

**OXOMOLYBDENUM- AND OXOTUNGSTEN (VI), (V) AND (IV)
COMPLEXES IN RELEVANCE TO ANALOGUE REACTIONS OF
MOLYBDO- AND TUNGSTOENZYMES**

*A Thesis Submitted
in Partial Fulfilment of the Requirements
for the Degree of
DOCTOR OF PHILOSOPHY*

by
SAMAR KUMAR DAS

to the
**DEPARTMENT OF CHEMISTRY
INDIAN INSTITUTE OF TECHNOLOGY, KANPUR**

SEPTEMBER, 1993

4 JUL 1986

CENTRAL LIBRARY
I.I.T. KANPUR

No A-121820

IIT-KANPUR - DAS - CXC



A121820

Dedicated
to
My Parents

STATEMENT

I hereby declare that the matter embodied in this thesis "Oxomolybdenum- and Oxotungsten (VI), (V) and (IV) Complexes in Relevance to Analogue Reactions of Molybdo- and Tungstoenzymes", is the result of investigations carried out by me in the Department of Chemistry, Indian Institute of Technology, Kanpur, India, under the supervision of Professor S. Sarkar.

In keeping with the general practice of reporting scientific observations, due acknowledgement has been made wherever the work described is based on the findings of other investigators.


Samar Kumar Das

Kanpur:

September 1993.



iv

CERTIFICATE

Certified that the work, "Oxomolybdenum- and Oxotungsten (VI), (V) and (IV) Complexes in Relevance to Analogue Reactions of Molybdo- and Tungstoenzymes", presented in this thesis has been carried out by Mr. Samar Kumar Das, under my supervision and the same has not been submitted elsewhere for a degree.

(S. Sarkar)

Thesis Supervisor

Department of Chemistry
I.I.T. Kanpur

Kanpur:

September 1993

DEPARTMENT OF CHEMISTRY
INDIAN INSTITUTE OF TECHNOLOGY KANPUR, INDIA

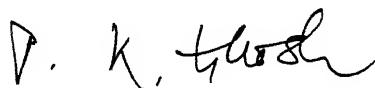
CERTIFICATE OF COURSE WORK

This to certify that Mr. Samar Kumar Das has satisfactorily completed all the courses required for the Ph.D. degree program.

The courses include:

chm 505 Principles of Organic Chemistry
chm 524 Modern Physical Methods in Chemistry
chm 525 Principles of Physical Chemistry
chm 545 Principles of Inorganic Chemistry
chm 668 Advanced Inorganic Chemistry II
chm 646 Bio-Inorganic Chemistry
chm 800 General Seminar
chm 801 Special Seminar
chm 900 Post-Graduate Research

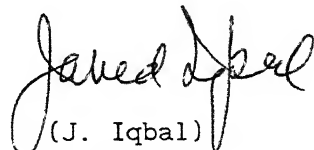
Mr. Samar Kumar Das was admitted to the candidacy of the Ph.D. degree in October 1989 after he successfully completed the written and oral qualifying examinations.



(P. K. Ghosh)

Head,

Department of Chemistry
Indian Institute of Technology
Kanpur - 208016



(J. Iqbal)

Convenor,

Department of Post-
graduate Committee,
Department of Chemistry
Indian Institute of
Technology, Kanpur
208016

ACKNOWLEDGEMENTS

It is great pleasure, I record my deep sense of gratitude to Professor Sabyasachi Sarkar, my thesis supervisor, for suggesting this research problem and for guiding me throughout the course of this research work and also for having been my friend, philosopher and guide.

I feel extremely grateful to Mrs. Sarkar for her patience, tolerance and hospitality during my discussions with professor sarkar at their apartment.

I am grateful to Prof. R. N. Mukherjee for providing me the necessary facilities and his keen interest in the progress of my work.

I sincerely thank Prof. P. K. Bharadwaj for helping to get the single crystal X-ray structure of one of the compounds and his constant encouragement and keen interest in my progress.

I thank Prof. S. Mukherji for his kind help and pleasant association.

I extend my thanks to Prof. T. K. Chandrashekhar and Prof. Y. D. Vankar for their kind help.

I am grateful to Prof. S Ranganathan for permitting me to record FT IR spectra in his laboratory.

I extend my heartfelt thank to Prof. J. Iqbal for his kind words during my times of trouble.

My special thank is due to Dr. P. K. Chaudhury for his constant help in kinetic study of my thesis work and pleasant association.

It was an experience worth remembering to have worked with Ramjee and Srinivasa. I thank them for their pleasant association.

I also thank khukudi (Mrs. Bharadwaj), Mama (Subrata Roy) and Rabin for pleasant association and cooperation throughout.

I offer my sincere thanks to all the faculty members and the students of the department for enlightening me with various aspects of chemistry.

I wish to make a special mention of Mr Promod Kumar and Dr. Manabendra Roy for their help in various aspects of my research work.

I thank my friends Manab, Bamdaa (Dr. Apurba K. Jana), Subrata (Mondal), Subir, Satpati, Joydeep, Surya, Rangan, Sunu, Shantanu, Sanjoy, Tarak, Pandian, Damoo, Ravikant, Goel, Jayraman, Patel, Dinu, Subit, Tapan, Mim, Bogadaa (Dr. Goutam Roy), Atanu, Ramdaa, Indra, Basakdaa, Somdaa, Indrani, kasi, imi etc for making my stay at I.I.T. enjoyable.

I sincerely thank Anu, my Pathfinder, who encourages me all the time.

Last but not the least I take the opportunity to acknowledge my parents, my younger brothers and my beloved Debi (Nibedita) for their love, encouragement and patience.

Samar Kumar Das

CONTENTS

	Page.
STATEMENT	iii
CERTIFICATE	iv
CERTIFICATE OF COURSE WORK	v
ACKNOWLEDGEMENTS	vi
SYNOPSIS	ix
CHAPTER 1 INTRODUCTION	1
CHAPTER 2 SCOPE OF THE INVESTIGATION	54
CHAPTER 3 SYNTHESIS AND CHARACTERIZATION	60
CHAPTER 4 FUNCTIONAL ANALOGUE REACTIONS	136
CHAPTER 5 OXIDATIVE ADDITION REACTION	205
CHAPTER 6 FUTURE SCOPE	216
REFERENCES	217
APPENDIX	230

SYNOPSIS

The thesis entitled, "Oxomolybdenum- and Oxotungsten (VI), (V) and (IV) Complexes in Relevance to Analogue Reactions of Molybdo- and Tungstoenzymes," consists of six chapters.

Chapter 1 presents an overview on the chemistry of molybdenum in contemporary inorganic chemistry and its role in biology. Based on this theme a general account, on (i) classification of molybdoenzymes, (ii) the presence of universal molybdenum cofactor in oxomolybdoenzymes and (iii) synthetic analogue reactions to mimic oxomolybdoenzymatic properties, has been presented.

Tungsten, the higher congener of molybdenum, has recently been shown to be an important trace element in biology. A brief survey of tungstoenzymes has also been presented.

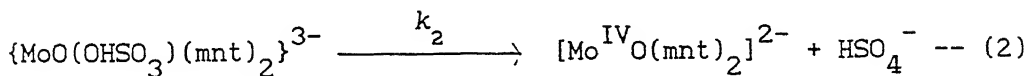
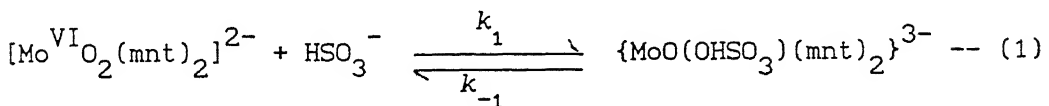
Chapter 2 deals with the scope of the present work. From the proposed structure of the molybdenum cofactor, a synthetic model compound should be comprised of a dithiolene type of ligation with oxomolybdenum group. The subtle difference in geometry between existing oxomolybdenum complexes and possible coordination number of molybdenum in cofactor has been stressed upon. An approach to exploit aqueous chemistry using MoO_4^{2-} as synthetic strategy to obtain suitable oxomolybdenum and oxotungsten compounds is outlined.

Chapter 3 describes the experimental procedures directed towards this research endeavour and has been divided into two sections: Section 3.1 presents work up manipulations of the complexes prepared and the methods to analyze them. Section 3.2

describes the physicochemical studies to characterize the synthesized complexes. These include infrared, electronic, nuclear magnetic resonance, electron spin resonance and FAB mass spectroscopy, magnetic moment, conductivity, X-ray powder diffractograms, X-ray single crystal study and cyclic voltammetry.

Chapter 4 presents functional analogue reactions carried out with the synthesized complexes and divided into seven parts.

Chapter 4.1 deals with the reaction between $[\text{Mo}^{\text{VI}}\text{O}_2(\text{mnt})_2]^{2-}$ (mnt^{2-} = maleonitriledithiolate = 1,2-dicyanoethylenedithiolate) and HSO_3^- in relevance to sulfite oxidase analogue reaction. The kinetics of the reaction



follows saturation behavior similar to biological substrate saturation kinetics at sufficient HSO_3^- concentration. This bisulfite saturation kinetics shows different inhibition patterns when the reaction is carried out in the presence of structurally similar anions such as SO_4^{2-} (competitive) and H_2PO_4^- (mixed noncompetitive).

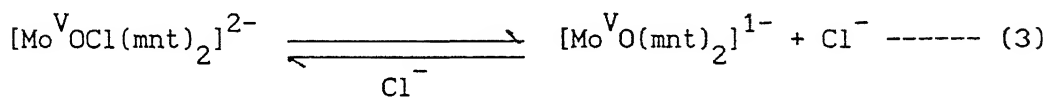
The anionic binding of HSO_3^- or the inhibitor (SO_4^{2-} or H_2PO_4^-) has been interpreted by invoking induced fit theory. Based on this, reaction mechanism has been proposed.

Part 4.2 describes the kinetics between $[\text{Mo}^{\text{VI}}\text{O}_2(\text{mnt})_2]^{2-}$ and PPh_3 in pure MeCN and in MeCN-water mixed solvent media and second order kinetics is observed in both the cases.

Chapter 4.3 presents the reductase type of synthetic analogue reaction. Kinetics of $[\text{Mo}^{\text{IV}}\text{O}(\text{mnt})_2]^{2-}$ with $(\text{CH}_3)_3\text{NO}\cdot 2\text{H}_2\text{O}$ follows enzymatic saturation behavior in acetone-acetic acid (effective pH = 6) ($K_m = 9.1 (\pm 0.9) \times 10^{-4}$ M, $V_{\max} (= k_2) = 3.81 \times 10^{-3}$ s^{-1}) which is inhibited competitively by Cl^- ion ($K_i = 2.40 (\pm 0.6) \times 10^{-3}$ M).

The unusual form of trimethylamine N-oxide like $(\text{CH}_3)_3\text{N}^+-\text{O}^-$ which in hydrated form remains as $[(\text{CH}_3)_3\text{NOH}]^+\text{OH}^-$ is stressed upon in relevance to the role of trimethylamine N-oxide reductase, an inducible terminal enzyme, for anaerobic respiration of bacteria like *Escherichia coli*.

Chapter 4.4 presents confirmations of competitive inhibitions by chloride anion in trimethylamine N-oxide saturation kinetics using cyclic voltammetry. This electrochemical reaction demonstrates the presence of chloride bound $\text{Mo}^{\text{IV}}\text{O}$ and $\text{Mo}^{\text{V}}\text{O}$ species. In the presence of high chloride concentration chemically oxidized species, $[\text{Mo}^{\text{V}}\text{O}(\text{mnt})_2]^{1-}$, responds to the following equilibrium:



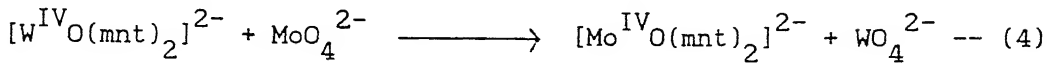
Detailed ESR investigations have been made to demonstrate the binding of Cl^- to molybdenum in *cis* position to Mo=O bond thus confirming the kinetic and electrochemical results.

Part 4.5 of this chapter presents proton coupled electron transfer reaction in the reduction of $[\text{Mo}^{\text{VI}}\text{O}_2(\text{mnt})_2]^{2-}$ by electrochemical means. All the experimental results obtained so far have been placed together to compare the suitability of the present model system in relevance to oxidoreductase reaction in

oxomolybdoenzymes.

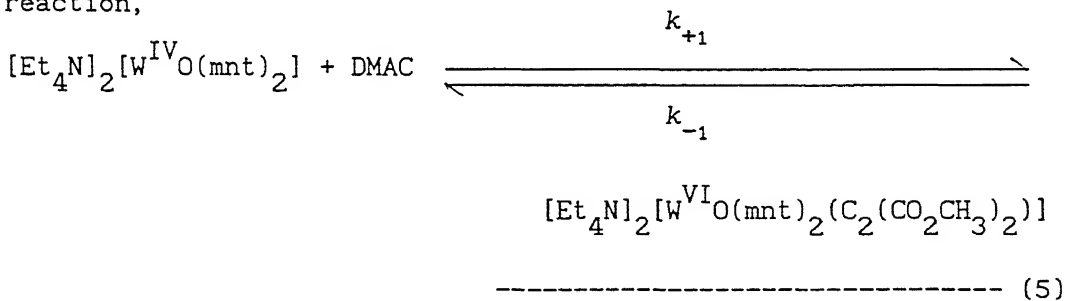
Part 4.6 presents the demonstration of CO_2 fixation by $[\text{W}^{\text{IV}}\text{O}(\text{mnt})_2]^{2-}$ in relevance to tungsten containing formate dehydrogenase from *Clostridium thermoaceticum*.

The last part (4.7) of this chapter describes the intermetallic electron transfer reaction,



implicating the displacement of tungsten by molybdenum. The similarity of this reaction to *Neurospora crassa nit-1* reconstitution assay of tungsten containing formate dehydrogenase in presence of MoO_4^{2-} has been discussed.

Chapter 5 deals with the reactivity of the $[\text{W}^{\text{IV}}\text{O}(\text{mnt})_2]^{2-}$. Oxidative addition reaction of dimethyl acetylenedicarboxylate (DMAC) to $[\text{W}^{\text{IV}}\text{O}(\text{mnt})_2]^{2-}$ has been described in part 5.1. For the reaction,



the K_{eq} (k_{+1}/k_{-1}) is found to be $14 (\pm 1) \text{ M}^{-1}$ and first order rate constants, found under pseudo first order condition with large excess of DMAC, are $k_{+1} = 11.2 (\pm 1.0) \times 10^{-4} \text{ s}^{-1}$ and $k_{-1} = 0.8 (\pm 0.01) \times 10^{-4} \text{ s}^{-1}$ respectively in MeCN at 25°C .

Part 5.2 describes similar oxidative addition of elemental sulfur to $[\text{Et}_4\text{N}]_2[\text{W}^{\text{IV}}\text{O}(\text{mnt})_2]$ with the formation of $[\text{Et}_4\text{N}]_2[\text{W}^{\text{VI}}\text{O}(\text{S}_2)(\text{mnt})_2]$. The reductive sulfur abstraction by PPh_3 of the oxidized disulfur complex, $[\text{W}^{\text{VI}}\text{O}(\text{S}_2)(\text{mnt})_2]^{2-}$, led to the

formation of $[W^{IV}O(\text{mnt})_2]^{2-}$. This reaction follows a second order A + 2B type kinetics with $k_{\text{obs}} = 4.3 (\pm 0.06) \text{ M}^{-1} \text{ S}^{-1}$ at 25°C . For this reaction the possible attack by phosphine across the W-S bond is proposed instead of across S-S bond based on monitoring the progress of this reaction cyclic voltammetrically.

Chapter 6 describes some insight about the scope of the future work for better understanding of synthetic analogue reactions of oxomolybdo- and oxotungstoenzymes.

CHAPTER 1

INTRODUCTION

One of the unique transition element is molybdenum. The chemistry of molybdenum compounds expanded many new fields in contemporary inorganic chemistry. Thus the formation of Mo-Mo bond of different multiplicities alongwith the formation of cluster compounds void of carbonyl ligand stimulated an enormous growth of its chemistry in its lower oxidation states in both molecular and solid state systems^{1,2}. The second important aspect of molybdenum chemistry is related to its applications as catalysts in organic transformations as well as in industrial processes³⁻⁵. The use of molybdenum as hydrodisulfurization catalyst in petroleum feed stocks is well recognized⁵. The third prominent use of this element is its role in biology.

From the last two decades conventional treatment of inorganic chemistry has been substantially changed and important contributions have been made to exploit the chemistry involved having some relation to their possible applicability or to reveal complex biological reactions. The present thesis is an attempt to understand the chemical aspects of some molybdenum complexes in relevance to some molybdoenzymes. Thus before presenting the present work the important contributions already existing in the literature have been briefly reviewed below.

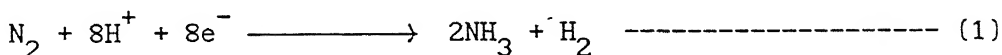
Molybdenum is only transition metal of 4d group having extensive role in biology. The abundance of this element in the

earth crust is rare (1.2 p.p.m.). The presence of molybdenum in the meteorites even led to the proposal of the involvement of this metal in chemical evolution according to Orgel's theory. Though its abundance in earth crust is very low yet its concentration in the sea water exceeded most of the transition metal ions by virtue of its existence in the form of water soluble MoO_4^{2-} ion. MoO_4^{2-} , being tetrahedral is isostructural to SO_4^{2-} or PO_4^{3-} anions and its accessibility across biological membrane is thus understood. Depending on the oxidation state molybdenum shows roughly equal affinity for hard donor oxo and soft donor sulfido ligands. The ready availability of different oxidation states with the possibility of a variety of different coordination numbers from 4 to 8 is another important aspect of this metal. All these properties taken together reflect the uniqueness of this metal which is reflected in its biological endeavour.

Till date molybdoenzymes can be divided into two different groups. In one group it is uniquely present in the enzyme, nitrogenase^{6,7}. The other group comprises of a fairly large number of oxomolybdoenzymes (molybdenum hydroxylases)⁷⁻¹¹.

NITROGENASE.

The nitrogenase catalyzes the reduction of molecular nitrogen as shown in equation (1).



The role of molybdenum for this enzyme was known since 1930¹². In 1978 Shah and Brill have isolated Fe-Mo cofactor from this enzyme¹³ and Zumft by acid base hydrolysis of the enzyme could

demonstrate the formation of thiomolybdate thus proving beyond all doubt the presence of molybdenum in this enzyme¹⁴. Several model compounds have been synthesized to mimic the structural if not functional properties of this enzyme but all these model compounds deviated from the basic atomic ratio of Fe:Mo:S found in the Fe-Mo cofactor. The EXAFS studies revealed that the basic minimum atomic aggregates around molybdenum center which could be a linear core or a cubane unit comprised of Fe_2MoS_5 or Fe_3MoS_5 aggregate respectively¹⁵. The basic problem of Mo-S chemistry related to dimerization via sulfur bridge eluted the synthesis of a heteronuclear Mo-Fe-S system comprising of only 1 Mo and 68 Fe via sulfur ligation as demonstrated by Fe-Mo cofactor analysis. Nevertheless an elaborate heteronuclear cluster chemistry in this regard has been developed and extensively reviewed elsewhere¹⁶. It is only in July 1992 the single crystal X-ray structure of the enzyme, nitrogenase has been solved¹⁷. A diagrammatic representation of this structure is shown in Fig. 1.1a. For comparison the proposed core structures around molybdenum, as analyzed by EXAFS, are also shown in Fig. 1.1b. The existence of Mo-O bonds from the homocitrate moiety reveals the limitation of EXAFS in predicting the first coordination sphere around molybdenum in nitrogenase. Thus the presence of Mo-O bonds can place nitrogenase even in the category of oxomolybdoenzymes.

The role of nitrogenase is the catalytic reduction of molecular nitrogen. The oxidation state of molybdenum in this enzyme is not clearly known. However, the extreme air sensitive nature of this enzyme and its role for reduction make one's belief

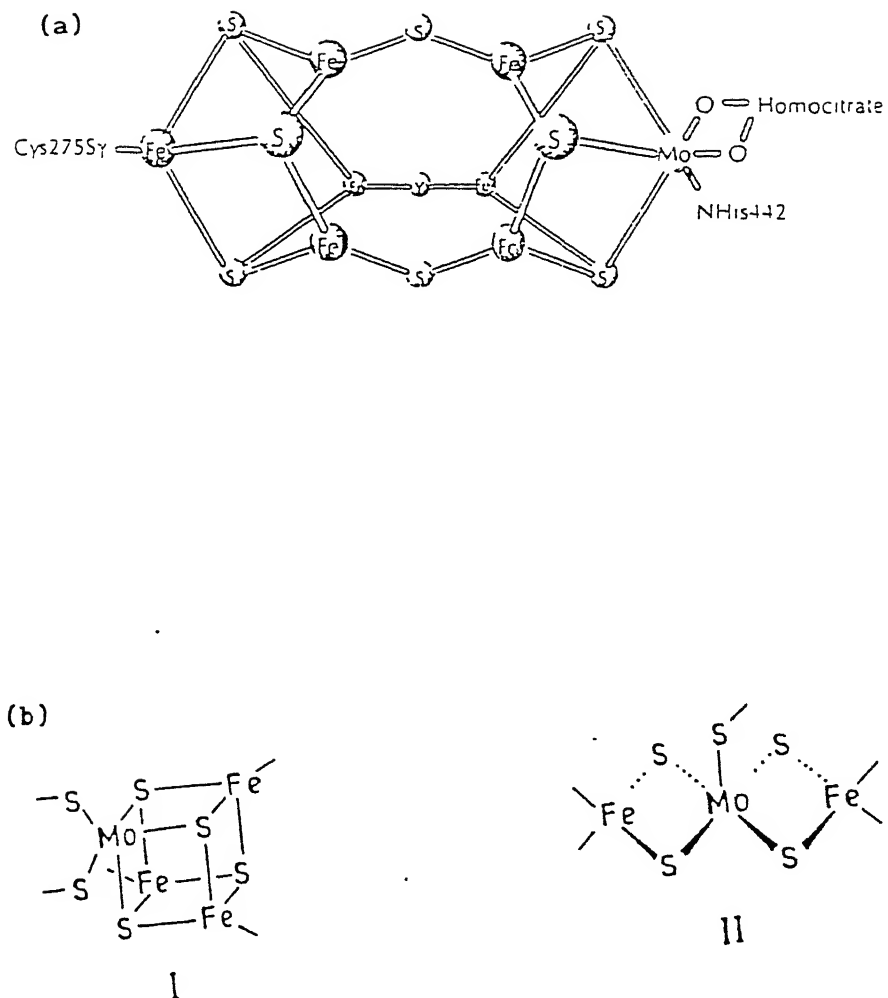
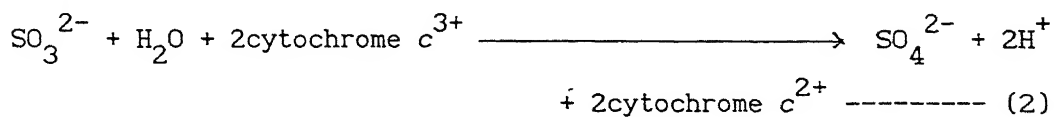


Fig. 1.1 (a) A diagrammatic representation of the FeMoco centre in the nitrogenase MoFe protein, showing the ligation by cysteine and histidine residues of the α subunit; (b) proposed core structures around molybdenum of nitrogenase as analyzed by EXAFS.

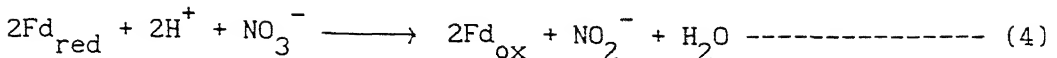
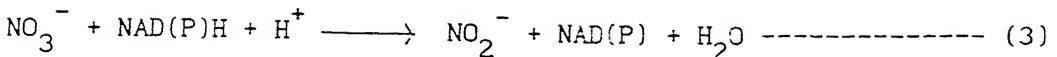
that oxidation state of molybdenum present here must be low. Molecular nitrogen is extremely inert and its reduction by one or two electron unit will not be attainable in aqueous medium because a strong reducing agent will react with water. However, from the basic relationship like $-\Delta G = nFE$ it is understandable that E can be minimized if the number of electrons involved are more which are to be supplied at a time. For a 6-electron reduction the E could be very low and will be accessible in aqueous medium. The cluster unit of the Fe-Mo cofactor comprises of 6 to 8 electron-flux at a time by changing one unit oxidation state from Fe(II) to Fe(III) of each iron present in the cluster. These requirements do not require a very low oxidation state of molybdenum. In the synthesized Fe-Mo heteronuclear cubane core¹⁸ the formal oxidation state of molybdenum can be as low as +3. Hence it is presumed that in the nitrogenase the oxidation state of molybdenum center may not be lower than +3. It is also understood that for a strong π -bonding ligand like NO^+ which is isoelctronic to molecular nitrogen, the minimum electrons available in the d orbital of molybdenum is 4 to have a stable mononitrosyl complex. A Mo(III) with d^3 electronic configuration may not provide enough bonding interaction with a π bonding NO^+ ligand. For the essential role of molybdenum in nitroganase to hold molecular nitrogen, which has not yet been substantiated, the substrate binding should not be too strong for the catalytic cycle of the enzyme. A functional model can clarify the essential requirements regarding the oxidation state of molybdenum.

OXOMOLYBDOENZYMES.

More than a dozen of molybdoenzymes of this class is known and many more may be still to be discovered. All these enzymes catalyze oxo transfer reaction coupled with two electrons. These enzymes can be eventually subdivided into two classes. A few are popularly known as "oxidase" type and the others are known as the "reductase" type. For the "oxidase" type of enzymes it is the reducing substrate which gets oxidized catalyzed by the enzyme. However, for the regeneration of enzyme which is now reduced, another half reaction sets in wherein an oxidizing substrate oxidizes back the reduced enzyme to complete a catalytic cycle. Thus these enzymes are best described as "oxidoreductase" type. For the "reductase" class of enzymes the two half redox reactions are reversed and the enzyme is informally named as "oxidizing substrate reductase", for example, nitrate reductase. Thus the enzyme, sulfite oxidase utilizes the reducing substrate sulfite or bisulfite bearing name of the enzyme. For the completion of the catalytic cycle the physiological electron acceptor is ferricytochrome c. Hence the proper nomenclature of this enzyme is sulfite:ferricytochrome c oxidoreductase. The oxidation of sulfite to sulfate is catalyzed by this enzyme. Thus the overall reaction is represented as below:



Similarly for the assimilatory nitrate reductase the following overall reactions take place.



From the reactions (3) and (4) it is clear that though the named enzyme nitrate reductase utilizes nitrate as the oxidizing substrate but for the regeneration stage it utilizes different types of electron donors like NAD(P)H for eucaryotic organisms and ferridoxin for prokaryotes respectively.

Largely studied and most complex enzyme of this class is xanthine oxidase. Contrary to sulfite oxidase it utilizes a wide variety of purines, pteridines, pyrimidines and other heterocyclic nitrogenous compounds as reducing substrates¹⁹. Specificity with regard to electron acceptors is also very broad including oxygen, NAD^+ , ferridoxin, cytochrome c and other *invitro* electron acceptors²⁰. Xanthine oxidase and the related dehydrogenase are widely distributed in bacteria, fungi, insects, birds and mammals. Some of the enzymes^{7-11,21} of this class are represented in Table 1.1.

Several important queries related to structure-function relationship of these enzymes have been addressed over the passed hundred years²². From a chemist's point of view the role of molybdenum in these enzymes is one of the most important fact to understand. The other important informations of relevance are substrate binding, electron transfer or oxo transfer, the source of oxygen in this oxo transfer reaction, inhibition role of certain related molecules with kinetics, and the minimal structural information around the molybdenum center with the absence of X-ray data.

Table 1.1 Examples of Some Oxomolybdoenzymes

Enzyme	Mo content ^a	Substrate	Source
sulfite oxidase	2	SO_3^{2-}	animals, microorganisms
xanthine oxidase	2	purines	bovine milk
xanthine dehydrogenase	2	purines	animals, microorganisms
Aldehyde oxidase	2	aldehydes	animals
formate dehydrogenase	2-4	CO_2 , HCOO^-	microorganisms
trimethylamine N-oxide reductase	2	trimethylamine N-oxide	microorganisms
nitrate reductase	4	NO_3^-	microorganisms (<i>C. vulgaris</i>)
nitrate reductase	1	NO_3^-	microorganisms (<i>E. coli</i>)
dimethylsulfoxide reductase	b	dimethyl-sulfoxide	microorganisms (<i>E. coli</i>)
biotinsulfoxide reductase	b	biotin-sulfoxide	microorganisms (<i>E. coli</i>)

^a Atoms/molecule^b not known

UNIVERSAL Mo-COFACTOR.

Pateman *et al* in 1964 first postulated the existence of a molybdenum cofactor common to several molybdenum enzymes²³. They investigated a series of pleiotropic mutants in *Aspergillus nidulans* each of which caused a deficiency of xanthine dehydrogenase and nitrate reductase. They proposed that these two enzymes have common molybdenum cofactor, the synthesis of which is controlled by five important genetic loci.

Nasons and coworkers using a mutant strain of *neurospora crassa* *nit-1* demonstrated that the inactive apoprotein of nitrate reductase in extract of *nit-1* could be reconstituted by the addition of acidified preparation of xanthine oxidase, aldehyde oxidase, sulfite oxidase or nitrate reductase from animals, fungal or bacterial origin²⁴. These important findings ,thus, established the presence of a common cofactor in this class of molybdoenzymes. Presently the presence of molybdenum cofactor in a purified enzyme is routinely assayed by *invitro* reconstitution of *neurospora crassa* nitrate reductase in extract of the *nit-1* mutant²⁵.

Unlike most of the known cofactors in biology the molybdenum cofactor is not isolable using normal procedures. The cofactor activity is extremely labile in the presence of air. For the structural characterization of the molybdenum cofactor elegant synthetic and spectroscopic analyses done by Rajagopalan and coworkers²⁶ led to the discovery of the structure of the molybdenum cofactor as shwon in Fig. 1.2. The worthnoting feaures of this cofactor are: (a) the presence of a pterin moiety, (b)

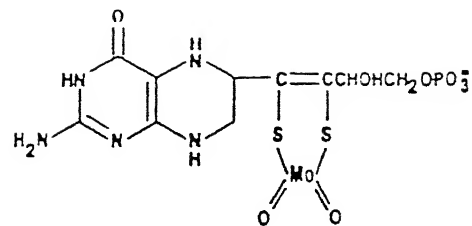


Fig. 1.2 Structure of the molybdenum cofactor. The dioxo structure shown is characteristic of the molybdenum center in sulfite oxidase and nitrate reductase. The other oxomolybdoenzymes such as xanthine oxidase require a terminal sulfide ligand in place of one of the oxo groups.

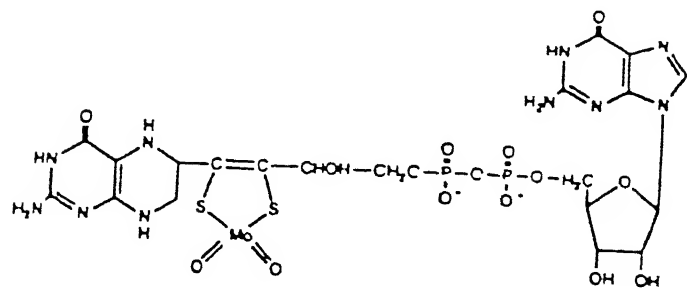


Fig. 1.3 Proposed structure of molybdenum cofactor of molybdopterin guanine dinucleotide form.

the side chain of the pterin contains a dithiolene group, (c) the presence of a phosphoester group and (d) the coordination to molybdenum via dithiol moiety to give a dithiolene coordination. The entire ligand without molybdenum is termed as molybdopterin which as well as the molybdenum cofactor are anionic in nature.

Kruger and Meyer have proposed the possibility of having a different form of molybdenum cofactor from carbon monooxide dehydrogenase of *Pseudomonas carboxydoflacea*²⁷. Rajagopalan and coworkers could isolate a new pterin derivative of molybdopterin guanine dinucleotide from dimethyl sulfoxide reductase from *Rhodobacter sphaeroides*²⁸. With this success of isolating another form of molybdenum cofactor, the cofactor of carbon monooxide dehydrogenase was recognized to be containing a molybdopterin cytosine dinucleotide form²⁹. In 1991 from *Methanobacterium thermoautotrophicum* molybdopterin moieties like molybdopterin guanine dinucleotide, molybdopterin adenine dinucleotide and molybdopterin hypoxanthine dinucleotide have been identified in formyl methanofuran dehydrogenase³⁰. The function of the ribonucleotide part of the molybdopterin dinucleotide is not understood. However, the diverse nature of this class of enzymes in relation to their availability from different species and their diverse role in the light of broad and specific substrate selectivity could be the reason for these variations. It is important to take note that the molybdopterin is the ligand of molybdenum and irrespective of different forms of cofactors available, the bonding of the molybdopterin ligand to molybdenum is exclusively through the dithiolene moiety. The proposed structure of

molybaenum cofactor of molybdopterin guanine dinucleotide form is shown in Fig. 1.3.

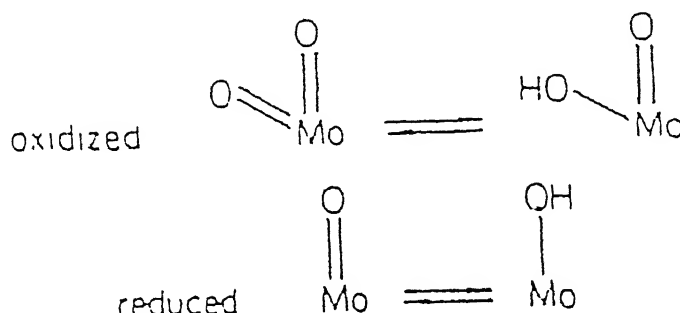
MINIMAL STRUCTURAL INFORMATION AROUND MOLYBDENUM IN THESE ENZYMES.

No X-ray structural data for this class of enzymes is available. The instability of molybdenum cofactor precludes its crystallization for X-ray structure analysis. The EXAFS is the only spectroscopic technique available to furnish some structural information around molybdenum center of these enzymes. As in the catalytic cycle a two electron oxo transfer reaction takes place, hence EXAFS studies are generally made in the oxidized as well as in the fully reduced forms of the enzyme. Analysis of EXAFS data revealed the existence of MoO_2 (VI) or MoOS(VI) core in oxidized forms of enzymes. However, in the reduced form it is only MoO(IV) core that is present in all forms of the enzymes. In some cases the semireduced or semioxidized form containing Mo(V) state of the enzyme has been subjected to EXAFS analysis. However, the use of phosphate or chloride buffer sometimes complicated the analysis of EXAFS data which strongly suggests the competition of phosphate or chloride group to bind to the molybdenum center³¹. The representative EXAFS data^{15b} are presented in Table 1.2. Sometimes EXAFS data³² when analyzed gave unexpected results which are not compatible to normal physicochemical properties of an enzyme. For example the molybdenum site in two different types of nitrate reductase, assimilatory enzyme from *Chlorella vulgaris* and dissimilatory enzyme from *Escherichia coli*, have been investigated by EXAFS spectroscopy³². For nitrate reductase from *Chlorella*

Table 1.2 Summary of EXAFS Results on Some Cxomolybacenzymes

Enzyme	Conditions	Mo=O		Mo-S	
		Number	R(A.)	Number	R(A.)
Sulfite oxidase (chicken liver)	50 mM KPi, pH 7.8, oxidized	2	1.68	2-3	2.41
Sulfite oxidase (chicken liver)	50 mM KPi, pH 7.8, dithionite-reduced	1	1.69	3	2.38
Xanthine oxidase (bovine milk)	100 mM Tris-HOAc, pH 8.5, oxidized	1.5	1.71	2.1	2.54
Xanthine oxidase (chicken liver)	5 mM KPi, pH 7.8, reduced	1	1.66	2-3	2.33
Nitrate reductase (<i>Chlorella</i>)	80 mM KPi, pH 7.6, reduced	1	1.67	3	2.38
Nitrate reductase (<i>Chlorella</i>)	80 mM KPi, pH 7.6, oxidized	2	1.72	2-3	2.44
Nitrate reductase (<i>E. coli</i>)	50 mM KPi, pH 7.0, reduced	0		2	2.37

vulgaris, the number of Mo-O terminal bonds found in the oxidized form is two and in the reduced form it is one as expected. However, in *Escherichia coli*, no terminal dioxoMo bonds could be predicted for oxidized form; instead only one terminal Mo=O bond could be located. In the reduced form of the enzyme apparently no terminal short Mo-O bond could be identified. However, the authors have suggested that the distinction between the oxo/dioxo and nonoxo/monooxo species may be due to pH effect. The oxidized and reduced forms of the molybdenum center in this enzyme may exist in the following forms (Scheme 1.1):



Scheme 1.1

Electron spin resonance (ESR) spectroscopy is a powerful tool to understand the role of specially molybdenum and other ESR active centers present in the oxomolybdenum enzymes. The six line hyperfine structure characteristic of molybdenum signals arises due to the presence of ^{95}Mo / ^{97}Mo ($I = 5/2$) which together constitute 25% of natural molybdenum. The other 75% consists of molybdenum isotopes with $I = 0$. As discussed earlier the viable oxidation state of molybdenum in biological system may be as low as Mo(III). From Mo(VI) to Mo(III), Mo(III) and Mo(V) are only

paramagnetic molybdenum species Mo(III) oxidation state containing molybdenum complexes generally show ESR signal only under stringent conditions because they are likely to lose intensity by exchange broadening. From the EXAFS analysis mentioned earlier the presence of atleast one terminal oxo group in most of the oxomolybdoenzymes exists. From the synthetic compounds it is well known that compounds containing MoO(V) core readily response to ESR signal compared to a simple Mo(V) complex of higher symmetry. One drawback for simple oxo Mo(V) complexes is their readiness for dimerization by hydrolysis. The Mo(V) dimer may be ESR inactive. Sometimes monomer dimer equilibria exist which are solvent dependent. An alternative source of ESR signal is a paramagnetic dimer containing a triplet state with two unpaired electrons. However, most of the oxomolybdoenzymes though contain a dimeric unit containing two active sites yet it is recognized that the catalytic cycle is independently carried out with each monomeric unit. Molybdenum ESR signals have characteristic g values and from several synthesized complexes these values are known. Thus the nature of g value can fairly predict the nature of donor atoms ligated to molybdenum. The hyperfine coupling constant is also related to the nature of donor ligand³³.

In fact it is the ESR study through which the presence of molybdenum in sulfite oxidase has been recognized³⁴. ESR spectroscopy has been extensively used by Bray and coworkers concerning the role of molybdenum mainly in xanthine oxidase³⁵. Using ESR method redox potentials of molybdenum in this class of enzymes have been determined which are tabulated³⁶ in Table 1.3.

Table 1.3 Redox Potentials for Molybdenum in Enzymes

Enzyme	Potential (mV) at pH 7		Reference
	Mo(VI)/Mo(V)	Mo(V)/Mo(IV)	
Xanthine oxidase (functional)	-355	-355	36a
Xanthine oxidase (desulfo)	-440	-480	36a
Xanthine dehydrogenase	-350	-362	36b
Nitrate reductase	+180	+220	36c

SUBSTRATE BINDING SITE.

From basic enzymatic principle it is reasonable to expect a substrate binding site in these enzymes. In all these enzymatic actions in the regeneration stage (the supporting half reaction as described earlier) a consecutive two one electron proton coupled electron transfer as predicted by Stiefel³⁷ have been observed. Thus in most of the cases substrates modify the ESR signal of molybdenum during enzymatic turnover confirming the fact that the enzyme has a substrate binding site. Some molecules and anions especially PO_4^{3-} , SO_4^{2-} and Cl^- have different inhibitory effects on enzymatic reactions. A direct probe to identify these effects is only by ESR study, as binding of these molecules or anions to molybdenum changes the shapes and g values of the signals. A representative example for the change of line shape and g value as presented by Gutteridge *et al*³⁸ for nitrate binding site with the slow signal from desulfoxanthine oxidase is shown in Fig. 1.4.

PROTON COUPLED Mo(V) SIGNAL.

In most enzymes of this class the Mo(V) ESR signal observed at low pH is proton coupled. Xanthine oxidase in fact shows interaction of two protons with molybdenum. On the other hand sulfite oxidase and nitrate reductase each show only one proton coupled signal. In the Table 1.4 representative superhyperfine coupling constant values³⁵ of some oxomolybdoenzymes are presented.

The interaction of proton with unpaired electron of Mo(V) furnishes the evidence about the fate of oxidized MoO_2 (VI) or

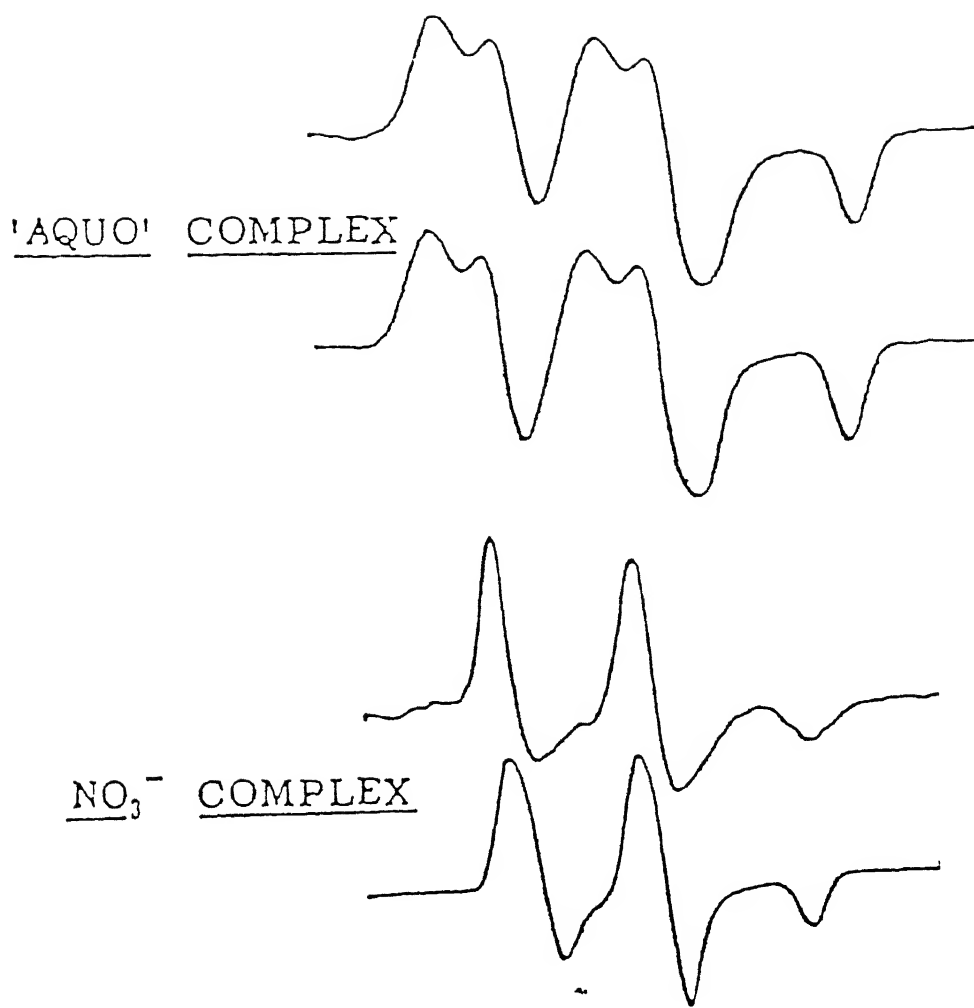


Fig. 1.4 Evidence for an anion binding site: the signal from desulfo xanthine oxidase. The top half of the figure shows ESR spectra in the absence, and the bottom half in the presence, of nitrate ions. For each pair of spectra, the upper one is experimental, lower one is a computer simulation. The weakly coupled proton in the "aquo" complex affects the linewidth.

Table 1.4 Exchangeable Protons Coupled to Mo(V) in Enzymes

Values of the Hyperfine Coupling Constants, $A(^1H)$, (in mT).

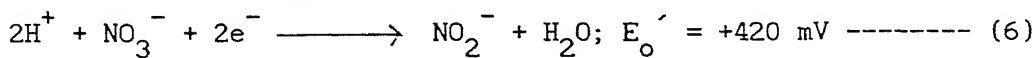
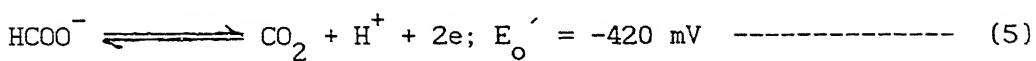
Enzyme	A_1	A_2	A_3	A_{av}
Xanthine oxidase (functional; type1)	1.30 0.40	1.39 0.30	1.40 0.20	1.36 0.30
Xanthine oxidase (desulfo)	1.66 0.16	1.66 0.16	1.56 0.16	1.63 0.16
Xanthine oxidase (functional; type2)	1.07 1.07	0.98 0.98	0.93 0.93	1.01 1.01
Nitrate reductase	1.11	0.84	0.81	0.92
Sulfite oxidase	0.85	0.80	1.20	0.95

MoOS(VI) core in the reduced pentavalent state which are MoO(OH)(V) or MoO(SH)(V) respectively. The nature of superhyperfine interaction suggests the presence of proton as MoO(OH)(V) or MoO(SH)(V) and not directly attached to molybdenum center. The interaction may be viewed as shown³⁹ in Fig 15.

The combined data from EXAFS and ESR help to understand the ligational aspect of dioxo- or oxosulfidoMo(VI) core and the respective conversion of the cores to monooxMo(IV) core in the fully reduced form via the intermediate participation of a MoO(OH) or MoO(SH) form in the pentavalent state. Based on these studies in the oxidized form of the molybdenum cofactor a dioxo or oxosulfido group directly attached to molybdenum has been proposed (*vide supra*).

REDOX PROPERTIES.

Metalloenzymes containing transition metals without fail involve the redox property of the metal center. Thus it is the thermodynamic necessity that a particular metal is involved in a specific metalloenzyme. For the oxomolybdenum class of enzymes the role of molybdenum is essentially to participate in the enzymatic reaction which is essentially a typical redox reaction. The diverse nature of redox reactions catalyzed by this class of molybdenum enzymes is surprising and to illustrate the extreme nature the following reactions are adequate.



Reaction (5) is catalyzed by the enzyme formate dehydrogenase

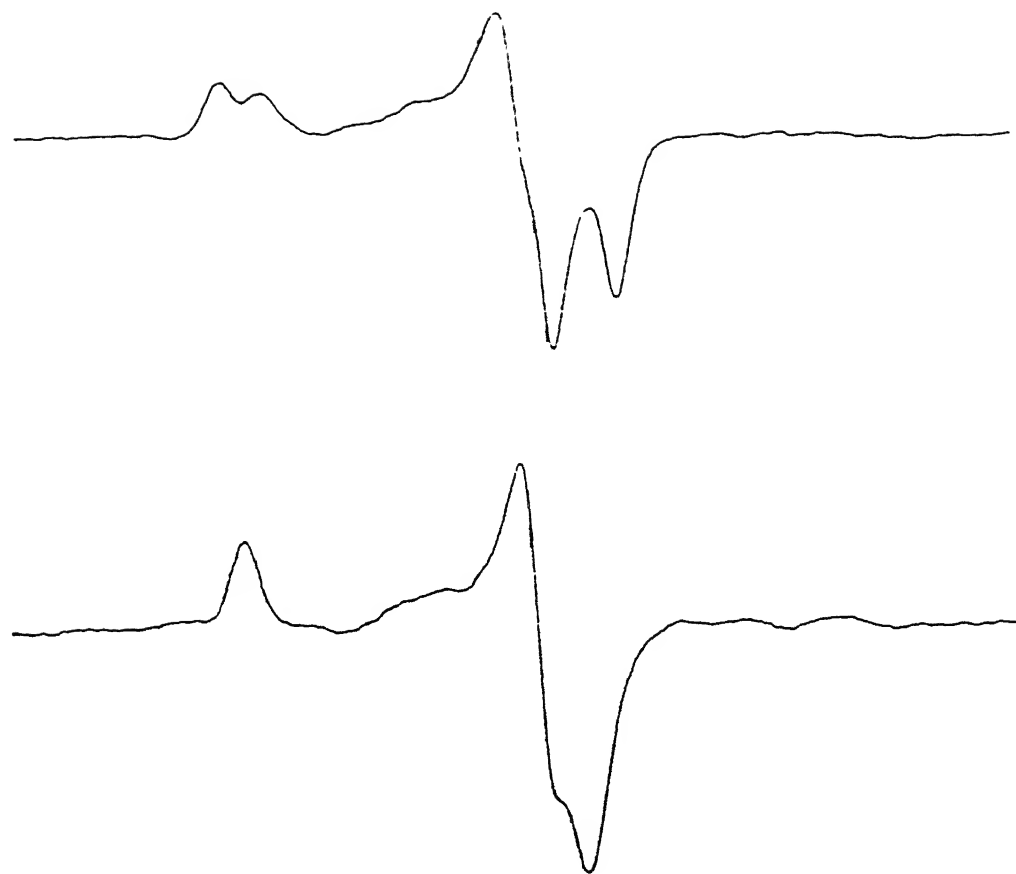
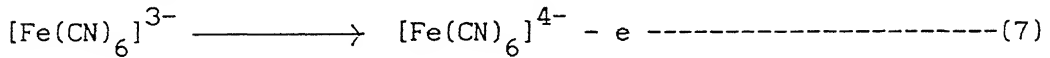


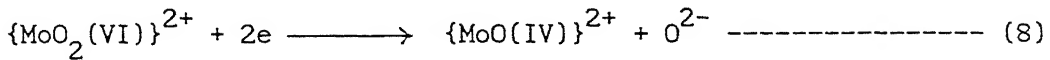
Fig. 1.5 ESR spectra at about 120 K from Mo(V) in chicken liver sulfite oxidase in H_2O (upper spectrum) or in D_2O (lower spectrum). The enzyme was reduced with sulfite in Tris buffer, pH 6.5 or pD 7.0.

whereas reaction (6) is catalyzed by nitrate reductase. Both these enzymes contain molybdenum which play a central role in these catalytic reactions. It is surprising that the total potential window for these two reactions span over 840 mV. This sort of diverse nature of redox potential mediated by molybdenum cofactor in this class of enzymes is difficult to understand. Furthermore if the molybdenum center is associated with a universal cofactor then it is even more intriguing to understand the role of apoenzyme; or the little variation in the molybdopterin ligand can impose this diversification. In a sense the reactions shown in equations (5) and (6) are widely different in nature. For formate dehydrogenase, for example, the reaction can be catalyzed both ways. However, for nitrate reductase the catalytic action is restricted to one direction i.e. the conversion of nitrate to nitrite only.

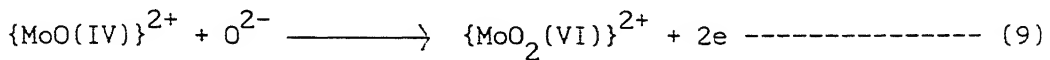
Furthermore the reversibility of a redox reaction as we understand is not valid for the redox reaction catalyzed by any molybdoenzyme. A simple reversible reaction which obeys Nernstian relationship can be represented as:



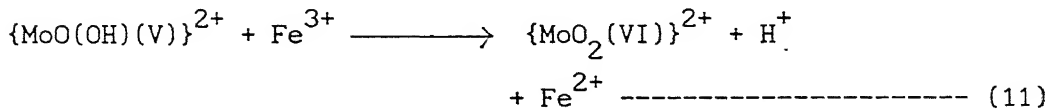
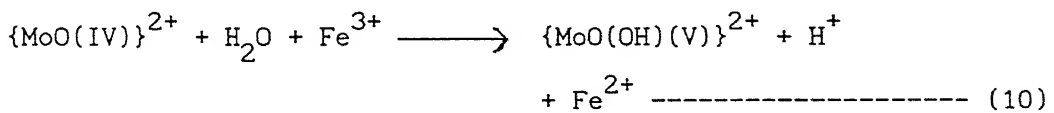
For this half reaction the conjugate redox pair differs by only an electron retaining their chemical entity identical. A reaction of this nature is an ideal reversible redox reaction. However, the redox reaction involved with the molybdenum center in a molybdoenzyme is essentially an atom transfer reaction as shown below:



In this case the conjugate redox partners are chemically not identical; hence it can not be reversible reaction in nature. In the sense of enzymatic reaction the reversibility implies that the reduced molybdenum center in the above stated equation may be smoothly reoxidized by another atom transfer reaction within its catalytic cycle as shown below:



Once again this reverse reaction is also an irreversible one. This argument would be clear in the light of two independent half cell reactions namely an oxidative half cell reaction followed by a reductive half cell reaction with respect to the enzyme. Thus the oxidation of sulfite by the oxidized form of sulfite oxidase is the oxidative half reaction and the reduction of ferricytochrome c by the reduced sulfite oxidase can be called as reductive half reaction with respect to the enzyme. For this reductive half reaction the situation is even more complicated because of the involvement of two successive one electron transfer reactions coupled with an oxo transfer which are shown below:



Both these successive reactions are irreversible in nature considering the chemical variation of the conjugate redox pairs.

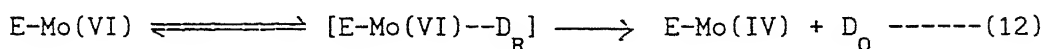
Most of the oxomolybdoenzymes contain multiple redox centers. The electron transfer processes will be more complicated if these

miltiple redox centers have very close redox potentials. Assuming that the electron donor donates electron at the molybdenum center, then if the reduction potential of molybdenum center is sufficiently close to the adjoining redox center, the distribution of electron in both the redox centers is possible. The situation may be like that that before the complete reduction of molybdenum center electron density may be funneled towards the next redox center. This situation is very much highlighted in reduction process of xanthine oxidase⁴⁰. Xanthine oxidase is comprised of four active redox centers namely molybdenum part, flavin and two nonequivalent ferridoxin cores of Fe_2S_2 type^{7,8}. For the catalytic role of this enzyme it is well known that the substrate molecule of general formula RH is hydrolysed to ROH which is a two electron process. In presence of the physiological substrate, xanthine oxidase showed very rapid Mo(V) ESR signal whose integration showed at the most 50% ESR active species and 100% signal could never be achieved. The 50% signal then decreased its intensity within the period of catalytic action. To explain the accountability with regard to number of electrons transferred from the substrate to the enzyme, it has been elegantly explained by the distribution of electron density from the molybdenum center to other redox centers. Bray and coworkers demonstrated the path of the electron by integrating ESR active signals of all the redox centers under variable conditions using rapid freezing technique⁴¹. As an illustrative example the equilibrium states of a four center enzyme, each center capable of accepting one electron, should give sixteen discrete microstates and the

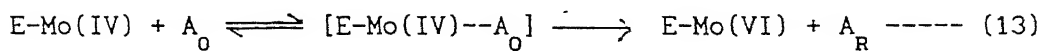
possible redox intermediates⁴² are shown in Fig. 1.6. One intensive feature about these enzymes is the variations of measured redox potentials on changing the conditions of the reaction medium. pH dependent change can be rationalized by invoking the existence of protonated / deprotonated forms of the enzyme. However, even the change of the nature of buffer ion in the reaction medium led to belief appreciable ionic interactions between the molybdenum center and the ions present in the medium. The mid point potential of most of the redox centers have been experimentally determined by potentiometric titration in conjunction with ESR technique using redox dye mediators⁸.

KINETICS OF THESE ENZYMES.

For the complete turnover of an enzymatic cycle two alternate redox reactions are in operation. For the oxidase class of enzyme the forward reaction is completed by electron donor substrate which reduces the molybdenum center, itself getting oxidized as shown below:



where D_R and D_O represent the reduced and oxidized states of substrate respectively. In the regeneration stage of the enzyme the reverse reaction occurs with another class of electron acceptor(A_O) as shown in equation (13).



(A_R = reduced electron acceptor)

Two important aspects have been considered in the reaction. First the oscillatory nature: these two alternative reactions led to the

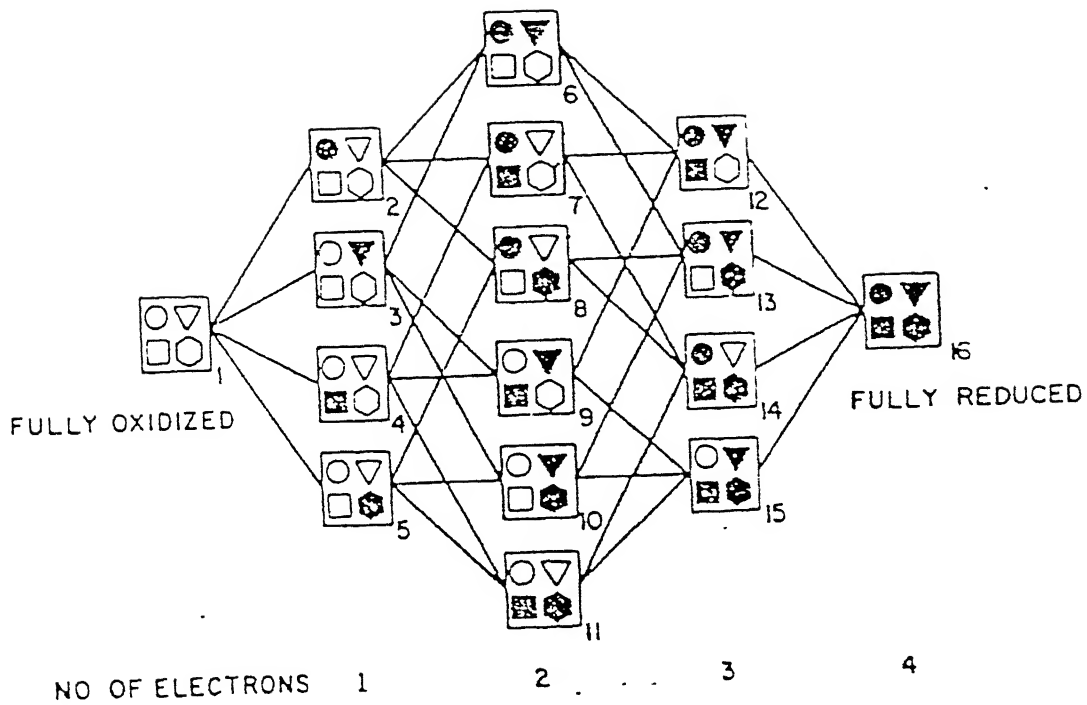


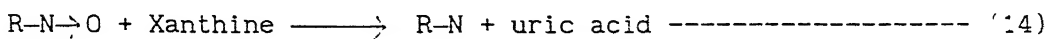
Fig. 1.6 Equilibrium distribution of electrons in four center enzyme. Four different shapes represent four redox centers. Empty symbols signify oxidized centers, solid symbols represent reduced centers. Each column contains all the enzyme species possessing the same total number of reducing equivalents, thus the five columns represent enzyme species with 0, 1, 2, 3, or 4 electrons.

proposal of the classical pingpong mechanism as proposed by Cleland⁴³. This pingpong mechanism assumes that after the oxidation of donor molecule the oxidized donor moiety dissociates from the reduced enzyme. Once this dissociation is over the acceptor molecule binds at the same site to complete the regeneration of the enzyme. Through a number of observations⁴⁴ it has been accepted that the electron donor and electron acceptor binding sites in these enzymes are different. The kinetic behavior of these enzymes have been interpreted in a manner analogous to that reported for pyruvate carboxylase⁴⁵. This type of mechanism is now called as "hybrid pingpong rapid equilibrium random" mechanism. In this mechanism it is assumed that substrates and products bind and dissociate independently in a rapid equilibrium random fashion. The transfer of electrons between the donor and acceptor sites is mediated by all the redox centers available in these enzymes. To illustrate this point the electron transfer mechanism for sulfite oxidase, the most simple enzyme of this class, may be viewed in the following way.

The physiological reducing substrate sulfite (or bisulfite) binds at the molybdenum center of this enzyme. After oxidation of sulfite (or bisulfite) to sulfate (or bisulfate) the regeneration of this enzyme takes place by electron acceptor ferricytochrome c via cytochrome b thus demonstrating two different sites for electron transfer in forward and backward reactions respectively⁴⁶.

The second important aspect is relative to the mechanism of oxo transfer reaction. It has been demonstrated by Murray *et al*⁴⁷ that the oxidation of reducing substrate takes place by oxygen

atom transfer from the solvent i.e. water, by ^{18}O isotopic experiment. Using broad substrate specificity they also showed that xanthine oxidase and xanthine dehydrogenase can catalyze direct transfer of ^{18}O from $^{18}\text{O-N-oxide}$ to xanthine for uric acid formation. Stohrer and Brown⁴⁸ have substantiated this view and generalized that heterocyclic N-oxides are biological oxygenating agent as represented below:



Recently Hille and Sprecher⁴⁹ using statistically probable single turn over experiments with isotopically labelled oxomolybdo-moieties in xanthine oxidase and water elegantly demonstrated that it is the oxo transfer reaction between Mo=O moiety and xanthine which is taking place. The participation of water as a source of oxygen takes place in the regeneration stages of the enzyme. Thus for the second and subsequent catalytic cycles, the oxygen from water is incorporated into the reduced molybdenum center to generate oxidized oxomolybdo species which in turn transfers oxygen into the reduced substrate. The picture is now clear atleast for xanthine oxidase class of enzymes that oxo transfer reactions proceeded via molybdenum center wherein the ultimate source of oxygen is derived from water. As the source of oxygen is water, these enzymes are generally classified as " hydroxylase " class of enzymes.

For a single substrate enzyme catalyzed reaction the Michaelis-Menten approach is well known. If E, S and ES represent enzyme, substrate and enzyme-substrate complex respectively then the rate of formation of product is given by the equation (16),



$$\text{rate } (v_0) = k_2 [ES] \quad \text{----- (16)}$$

The fundamental assumption of this theory is that k_2 is small so that the second step in the process does not influence the equilibrium formation of the ES complex. Thus for constant enzyme concentration, when the substrate concentration is low, only a fraction of the total number of enzyme molecules will be present in the form of the enzyme-substrate (ES) complex. The concentration of ES increases with the increase of substrate concentration and therefore the rate of the overall reaction rises. At very high substrate concentration the equilibrium will be such that virtually all the enzyme molecules would be present as the ES complex. This means that the enzyme is saturated with substrate and in this situation the increase in substrate concentration will not produce any further increase in reaction rate. Therefore for a given enzyme concentration there is a maximal velocity attainable on increase in the substrate concentration. The plot of the rate of reaction, v_0 against substrate concentration would be a linear hyperbolic curve, very much similar to oxygen saturation curve of myoglobin. At high substrate concentration the rate approach is a maximum value V_{\max} and K_m = the substrate concentration at half maximal rate.

If we define K_s as the equilibrium constant for the dissociation of the ES complex into E and S and $[E']$ is the

concentration of the enzyme initially added, then the concentration of free enzyme E will be equal to ($[E'] - [ES]$).

Hence,

$$K_s = \frac{[E][S]}{[ES]} = \frac{([E'] - [ES])[S]}{[ES]} = \frac{[S][E'] - [ES][S]}{[ES]}$$

$$\text{or } K_s[ES] = [S][E'] - [ES][S] \quad \text{or } [ES](K_s + [S]) = [E'][S]$$

$$\text{or } [ES] = \frac{[E'][S]}{K_s + [S]} \quad \text{----- (17)}$$

now from the equation (16),

$$v_o = \frac{k_2[E'][S]}{K_s + [S]} = \frac{k_2[E']}{1 + \frac{K_s}{[S]}} \quad \text{----- (18)}$$

At enzyme saturation with substrate,

$$V_{\max} = k_2[E'] \quad \text{and hence}$$

$$v_o = \frac{V_{\max}}{1 + \frac{K_s}{[S]}} \quad \text{----- (19)}$$

In practice the assumption is $K_m = K_s$ which , for any enzyme with a given substrate, is a direct measure of the strength of the binding between the enzyme and the substrate.

Therefore,

$$v_0 = \frac{V_{\max}}{K_m + \frac{[S]}{V_{\max}}} \quad \text{--- (20)}$$

This equation may be also written in the form,

$$v_0 = \frac{V_{\max}[S]}{[S] + K_m} \quad \text{--- (21)}$$

This is the Michaelis-Menten equation, the rate equation for a single substrate enzyme-catalyzed reaction.

An important numerical relationship emerges from this equation (21) in the special case when the initial reaction rate is exactly one half the maximum velocity, i.e. $v_0 = 1/2 V_{\max}$. Then

$$\frac{V_{\max}}{2} = \frac{V_{\max}[S]}{K_m + [S]}$$

solving,

$$K_m + [S] = 2[S] \quad \text{or } K_m = [S] \text{ when } v_0 \text{ is exactly } 1/2 V_{\max}.$$

From the hyperbolic saturation curve it is difficult to accurately evaluate V_{\max} and K_m . The equation (20) may be changed to reciprocal form as

$$\frac{1}{v_0} = \frac{K_m + [S]}{V_{\max}[S]} \quad \text{or}$$

$$\frac{1}{v_0} = \frac{K_m}{V_{\max}} \frac{1}{[S]} + \frac{1}{V_{\max}} \quad \text{--- (22)}$$

Thus a plot of $1/v_0$ against $1/[S]$, known as double reciprocal plot or Lineweaver-Burk plot, should be straight line with an intercept on the ordinate $1/v_0$ and slope K_m/V_{max} . The intercept on the abscissa gives $-1/K_m$. This Lineweaver-Burk plot has the great advantage of allowing a more accurate determination of V_{max} , which can only be approximated from a simple plot of v_0 vs $[S]$. The double reciprocal plot of enzyme rate data is very useful in analyzing enzyme inhibition.

Chemical species whose presence causes a decrease in the ability of an enzyme to catalyze its particular reaction is called inhibition. An inhibitor may be reversible or irreversible. Irreversible inhibitor generally binds at the site of the enzyme via covalent bond, does not dissociate away from the enzyme and can not be removed by usual means. A reversible inhibitor is usually bound to the enzyme in such a manner so that an equilibrium situation prevails which is similar to ES type complex formation as described above.

There are two kinds of reversible inhibitors: competitive and noncompetitive. When the inhibitor is structurally close to the substrate the inhibition is often found to be competitive meaning thereby that both substrate and inhibitor bind at the same site of enzyme and they therefore compete for that site. By definition and on the principle of microscopic reversibility the product of any substrate must be competitive inhibitor.

A noncompetitive inhibitor binds reversibly to a site on the enzyme which is not the binding site for the substrate. These inhibitors need not be structurally related to the substrates.

Double reciprocal plots are very useful in determining whether reversible enzyme inhibition is competitive or noncompetitive. Two sets of rate experiments are carried out, the enzyme concentration is held constant in both sets. In one set the substrate concentration is held constant and the effect of increasing the inhibitor concentration on the initial rate v_0 is determined. In the other set the inhibitor concentration is held constant and the substrate concentration is varied. The $1/v_0$ is plotted against $1/[S]$. Competitive inhibitors yield a family of lines with a common intercept on the $1/v_0$ axis but with different slopes. Since the intercept on the $1/v_0$ axis is equal to the $1/V_{max}$, so V_{max} is unchanged by the presence of a competitive inhibitor. In the case of noncompetitive inhibition similar plots give the family of lines where a common intercept is found on the $1/[S]$ axis, indicating that K_m for the substrate is not altered by a noncompetitive inhibitor but V_{max} changes^{50a}.

Various mixed type inhibitions can arise when an inhibitor combines not with the initial enzyme-substrate (ES) complex but with a later intermediate in the reaction^{50b}.

For alternative two substrate reactions as the case with molybdenum enzymes following so called pingpong mechanism the double reciprocal plots are made keeping a fixed concentration of one substrate and varying the concentration of other substrate and vice versa. In both the cases the double reciprocal plots result in a series of parallel lines which is diagnostic of a pingpong mechanism⁵¹. The relationship of kinetic parameters with different types of inhibitors are briefly summarized⁴⁶ in Table 1.5.

Table 1.5 Relationship of kinetic parameters with different types of inhibitions.

Type of inhibition	Slope of the plot	Intercept in the ordinate ($1/v_0$ axis)	Intercept on the $1/[S]$, axis
None	$\frac{K_M}{v_m}$	$1/v_m$	$-1/K_M$
Competitive	$\frac{K_M}{v_m} \left(1 + \frac{[I]_0}{K_I} \right)$	$1/v_m$	$-\frac{1}{K_M} \left(1 - \frac{[I]_0}{K_I} \right)$
Uncompetitive	$\frac{K_M}{v_m}$	$\frac{1}{v_m} \left(1 + \frac{[I]_0}{K'_I} \right)$	$-\frac{1}{K_M} \left(1 + \frac{[I]_0}{K'_I} \right)$
Non-competitive			
(a) $K_I = K'_I$	$\frac{K_M}{v_m} \left(1 + \frac{[I]_0}{K_I} \right)$	$\frac{1}{v_m} \left(1 + \frac{[I]_0}{K_I} \right)$	$-\frac{1}{K_M}$
(b) Mixed	$\frac{K_M}{v_m} \left(1 + \frac{[I]_0}{K_I} \right)$	$\frac{1}{v_m} \left(1 + \frac{[I]_0}{K'_I} \right)$	$-\frac{1}{K_M} \left[\frac{\left(1 + [I]_0 / K'_I \right)}{\left(1 + [I]_0 / K_I \right)} \right]$

TUNGSTEN CONTAINING SIMILAR ENZYMES.

Tungsten being the higher congener of molybdenum generally shows similar chemical reaction to molybdenum. Compare to molybdenum, reaction of tungsten is sluggish in nature. For an example, even for a simple substitution reaction like $[MoO_4]^{2-}$ to $[MS_4]^{2-}$ ($M = Mo, W$), the formation of $[MoS_4]^{2-}$ is sufficiently faster at ambient conditions. For the formation of $[WS_4]^{2-}$ a higher temperature and longer time is essential. When simple σ bonding ligands are attached to tungsten it is generally been observed that reduction is difficult compared to the corresponding molybdenum system⁵². However, for strongly π bonding ligated complexes redox properties are very similar for molybdenum and tungsten systems.

In the early 80's only a single tungsten containing enzyme, tungsten containing formate dehydrogenase, has been identified⁵³. Very recently several other tungstoenzymes like aldehyde ferredoxin oxidoreductase, carboxylic acid reductase etc have been discovered⁵⁴. Some of the tungstoenzymes with their functions are tabulated in the Table 1.6.

Table 1.6 Examples of Some Tungstoenzymes

Enzyme	Source	Function	Reference
Tungsten containing formate dehydrogenase	<i>Clostridium thermoaceticum</i>	CO_2 to HCOO^-	50
Carboxylic acid reductase	<i>Clostridium thermoaceticum</i>	Carboxylic acid to aldehyde	54a
Aldehyde oxidase	<i>Pyrococcus furiosus</i>	Aldehyde to carboxylic acid	54b
Aldehyde ferredoxin oxidoreductase	<i>Pyrococcus furiosus</i>	Aldehyde to carboxylic acid	54c

MODEL STUDIES

Is it possible to synthesize a particular enzyme *in vitro*? For any enzyme of this class high molecular weight of the whole enzyme and sequential assembly of different redox centers present there make it extremely difficult if not impossible to synthesize in the test tube. By definition a model system represents the simplified description of system to assist prediction of structural information of the original one. Unfortunately X-ray three dimensional structural information of any enzyme of this class is lacking. The presence of a dissociable common molybdenum cofactor in these enzymes thus may permit to model this cofactor. The relevant spectral and other physiochemical properties of this cofactor reflect its importance of existence in the enzyme. Thus for designing a model for this cofactor two important factors are to be kept in mind. Firstly the synthesized complexes should have very similar donor atom ligation around molybdenum to the cofactor which would be reflected by the resemblance of spectral and other physiochemical properties of the model compound to those of the cofactor. Three dimensional structural information of these model compounds may then be used to predict the geometry around molybdenum in the cofactor for which similar structural information is not yet known. This part of the model may be called as "structural analogue"⁵⁵ to molybdenum cofactor or in a sense to molybdoenzyme in relevance to the role played by molybdenum in this.

Secondly an even more important criterion for the model

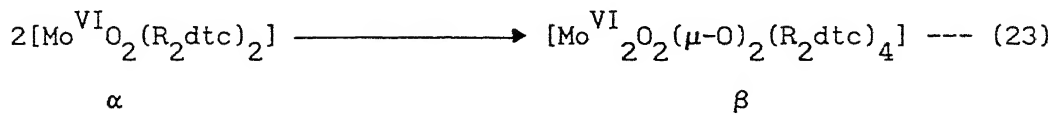
compound lies in its ability to function similarly in relation to the native enzyme. This "functional" model⁵⁵ may not demonstrate exactly identical activity of the molybdenum center present in the enzyme. This is simply because of the fact that the activity of these enzymes generally follow pingpong kinetic mechanism of hybrid nature where it has already been discussed that for the regeneration of the enzyme in one catalytic cycle the second half of the redox reaction originates via another redox center. As direct electron (oxo) transfer in catalytic cycle is only half way via molybdenum and the other complementary half via another redox center attached to molybdenum, a full catalytic cycle resembling enzymatic reaction is not viable with a simple molybdenum model compound. It is to be noted that functional analogue or enzymatic reactions are essentially solution chemistry. The paramount role of water as an essential chemical reactant in enzymatic function is to be borne in mind because a functional analogue reaction in nonaqueous media definitely will be far away from functional mimicry of the real enzyme.

Based on the above stated limitations and essential qualifications of a model compound several contributions have been made. It is to be kept in mind that during the development of this aspect all the biochemical informations related to these enzymes were not available. The improvement of the synthetic strategies to achieve the goal has been all the time helped by newer findings from biochemical studies. Keeping this view point in mind contributions from the synthetic chemists in this regard is briefly outlined below.

COMPLEXES CONTAINING MoO_2 (VI) MOIETY.

Simple oxohalo complexes of the type MoO_2X_2 (X = halide anion) have long been known. Derivatives like $\text{MoO}_2\text{Cl}_2\text{L}_2$ (L = CH_3COCH_3 , DMF, DMSO, Ph_3PO , Ph_3AsO , PyO)⁵⁶ have been prepared by direct reaction of MoO_2Cl_2 and L. These complexes are good starting materials for the chelated species like $\text{MoO}_2(\text{acac})_2$, $\text{MoO}_2(\text{oxine})_2$ ^{56a}. The complex anion like $[\text{MoO}_2\text{Cl}_4]^{2-}$ is generally present in aqueous HCl acid solution of molybdate(VI)⁵⁷. $\text{MoO}_2(\beta\text{-diketonate})_2$ complexes are alternatively prepared by acidification of aqueous MoO_4^{2-} - $\beta\text{-diketone}$ solution⁵⁸. Among these $\text{MoO}_2(\text{acac})_2$ has been found to be the most effective starting material for the syntheses of other dioxoMo(VI) derivatives. Complexes of the type $\text{MoO}_2(\text{R}_2\text{dtc})_2$ ($\text{R} = \text{CH}_3, \text{C}_2\text{H}_5$) were prepared by Malatesta⁵⁹ by reacting aqueous MoO_4^{2-} solution with the appropriate ligand followed by acidification. Improved synthetic routes have been devised for these complexes⁶⁰.

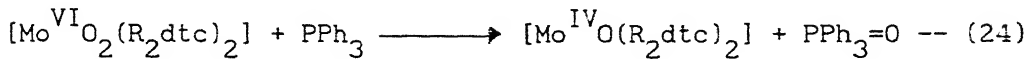
The dioxomolybdenum complexes briefly mentioned above display some important chemical reactions. Thus the isolation of two forms of $\text{MoO}_2(\text{R}_2\text{dtc})_2$ complexes from two different synthetic routes displaying different properties finally led to the suggestion that the β form is dimer^{60d} of the α form as shown below.



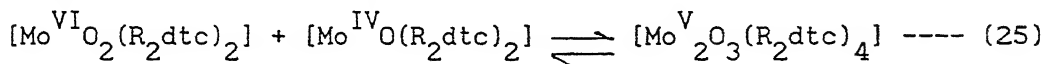
The dimerization revealed an interesting aspect of oxomolybdenum

chemistry with regard to its readiness to interconvert between monomer-dimer equilibrium. Furthermore the ability of terminal oxomolybdenum entity to function as a nucleophile is realized

The reactions of monomeric $\text{MoO}_2(\text{R}_2\text{dtc})_2$ with phosphines^{60c,61} lead to oxotransfer reaction according to equation (24).



Here again the course of the reaction follows in a way similar to $\alpha-\beta$ conversion (reaction 23). Thus when 0.5 mol of PPh_3 is used per mol of $\text{MoO}_2(\text{R}_2\text{dtc})_2$ half of its is reduced to $\text{MoO}(\text{R}_2\text{dtc})_2$. The mixture of equimolar quantity of the oxidized and reduced forms leads to the following equilibrium.



The forward reaction of (25) is similar to what is known for β form formation of $\text{MoO}_2(\text{R}_2\text{dtc})_2$. This reaction can be rationalized in the following way. One of the terminal oxomolybdenum group in $\text{MoO}_2(\text{R}_2\text{dtc})_2$ functioning as a nucleophile attacks coordinatively unsaturated molybdenum center in $\text{MoO}(\text{R}_2\text{dtc})_2$. This process is followed through an electron transfer from Mo(IV) to Mo(VI) through oxygen thereby leading to the formation of $\{\text{Mo}^{\text{V}}_2\text{O}_3\}$ moiety. The reversible nature of the reaction (25) suggests the subtle energetics to push the equilibrium in the forward or backward direction.

The important reactions of dioxomolybdenum complexes lead to correlate electron or oxotransfer capability of synthesized complexes in relevance to oxomolybdoenzymes. The surge in the

syntheses of complexes containing MoO_2 (VI) core stem from unusual reactivity of this core. The diverse interests related to structural varieties, donor atom dependence, electrochemical behavior and correlation of these in relevance to oxo transfer capability have been undertaken. This resulted in the designing of multidonor sites containing ligand to hold the MoO_2 (VI) moiety. As in electron (atom) transfer reaction in oxomolybdoenzymes there is no intervening formation of Mo_2O_3 type dimeric core. Special designing of the ligands have been made to create steric crowding of the multidonor ligand in such a way to mimic partly the role of protein part (apoenzyme) of the oxomolybdoenzymes to prevent this undesirable event of dimerization.

In synthesizing or choosing already available ligands it has been in general kept in mind to have minimum 2-3 thiolate type of sulfur ligation in the oxidized MoO_2 (VI) species. The identity of other donor in the real enzyme is unknown but it could be nitrogen, oxygen or thioether sulfur type. This led to work with ligands having combinations of S/N/O donor atoms. The complexes $[\text{MoO}_2((R)-\text{cysOMe})_2]$ and $[\text{MoO}_2((S)-\text{PenOMe})_2]$ (Cys = cysteine, Pen = Penisilimine) are readily synthesized by reacting MoO_4^{2-} with the hydrochloride of the corresponding ligand in water⁶². The success in getting oxygen atom transfer reaction with $\text{MoO}_2(\text{R}_2\text{dtc})_2$ by phosphine prompted to explore the reaction between $[\text{MoO}_2((R)-\text{cysOMe})_2]$ and aldehyde to model the reaction of aldehyde oxidase. Some apparent contradictions are present to interpret these results when product analysis was not reported⁶³. A series of complexes of the type $\text{MoO}_2(L-L)_2$ ($L-L$ = tox, 8-mercaptopquinoline; mee, N,N' -

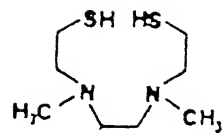
dimethyl-N,N'-bis(2-mercaptoproethyl)ethylenediamine; mpe, N,N'-bis(2-mercaptoproethyl)ethylenediamine; sap, salicylaldehyde o-hydroxyanil) have been prepared⁶⁴. Some of these complexes have been studied for the reaction like dehydrogenation of hydrazobenzene to azobenzene⁶⁵. A dioxo derivative, $\text{MoO}_2[\text{CH}_3\text{NHCH}_2\text{C}(\text{CH}_3)_2\text{S}]_2$, with interesting structure has been reported⁶⁶. Amongst anionic complexes of MoO_2 (VI) core, $[\text{Et}_4\text{N}]_2[\text{MoO}_2(\text{bdt})_2]^{2-}$ = benzene dithioclate)⁶⁷ and $[\text{NH}_4]_2[\text{MoO}_2\{\text{O}_2\text{CC(S)Ph}_2\}_2]^{68}$ are known. Very recently Holm and coworkers have reported the analogue reaction system of the molybdenum oxotransferases using $\text{Mo}^{\text{VII}}\text{O}_2$ and $\text{Mo}^{\text{IV}}\text{O}$ cores with the bidentate ligand bis(4-tert-butylphenyl)-2-pyridylmethanethiolate(1-)(tBuL-NS)⁶⁹.

Amongst tridentate schiff's base ligands with O, N, S donor atoms the 5-H-sspH₂ ligand has been shown to coordinate to MoO_2 (VI) core as dianionic tridentate ligand with a solvent molecule like DMF present in the molecule⁷⁰ (5-H-ssp)²⁻ = 2-(salicylideneamino)benzenethiolato(2-)). Complex of the type $[\text{MoO}_2(\text{ssp})]$ has also been made⁷¹. Several derivatives of tridentate schiff's bases like ssp, sap and sae have been made with MoO_2 (VI) moiety (sae = 2-(salicylideneamino)ethanolate (2-))⁷². A mixed ligand complex, $[\text{MoO}_2(\text{pdmt})(\text{tmso})]$ is also known⁷³. For this complex, the use of the ligand, pyridine-2,6-dimethane thiolate (pdmt) favors the facial coordination. Oxo transfer reaction has been demonstrated using the MoO_2 (VI) complexes with the schiff's base ligands, S-benzyl 3-(5-R-2-hydroxyphenyl)methylene dithiocarbazate and S-methyl 3-(2-hydroxyphenyl)methylene dithiocarbazate⁷⁴.

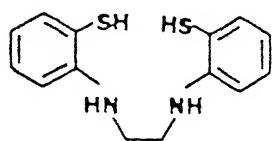
The ligand, hydrotris(3,5-dimethylpyrazolyl)borate ($\text{HB}(\text{3},\text{5}-\text{Me}_2\text{pz})_3$) forms complexes of the type $[\text{MoO}_2\text{X}(\text{HB}(\text{3},\text{5}-\text{Me}_2\text{pz})_3)]$, which also possesses a frame work to impose facial coordination⁷⁵. The interesting aspect of this complex, though void of sulfur ligation, is the presence of an exchangeable monodentate anionic ligand (X). This aspect has been exploited to synthesize a series of complexes varying X (X = F⁻, Cl⁻, Br⁻, NCS⁻, OPh⁻, OMe⁻, SPh⁻)⁷⁶. To introduce sulfur coordination, monodentate dithiophosphate ligand has been used to synthesize the complex $[\text{HB}(\text{Me}_2\text{pz})_3][\text{MoO}_2(\text{S}_2\text{P}(\text{OEt})_2)]^{77}$.

The most successful synthesis with regard to synthetic as well as functional analogue of molybdenum site in oxomolybdo-enzymes has been developed by Holm and Berg⁷⁸. The complex, $\text{MoO}_2(\text{LNS}_2)$ (LNS_2 = 2,6-bis(2,2-diphenyl-2-sulfidoethyl)pyridine-(2-)), and the oxo version with respect to the ligand, $\text{MoO}_2(\text{LNO}_2)-(\text{Me}_2\text{SO})$ have been synthesized. A dioxo molybdenum(VI) complex with the ligand, *threo*- α,α -di-*tert*-butyl-2,6-pyridinedimethanol, has also been reported⁷⁹.

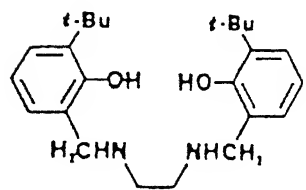
Several complexes with tetradentate pseudomacrocyclic ligands have been designed to complex with $\{\text{MoO}_2\}^{2+}$ moiety. The protonated forms of these ligands are presented⁸⁰ in the Fig. 1.7.

*N,N'*-dimethyl-*N,N*-bis-2'-mercaptoproethyl-1,2-diaminoethane

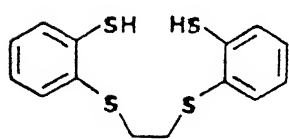
Ref. 80

*N,N'*-bis-2'-mercaptophenyl-1,2-diaminoethane

Ref. 80t

*N,N'*-bis-(3'-1",1"-dimethylethyl-2'-hydroxyphenylmethyl)-1,2-diaminoethane

Ref. 80c

*S,S'*-bis-2'-mercaptophenyl-1,2-dimercaptoethane

Ref. 80d

Fig. 1.7 The protonated forms of tetradeятate pseudomacrocyclic ligands.

COMPLEXES CONTAINING $\{CIS\text{-MoO(OH)}\}^{2+}$ MOIETY

Syntheses of complexes containing above core has not yet been reported. A long known TPP complex with $\{\text{trans-MoC}_5\text{OH}\}^{2+}$ moiety is reported⁸¹ (TPP = dianion of *meso*-tetraphenyl porphyrin). It is even more difficult to stabilize similar core using SH^- instead of OH^- in relevance to xanthine oxidase and aldehyde oxidase. The presence of these moieties have been accounted for during the catalytic cycle as transient species in native enzymes. Even from the knowledge of enzymatic systems the instability of these cores suggests that the efficiency of the system to flip from MoO_2 (VI) (or MoOS(VI)) to MoO(IV) required for the regeneration stage of the relevant ("reductase" or "oxidase" type) enzyme is mostly done by one electron donor or acceptor. This accounts for two successive one electron transfer processes which must proceed via pentavalent molybdenum in either way. This oxidation state is thus not relevant for actual substrate's reduction or oxidation except xanthine oxidase class of enzymes where internal redistribution of electron density occurs which has already been discussed. For most of the other enzymes of this class this oxidation state is passage for achieving the next oxidation state in both ways. For the regeneration stage which should be faster and thus a transient Mo(V) species is seen by ESR^{7,8}. It is important to note that from $\{\text{MoO}\}^{2+}$ core in real enzymatic reaction, $\{\text{MoO}_2\}^{2+}$ core is achieved by aquation with successive deprotonation. Thus in some elegant experiments demonstrations have been made by electrochemically generated MoO(V) species either from MoO_2 (VI) or MoO(IV) species wherein ${}^1\text{H}$ superhyperfine coupled ESR spectra were observed^{21,82}.

MoO(IV) complexes are relatively rare in comparison to dioxo Mo(VI) complexes. Considering the model aspect, only few such complexes have been synthesized. The best studied compound of this class is $MoO(R_2dtc)_2$ which was synthesized by reacting Na_2MoC_4 and R_2dtc^- in the presence of excess of sodium dithionite in aqueous medium⁸³. The same complex can also be synthesized by reacting $MoO_2(R_2dtc)_2$ with $PhSH$ ⁸⁴. However, the formation of $MoO(R_2dtc)_2$ by reacting $MoC_2(R_2dtc)_2$ with PPh_3 has been exploited very much⁸⁵. The synthesis of $[MoO(mnt)]^{2-}$ has long been reported⁸⁶. Report of the same compound as a byproduct in other reactions has also been made⁸⁷. Though this complex is very much alike to $MoO(R_2dtc)_2$ with regard to donor atom and specially containing direct dithiolen linkage in relevance to molybdenum cofactor, yet no attempt has been made to test its reactivity. For the synthesis of tetravalent oxomolybdenum complex oxo abstracting phosphines are largely employed, thus from $MoO_2(LNS_2)$, $MoO(LNS_2)(DMF)$ has been synthesized by PPh_3 in DMF medium⁷⁸. Similarly $[MoO_2(dttd)]$ which is reactive with more basic phosphine, PPh_2Et , produced $[MoO(PPh_2Et)(dttd)]^{80d}$. However, this reaction requires special precautions with respect to the time of reaction as the shorter times give the mixture of monooxo complex and $Mo_2O_3(dttd)$ dimer and longer times yield uncharacterized nonoxo species^{80d}. The recently reported complex, $MoO_2(tBuL-NS)_2$, reacts with one of the strongest basic phosphines, Et_3P , to form corresponding tetravalent monooxo complex, $MoO(tBuL-NS)_2^{69}$. The complex,

$[\text{Et}_4\text{N}]_2[\text{MoO}(\text{S}_2\text{C}_2(\text{CCPh})_2)_2]$, has been synthesized⁸⁸. The similar complex, $[\text{Et}_4\text{N}]_2[\text{MoO}(\text{S}_2\text{C}_2(\text{COCMe})_2)_2]$, has also been reported⁸⁹. In the syntheses of above two compounds the dithiolene type of ligands have been incorporated by the reaction of coordinated S_4^{2-} ligand with respective activated acetylenes. One more oxo-molybdenum(IV) dithiolene complex, $[\text{Et}_4\text{N}]_2[\text{MoO}(\text{bdt})_2]$ has been reported⁹⁰ which was prepared by the reaction of $\text{K}_4[\text{MoO}_2(\text{CN})_4] \cdot 6\text{H}_2\text{O}$ with H_2bdt (1:2) in $\text{H}_2\text{O}-\text{EtOH}$ followed by the addition of $[\text{Et}_4\text{N}]\text{Br}$.

RELATED TUNGSTEN COMPLEXES.

Tungsten complexes analogous to molybdenum compounds are less known. It is generally observed that though tungsten shows chemistry similar to that of molybdenum, yet its reactivity is many fold less compared to that of molybdenum because of thermodynamic as well as kinetic reasons. Nevertheless it is important to synthesize relevant tungsten complexes analogous to molybdenum series because the sluggish nature of reactivity of tungsten compounds may sometimes help to understand the course of reaction of analogous molybdenum complexes which may occur in much faster rates. Besides, several tungsten containing enzymes are recently discovered and so studies on tungsten system would be equally important on this ground. Only few dioxo tungsten(VI) complexes are known. The complexes $\text{WO}_2(\text{R}_2\text{dtc})_2$ have been synthesized by intermetallic electron (atom) transfer reaction⁹¹.

Compelexes of the type $\text{WO}_2(\text{sap})$, $\text{WO}_2(\text{ssp})$ have been reported by Holm and Yu⁹². Very recently Nakamura and coworkers have synthesized dioxo tungsten(VI) complex, $[\text{PPh}_4]_2[\text{WO}_2(\text{bdt})_2]$, by the reaction of corresponding W(IV) complex and trimethylamine N-oxide in DMF⁹³.

WO(IV) core containig complex, $[\text{WO}(\text{bdt})_2]^{2-}$, has been isolated by a simple borohydride reduction of $[\text{WO}(\text{bdt})_2]^{1-}$ which has been prepared by the ligand exchange reaction between $[\text{WO}(\text{SPh}_4)]^-$ and H_2bdt ⁹³. The same WO(IV) complex may be prepared by exploiting the oxo transfer reaction of $[\text{WO}_2(\text{bat})_2]^{2-}$ with benzoin⁹³. A brief mention about the formation of $\text{WO}(\text{R}_2\text{dtc})_2$ from $[\text{WO}(\text{S}_2)(\text{R}_2\text{dtc})_2]$ and CN^- has also been made⁹⁴.

PHYSICOCHEMICAL PROPERTIES.

Vibrational and electronic spectral studies of oxomolybdenum and related oxotungsten complexes are well documented in the literature⁹⁵. One of the most important observations related to dioxomolybdenum(VI) moiety is the *cis* disposition of the two oxo groups. This accounts for the maximum formal bond order of an Mo-O_t (*t* = terminal) bond as three. This is comprised of one σ component along the Z axis and two orthogonal π components formed by the overlap of two terminal oxygen's $p\pi$ orbitals (P_x and P_y) with the appropriate metal $d\pi$ orbitals (d_{xz} and d_{yz}). *Cis* arrangement of the MoO_2 (VI) core thus permits the two terminal oxo groups to utilize all the three metal $d\pi$ orbitals. A *trans* dioxo

arrangement does not allow to utilize all the three metal $d\pi$ orbitals for bonding. Hence for d^0 system containing MoC_2 (VI) moiety *cis* dioxo disposition is expected. For local C_2 symmetry of MoO_2 (VI) moiety both Mo-O stretching vibrations are infrared active. Thus the presence of a dioxomolybdenum(VI) group, without fail, can be observed in the infrared spectrum.

The σ and π bonding in the $\text{Mo}-\text{O}_t$ moiety would give rise to the corresponding antibonding component with expected energy order $\pi^* < \sigma^*$. For the reduction of dioxomolybdenum(VI) to monooxo-molybdenum(IV), the addition of electrons would be in the π^* orbitals resulting in the weakening of $\text{Mo}-\text{O}_t$ (bonds). The accommodation of a pair of electrons in d_{xy} orbital of $\text{MoO}(\text{IV})$ moiety places it as a nonbonding orbital at a significant lower energy. Qualitatively it can be stated that in the complexes containing $\text{MoO}(\text{IV})$ moiety with $(d_{xy})^2$ configuration, besides a σ bond along Z axis, overlap between vacant metal d_{xz} and filled oxygen $2P_x$ orbitals contributes a π bond. Furthermore overlap between vacant metal d_{yz} and filled oxygen $2P_y$ orbitals will give another π contribution. This makes once more a formal bond order of three in $\text{Mo}-\text{O}_t$ in tetravalent oxo molybdenum complexes. Thus for *cis* MoO_2 (VI) core the bond order in each $\text{Mo}-\text{O}_t$ is 2.5 and for reduced $\text{MoO}(\text{IV})$ core this bond order is increased. Infrared spectra clearly identify these differences in bond order and between identical pair like $[\text{Mo}^{\text{VI}}\text{O}_2(\text{L-L})_2]$ ($\text{L-L} =$ mononegative bidentate ligand) and $[\text{Mo}^{\text{IV}}\text{O}(\text{L-L})_2]$, the $\nu_{\text{Mo}-\text{O}}$ stretching band for the tetravalent compound generally appears at higher wave number compared to $\nu_{\text{Mo}-\text{O}}$ stretching vibrations of the oxidized species.

This trend is shown^{58b, 60a, 69, 96} in the Table 1.7. This bond order formalism has nicely been verified by X-ray structural data of Mo-O bond lengths and are also included in the Table 1.7.

Electronic spectral data for dioxo molybdenum(VI) species are comprised of only charge transfer transitions. The general trends are, when the donor atom is changed from oxygen to sulfur, transitions are shifted to lower energy. Thus the sulfur ligated dioxomolybdenum complexes are generally yellow-orange in color. For the tetravalent monooxo complexes comprised of $(d_{xy})^2$ electronic configuration, d-d transitions along with charge transfer transitions are expected. However, most of the complexes have transitions of charge transfer origin even in the visible range thus obscuring the d-d transitions^{7,8}.

Resonance Raman (RR) study is a powerful tool to identify low energy symmetric metal-ligand vibrations. Interestingly DMSO reductase has been shown to possess dithiolene ligatation by this study⁹⁷. Similar studies have been made for complexes like $[\text{MoO}_2(\text{dttd})]$, $[\text{Et}_4\text{N}]_2[\text{MoO}(\text{S}_2\text{C}_2(\text{COOMe})_2)_2]$ ⁹⁸. For native sulfite oxidase, a preliminary RR report has appeared for the identification of cis dioxo grouping⁹⁹.

Electrochemically or chemically generated ESR active pentavalent molybdenum species from either isolated dioxo-molybdenum(VI) or from monooxomolybdenum(IV) complex have been made^{21,82}. Interests were shown to evaluate hyperfine and superhyperfine interactions in relevance to the data obtained from native enzymes¹¹.

Table 1.7 IP and Bond Distance Data of $\{c\text{-}s\text{-Mo}^{\text{VI}}\text{C}_2\}$ and $\{\text{Mo}^{\text{IV}}\text{O}\}$ Moieties in Dioxo and Corresponding Monooxo Complexes

Complex	IR (cm^{-1})	Bond Distance (\AA°)
	$\nu(\text{Mo=O})$	M-O
$\text{MoO}_2(\text{Pr}^n\text{2}^{\text{dtc}})_2$	909, 875 ^a	1.695(5) ^b
$\text{MoO}(\text{Pr}^n\text{2}^{\text{dtc}})_2$	975 ^c	1.665 ^c
$\text{MoO}_2(\text{tBuL-NS})_2$	936, 901 ^d	1.696(4) ^d
$\text{MoO}(\text{tBuL-NS})_2$	943 ^d	1.681 ^d

Pr^n = normal propyl; tBuL-NS = bis(4-*tert*-butylphenyl)-2-pyridyl-methanethiolate(1-); ^aRef. 60a, ^bRef. 58b, ^cRef. 96, ^dRef. 69.

NMR studies are seldomly done for characterization of these complexes. However, the important contributions by Rajagopalan and his group to advance the proposed structure of molybdenum cofactor, a judious synthetic strategy, were associated with NMR and FAB mass spectroscopy^{26d}.

Electrochemical investigations are important in relevance to thermodynamic stability of model complexes. As expected one electron reduction of MoO₂(VI) core did not show reversible couple in aprotic media wherein the more basic MoO₂(V) core is immediately protonated⁷⁸. Another important feature is the oxidation of MoO(IV) core to MoO(V) core. Here if the supporting electrolytes contain Cl⁻ anion which invariably coordinates to molybdenum, a new redox couple appears^{78,80d}. The third important aspect is that further electrochemical oxidation of generated pentavalent species to change into MoO₂(VI) core even in the protic solvent has not been achieved⁸.

Most of the synthesized complexes have been subjected to three dimensional X-ray structure analysis^{7,8,69,78,80}. Though varieties of structural types are known yet the understanding of the molybdenum site in the enzyme is far away because the structure of the enzyme is not known. Deliberate imposition of facial tridentate and tetradentate ligands with effective substituents to restrict dimerization have been made by atleast two different types of ligands^{76,78,80}. Once more it is to be kept in mind that the dimerization process is a thermodynamical one where comproportionation type of reaction takes place. Proper energetics can dictate the favorable disproportionation reaction

wherein haxavalent and tetravalent centers may stay together

The physicochemical studies done for the synthesized complexes generally on the line of the principles of chemistry related to molybdenum and tungsten. Further discussion on this aspect will be done in the succeeding chapters.

CHAPTER 2

SCOPE OF THE INVESTIGATION

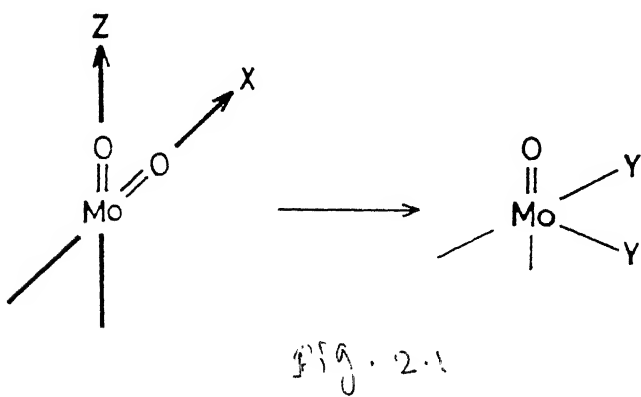
If one takes into account the proposed structure of the molybdenum cofactor the following salient features are worthnoting: (i) the ligational atoms around molybdenum are two terminal oxo groups and a dithiolene type of coordination, (ii) this dithiolene is attached to a pterin moiety; (iii) at the other end of the carbon of dithiolene a phosphate ester is linked; (iv) the overall charge of the molybdenum cofactor is dinegative [Fig. 2].

From the known chemistry of MoO_2 (VI) core a tetracoordinated arrangement around molybdenum is unlikely except for $[\text{MoO}_2\text{S}_2]^{2-}$ where the structure is stabilized by resonance and the cause of ready expansion of its coordination number without affecting the oxidation state of molybdenum is unknown¹⁰⁰.

The minimum coordination number around molybdenum in molybdenum cofactor is four (Fig. 2). Then the attachment of apo-protein as well as the presence of apparently a reserved site for substrate binding demand that the minimal coordination around molybdenum center should be six in these enzymes. Now the cofactor is readily dissociable from the whole enzyme suggesting that the apoenzyme independently binds to molybdenum center without the association of dithiolene moiety. This would lead to the suggestion that only dithiolene is the bidentate chelating ligand attached to molybdenum center and apoenzyme is in principle then

be a monodentate ligand. In the absence of bonded substrate the coordination number around molybdenum would be five. From the known model chemistry of dioxomolybdenum(VI) complexes pentacoordination is known⁷⁸. However this trigonal bipyramidal geometry is specially attained by the use of a tridentate robust ligand. In another type of tridentate ligand the stabilization is achieved by six coordination with the presence of a labile monodentate ligand⁷⁶. The separable entity of dithiolene coordination in molybdenum cofactor clearly suggests the absence of any strong tridentate or tetradeятate ligation. If it is assumed that the apoprotein can function as a tridentate ligand then the coordination number around molybdenum would approach to eight. In molybdenum complexes of lower oxidation states octacoordination is known but not associated with terminal oxo group. Thus with $\text{MoO}_2(\text{VI})$ core, hepta- or octacoordination is highly unlikely. On this ground the most readily accessible dioxomolybdenum(VI) moiety containing complexes are hexacoordinated type with bidentate coordination. For minimal stability of molybdenum center in the resting enzyme a bidentate chelation from the apoenzyme may not be a wild guess. This is because of the fact that synthesized complexes of the type $\text{MoO}_2(\text{R}_2\text{dtc})_2$ readily reacts with catechol type of ligands (cat) to expand its coordination number seven to form $[\text{MoO}(\text{R}_2\text{dtc})_2(\text{cat})]^{101}$. Furthermore $\text{MoO}(\text{R}_2\text{dtc})_2$ responds to oxidative addition with elemental sulfur¹⁰² or with activated acetylenes¹⁰³. For the hexacoordinated $\text{MoO}_2(\text{VI})$ complex the π bonding of MoO_2 unit suggests that each terminal oxo uses one $d\pi$ orbital (d_{xz} and d_{yz}) of molybdenum sharing the third $d\pi$ orbital

$(d_{xy})^{103}$. The availability of d_{xy} orbital to form π bond with one of the terminal oxygen in dioxomolybdenum(VI) moiety and accomodation of $(d_{xy})^2$ electrons in pentacoordinated molybdenum(IV) species followed by disposing of d_{xy} orbital in the complex like $[\text{Mo}^{\text{VI}}\text{O}(\text{R}_2\text{dtc})_2(\text{activated acetylene})_2]^{103}$ clearly indicate that the conversion of hexacoordinated $\text{MoO}_2(\text{R}_2\text{dtc})_2$ to $[\text{MoO}(\text{R}_2\text{dtc})_2(\text{cat})]$ is attained by disposing of the second terminal oxygen π bond which is energetically stabilized by the formation of another σ bond in the heptacoordinated Mo(VI) complex. In a formal book keeping sense it can be stated that in dioxomolybdenum(VI) compound a σ bond followed by a π bond across the terminal Mo=O bond can favorably be replaced by two σ bonds as shown in the Fig. 2.1.



where the position of two σ bonded ligands would remain *cis* to another terminal Mo=O bond of the Z axis. Based on the above qualitative arguments a model complex of MoO_2 (VI) moiety with

dithiolene ligation should be attempted wherein besides the bidentate dithiolene another bidentate ligand may be incorporated to represent the apoprotein's mode of binding

As the cofactor contains a phosphate ester group with dinegative charge which has recently been shown to be fairly soluble in water¹⁰⁴, attempts can be made to synthesize dianionic complexes of MoO₂(VI) core with dithiolene ligation. Direct use of MoO₄²⁻ in aqueous medium using water soluble dithiolene ligand under suitable buffer conditions may thus be interesting. If such type of complexes are designed then these should respond to facile oxo transfer reaction with the formation of corresponding MoO(IV) species. This type of reaction can be achieved by largely used oxophilic phosphines in non aqueous medium. As the complex should be anionic in nature it would be possible to solubilize it if not in pure water (because of bulky counter cation) but in aqueous-organic solvent mixture to try to react with anionic physiological substrate like sulfite (or bisulfite). For the reduced MoO(IV) species it would be equally important to test its reactivity with different electron acceptors in aqueous-organic solvent media in the light of oxo incorporation into it from water. This would, if achieved, be a perfect functional model of sulfite oxidase.

The monooxo species, MoO(IV), can further be tested by biologically important oxo donor agents like NO₃⁻, trimethylamine N-oxide or DMSO to verify its response as a model for "reductase" class of enzymes. It is important to note that recently conversions of [M^{IV}O(bdt)₂]²⁻ to [M^{VI}O₂(bdt)₂]²⁻ (M = Mo, W) have

been achieved using oxo transfer capability of trimethylamine N-oxide in DMF medium^{67,93}.

From the chemistry point of view it will be of interest to try to the syntheses of tungsten analogues of the molybdenum complexes. The recent reports of several tungstoenzymes^{53,54} like formate dehydrogenase, carboxylic acid reductase (aldehyde oxidase) and aldehyde oxidoreductase have opened the possibility to synthesize tungsten complexes. The involvement of tungsten redox couple in formate dehydrogenase is not well known. However, its response towards reconstitution assay with *neurospora crassa nit-1 mutant* strongly suggests that a very similar ligational environment to molybdenum enzyme is present in this enzyme^{53c}. Furthermore EXAFS analysis of aldehyde ferredoxin oxidoreductase (tungsten containing enzyme) from *Pyrococcus furiosus* shows that minimal coordination around tungsten is very much similar to that around molybdenum in sulfite oxidase^{54e}.

Once the complexes are synthesized, established characterization procedures should be followed to understand the chemistry of these compounds in the light of existing theories as well as with the comparative chemistry of already established complexes of similar nature. Once the characterization part is achieved, the reactivity of these complexes could be tested with different reagents for possible oxo and electron transfer reactions. Electrochemical studies would be of much help to understand these reactions. Finally in the case of positive reaction, kinetics may be done in the light of native enzymatic reactions. If such reaction kinetics can be achieved it would be

of paramount interest to check inhibitory effects of certain common anions in the light of similar studies based on real enzymatic reactions. The outcome of all these results may comprehensively be viewed to understand thermodynamic as well as kinetic controlled reactions in this class of enzymes.

CHAPTER 3

SYNTHESIS & CHARACTERIZATION

3.1 EXPERIMENTAL SECTION.

3.1.1 Materials. $[Bu_4N]Br$, $[Bu_4P]Br$, $[Et_4N]Br$, PPh_3 , $[Ph_3PNPPh_3]Cl$, trimethylamine N-oxide and dimethyl acetylenedicarboxylate were obtained from Aldrich; $NaHSO_3$, Na_2SO_4 and citric acid from Merck; KH_2PO_4 from Glaxo; NaCN from May and Baker Ltd; $Na_2MoO_4 \cdot 2H_2O$ from John Backer Inc; Na_2WO_4 from BDH (India) Private Ltd.; Molybdic acid and sodium dithionite from Thomas Baker and Co.; iodine, catechol and elemental sulfur from s.d. fine-cHEM Ltd.; thiophenol from Sisco Research Laboratories Pvt. Ltd.; sodium diethyl dithiocarbamate from BDH Chemicals Ltd. Poole England. The chemicals were used as purchased. All solvents were reagent grade, purified and dried by standard methods. Double distilled water was used to make buffer solutions. Anaerobic syntheses, when necessary, were carried out in argon atmosphere.

3.1.2 Physical Measurements. Elemental analyses for CHN were determined with a EA 1108-Elemental Analyzer. Sulfur was estimated gravimetrically as $BaSO_4$ (*vide infra*). Infrared spectra were recorded as CsI and KBr pellets on Perkin Elmer 577, 1320 and FT 1600 Series IR spectrophotometers. UV-Visible electronic spectra were measured in different solvents on a Shimadzu 160 UV-Visible

spectrophotometer. Negative ion FAB (FAB⁻) mass spectra were recorded on a Jeol SX 102/DA-6000 Mass Spectrometer/Data system using argon (6 KV, 10 mA) as the FAB gas. The accelerating voltage was 10 kV and spectra were recorded at room temperature using m-nitrobenzyl alcohol (3-NBA) as the matrix. ¹³C NMR (100 MHz) spectra were obtained on a Bruker WM-400 FT NMR spectrometer using DMSO-d₆. ¹H NMR (80 MHz) spectra were recorded with a Bruker WM-80 FT NMR spectrometer. Tetramethylsilane was used as an internal standard for NMR studies. Conductances were determined at room temperature on MeCN solutions with an Elicotype CM-82T conductivity bridge (Hydrabad, India) with solute concentrations of ca 10⁻³M. ESR spectra were obtained with a Varian E-109 spectrometer. Sample solutions were prepared under argon, transferred to ESR tubes with gas-tight syrings, and frozen immediately into liquid nitrogen. Room temperature spectra were obtained with a flat cell. ESR parameters were obtained from the measured spectra by inspection, using DPPH as standard.

Cyclic voltammetric measurements were made with CV 27 BAS Bioanalytical Systems and PAR Model 370-4 Electrochemistry System. Cyclic voltammograms of 10⁻³ M solutions of the compounds were recorded either at a glassy carbon or platinum working electrode in MeCN / 0.1 M [Et₄N]ClO₄ or in CH₂Cl₂ / 0.1 M [Bu₄N]ClO₄. The experiments employed a Ag/AgCl or SCE reference electrode and platinum auxiliary elecrode. Controlled-potential electrolysis experiments were performed with a PAR Model 370-4 Electrochemistry System using a platinum-wire-gauze working electrode. Solid state magnetic moment was measured on Cahn Faraday Balance using

$\text{Hg}[\text{Co}(\text{NCS})_4]$ as calibrant and diamagnetic corrections were made using Pascal's constants. X-ray powder diffraction patterns were measured using a Reich Seifert Isodebyeflex 2002 X-ray Diffractometer.

3.1.3 Syntheses.

1. Procedure for the gravimetric estimation of sulfur.

About 0.3 g of the sulfur containing complex was oxidized with an excess of alkaline bromine water. The excess bromine was evaporated off by warming the solution slowly on a water bath. To the resulting solution hydrochloric acid was added slowly and the liberated bromine was again evaporated off by boiling the solution. The solution was then filtered and the sulfate in the filtrate was estimated gravimetrically as BaSO_4 by standard method¹⁰⁵.

2. Preparation of the ligand, 1,2-dicyanoethylenedithiolate, disodium salt or maleonitriledithiolate, disodium salt (Na_2mnt):

The ligand, Na_2mnt , was prepared by the procedure⁸⁷ published by Stiefel *et al.* Sodium cyanide (15 g) was suspended in 50 ml of DMF, 20 ml of CS_2 was added dropwise to the suspension with vigorous stirring and constant cooling. The cooling was removed and the stirring was continued for 1 h. The resulting dark brown mass was dissolved in 200 ml of CHCl_3 and filtered. The CHCl_3 solution was then refluxed for 24 h during which time a yellow precipitate formed. The solution was filtered hot to avoid the soluble elemental sulfur. The yellow product was then washed with CHCl_3 . Yield 14 g.

The compound gave characteristic bands at 2190 and 1440 cm^{-1} in the IR spectrum due to $\nu(\text{CN})$ and $\nu(\text{C}=\text{C})$ vibrations respectively. λ_{max} (MeOH): 370 nm ($\epsilon = 11500$).

3. Preparation of $[\text{Bu}_4\text{N}]_2[\text{Mo}^{\text{VI}}\text{O}_2(\text{mnt})_2]$:

2 mmol of $\text{Na}_2\text{MoO}_4 \cdot 2\text{H}_2\text{O}$ (0.485 g) and 4 mmol of Na_2mnt (0.745 g) were taken in 40 ml of citric acid-phosphate buffer (pH ~ 6) at 10°C. 5 mmol of Bu_4NBr (1.6 g) was added when a red-brown oily mass was formed. The oily mass solidified at room temperature. The red-brown solid was washed with cold water and then with isopropanol and diethylether. This product was dissolved in minimum (3-4 ml) MeCN and crystallized by adding isopropanol and diethyl ether. Yield 1.1 g (61% based on $\text{Na}_2\text{MoO}_4 \cdot 2\text{H}_2\text{O}$).

Anal. calcd. for $\text{C}_{40}\text{H}_{72}\text{MoN}_6\text{O}_2\text{S}_4$: C, 53.78; H, 8.12; N, 9.40; S, 14.35. Found: C, 53.99; H, 7.87; N, 9.66; S, 14.66.

m.p. 100-103°C. Conductivity: $247 \text{ cm}^2 \text{ ohm}^{-1} \text{ mol}^{-1}$ in 10^{-3} M MeCN, consistent for a 2:1 electrolyte.

The $[\text{Bu}_4\text{P}]^+$ salt was prepared and isolated in the same way as the $[\text{Bu}_4\text{N}]^+$ salt. Anal. calcd. for $\text{C}_{40}\text{H}_{72}\text{MoN}_4\text{O}_2\text{P}_2\text{S}_4$: C, 51.81; H, 7.82; N, 6.04; S, 13.83. Found. C, 51.94; H, 7.71; N, 5.98; S, 13.94.

4. Preparation of $[\text{Bu}_4\text{N}]_2[\text{Mo}^{\text{IV}}\text{O}(\text{mnt})_2]$:

This compound was already reported earlier^{86,87}. The alternative methods are:

Method A. 2 mmol of molybdic acid (0.36 g) and 4 mmol of Na_2mnt (0.372 g) were taken in 100 ml of water. The reaction mixture was slightly heated when undissolved molybdic acid reacted and went into solution. 2 mmol of NaHSO_3 (0.209 g) was then added when the

yellow red solution changed to green-brown solution. Addition of 5 mmol (1.61 g) of Bu_4NBr caused precipitation of dirty green solid, which was collected by filtration and washed with water, then with isopropanol and diethylether. This green product was crystallized from acetonitrile, isopropanol and diethylether. Yield 1.17 g (66 % based on $\text{H}_2\text{MoO}_4 \cdot \text{H}_2\text{O}$).

Anal. calcd. for $\text{C}_{40}\text{H}_{72}\text{MoN}_6\text{OS}_4$: C, 54.76; H, 8.27; N, 9.58, S, 14.62. Found: C, 54.88; H, 8.12; N, 9.66; S, 14.77.

m.p. 150-153°C.

The $[\text{Et}_4\text{N}]^+$ salt was obtained in the same way as $[\text{Bu}_4\text{N}]^+$ salt.

Anal. calcd. for $\text{C}_{24}\text{H}_{40}\text{MoN}_6\text{OS}_4$: C, 44.15; H, 6.17; N, 12.87; S, 19.64. Found: C, 44.03; H, 6.26; N, 13.04; S, 19.59.

Conductivity: $274 \text{ cm}^2 \text{ ohm}^{-1} \text{ mol}^{-1}$ in 10^{-3} M MeCN, consistent for 2:1 electrolyte.

The $[\text{Bu}_4\text{P}]^+$ salt was also obtained. Anal. calcd. for $\text{C}_{40}\text{H}_{72}\text{MoN}_4\text{OP}_2\text{S}_4$: C, 52.73; H, 7.96; N, 6.15; S, 14.07. Found: C, 52.88. H, 8.01; N, 6.09; S, 14.13.

Method B. A solution of 0.648 mmol (0.579 g) of $[\text{Bu}_4\text{N}]_2^{+}$
 $[\text{Mo}^{\text{VI}}\text{O}_2(\text{mnt})_2]$ in 6 ml of acetonitrile was treated with a solution of 1.62 mmol (0.169 g) of NaHSO_3 in 4 mmol of water resulting immediately in a green oily mass. This oily mass solidified after 5-6 h at room temperature which was then filtered and washed with isopropanol and diethyl ether. Yield 0.524 g (92 %)

Method C. A solution of 0.191 mmol (0.050 g) of PPh_3 in 4ml acetonitrile was added to a solution of 0.107 mmol (0.096 g) of $[\text{Bu}_4\text{N}]_2[\text{Mo}^{\text{VI}}\text{O}_2(\text{mnt})_2]$ in 3 ml of acetonitrile. This was stirred for 2h when deep red solution was converted to dirty green solution. Addition of isopropanol and excess diethylether caused crystalline green solid mass of $[\text{Bu}_4\text{N}]_2[\text{Mo}^{\text{IV}}\text{O}(\text{mnt})_2]$. Yield 0.075 g (80 %).

5. Preparation of $(\text{PyH})_2[\text{Mo}^{\text{IV}}\text{O}(\text{mnt})_2]$:

2 mmol of molybdic acid (0.36 g) and 4 mmol of Na_2mnt (0.372 g) were taken in 15 ml of water. The reaction mixture was heated to get the clear solution. 2 mmol of NaHSO_3 (0.209 g) was then added when the color of the solution became green-brown. It was filtered. Addition of 0.5 ml of CH_3COOH and 0.8 ml of pyridine to the filtrate caused the precipitation of crystalline solid of $(\text{PyH})_2[\text{Mo}^{\text{IV}}\text{O}(\text{mnt})_2]$. This was recrystallized from MeCN, isopropanol and diethylether. Yield 0.75 g (58 % based on $\text{H}_2\text{MoO}_4 + \text{H}_2\text{O}$).

Anal. calcd. for $\text{C}_{18}\text{H}_{12}\text{MoN}_6\text{OS}_4$: C, 39.13; H, 2.19; N, 15.21; S, 23.21. Found: C, 39.21; H, 2.30; N, 15.18; S, 23.31.

6. Attempted synthesis of $[\text{Mo}^{\text{V}}\text{O}(\text{mnt})_2]^{1-}$: Preparation of $[\text{Et}_4\text{N}]_2[\text{Mo}^{\text{IV}}(\text{mnt})_3]$.

1.02 mmol of iodine (0.13 g) in 5 ml CH_2Cl_2 was added with stirring to a green-brown solution of $[\text{Et}_4\text{N}]_2[\text{Mo}^{\text{IV}}\text{O}(\text{mnt})_2]$ in 15 ml of CH_2Cl_2 . The color of the solution immediately turned bright green. Stirring was continued for 2 h. Isopropanol (20 ml) was

added when bright green solid separated. This solid was collected by filtration, washed with isopropanol and diethylether. This product was crystallized from MeCN, isopropanol and diethylether giving needle shaped crystals. Yield 50 %.

Anal. calcd. for $C_{28}H_{40}MoN_8S_6$: C, 43.28; H, 5.18; N, 14.42; S, 24.75. Found: C, 43.30; H, 5.23; N, 14.40; S, 24.79.

The electronic spectrum of this complex was exactly matched with that of reported^{87,106} $[Bu_4N]_2^{[Mo^{IV}O(mnt)]_3}$.

7. Preparation of $[Ph_3PNPPh_3][Et_4N][Mo^VCl(mnt)]_2$:

1.02 mmol of iodine (0.13 g) in 5 ml CH_2Cl_2 was added with stirring to a solution of 0.99 mmol (0.65 g) $[Et_4N]_2^{[Mo^{IV}O(mnt)]_2}$ in 15 ml CH_2Cl_2 containing excess $[Ph_3PNPPh_3]Cl$. Stirring continued for half an hour. 10 ml MeOH and excess petroleum ether were added when needle shaped microcrystals separated. The microcrystalline product was washed with petroleum ether and dried in vacuo at room temperature. Yield 80 %.

Anal. calcd. for $C_{52}H_{50}MoN_6OClP_2S_4$: C, 56.96; H, 4.59; N, 7.66; S, 11.69. Found: C, 56.98; H, 4.63; N, 7.63; S, 11.72.

Magnetic moment: $\mu_{eff} = 1.86$ B.M.

8. Preparation of $[Bu_4N]_2^{[W^{VI}O_2(mnt)]_2}$:

2 mmol of $Na_2WO_4 \cdot 2H_2O$ (0.66 g), 4 mmol of Na_2mnt (0.75 g) and 9.6 mmol (1 g) $NaHSO_3$ were dissolved in 80 ml of water and the pH was adjusted to 5.5 by adding CH_3COOH . 4.5 mmol of $[Bu_4N]Br$ (1.45 g) was then added to precipitate the orange-red solid. This solid was collected by filtration, washed with isopropanol and

diethylether. This orange-red product was crystallized from CH_3CN , isopropanol and diethylether. The orange-red solid can also be crystallized from CH_2Cl_2 , isopropanol and diethylether. Yield 60%. Anal. calcd. for $\text{C}_{40}\text{H}_{72}\text{N}_6\text{O}_2\text{S}_4\text{W}$: C, 48.96; H, 7.39; N, 8.56, S, 13.07. Found: C, 49.07; H, 7.31; N, 8.63; S, 13.11.

Conductivity: $267 \text{ cm}^2 \text{ ohm}^{-1} \text{ mol}^{-1}$ in 10^{-3} M MeCN , consistent for a 2:1 electrolyte.

9. Preparation of $[\text{Et}_4\text{N}]_2[\text{W}^{\text{VI}}\text{O}_2(\text{mnt})_2]$:

2 mmol of $\text{Na}_2\text{WO}_4 \cdot 2\text{H}_2\text{O}$ (0.66 g), 4 mmol of Na_2mnt (0.75 g), 9.6 mmol of NaHSO_3 (1 g) and 6 mmol of $[\text{Et}_4\text{N}]\text{Br}$ (1.26 g) were dissolved in 100 ml of water and then pH of this solution was adjusted to 5.5 by adding CH_3COOH when orange-red solid mass separated. This solid was collected by filtration, washed with isopropanol and diethylether. This orange-red solid was crystallized from dry MeCN and dry diethylether. Yield 50 % based on $\text{Na}_2\text{WO}_4 \cdot 2\text{H}_2\text{O}$.

Anal. calcd. for $\text{C}_{24}\text{H}_{40}\text{N}_6\text{O}_2\text{S}_4\text{W}$: C, 38.09; H, 5.32; N, 11.10; S, 16.94. Found: C, 37.98; H, 5.02; N, 10.94; S, 16.89.

10. Preparation of $[\text{Et}_4\text{N}]_2[\text{W}^{\text{IV}}\text{O}(\text{mnt})_2]$:

2 mmol of $\text{Na}_2\text{WO}_4 \cdot 2\text{H}_2\text{O}$ (0.66 g) and 4 mmol of Na_2mnt (0.75 g) were dissolved in 100 ml of water under dinitrogen atmosphere and pH of this solution was adjusted to 5.5 by adding CH_3COOH . 58 mmol sodium dithionite (10 g) was added into it and then the addition of 6 mmol of $[\text{Et}_4\text{N}]\text{Br}$ (1.26 g) caused the precipitation of pink colored solid. This solid was collected by filtration, washed with

water, isopropanol and diethylether. This solid was crystallized from CH_3CN and diethylether giving needle shaped purple-pink crystals. Yield 60 % based on $\text{Na}_2\text{WO}_4 \cdot 2\text{H}_2\text{O}$.

Anal. calcd. for $\text{C}_{24}\text{H}_{40}\text{N}_6\text{OS}_6\text{W}$: C, 38.91; H, 5.44, N, 11.34; S, 17.31. Found: C, 38.88, H, 5.56; N, 11.44; S, 17.40

Conductivity: $280 \text{ cm}^2 \text{ ohm}^{-1} \text{ mol}^{-1}$ in 10^{-3} M MeCN, consistent for a 2:1 electrolyte.

11. Preparation of $[\text{Et}_4\text{N}]_2[\text{W}^{\text{VI}}\text{O}(\text{mnt})_2(\text{S}_2)]$:

1 mmol of $[\text{Et}_4\text{N}]_2[\text{W}^{\text{IV}}\text{O}(\text{mnt})_2]$ (0.74 g) and 2.49 matom of elemental sulfur (0.08 g) were heated under reflux in acetone (60 ml) under dinitrogen for 36 h when the purple color of $[\text{Et}_4\text{N}]_2[\text{W}^{\text{IV}}\text{O}(\text{mnt})_2]$ turned red. This reddish reaction mixture, after filtration, was evaporated to a concentrated oily mass under vacuum. This oily mass was purified by crystallization from MeOH and diethylether to give red crystals of $[\text{Et}_4\text{N}]_2[\text{W}^{\text{VI}}\text{O}(\text{S}_2)(\text{mnt})_2]$. These crystals were recrystallized from acetonitrile, isopropanol and diethylether. Yield 0.42 g (52 %).

Anal. calcd. for $\text{C}_{24}\text{H}_{40}\text{N}_6\text{OS}_6\text{W}$: C, 35.81; H, 5.01; N, 10.44; S, 23.90. Found: C, 35.83; H, 4.90; N, 10.57; S, 23.85.

m.p. $124\text{--}126^\circ\text{C}$ (with decomposition).

Couductivity: $300 \text{ cm}^2 \text{ ohm}^{-1} \text{ mol}^{-1}$ in 10^{-3} M MeCN, consistent for a 2:1 electrolyte.

12. Preparation of $[\text{Et}_4\text{N}]_2[\text{W}^{\text{VI}}\text{O}(\text{mnt})_2(\text{C}_2(\text{CO}_2\text{CH}_3)_2)]$:

1 mmol of $[\text{Et}_4\text{N}]_2[\text{W}^{\text{IV}}\text{O}(\text{mnt})_2]$ (0.74 g) was dissolved in dry MeCN (15 ml) under argon and 10 mmol of dimethyl acetylenedicarboxylate (DMAC) (1.2 ml) was added into it. The reaction mixture was kept with stirring for 6 h at room temperature. Addition of dry diethylether (20 ml) and keeping it overnight in the fridge resulted in the separation of red microcrystalline solid. This was filtered, washed with diethylether and then recrystallized from MeCN and diethylether to yield $[\text{Et}_4\text{N}]_2[\text{W}^{\text{VI}}\text{O}(\text{mnt})_2(\text{C}_2(\text{CO}_2\text{CH}_3)_2)]$. Yield 0.53 g (60 %).
Anal. calcd. for $\text{C}_{30}\text{H}_{46}\text{N}_6\text{O}_5\text{S}_4\text{W}$: C, 40.81; H, 5.25; N, 9.52; S, 14.53. Found: C, 40.46; H, 5.38; N, 9.70; S, 14.60.

3.2 CHARACTERIZATION OF THE SYNTHESIZED COMPLEXES.

3.2.1 SYNTHESES.

The synthetic aspect of $[\text{Mo}^{\text{VI}}\text{O}_2(\text{mnt})_2]^{2-}$ has special relevance in relation to its model behavior (*vide infra*). The tetrahedral $[\text{MoO}_4]^{2-}$ anion is readily soluble in water in common pH range. The similarity of this anion with PO_4^{3-} and SO_4^{2-} may be the main reason for its bioassimillation¹⁰⁷. It is well known that MoO_4^{2-} started polymerization below pH 7 with the expansion of its coordination number. In lower pH the ready availability of the hydrated $\{\text{MoO}_2\}^{2+}$ moiety favors to form complexes containing this core⁸. However, ligands like mnt^{2-} which are susceptible to easy oxidation may create problems as molybdenum(VI) at lower pH is a potent reductant. Even for the ligand like acetylacetone (acac), the synthesis of $\text{MoO}_2(\text{acac})_2$ is accomplished under dilute nitric acid which prevents the reduction as well as makes the pH lower for ready availability of $\{\text{MoO}_2\}^{2+}$ moiety in solution.

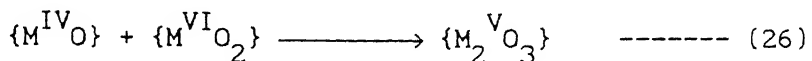
In the present case mnt^{2-} is readily oxidized at very low potential¹⁰⁸. Hence use of nitric acid is unwarranted. The reaction between molybdic acid and Na_2mnt does show chelating ability of the mnt^{2-} ligand which solubilize molybdic acid in aqueous medium but at the expense of side reaction (reduction of molybdic acid by mnt ligand i.e. oxidation of mnt ligand) with the loss of approximately 2/3 of this ligand involved in the process of oxidation of ligand resulting in the isolation of the reduced monooxo speceis, $[\text{Mo}^{\text{IV}}\text{O}(\text{mnt})_2]^{2-}$ in approximately 30% yield. This

oxidation of the ligand is prevented by adding excess of NaHSO_3 into the reaction mixture to improve the yield of the reduced species, $[\text{Mo}^{\text{IV}}\text{O}(\text{mnt})_2]^{2-}$, to near quantitative. However, to achieve only complexation preventing any redox reaction for the isolation of $[\text{Mo}^{\text{VI}}\text{O}_2(\text{mnt})_2]^{2-}$, a pH window of 6-6.6 with phosphate or citric acid-phosphate buffer has been optimized. This reaction is demonstrative in nature to incorporate molybdate, MoO_4^{2-} in molybdopterin ligand to form molybdenum cofactor.

Analogue complexes of tungsten described here deserve some comments: In the synthesis of $[\text{W}^{\text{VI}}\text{O}_2(\text{mnt})_2]^{2-}$ an optimum pH around 5.5 is required as lower pH below this would result in the precipitation of tungstic acid. However, Na_2mnt is even oxidized by tungsten(VI) in this medium. No definite reduced tungsten species is formed and thus a meaningful compound could not be isolated. Addition of HSO_3^- prevents this oxidation of mnt^{2-} wherein $[\text{W}^{\text{VI}}\text{O}_2(\text{mnt})_2]^{2-}$ can be isolated. For the isolation of reduced monooxo species, $[\text{W}^{\text{IV}}\text{O}(\text{mnt})_2]^{2-}$, we have used excess of sodium dithionite. Early studies to synthesize $\text{WO}(\text{R}_2\text{dtc})_2$ analogous to $\text{MoO}(\text{R}_2\text{dtc})_2$ ⁸³ using dithionite reduction led to the isolation of pentavalent dimeric species¹⁰⁹. This may be due to the fact that when R_2dtc^- and WO_4^{2-} are present together and dithionite was added in slightly acidified condition the reduction of tungsten(VI) to tungsten(IV) is not fully achieved which comproportionated to $\{\text{W}_2^{\text{V}}\text{O}_3\}$ moiety from the reaction: $\text{W(VI)} + \text{W(IV)}$, and thus precipitating out from the reaction solution with the aid of R_2dtc chelation. In the present case the addition of counter cation to precipitate the anionic complex was

delayed till the completion of the reaction. Fortunately, even after addition of the counter cation the precipitation did not take place immediately rather slowly which help further for the completion of the reaction.

It is interesting to note that with this dithiolene ligand system comproportionation reaction like



did not take place. This is also true for other recently reported anionic dithiolate complex⁹³.

It is surprising that all neutral complexes of molybdenum with dioxo and monoxo moieties invariably respond to this comproportionation reaction even with bulky ligands^{69, 78, 80}.

Characterization of the synthesized complexes has been made by infrared, electronic, nuclear magnetic resonance, electron spin resonance, and FAB mass spectroscopy, magnetic moment, conductivity, X-ray powder diffractograms, X-ray single crystal study and cyclic voltammetry.

3.2.2 IR SPECTROSCOPY.

Characterization of the presence of *cis* dioxo moiety in *cis*-MoO₂(VI) and *cis*-W₂(VI) complexes can be readily made from infrared spectroscopy as discussed in the earlier chapter. A set of two M-O (M = Mo, W) stretching vibrations have been observed in both the dioxo complexes synthesized here. For the Mo(IV)-O vibrations in monooxo complexes, appearance of a strong infrared

Table 3.1 IR (cm^{-1}) Spectral Data^a for Complexes

compound	$\nu(\text{M=O})$	$\nu(\text{C=C})$	$\nu(\text{M-S})$	$\nu(\text{CN})$
$[\text{Bu}_4\text{N}]_2[\text{Mo}^{\text{VI}}\text{O}_2(\text{mnt})_2]$	854s, 889vs	1471vs	320s	2198vs
$[\text{Bu}_4\text{N}]_2[\text{Mo}^{\text{IV}}\text{O}(\text{mnt})_2]$	928vs	1482vs	335s	2194vs
$[\text{Ph}_3\text{PNPPh}_3][\text{Et}_4\text{N}]$ $[\text{Mo}^{\text{V}}\text{OCl}(\text{mnt})_2]$	933s	1483vs	b	2195vs
$[\text{Et}_4\text{N}]_2[\text{W}^{\text{IV}}\text{O}(\text{mnt})_2]$	935vs	1483vs	325w	2192vs
$[\text{Et}_4\text{N}]_2[\text{W}^{\text{VI}}\text{O}_2(\text{mnt})_2]$	860s, 906vs	1476vs	310m	2200vs
$[\text{Bu}_4\text{N}]_2[\text{W}^{\text{VI}}\text{O}_2(\text{mnt})_2]$	874s, 916vs	1476vs	314m	2198vs

^aas CsI disk; w = weak, m = medium, s = strong, vs = very strong.

^bnot known.

vibration in the range 900-1010 cm^{-1} is characteristic to $\nu(\text{Mo}-\text{O}_t)$ ¹¹⁰. As discussed earlier terminal W-O_t bonds are stronger than Mo-O_t bonds in analogous complexes. Therefore M-O stretching vibrations in tungsten complex generally appear at higher wave number compared to that of the corresponding Mo-O stretching vibration.

All the complexes synthesized here contain mnt²⁻ as chelating ligand. Detailed infrared spectral analysis of dithiolene coordinated complexes is known¹¹¹. Thus identification of chelated dithiolene group in these complexes is easier. Based on these assignments of vibrations due to oxo and dithiolene coordination are tabulated in Table 3.1. All these infrared spectra are reproduced in Figs 3.1 to 3.13. It is important to take note that $\nu(\text{M-S})$ vibrations in monoxo complexes appear at higher wave number compared to the corresponding dioxo complexes. This is fully in agreement with the chemical properties of these complexes where it was found that chelation from dithiolene to monooxo species are stronger and hence these species are more stable compared to corresponding dioxo species. Interestingly, the separation of molybdenum cofactor under reduced state is reported to be quantitative compared to that in the oxidized state. This difference has been interpreted due to the linkage of the dithiolene ligand to molybdenum(IV) as stronger than that to molybdenum(VI)¹¹².

For the complex, $[\text{Et}_4\text{N}]_2[\text{W}^{\text{VI}}\text{O}(\text{mnt})_2(\text{C}_2(\text{CO}_2\text{CH}_3)_2)]$, $\nu(\text{W=O})$ is 20 cm^{-1} lower than that of $[\text{Et}_4\text{N}]_2[\text{W}^{\text{IV}}\text{O}(\text{mnt})_2]$ which suggests an effective increase in the oxidation state and coordination number

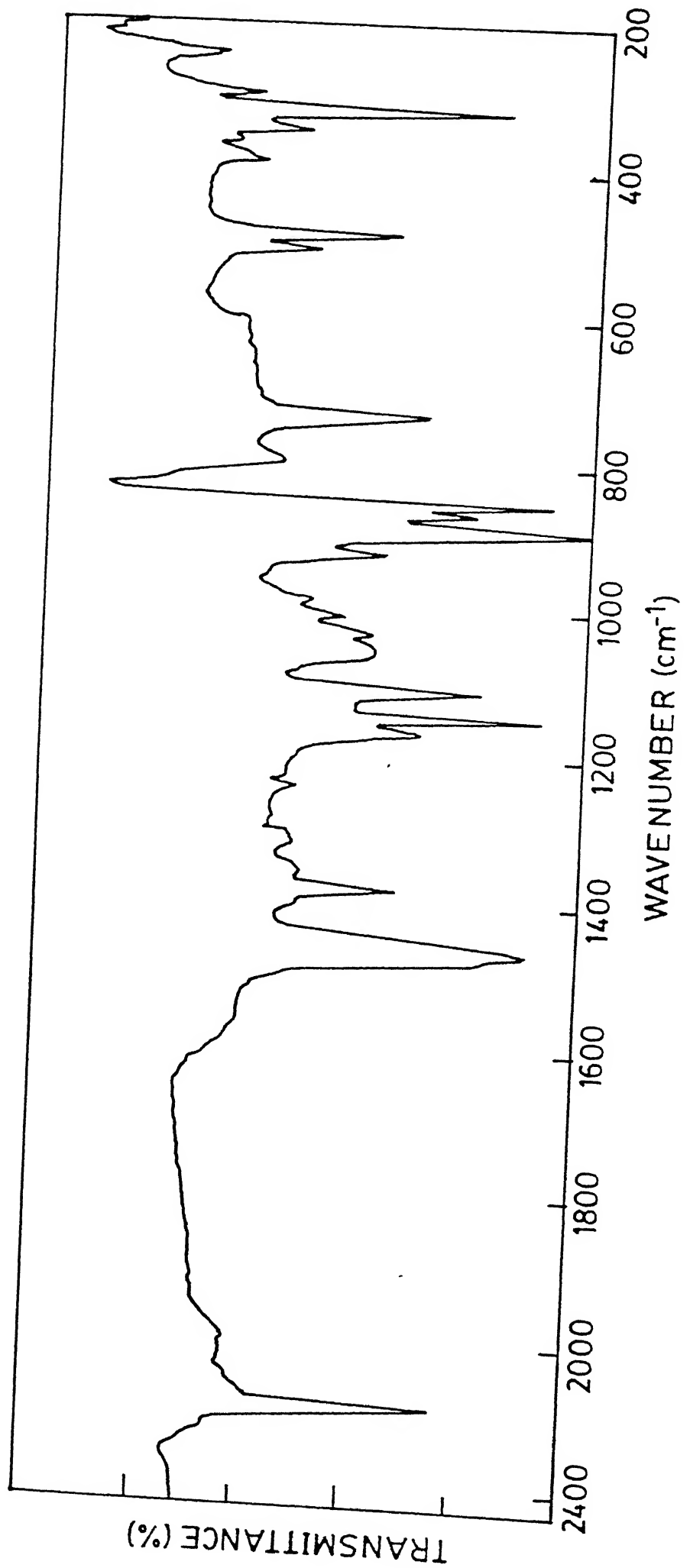


Fig. 3.1 IR spectrum of $[Bu_4N]^2[Mo^{Vl}O_2(mnt)_2]$

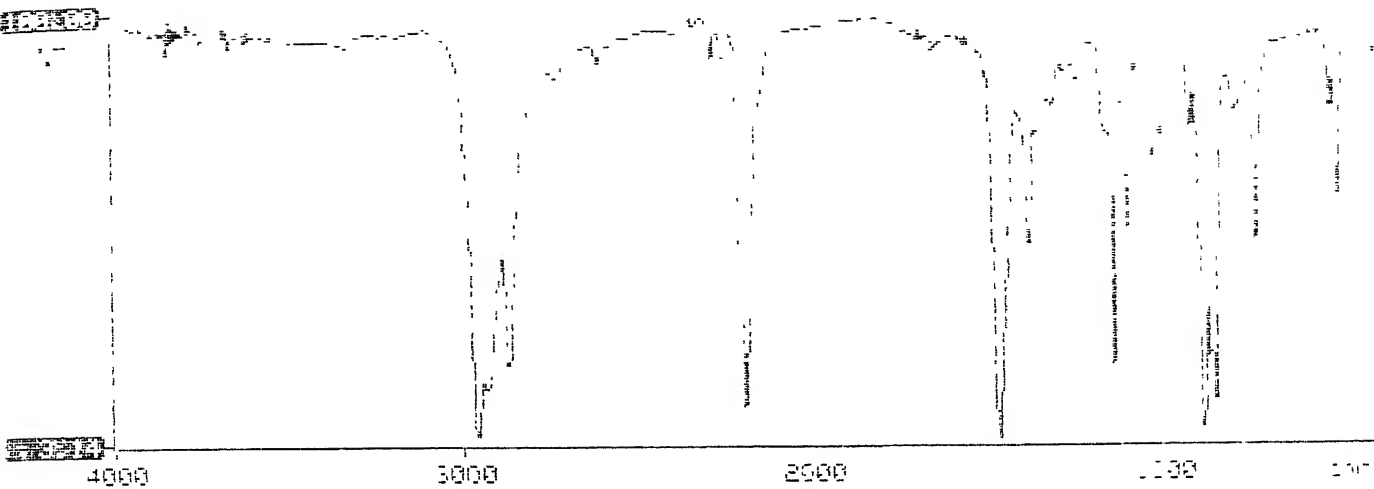


Fig. 3.2 FT IR spectrum of $[Bu_4N]_2[Mo^{VI}O_2(\text{mnt})_2]$

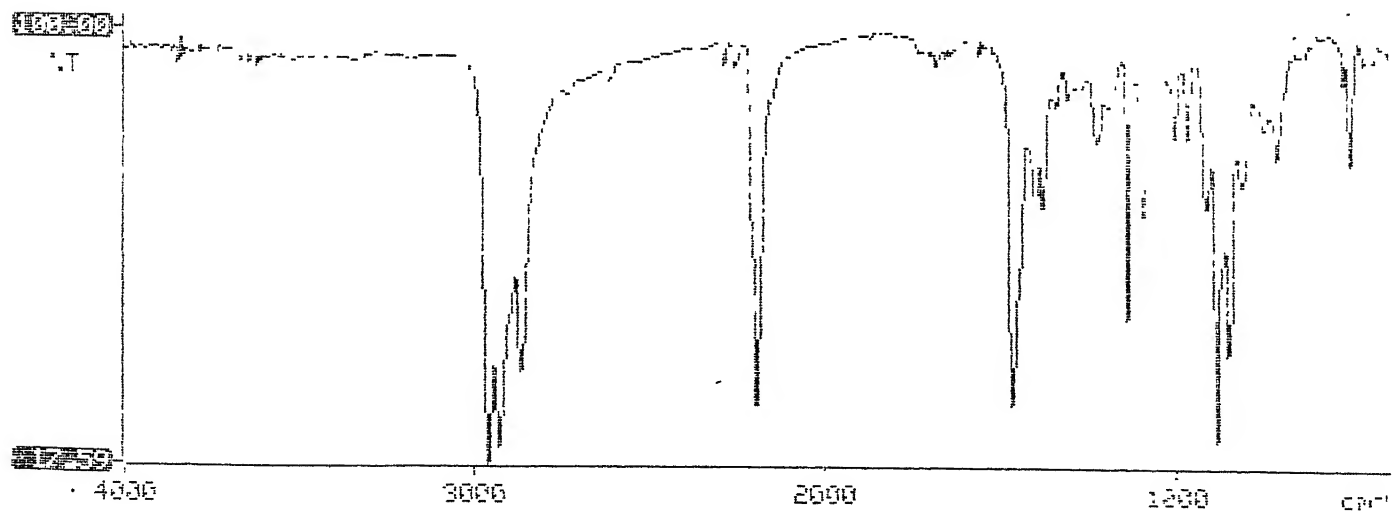


Fig. 3.3 FT IR spectrum of $[Bu_4P]_2[Mo^{VI}O_2(\text{mnt})_2]$

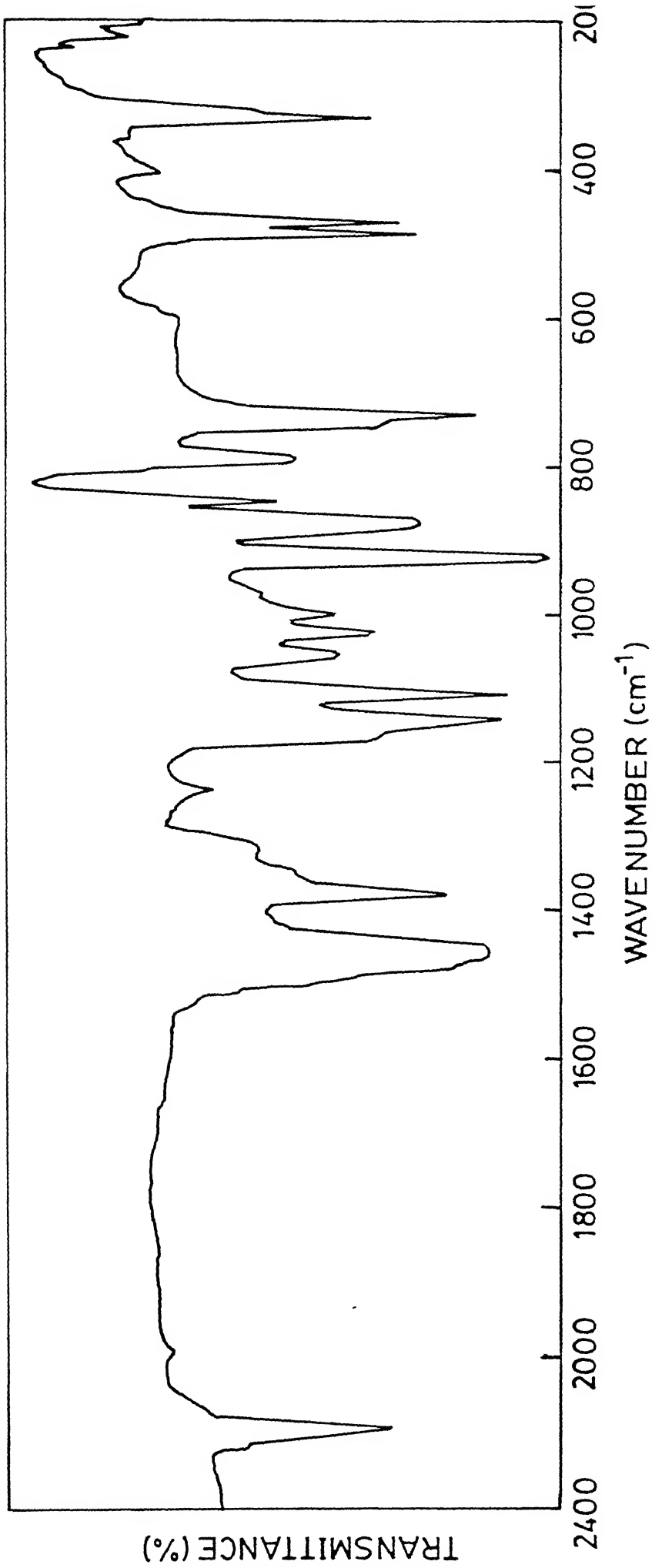


Fig. 3.4 IR spectrum of $[Bu_4N]^2[Mo^{1V}O(mnt)_2]$

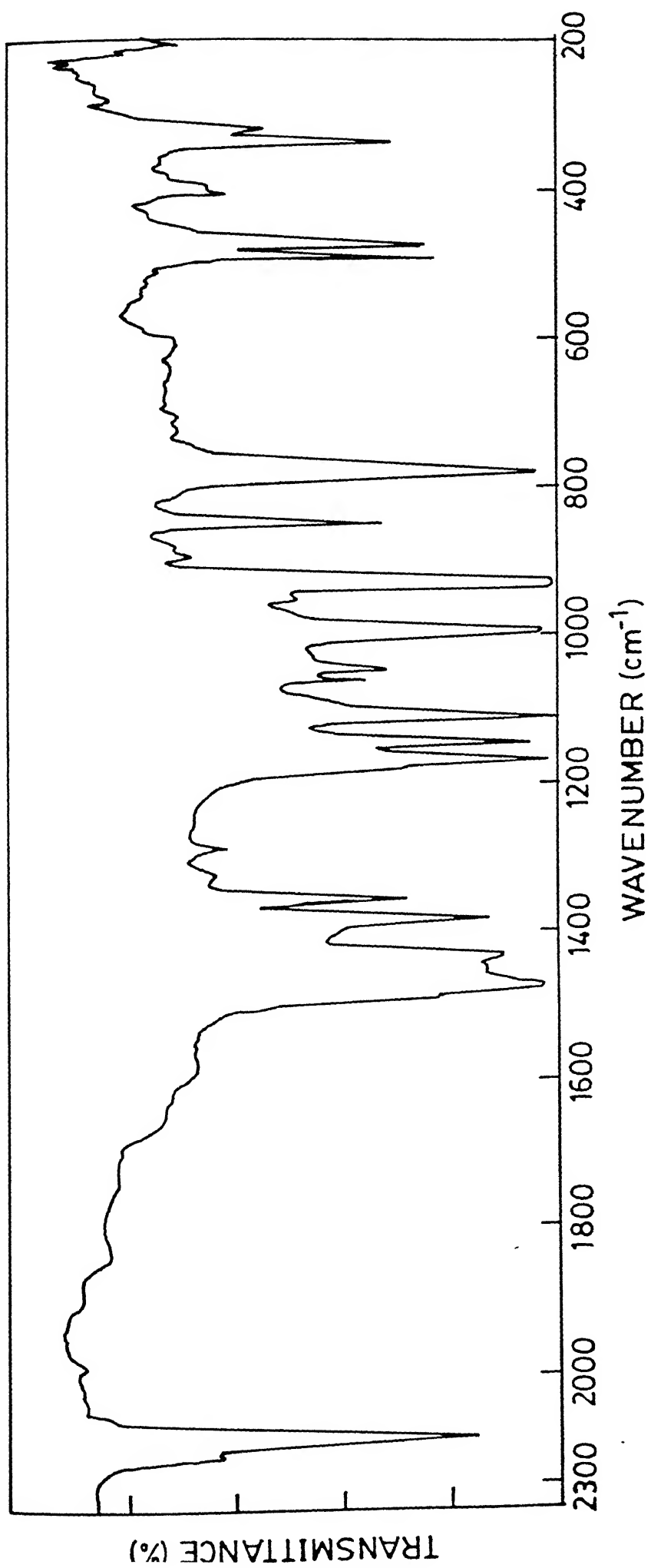


Fig. 3.5 IR spectrum of $[\text{Et}_4\text{N}]_2[\text{Mo}^{\text{IV}}\text{O}(\text{mnt})_2]$

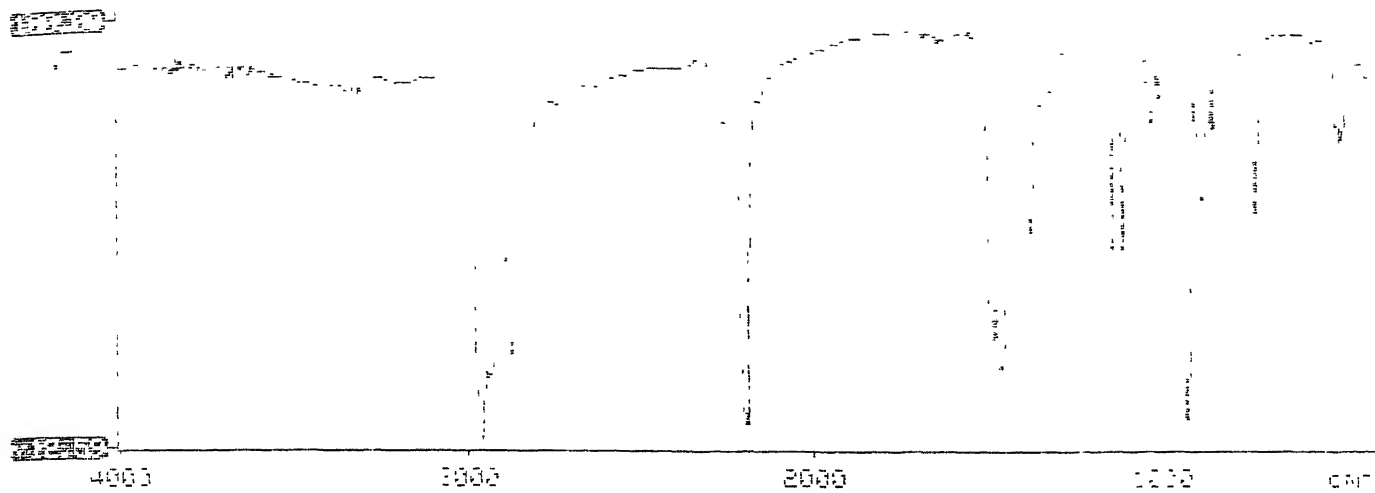


Fig. 3.6 FT IR spectrum of $[\text{Bu}_4\text{N}]_2[\text{Mo}^{\text{IV}}\text{O}(\text{mnt})_2]$

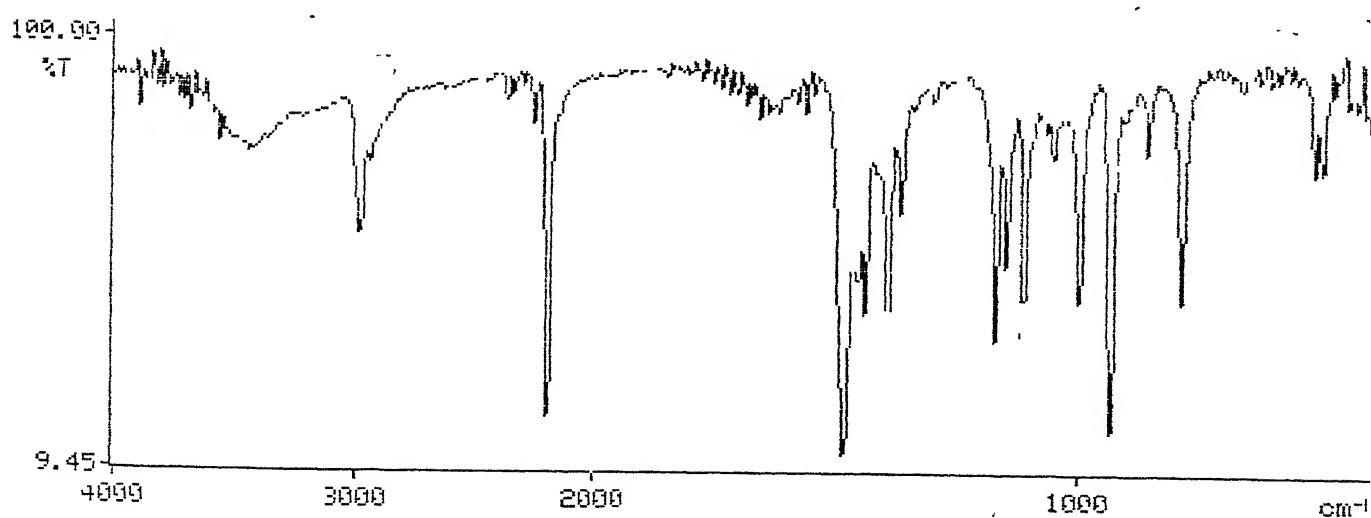


Fig. 3.7 FT IR spectrum of $[\text{Et}_4\text{N}]_2[\text{Mo}^{\text{IV}}\text{O}(\text{mnt})_2]$

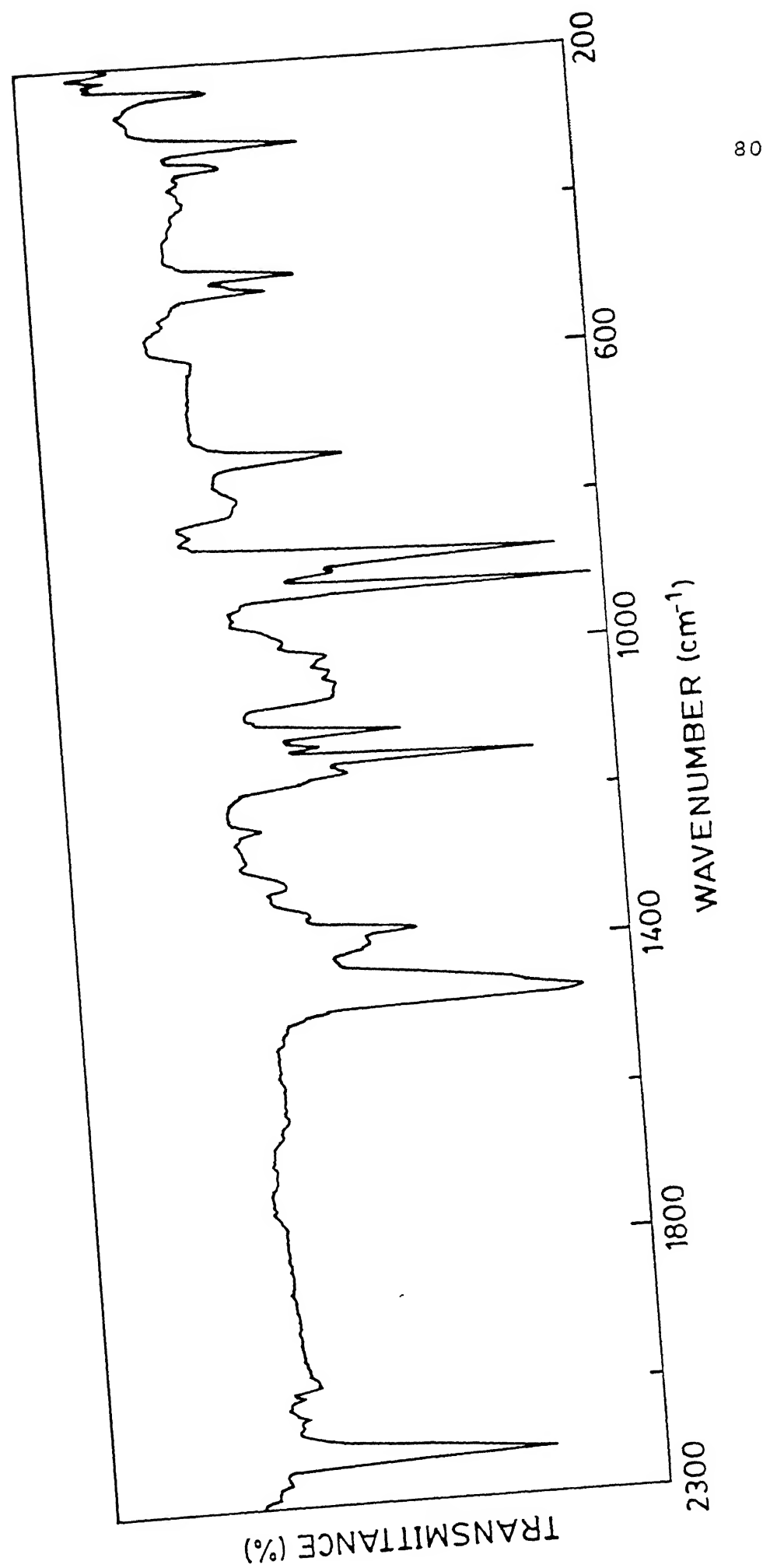


Fig. 3.8 IR spectrum of $[Bu_4N]_2[W^{VI}O_2(mnt)]_2$

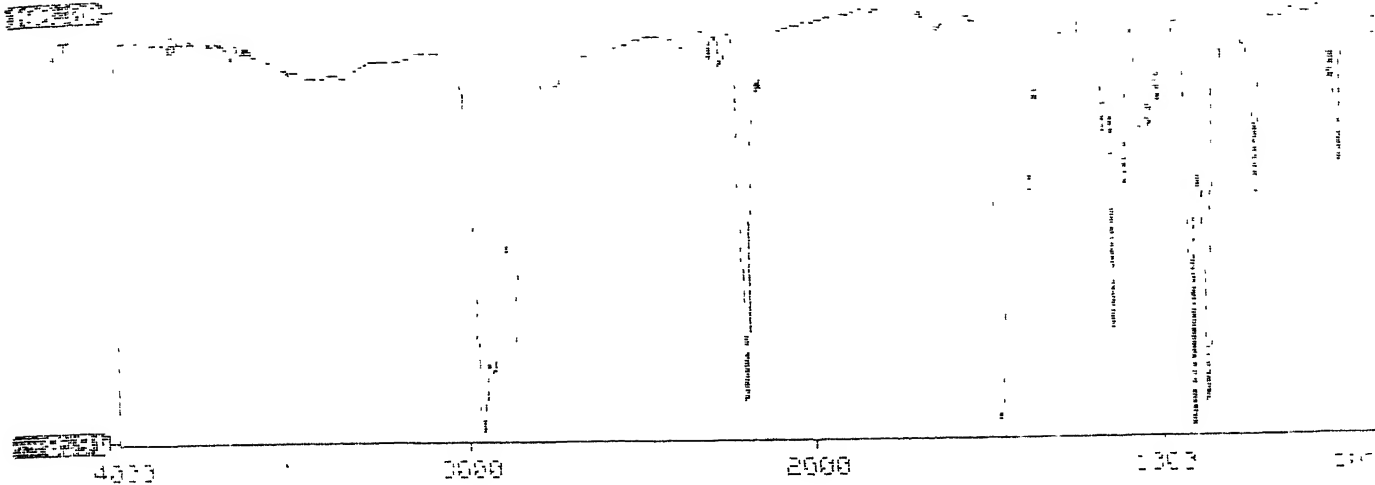


Fig. 3.9 FT IR spectrum of $[Bu_4N]_2[W^{VI}O_2(\text{mnt})_2]$

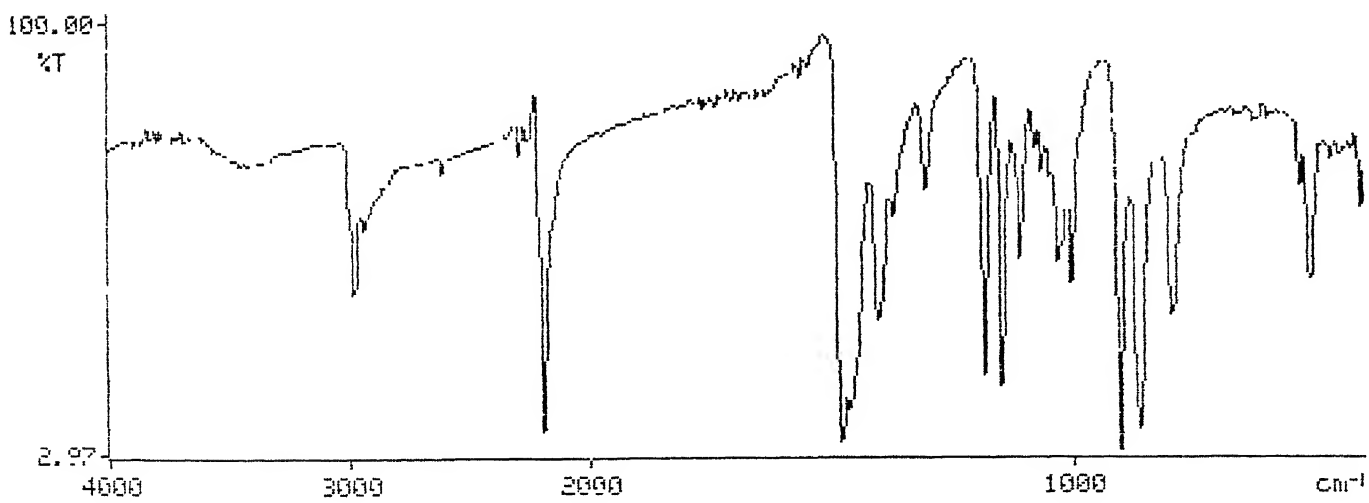


Fig. 3.10 FT IR spectrum of $[Et_4N]_2[W^{VI}O_2(\text{mnt})_2]$

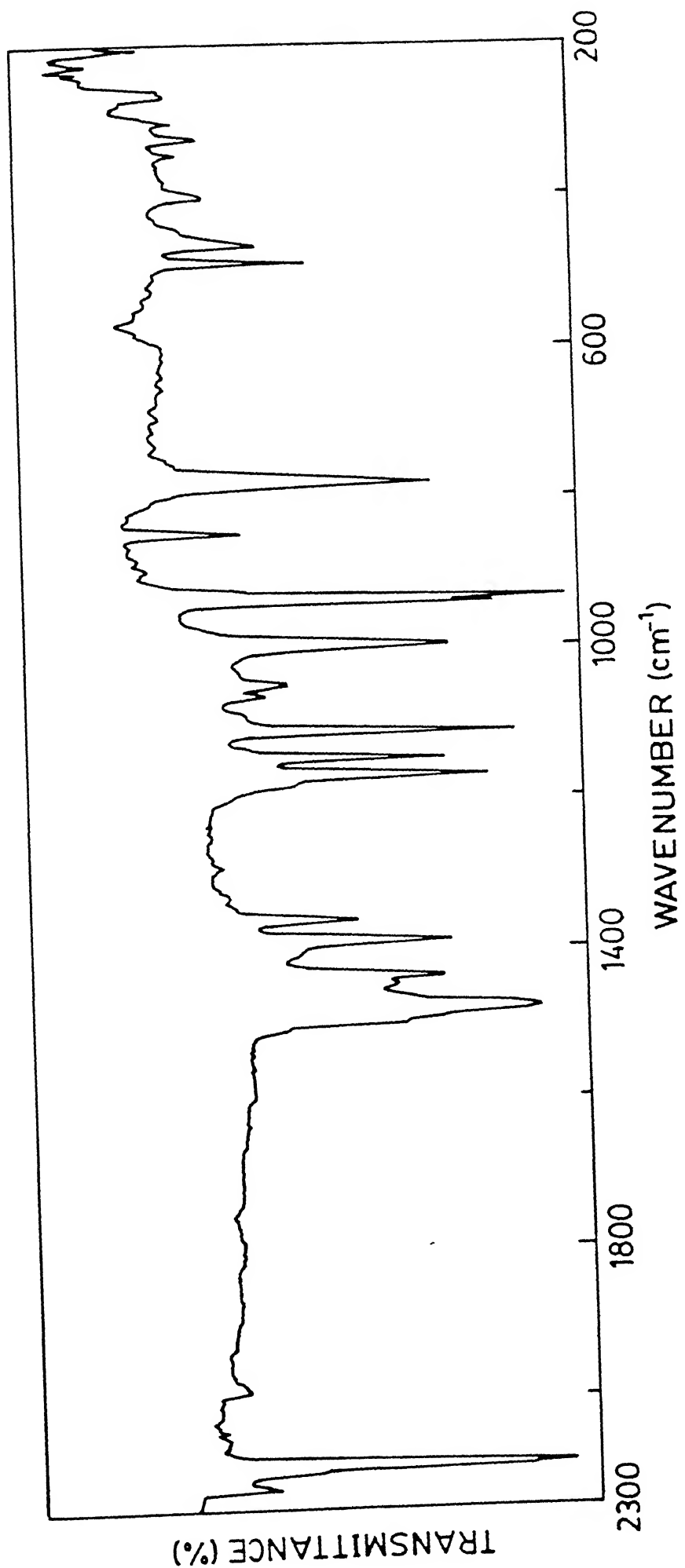


Fig. 3.11 IR spectrum of $[\text{Et}_4\text{N}]_2[\text{W}^{\text{IV}}\text{O}(\text{mnt})_2]$

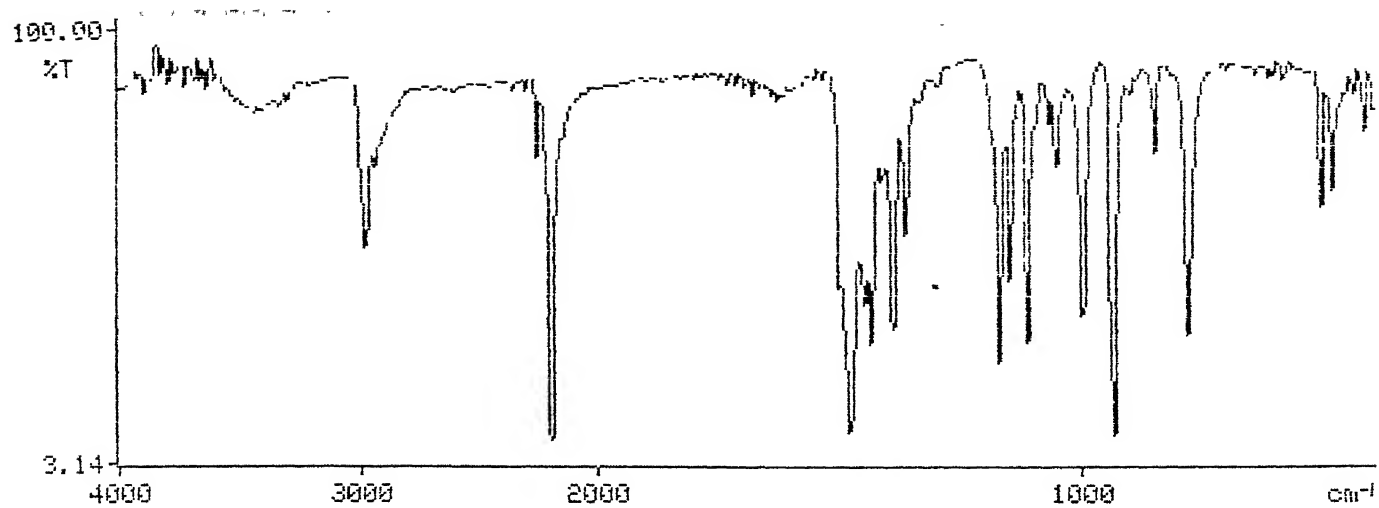


Fig. 3.12 FT IR spectrum of $[\text{Et}_4\text{N}]_2[\text{W}^{\text{IV}}\text{O}(\text{mnt})_2]$

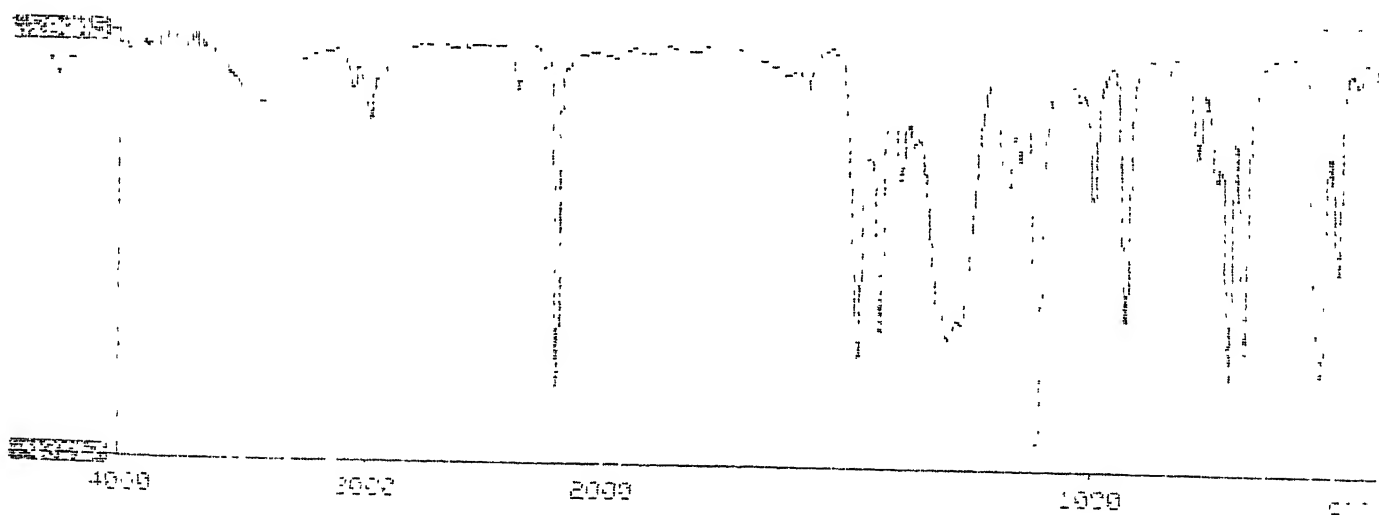


Fig. 3.13 FT-IR spectrum of $[\text{Ph}_3\text{PNPPh}_3][\text{Et}_4\text{N}][\text{Mo}^{\text{V}}\text{OC}_1(\text{mnt})_2]$

Table 3.2 IR (cm^{-1}) Spectral Data^a for Complexes

complex	$\nu(\text{M=O})$	$\nu(\text{C=C})^b$	$\nu(\text{C=O})$	$\nu(\text{C=C})^c$	$\nu(\text{S-S})$	Ref.
$[\text{Et}_4\text{N}]_2^-$ $[\text{W}^{\text{VI}}\text{O}(\text{mnt})_2^-$ $(\text{C}_2(\text{CO}_2\text{CH}_3)_2)]$	915s	1790m	1700vs	1460s	---	present work
$[\text{MoO}(\text{Et}_2\text{dtc})_2^-$ (DMAC)]	925	1850	1715	---	---	103
$[\text{MoO}(\text{Me}_2\text{dtc})_2^-$ (DMAC)]	940	1870	1720	---	---	103
$[\text{Et}_4\text{N}]_2[\text{W}^{\text{VI}}\text{O}-$ $(\text{S}_2)_2(\text{mnt})_2]$	920s	---	---	1470s	532m	present work
$[\text{MoO}(\text{S}_2)_2(\text{Et}_2-$ $\text{dtc})_2]$	908s, 922s	---	---	---	560m	102
$[\text{MoO}(\text{S}_2)_2(\text{Me}_2-$ $\text{dtc})_2]$	916s	---	---	---	555m	102

^aas CsI pellet, vs = very strong, s = strong, m = medium.

^bC=C of coordinated DMAC. ^cC=C of mnt²⁻.

of tungsten. The coordinated dimethyl acetylenedicarboxylate (DMAC) showed $\nu(C=C)$ at 1790 cm^{-1} which is lower than that in $MoO(Et_2dtc)_2(\text{DMAC})^{103}$. Important infrared vibrations in the present complex alongwith data of the related molybdenum complexes have been tabulated in Table 3.2. In this table the related vibrations of $[Et_4N]_2[W^{\text{VI}}O(S_2)(\text{mnt})_2]$ alongwith the reported vibrations for oxomolybdenum disulfur complexes are also included. The infrared spectra of $[Et_4N]_2[W^{\text{VI}}O(\text{mnt})_2(C_2(\text{CO}_2\text{CH}_3)_2)]$ and $[Et_4N]_2[W^{\text{VI}}O(S_2)(\text{mnt})_2]$ are shown in Fig. 3.14 and Fig. 3.15 respectively.

3.2.3 ELECTRONIC SPECTROSCOPY.

Electronic absorption spectra of $[Bu_4N]_2[Mo^{\text{VI}}O_2(\text{mnt})_2]$ and $[Bu_4N]_2[W^{\text{VI}}O_2(\text{mnt})_2]$ are reproduced in Fig. 3.16 and Fig. 3.17 respectively. All the absorptions occurred in the molybdenum complex are charge transfer type as evidenced by molar extinction coefficient values. As expected for the corresponding tungsten complex all the absorptions are blue shifted. Most of the other synthesized dioxomolybdenum(VI) complexes containing sulfur ligands are yellow in color. Amongst these, the complex, $MoO_2(\text{dttd})$ has absorption at 410 nm^{80d} containing $\{Mo^{\text{VI}}O_2S_4\}$ core. Resonance Raman studies on this complex demonstrated that this 410 nm electronic absorption is due to O to Mo charge transfer transition¹¹³. In these studies it has also been demonstrated that a weak transition at $\sim 480\text{ nm}$ is attributed to thiolate-Mo charge transfer transition. The present complex, $[Bu_4N]_2[Mo^{\text{VI}}O_2(\text{mnt})_2]$ distinctly shows three electronic absorptions at 525 nm , 425 nm

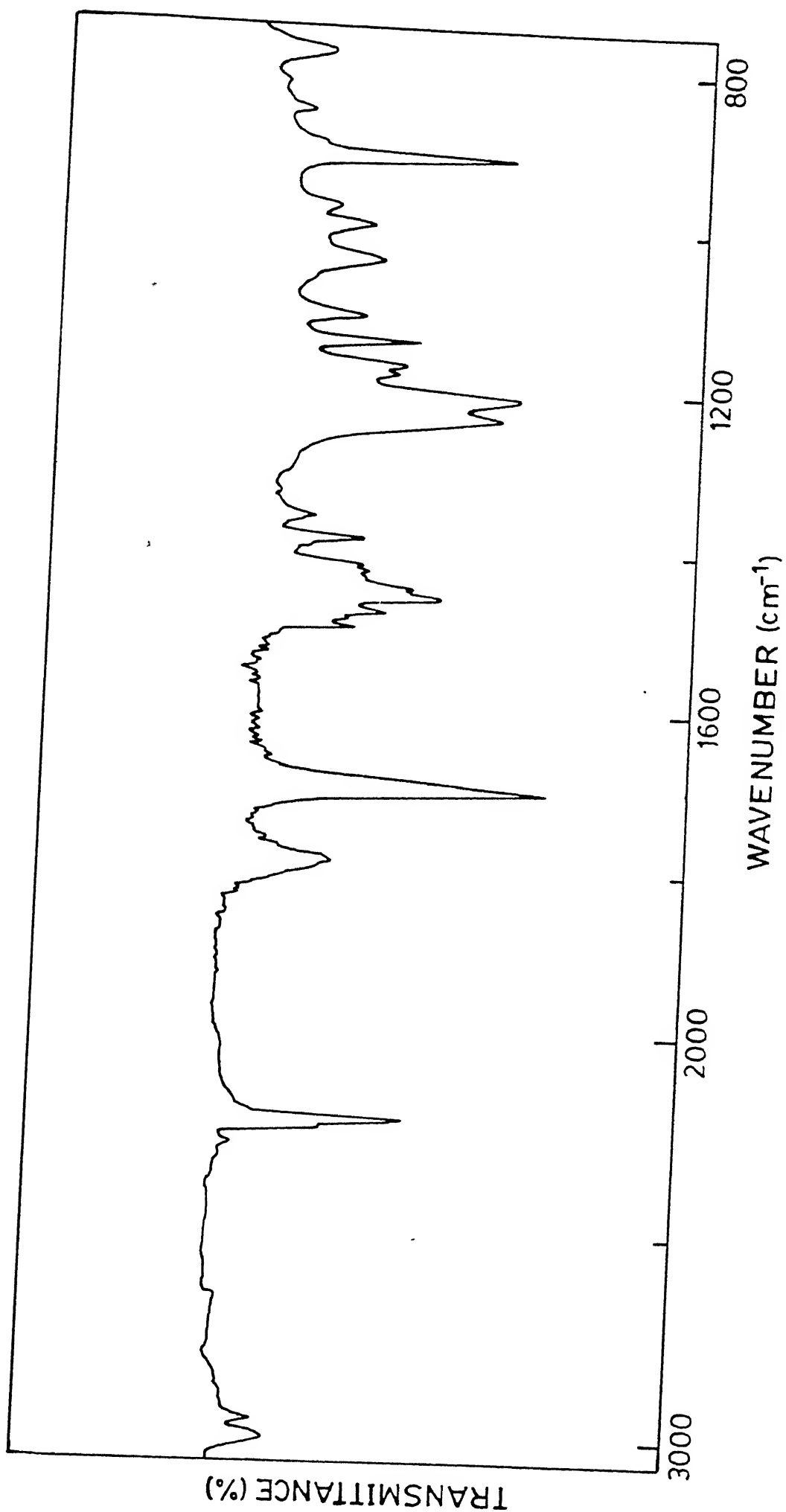


Fig. 3.14 IR spectrum of $[Et_4N]_2[W^{V1}O(mnt)_2(C_2(CO_2CH_3)_2)]$

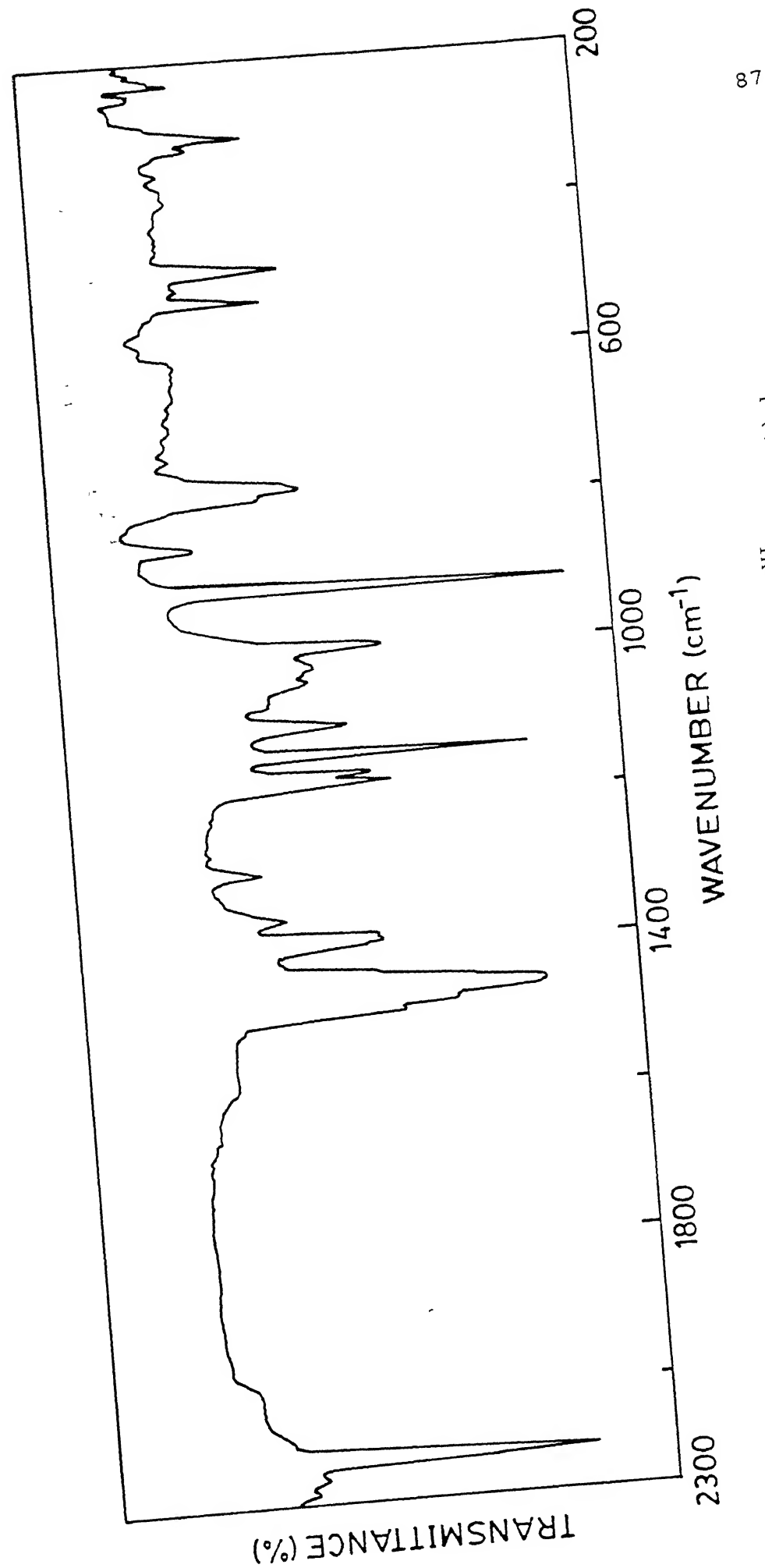


Fig. 3.15 IR spectrum of $[\text{Et}_4\text{N}]_2[\text{W}^{\text{VI}}\text{O}(\text{S}_2)_2(\text{mnt})_2]$

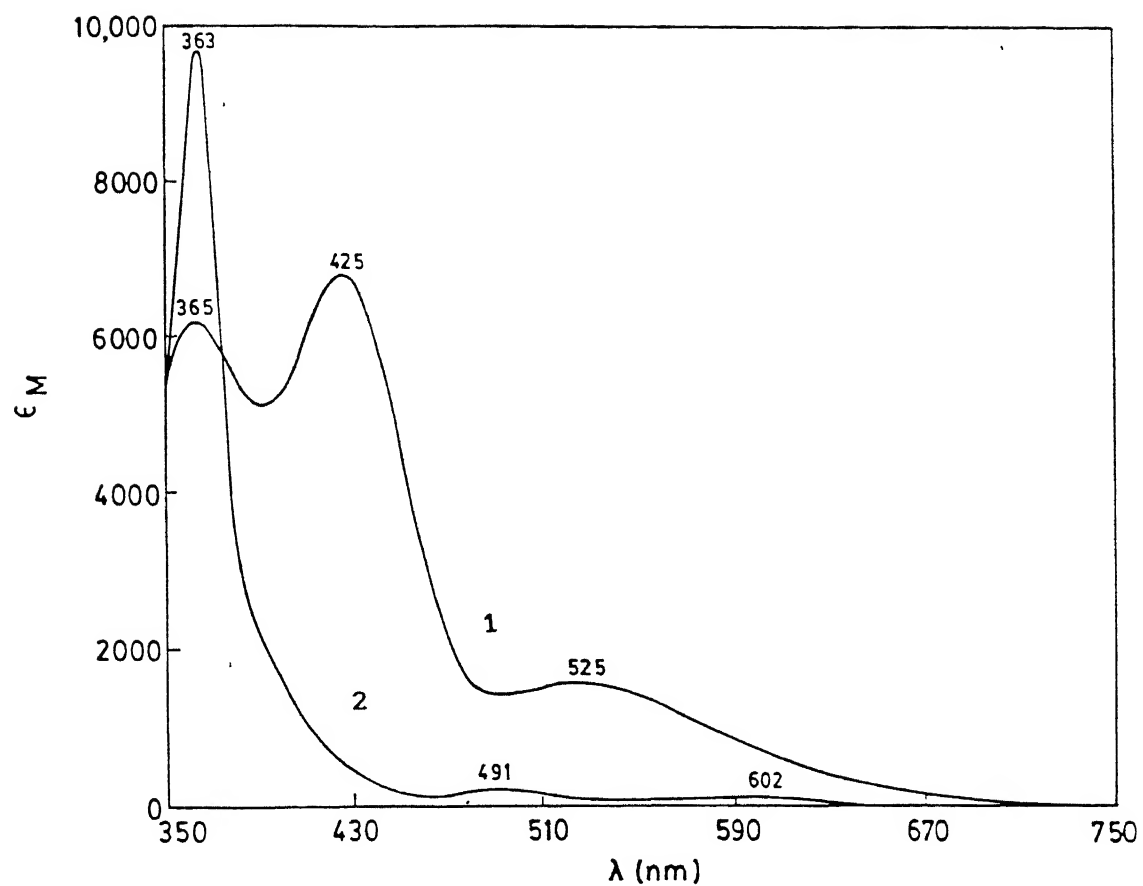


Fig. 3.16 UV-visible absorption spectra of $[\text{Bu}_4\text{N}]_2^{+} [\text{Mo}^{\text{VI}} \text{O}_2(\text{mnt})_2]^-$ 1 and $[\text{Bu}_4\text{N}]_2^{+} [\text{Mo}^{\text{IV}} \text{O}(\text{mnt})_2]^-$ 2 in MeCN. Conc. 1×10^{-4} M.

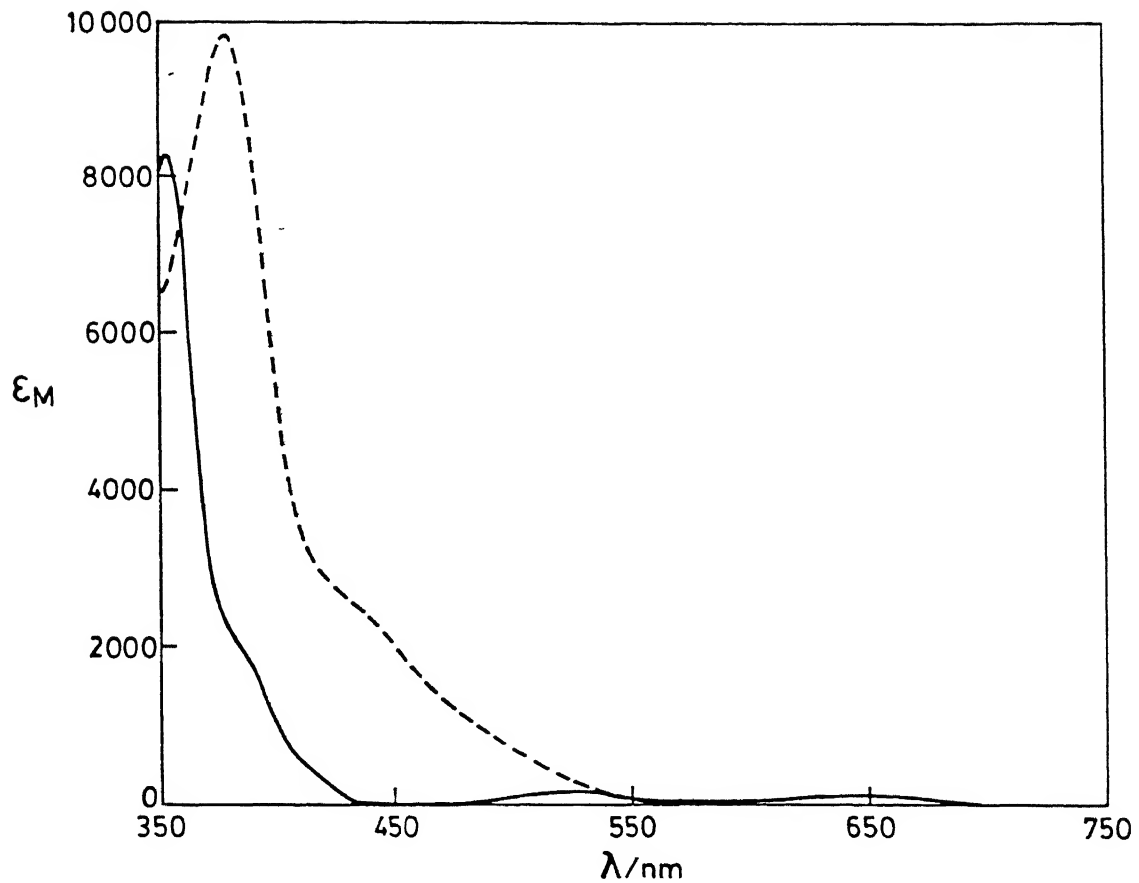


Fig. 3.17 UV-visible absorption spectra of $[\text{Et}_4\text{N}]_2[\text{W}^{\text{VI}}\text{O}_2(\text{mnt})_2]$ (-----) and $[\text{Et}_4\text{N}]_2[\text{W}^{\text{IV}}\text{O}(\text{mnt})_2]$ (—) in MeCN. Conc. 1×10^{-4} M.

and 365 nm. These could be assigned to dithiolate-Mo charge transfer transition, O-Mo charge transfer transition and dithiolene intraligand charge transfer transition respectively. However, confirmation of these assignments should have been made by resonance Raman study.

The electronic spectra of $[\text{Et}_4\text{N}]_2[\text{W}^{\text{VI}}\text{O}(\text{mnt})_2(\text{C}_2(\text{CO}_2\text{CH}_3)_2)]$ and $[\text{Et}_4\text{N}]_2[\text{W}^{\text{VI}}\text{O}(\text{S}_2)(\text{mnt})_2]$ are reproduced in Fig. 3.18 and Fig. 3.19 respectively. For the later complex, the lowest energy band at 478 nm may be assigned to $\pi_v^* \longrightarrow \text{d}(\text{W})$ as has been assigned for $[\text{MoO}(\text{S}_2)(\text{R}_2\text{dtc})_2]^{114}$.

For the complex, $[\text{Et}_4\text{N}]_2[\text{W}^{\text{VI}}\text{O}(\text{mnt})_2(\text{C}_2(\text{CO}_2\text{CH}_3)_2)]$ the lowest energy band at 435 nm can similarly be assigned to ligand (olefin) to metal charge transfer transition. The higher energy bands for both the complexes could not be assigned properly. The band positions of all these complexes are tabulated in Table 3.3.

Electronic spectra of the complex anions, $[\text{Mo}^{\text{V}}\text{OCl}(\text{mnt})_2]^{2-}$, $[\text{Mo}^{\text{IV}}\text{O}(\text{mnt})_2]^{2-}$ and $[\text{W}^{\text{IV}}\text{O}(\text{mnt})_2]^{2-}$ are shown in Fig. 3.20, Fig. 3.16 and Fig. 3.17 respectively. The interpretation of the electronic spectrum of the chloro complex can be made relatively easier because several theoretical treatments for the interpretation of electronic spectra of such complexes have been made¹¹⁵. As the complex contains *cis*-chloro attachment (*vide infra*) the symmetry will be reduced and detailed assignments are not possible. However, the lowest energy band at 650 nm may be assigned as $(\text{d}_{xy})^1 \longrightarrow (\text{d}_{xz,yz})^1$ transition. The second absorption at 491 nm may be then due to $(\text{d}_{xy})^1 \longrightarrow (\text{d}_{x^2-y^2})^1$ promotion. The shoulders on the intense absorption of charge transfer origin

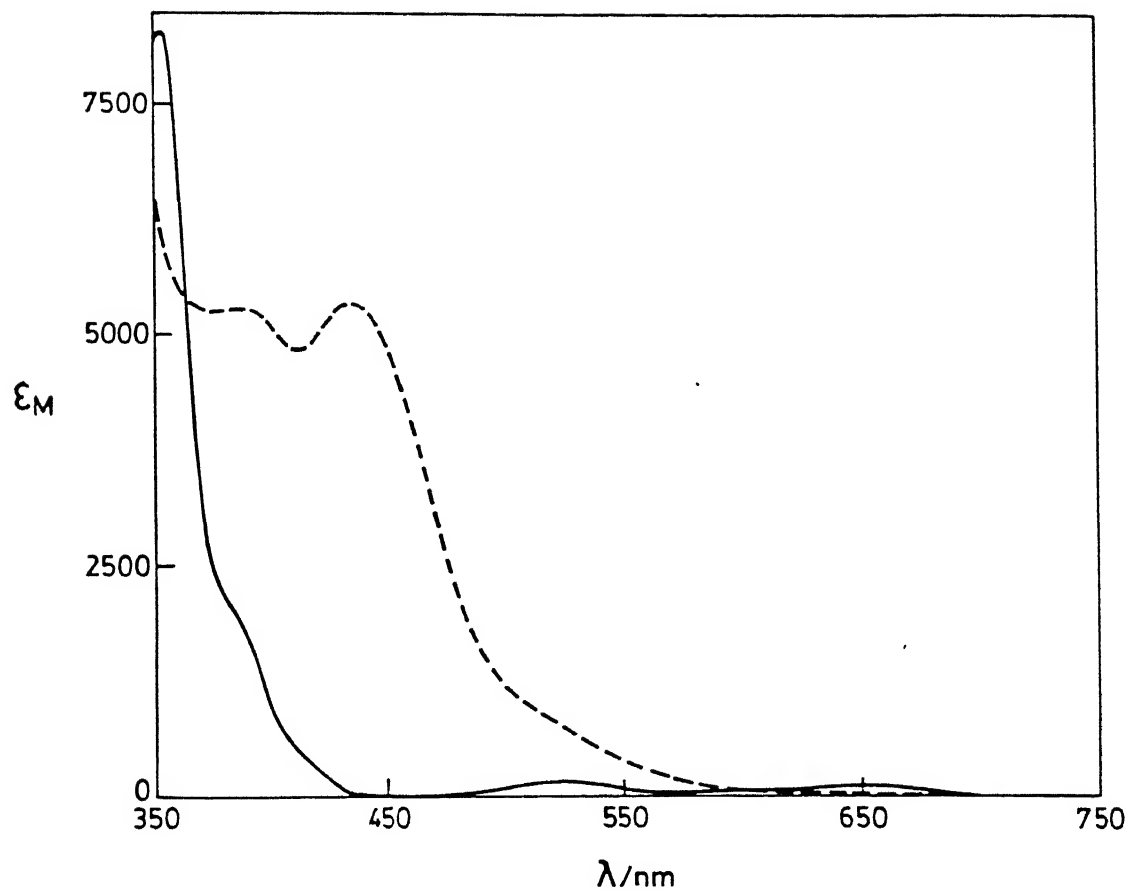


Fig. 3.18 UV-visible absorption spectra of $[\text{Et}_4\text{N}]_2[\text{W}^{\text{IV}}\text{O}(\text{mnt})_2]$ (—) and $[\text{Et}_4\text{N}]_2[\text{W}^{\text{VI}}\text{O}(\text{mnt})_2(\text{C}_2(\text{CO}_2\text{CH}_3)_2)]$ (----) in MeCN.
Conc. $1 \times 10^{-4}\text{M}$.

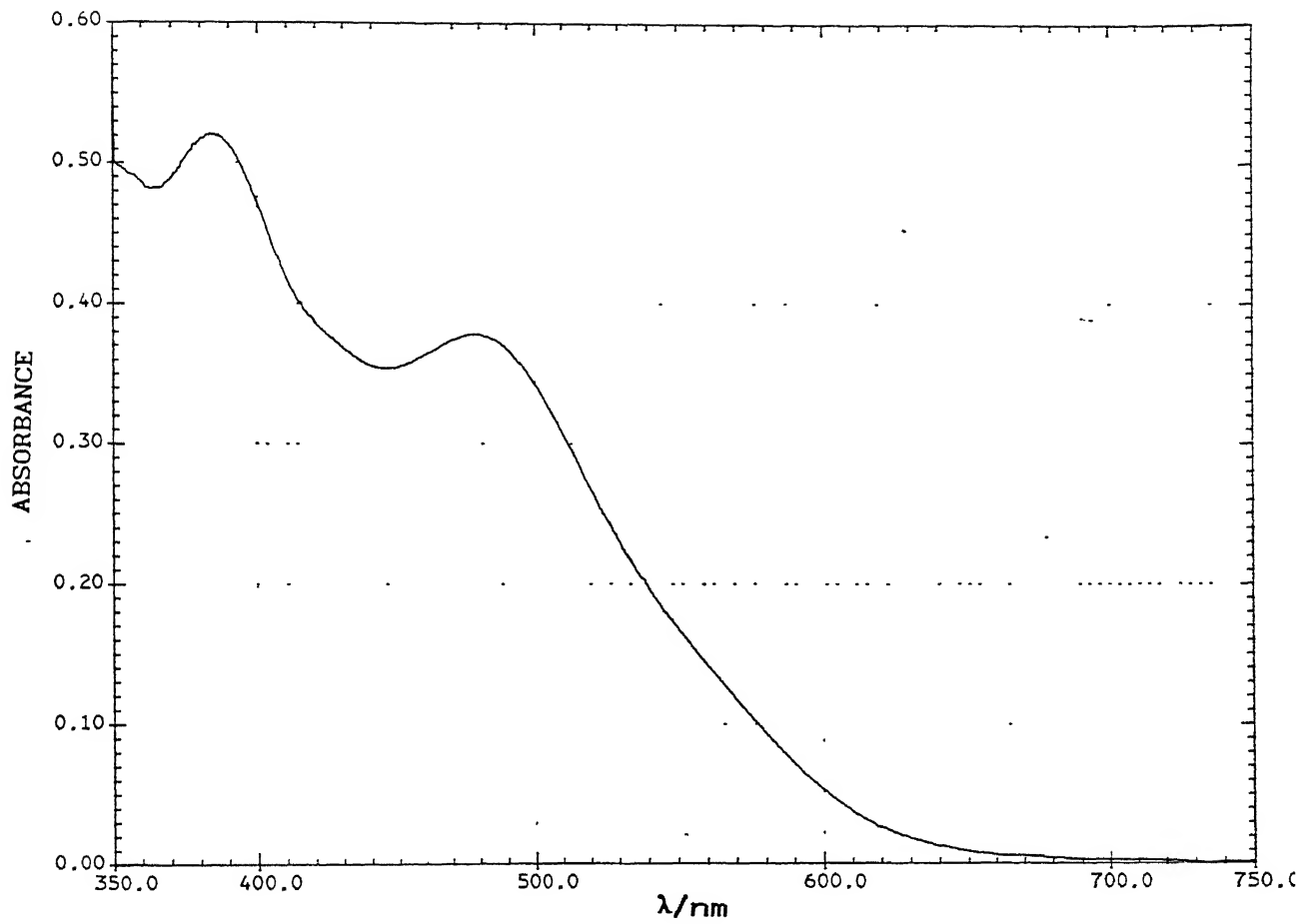


Fig. 3.19 UV-visible absorption spectrum of $[\text{Et}_4\text{N}]_2^{+} [\text{W}^{\text{VI}} \text{O}(\text{S}_2^-)_2 (\text{mnt})_2^-]$ in MeCN. Conc. 1×10^{-4} M.

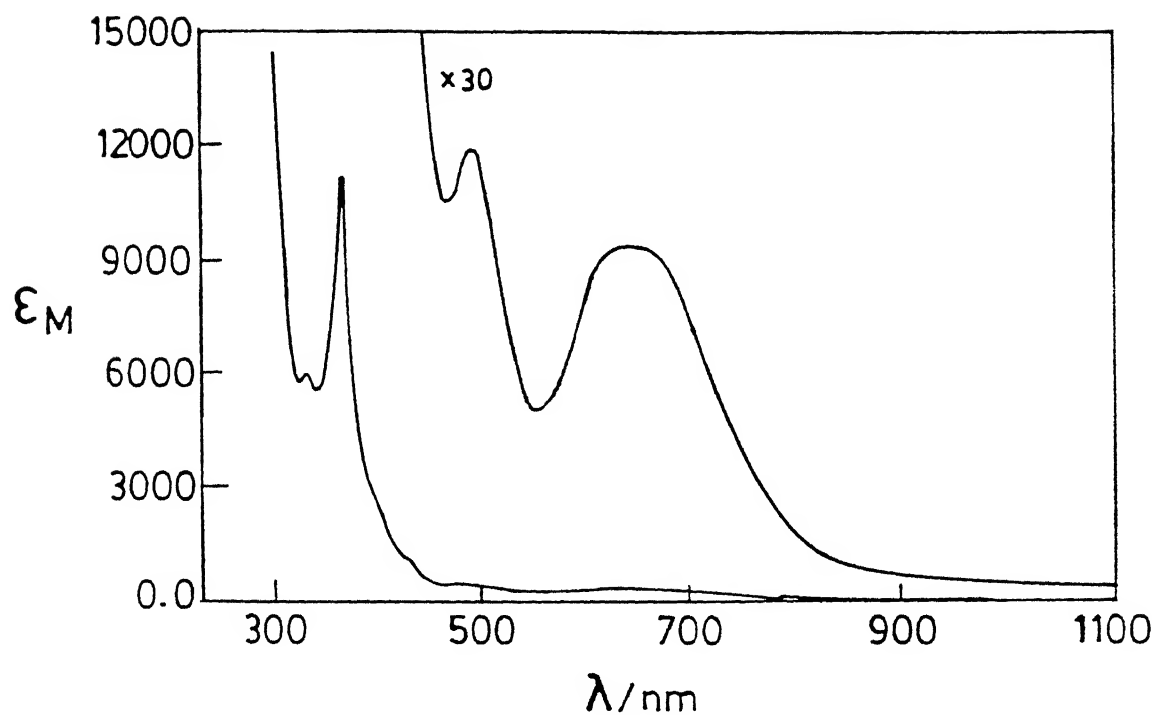


Fig. 3.20 UV-visible absorption spectrum of $[\text{Mo}^{\text{V}}\text{OCl}(\text{mnt})_2]^{2-}$ in CH_2Cl_2 in presence of excess of $[\text{Ph}_3\text{PNPPh}_3]\text{Cl}$. Conc. 1×10^{-4} M.

Table 3.3 UV-Vis Spectroscopic Data for Complexes^a in MeCN

complex	λ_{max} , nm (ϵ , M ⁻¹ cm ⁻¹)
[Mo ^{VI} O ₂ (mnt) ₂] ²⁻	525 (1620), 425 (6866), 365 (6244)
[W ^{VI} O ₂ (mnt) ₂] ²⁻	440 (sh), 380 (9880)
[W ^{VI} O(mnt) ₂ (C ₂ (CO ₂ CH ₃) ₂)] ²⁻	435 (5350), 388 (5290)
[W ^{VI} O(S ₂)(mnt) ₂] ²⁻	478 (3340), 385 (4550)

^aconc. taken 1×10^{-4} M.

could not be assigned properly. For the complex anion, $[\text{Mo}^{\text{IV}}\text{O}(\text{mnt})_2]^{2-}$ the two weak absorptions at 602 nm and 491 nm are definitely due to d-d transitions because of their low molar extinction coefficients. The shoulder is present at 395 nm on the strong charge transfer intraligand transition. The origin of this transition is not known. Curiously the corresponding tungsten complex, $[\text{Et}_4\text{N}]_2[\text{W}^{\text{IV}}\text{O}(\text{mnt})_2]$ showed very similar electronic spectrum with that of the molybdenum complex (Fig. 3.21). However, contrary to the normal expectation the two d-d bands in the tungsten complex are red shifted; whereas the strong intraligand charge transfer transition at 354 nm as well as the shoulder at 385 nm are expectedly blue shifted. The reason for this behavior is not known. There is no solvent dependency of these bands to cause such discrepancies as have been checked by taking electronic spectra of these two complexes in different solvents. However, the main feature remains the same. Solid state diffused reflectant spectra of these two species showed identical trends of d-d absorptions to those in solution state. Powder diffraction patterns of these two compounds suggest that they are isostructural (*vide infra*). All the band positions are tabulated in Table 3.4.

3.2.4 NMR SPECTROSCOPY.

The ^{13}C NMR spectra of the dimagnetic complexes, $[\text{Bu}_4\text{N}]_2[\text{Mo}^{\text{VI}}\text{O}_2(\text{mnt})_2]$, $[\text{Bu}_4\text{N}]_2[\text{Mo}^{\text{IV}}\text{O}(\text{mnt})_2]$, are presented in Fig. 3.22 and those of $[\text{Bu}_4\text{N}]_2[\text{W}^{\text{VI}}\text{O}_2(\text{mnt})_2]$, $[\text{Et}_4\text{N}]_2[\text{W}^{\text{IV}}\text{O}(\text{mnt})_2]$ and $[\text{Et}_4\text{N}]_2[\text{W}^{\text{VI}}\text{O}(\text{S}_2)(\text{mnt})_2]$ are shown in Fig. 3.23, Fig. 3.24, and Fig.

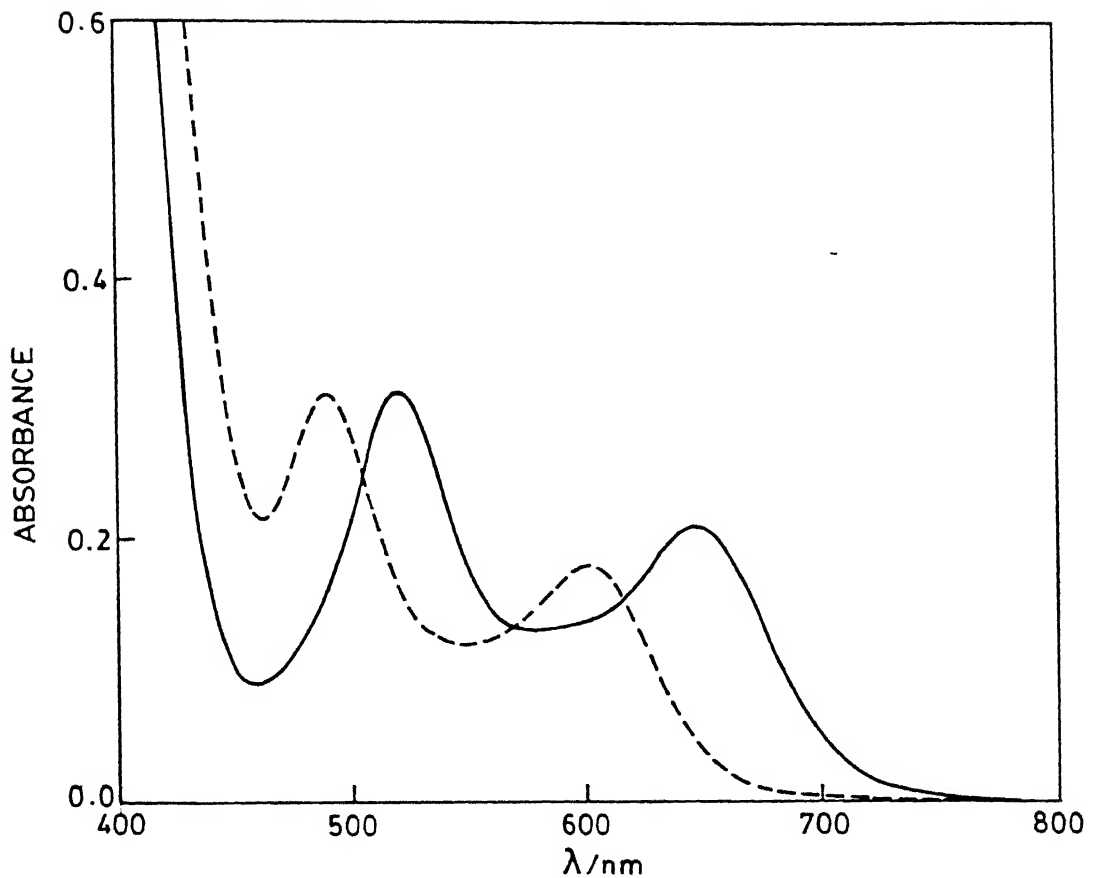


Fig. 3.21 UV-visible absorption spectra of $[\text{Mo}^{\text{IV}}\text{O}(\text{mnt})_2]^{2-}$ (----) and $[\text{W}^{\text{IV}}\text{O}(\text{mnt})_2]^{2-}$ (—) in MeCN. Conc. 1.2×10^{-3} M.

Table 3.4 UV-Vis Spectroscopic Data for Complexes^a

complex	λ_{max} , nm (ϵ , M ⁻¹ cm ⁻¹)
[Mo ^V OCl(mnt) ₂] ²⁻ ^b	650 (313), 491 (400), 336 (11300), 330 (6160)
[Mo ^{IV} O(mnt) ₂] ²⁻ ^c	602 (110), 491 (187), 395 (sh), 363 (10055)
[W ^{IV} O(mnt) ₂] ²⁻ ^c	649 (145), 521 (219), 385 (sh), 354 (8440)

^aconc. taken 1×10^{-4} M.

^bCH₂Cl₂ in presence of excess of [Ph₃PNPPh₃]Cl

^cMeCN

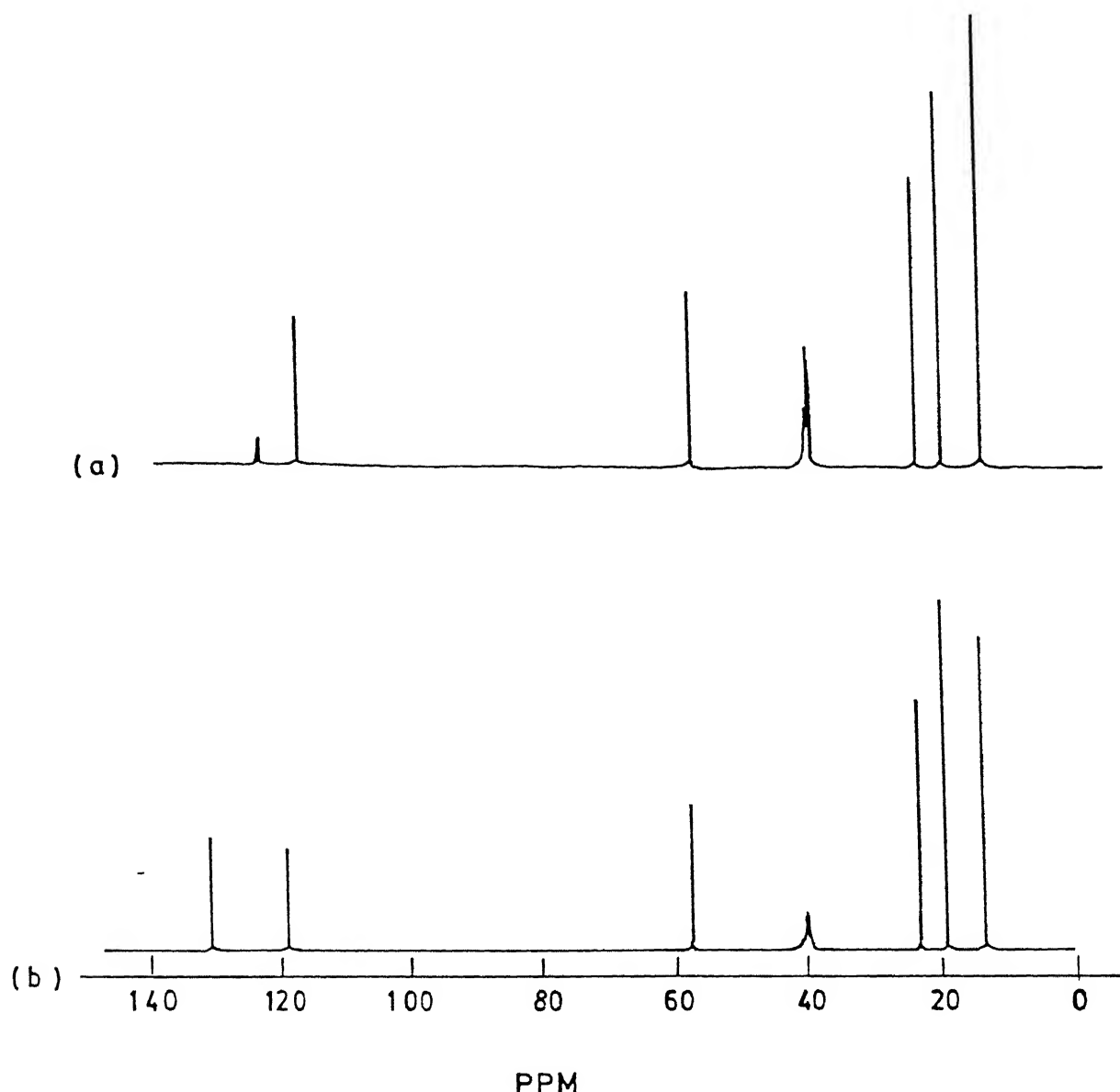


Fig. 3.22 ^{13}C NMR spectra of $[\text{Bu}_4\text{N}]_2[\text{Mo}^{\text{VI}}\text{O}_2(\text{mnt})_2]$ (a) and $[\text{Bu}_4\text{N}]_2[\text{Mo}^{\text{IV}}\text{O}(\text{mnt})_2]$ (b) in DMSO-d_6 .

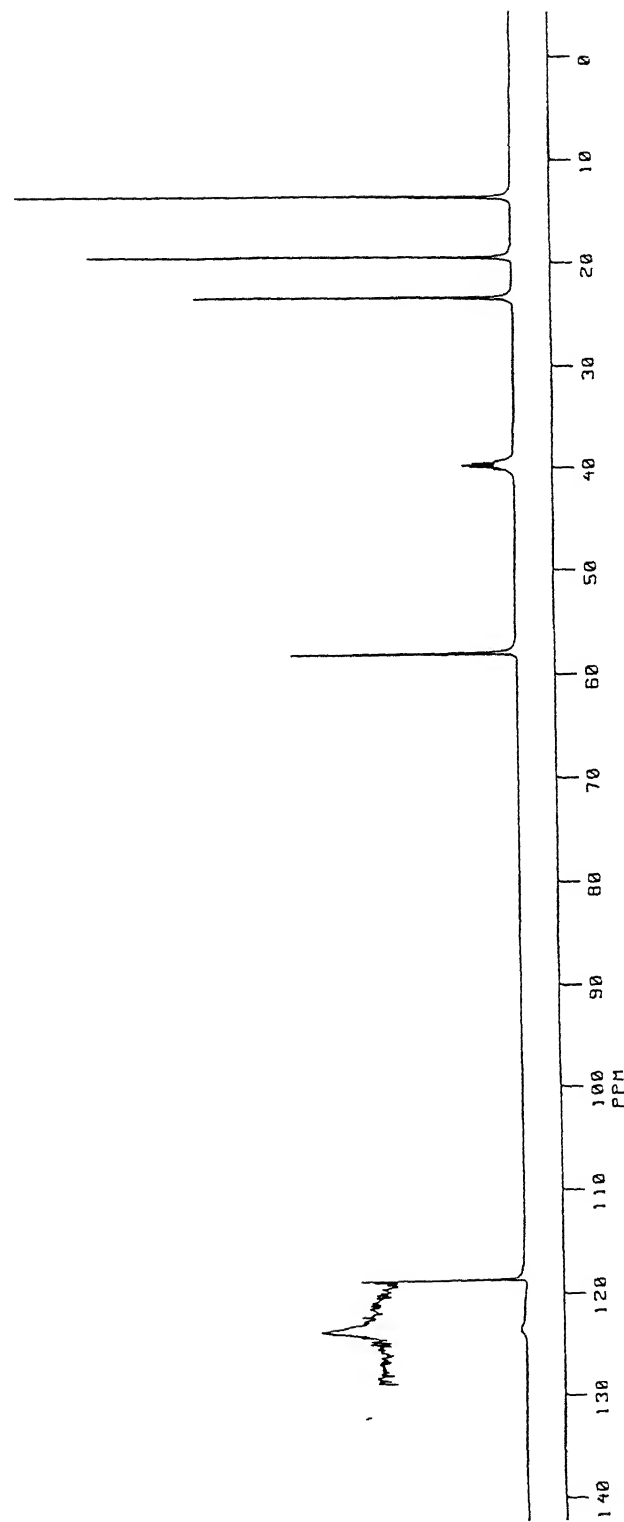


Fig. 3.23 ^{13}C NMR spectrum of $[\text{Bu}_4\text{N}]_2[\text{W}^{\text{Vl}}\text{O}_2(\text{mn})_2]$ in $\text{DMSO}-\text{d}_6$.

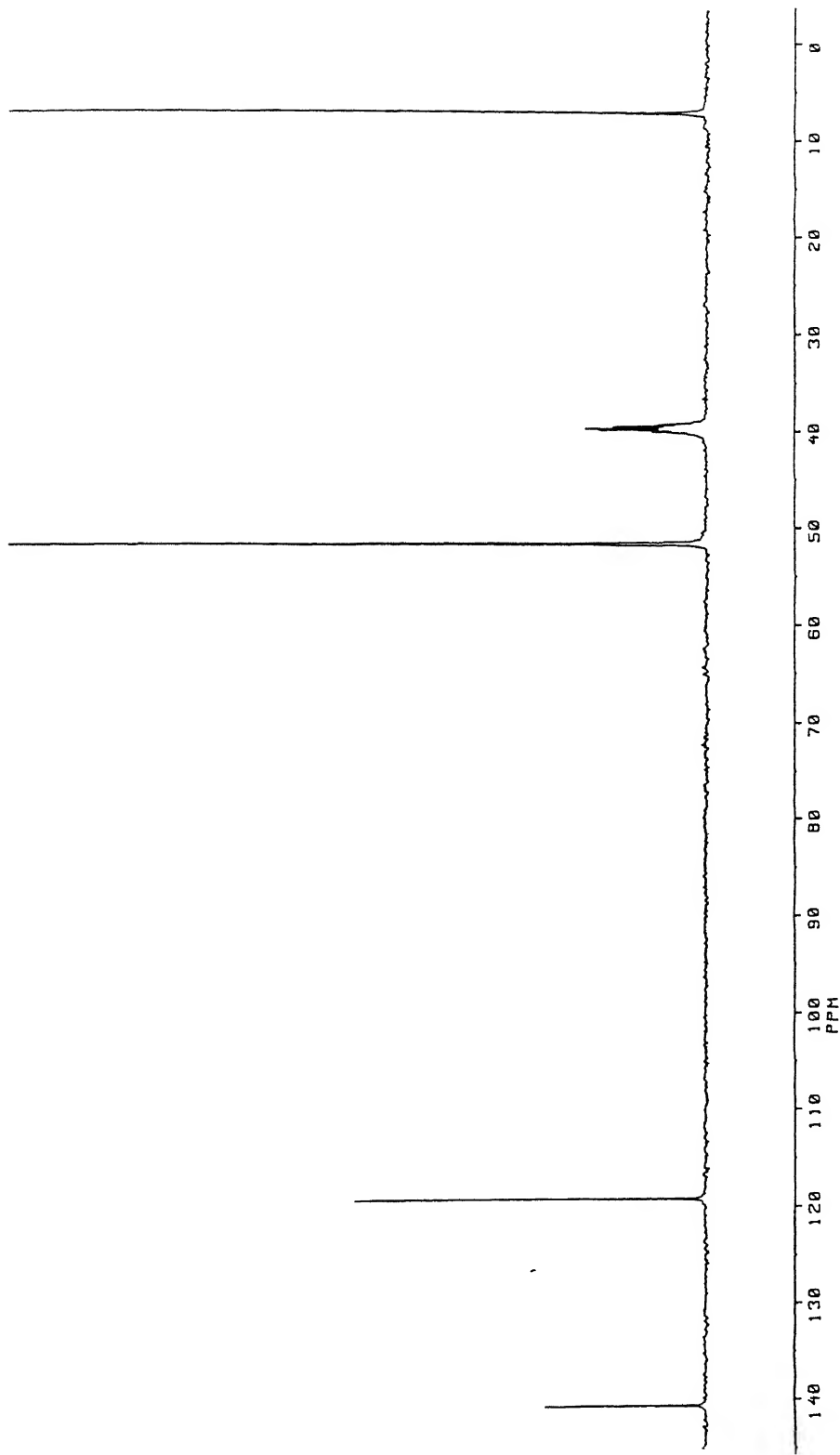


Fig. 3.24 ^{13}C NMR spectrum of $[\text{Et}_4\text{N}]_2[\text{W}^{\text{IV}}\text{O}(\text{mnt})_2]$ in DMSO-d_6 .

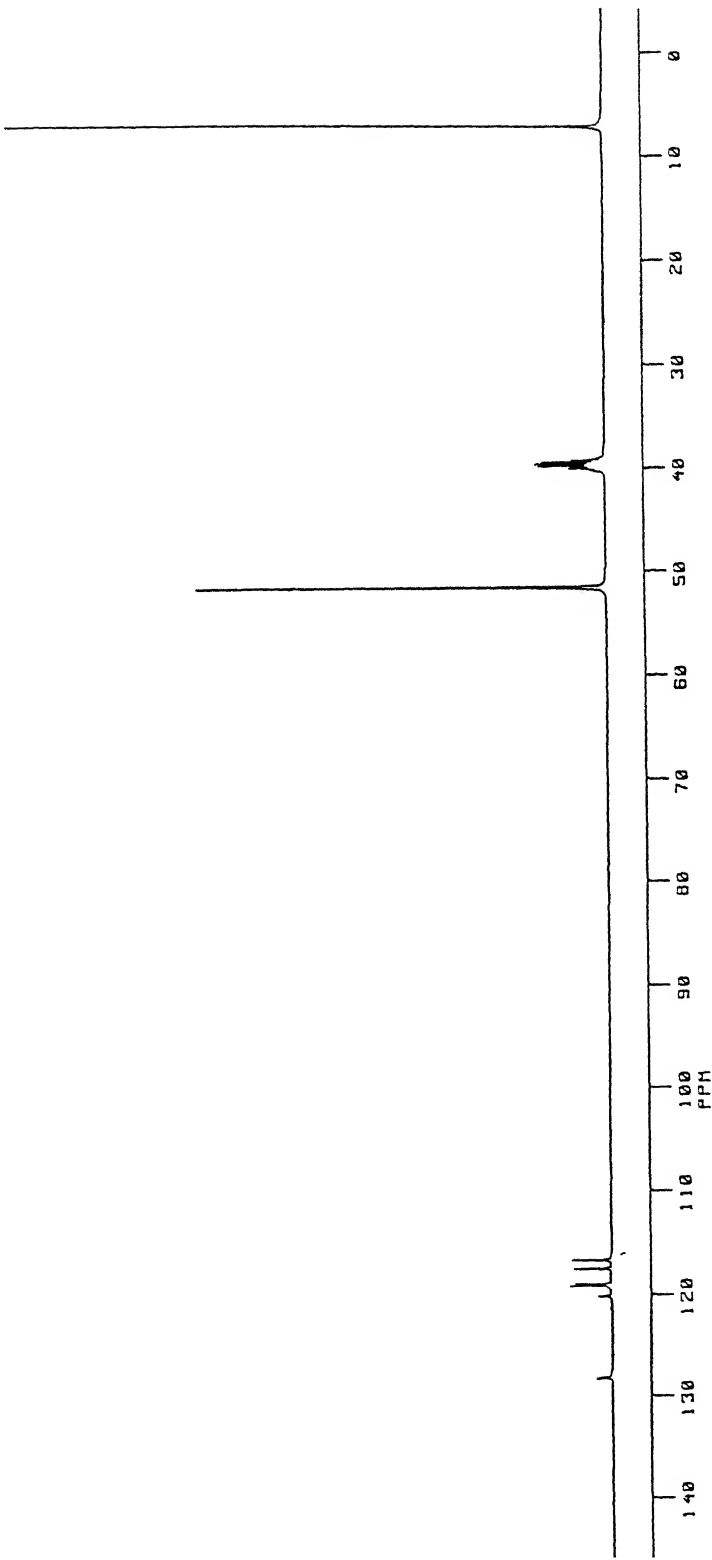


Fig. 3.25 ^{13}C NMR spectrum of $[\text{Et}_4\text{N}]_2[\text{W}^{\text{VI}}\text{O}(\text{S}_2^-)\text{(mnt)}_2]$ in DMSO-d_6 .

Table 3.5 ^{13}C NMR Spectral Data

102

 ^{13}C chemical shifts^a

compound	mnt (-CN, -C=C-)		$\alpha\text{-CH}_2$	$\beta\text{-CH}_2$	$\gamma\text{-CH}_2$	CH_3
	ligand		cation			
1	123.2	117.5	57.8	23.21	19.30	13.52
2	130.52	118.90	57.56	22.98	19.07	13.26
3	123.34	118.48	57.83	23.20	19.26	13.44
4	140.42	118.99	51.53	---	---	7.05
5	128.2 120.2 118.9 116.6	128.0 119.1 117.4	51.6	---	---	7.10

^a in DMSO-d₆; in parts per million relative to tetramethylsilane

1: [Bu₄N]₂[Mo^{VI}O₂(mnt)₂], 2: [Bu₄N]₂[Mo^{IV}O(mnt)₂]

3: [Bu₄N]₂[W^{VI}O₂(mnt)₂], 4: [Et₄N]₂[W^{IV}O(mnt)₂]

5: [Et₄N]₂[W^{VI}O(S₂)(mnt)₂].

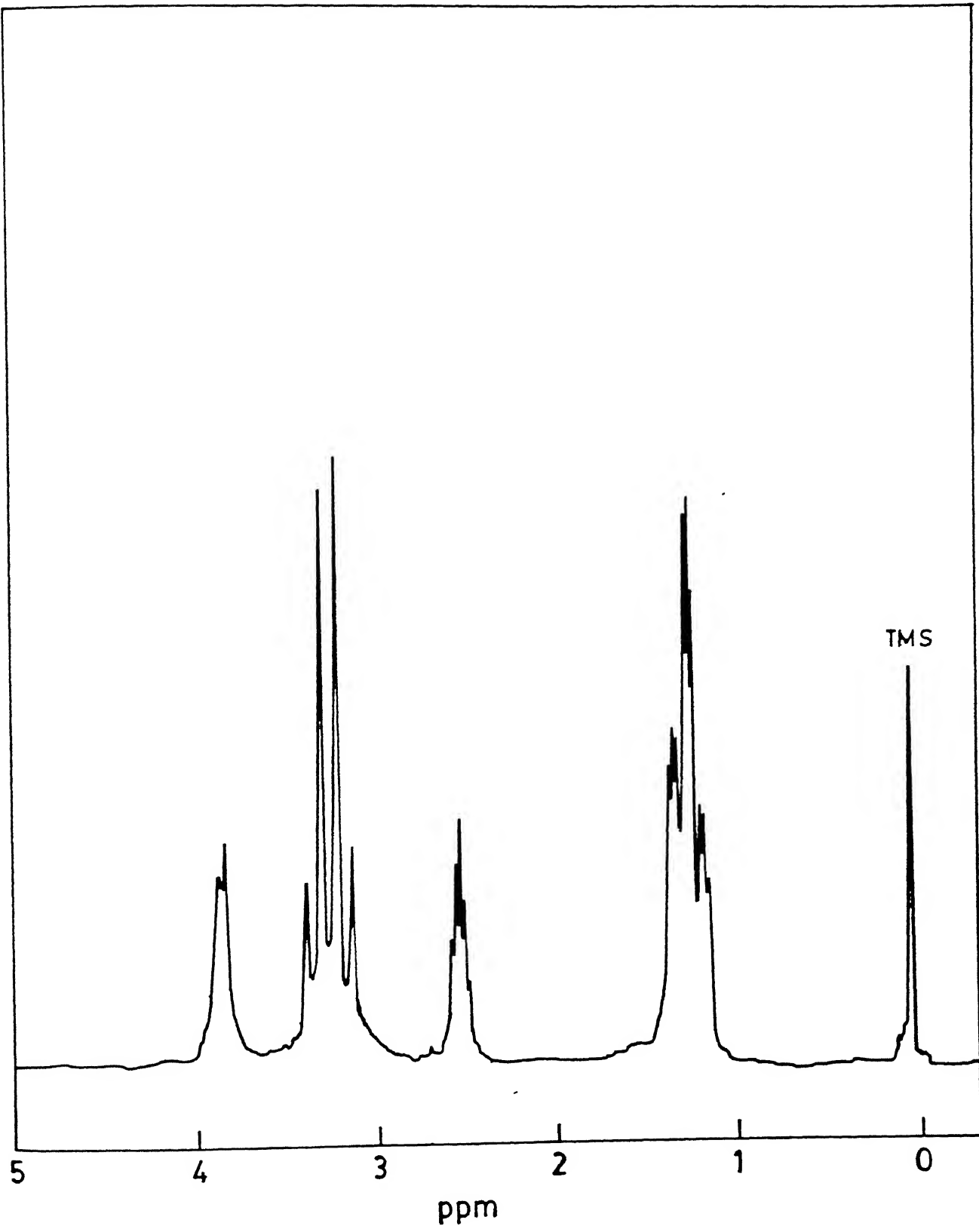


Fig. 3.26 ^1H NMR spectrum of $[\text{Et}_4\text{N}]_2[\text{W}^{\text{VI}}\text{O}(\text{mnt})_2(\text{C}_2(\text{CO}_2\text{CH}_3)_2)]$ in DMSO-d_6 .

Table 3.6 ^1H NMR Data for $[\text{Et}_4\text{N}]_2[\text{W}^{\text{VI}}\text{O}(\text{mnt})_2(\text{C}_2(\text{CO}_2\text{CH}_3)_2)]$

^1H chemical shifts ^a		
δ (ester CH_3)	δ (cation CH_2)	δ (cation CH_3)
3.86 (s, 3)	3.24 (q, 16)	1.21 (t, 24)
3.83 (s, 3)		

^ain DMSO-d₆; in parts per million relative to tetramethylsilane.

3.25 respectively. Nonprotonated carbon atoms have longer relaxation times and give small peaks. So it is very easy to recognize the nonprotonated nuclei, -C=C- and -CN of mnt²⁻ in these complexes. The spectral data are summarized in Table 3.5.

The ¹H NMR spectrum of [Et₄N]₂[W^{VI}O(mnt)₂C₂(CO₂CH₃)₂] in DMSO-d₆ at room temperature is displayed in Fig. 3.26 along with the assignments given in Table 3.6. Two methoxy carbonyl resonances at room temperature is consistent with the addition of DMAC *cis* to oxotungsten group suggesting a pentagonal bipyramidal geometry similar to oxomolybdenum-alkyne complex, MoO(Et₂dic)₂(DMAC)¹⁰³.

3.2.5 FAB MASS SPECTROSCOPY.

The negative ion FAB mass spectra of the complexes [Bu₄N]₂[Mo^{VI}O₂(mnt)₂] and [Bu₄N]₂[Mo^{IV}O(mnt)₂] can be divided into two parts: a "lower part" (M/Z < 350) where the matrix including their fragment ions, and some fragment ions of molecular anion can be observed and an "upper part" (M/Z > 350) with characteristic multiplet of the mononuclear unit. The upper division of the negative ion FAB mass spectra of these complexes are presented in Fig. 3.27. In Fig. 3.27b the entire complex, [Bu₄N]₂[Mo^{IV}O(mnt)₂] appears as molecular anion [MoO(mnt)₂]⁻ (M/Z = 394) and the ion pair [(Bu₄N)(MoO(mnt)₂)]⁻ (M/Z = 636). In Fig. 3.27a the entire complex, [Bu₄N]₂[Mo^{VI}O₂(mnt)₂] is observed with relatively low abundance as either [MoO₂(mnt)₂]⁻ (M/Z = 410) or [(Bu₄N)(MoO₂(mnt)₂)]⁻ (M/Z = 652). This spectrum (Fig. 3.27a) is dominated by reduced monooxo [MoO(mnt)₂]⁻. This is due to low

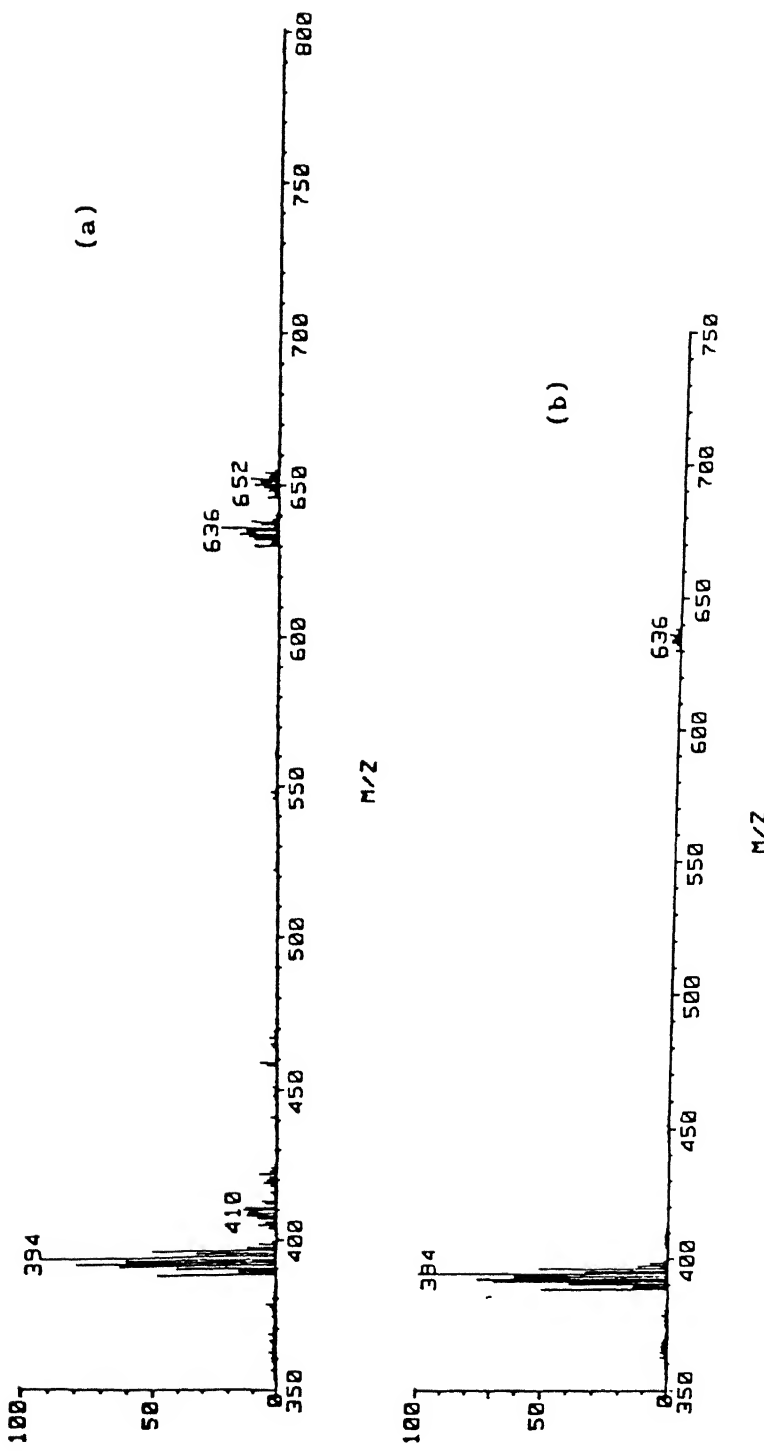


Fig. 3.27 Negative ion FAB mass spectra of $[Bu_4N]_2[Mo^{IV}O_2(mnt)_2]$ (a) and $[Bu_4N]_2[Mo^{IV}O_2(mnt)_2]$ (b).

thermal stability of the dioxo species. The degradation of MoO_2^{2+} to MoO^{2+} obviously indicates the conversion of dioxo to monooxo species which can be correlated with the facile oxo transfer reaction of $[\text{Mo}^{\text{VI}}\text{O}_2(\text{mnt})_2]^{2-}$ in solution (*vide infra*).

Similarly the negative ion FAB mass spectra of $[\text{Et}_4\text{N}]_2[\text{W}^{\text{VI}}\text{O}_2(\text{mnt})_2]$ and $[\text{Et}_4\text{N}]_2[\text{W}^{\text{IV}}\text{O}(\text{mnt})_2]$ excluding the lower parts are reproduced in Fig. 3.28. In Fig. 3.28a the complex $[\text{Et}_4\text{N}]_2[\text{W}^{\text{VI}}\text{O}_2(\text{mnt})_2]$ is observed as molecular anion $[\text{WO}_2(\text{mnt})_2]^-$ ($M/Z = 496$) and the ion pair $[(\text{Et}_4\text{N})(\text{WO}_2(\text{mnt})_2)]^-$ ($M/Z = 626$). In Fig. 3.28b the $M/Z = 480$ corresponds to the molecular anion, $[\text{WO}(\text{mnt})_2]^-$.

The negative ion FAB mass spectrum of the tungsten disulfur complex, $[\text{Et}_4\text{N}]_2[\text{W}^{\text{VI}}\text{O}(\text{S}_2)(\text{mnt})_2]$ is shown in Fig. 3.29 in which the entire complex is appeared with low abundance as either $[\text{WO}(\text{S}_2)(\text{mnt})_2]^-$ ($M/Z = 544$) or $[(\text{Et}_4\text{N})(\text{WO}(\text{S}_2)(\text{mnt})_2)]^-$ ($M/Z = 674$). The spectrum is fully dominated by the reduced monooxo $[\text{WO}(\text{mnt})_2]^-$ ($M/Z = 480$). This due to the larger reactivity of the disulfur complex and the degradation of WOS_2^{2+} to WO^{2+} indicates the easy conversion to disulfur to nonsulfur species which can be correlated with the facile sulfur abstraction reaction of this disulfur complex in solution (*vide infra*).

The negative ion FAB mass spectrum of the activated acetylene complex, $[\text{Et}_4\text{N}]_2[\text{W}^{\text{VI}}\text{O}(\text{mnt})_2(\text{C}_2(\text{CO}_2\text{CH}_3)_2)]$ is presented in Fig. 3.30 which shows the appearance of molecular anion $[\text{WO}(\text{mnt})_2(\text{C}_2(\text{CO}_2\text{CH}_3)_2)]^-$ ($M/Z = 622$) with relatively low abundance. Here again the spectrum is dominated by the reduced monooxo $[\text{WO}(\text{mnt})_2]^-$ ($M/Z = 480$). In all these FAB mass spectra,

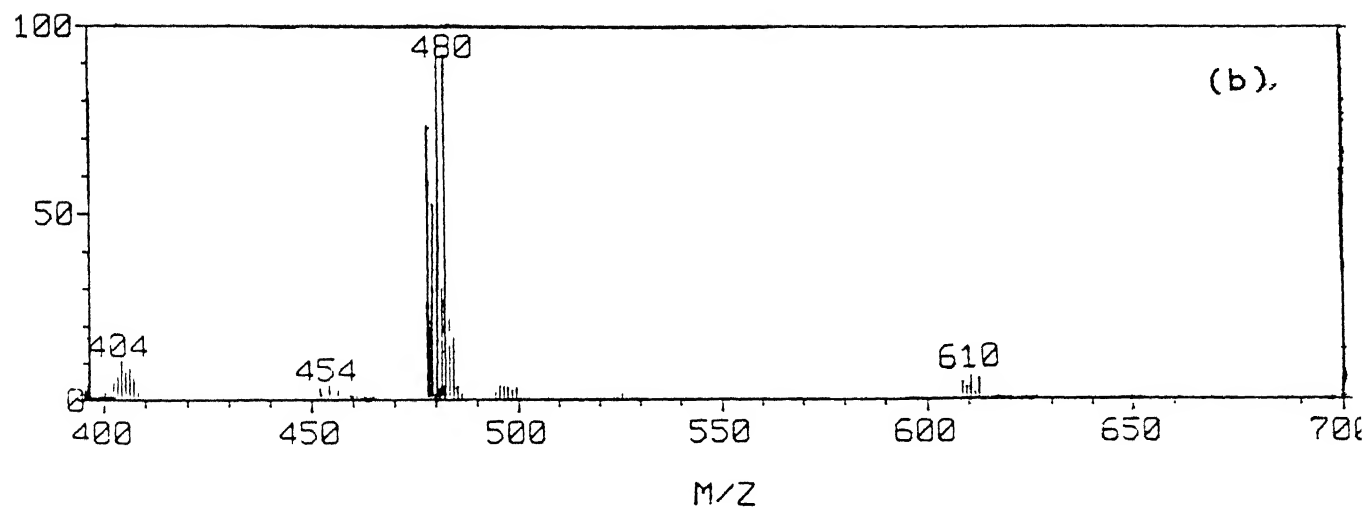
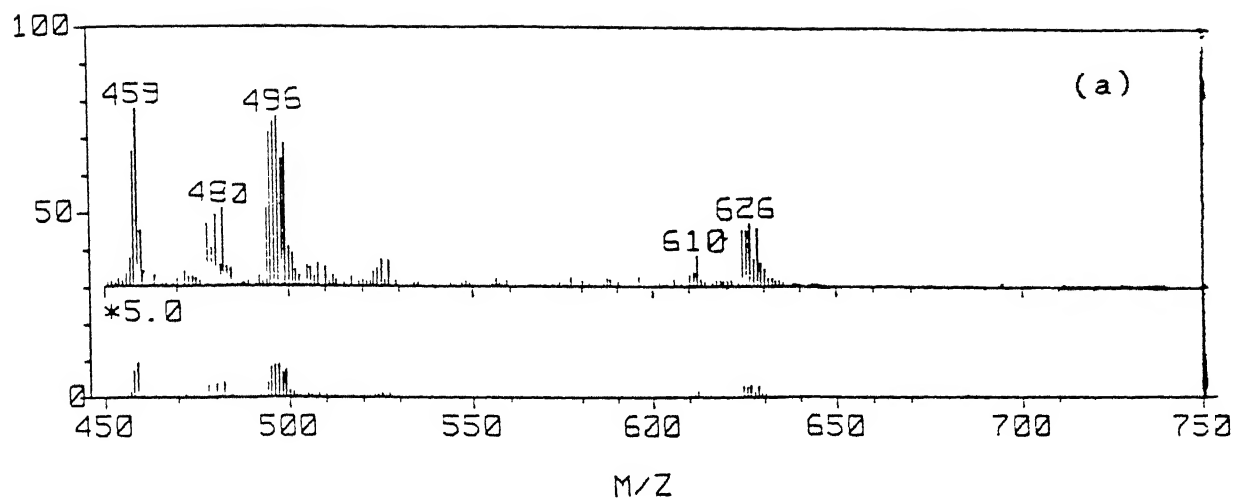


Fig. 3.28. Negative ion FAB mass spectra of $[Et_4N]_2[W^{VI}O_2(mnt)]_2$ (a) and $[Et_4N]_2[W^{IV}O_2(mnt)]_2$ (b).

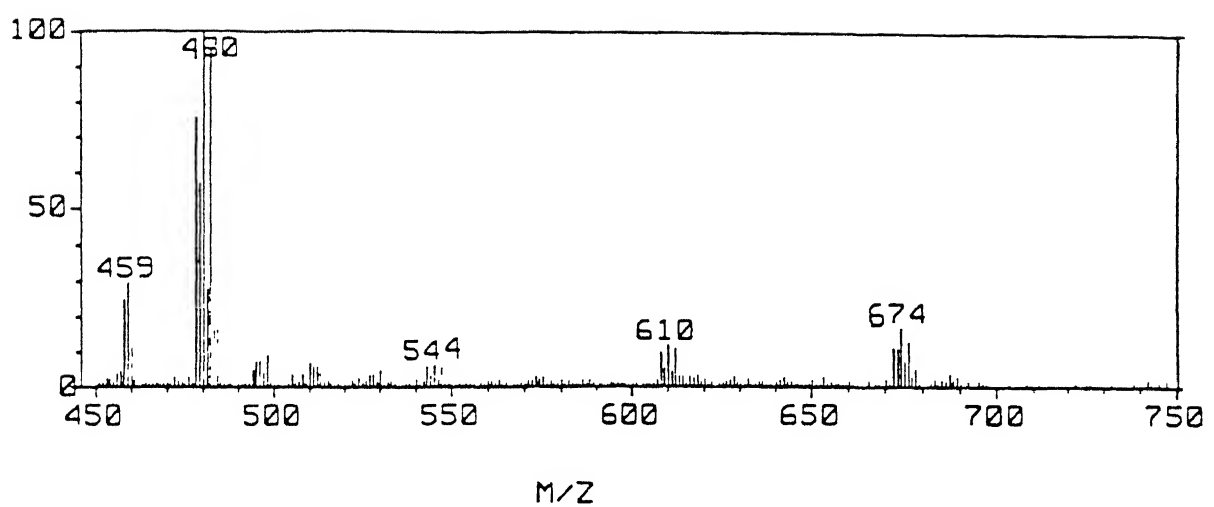


Fig. 3.29 Negative ion FAB mass spectrum of $[\text{Et}_4\text{N}]_2[\text{W}^{\text{VI}}\text{O}(\text{S}_2)^{-}(\text{mnt})_2]$.

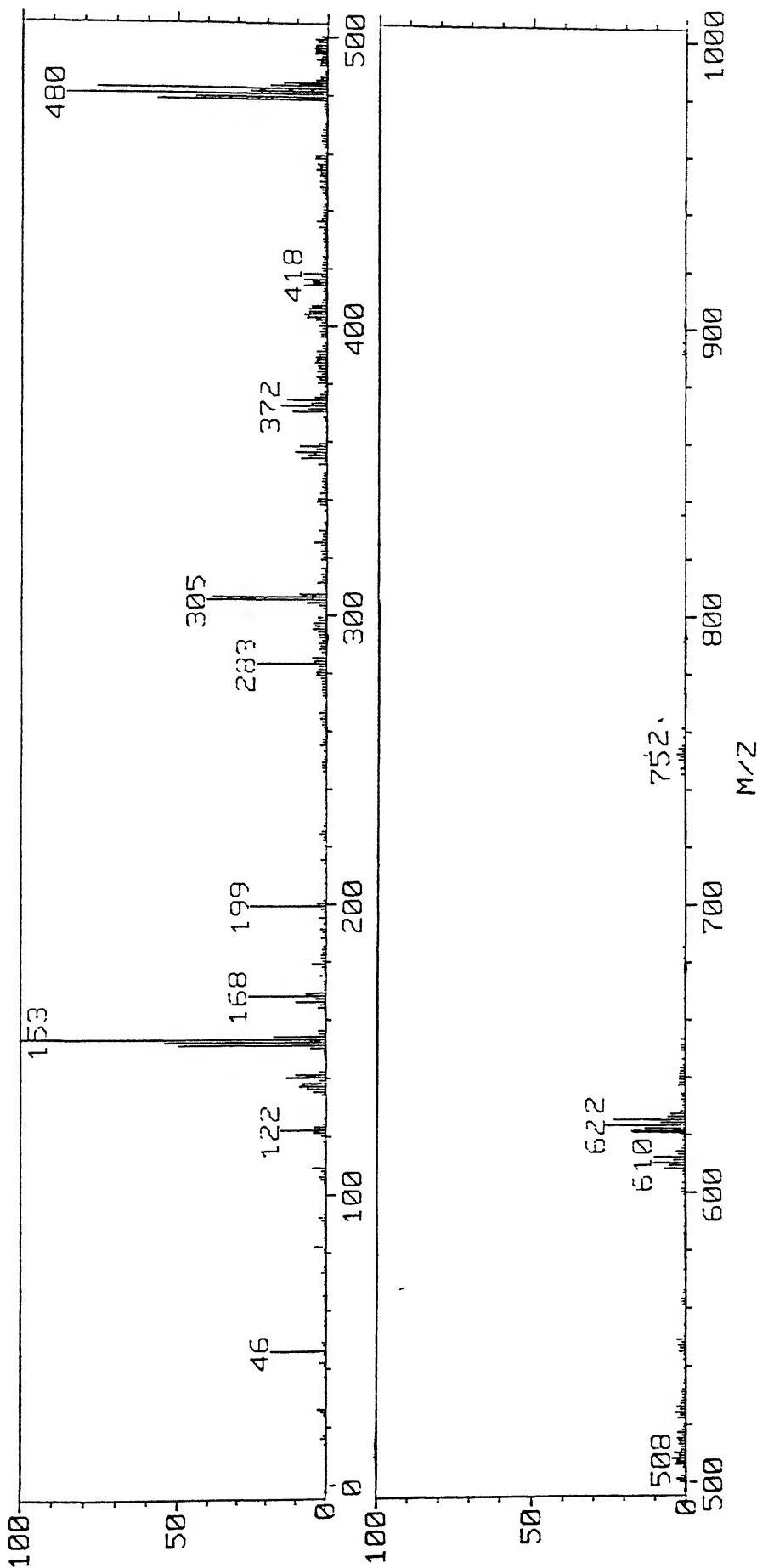


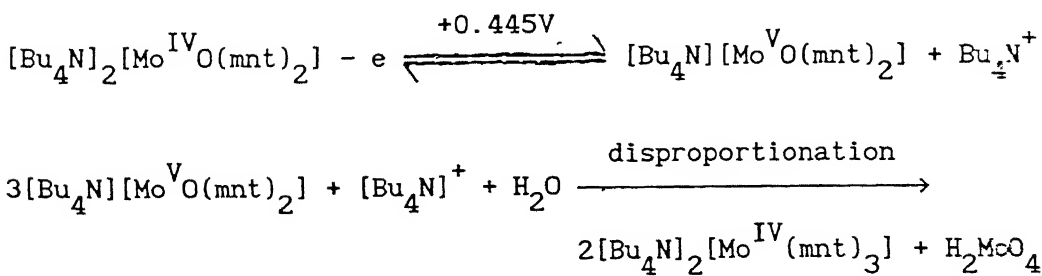
Fig. 3.30 Negative ion FAB mass spectrum of $[Et_4N]_2[W^{VI}O(O(mnt))_2(C_2(CO_2CH_3)_2)]$.

the observed isotope multiplets caused by the polyisotopic nature of Mo, W, O, S, N, C,H allowed an unambiguous assignment of the detected signals.

3.2.6 ELECTROCHEMISTRY.

The cyclic voltammogram (CV) $[\text{Bu}_4\text{N}]_2[\text{Mo}^{\text{VI}}\text{O}_2(\text{mnt})_2]$ in MeCN in the presence of Et_4NClO_4 exhibits a quasireversible reduction centered at -1.1V vs Ag/AgCl with $\Delta E_p = 100$ mV (Fig. 3.31a). The reduction remained quasireversible at lower temperature (0°C). Coulometric reduction of this complex in MeCN at -1.3V gave yellow red solution after addition of 2.28 electrons / molecule after a period of half an hour (when coulomb count was still increasing). The bands in the electronic spectrum of this yellow red solution are associated with the oxidized product of the free dithiolene ligand indicating that this electrolyzed solution is decomposed product lacking Mo-dithiolene ligation. A similar decomposed product has been obtained by the coulometric reduction of neutral compound, $\text{MoO}_2(\text{LNS}_2)$ (*vide infra*) which showed a nearly reversible CV centered at -0.88V vs SCE⁷⁸. A possible cause for the decomposition of $[\text{Bu}_4\text{N}]_2[\text{Mo}^{\text{VI}}\text{O}_2(\text{mnt})_2]$ in coulometric time scale may be the instability of this complex in the presence of OH^- generated in the reduction by traces of H_2O in the solvent. The electronic spectrum of this complex in 1:1 MeCN:phosphate buffer in water (pH ~ 8) exhibited rapid decrease in the height of the peaks (525 nm and 425 nm) with the end feature identical to the absorption spectrum of free dithiolene ligand within a period of

The tetravalent monooxo complex, $[\text{Bu}_4\text{N}]_2[\text{Mo}^{\text{IV}}\text{O}(\text{mnt})_2]$ undergoes a reversible one electron oxidation (with $\Delta E_p = 70 \text{ mV}$) in MeCN in the presence of Et_4NClO_4 at $+0.445\text{V}$ vs Ag/AgCl (Fig. 3.31b). However, on the coulometric time scale, this complex anion, $[\text{Mo}^{\text{IV}}\text{O}(\text{mnt})_2]^{2-}$ is converted to the tris dithielen complex $[\text{Mo}^{\text{IV}}(\text{mnt})_3]^{2-}$. Coulometric oxidation of $[\text{Bu}_4\text{N}]_2[\text{Mo}^{\text{IV}}\text{O}(\text{mnt})_2]$ at 0.70V , after the oxidation of ~ 1 electron / molecule (when coulomb count was still increasing rapidly) gave a bright green ESR silent solution. The CV of this bright green solution exhibits a new quasireversible oxidation at 0.70V vs Ag/AgCl and a new reversible oxidation process centered at -1.12V vs Ag/AgCl. This CV was identical with the CV obtained from the authentic molybdenum(IV) tris dithiolene complex, $[\text{Et}_4\text{N}]_2[\text{Mo}^{\text{IV}}(\text{mnt})_3]$ ^{87,106}. The electronic spectrum of this bright green solution was same as that of the authentic tris dithiolene complex. These results indicate that the initial one electron oxidized molybdenum(V) product, $[\text{Mo}^{\text{V}}\text{O}(\text{mnt})_2]^{1-}$, which is very unstable in MeCN, rapidly changes to tris dithielen complex, $[\text{Mo}^{\text{IV}}(\text{mnt})_3]^{2-}$, by disproportionation reaction with trace amount of water present in the solvent. These results are interpreted in Scheme 3.1.



Scheme 3.1

The CV of the complex, $[Bu_4N]_2[Mo^{IV}O(mnt)_2]$ in CH_2Cl_2 in the presence of Bu_4NCIO_4 as supporting electrolyte includes a chemically reversible ($i_{PA}/i_{PC} = 0.90$) one electron oxidation at +0.44V vs SCE (Fig. 3.32a). Coulometric oxidation of this complex at +0.70V removed 0.7 electron / molecule after a period of half an hour (when coulomb count was increasing slowly) and gave ESR active solution (*vide infra*). After coulometry the CV was almost intact but an additional weak redox couple (~~marked at Fig. 3.32b~~) was observed at ~ 0.60V vs SCE. The authentic tris dithiolene complex, $[Mo^{IV}(mnt)_3]^{2-}$ also exhibited a reversible couple in CH_2Cl_2 at 0.61V vs SCE. Thus after coulometry the solution contains mainly the MoO(V) species, $[Mo^V_2O(mnt)_2]^{1-}$ with some amount of $[Mo^{IV}(mnt)_3]^{2-}$. After one hour this solution did not give any ESR spectrum and the electronic spectrum of this was almost identical to the spectrum of the authentic tris dithiolene complex, $[Et_4N]_2[Mo^{IV}(mnt)_3]$ in CH_2Cl_2 . These results suggest that the initial one electron oxidized species, $[Mo^V_2O(mnt)_2]^{1-}$ disproportionate ultimately to $[Mo^{IV}(mnt)_3]^{2-}$ but in slow rate in CH_2Cl_2 and in faster rate in MeCN as shown in Scheme 3.1.

The pentavalent species, $[Mo^V_2OCl(mnt)_2]^{2-}$ exhibits a quasireversible CV in CH_2Cl_2 in the presence of large excess of $[Ph_3PNPPh_3]Cl$ with reduction centered at -0.20V vs SCE (Fig. 3.32). The reported MoOCl(V) complex with S_4 donor ligand, $Mo^V_2OCl(dttd)$ also shows the reversible reduction in DMF in the presence of excess Et_4NCl at -0.18V vs SCE^{80d}.

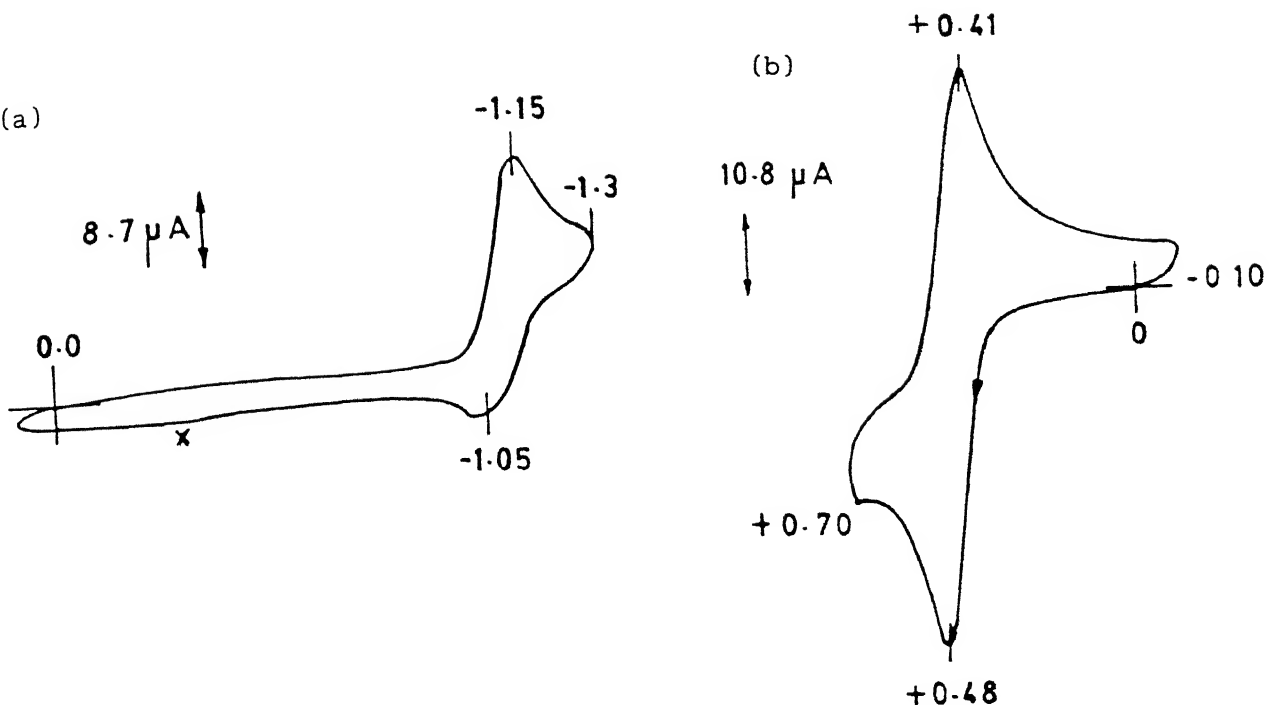


Fig. 3.31 Cyclic voltammograms of $[Bu_4N]^2[Mo^{VI}O_2(mnt)_2]$ (a) and $[Bu_4N]^2[Mo^{IV}O(mnt)_2]$ (b) in MeCN. Potential vs Ag/AgCl, 0.1M Et_4NCIO_4 , 100 mV/s. x, unidentified species

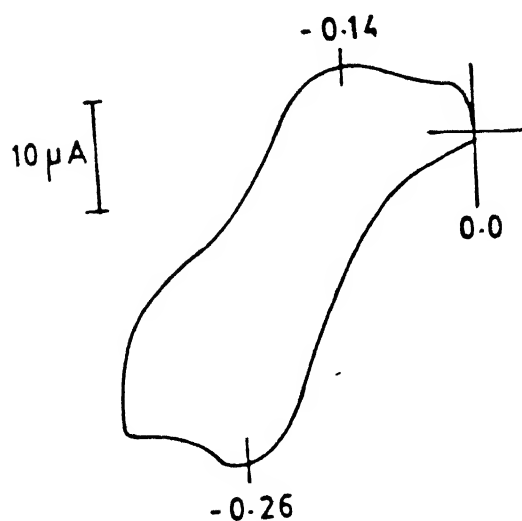


Fig. 3.32 Cyclic voltammogram of $[Ph_3PNPPh_3][Et_4N][Mo^V OCl(mnt)_2]$

The CV of the complex, $[\text{Et}_4\text{N}]_2[\text{W}^{\text{VI}}\text{O}_2(\text{mnt})_2]$ in MeCN in the presence of Et_4NClO_4 as supporting electrolyte shows an irreversible reduction at -1.50V vs Ag/AgCl as shown in Fig. 3.33b. Coulometric reduction of this complex in MeCN at -1.70V gave yellow brown solution which was found to be composed of decomposed products. The tetravalent monooxo complex, $[\text{Et}_4\text{N}]_2[\text{W}^{\text{IV}}\text{O}(\text{mnt})_2]$ exhibits a reversible CV at $+0.25\text{V}$ vs Ag/AgCl in MeCN as shown in Fig. 3.33a. Coulometric oxidation of this complex in MeCN at $+0.50\text{V}$, after addition of \sim one electron / molecule (when coulomb count was still increasing rapidly) gave a red pink ESR silent solution. The CV of this solution was identical to that of the authentic tris dithiolene complex, $[\text{Et}_4\text{N}]_2[\text{W}^{\text{IV}}(\text{mnt})_3]$ ^{87,106}. The electronic spectrum of this electrolyzed solution was also identical to that of the authentic tris dithiolene complex^{87,106}. Here also it can be concluded that $[\text{Et}_4\text{N}]_2[\text{W}^{\text{IV}}\text{O}(\text{mnt})_2]$ on electrolysis in MeCN (in coulometric time scale) disproportionates to $[\text{W}^{\text{IV}}(\text{mnt})_3]^{2-}$, a phenomenon similar to that of corresponding molybdenum complex (*vide supra*).

The tungsten disulfur complex, $[\text{Et}_4\text{N}]_2[\text{W}^{\text{VI}}\text{O}(\text{S}_2)(\text{mnt})_2]$ shows an irreversible reduction in MeCN at -1.45V vs Ag/AgCl as shown in the Fig. 3.34. The electrochemical behavior of the activated acetylene complex, $[\text{Et}_4\text{N}]_2[\text{W}^{\text{VI}}\text{O}(\text{mnt})_2(\text{C}_2(\text{CO}_2\text{CH}_3)_2)]$ in MeCN in the presence of Et_4NClO_4 includes an irreversible reduction at -1.75V vs Ag/AgCl (Fig. 3.35). The electrochemical parameters of the complexes are described in Table 3.7.

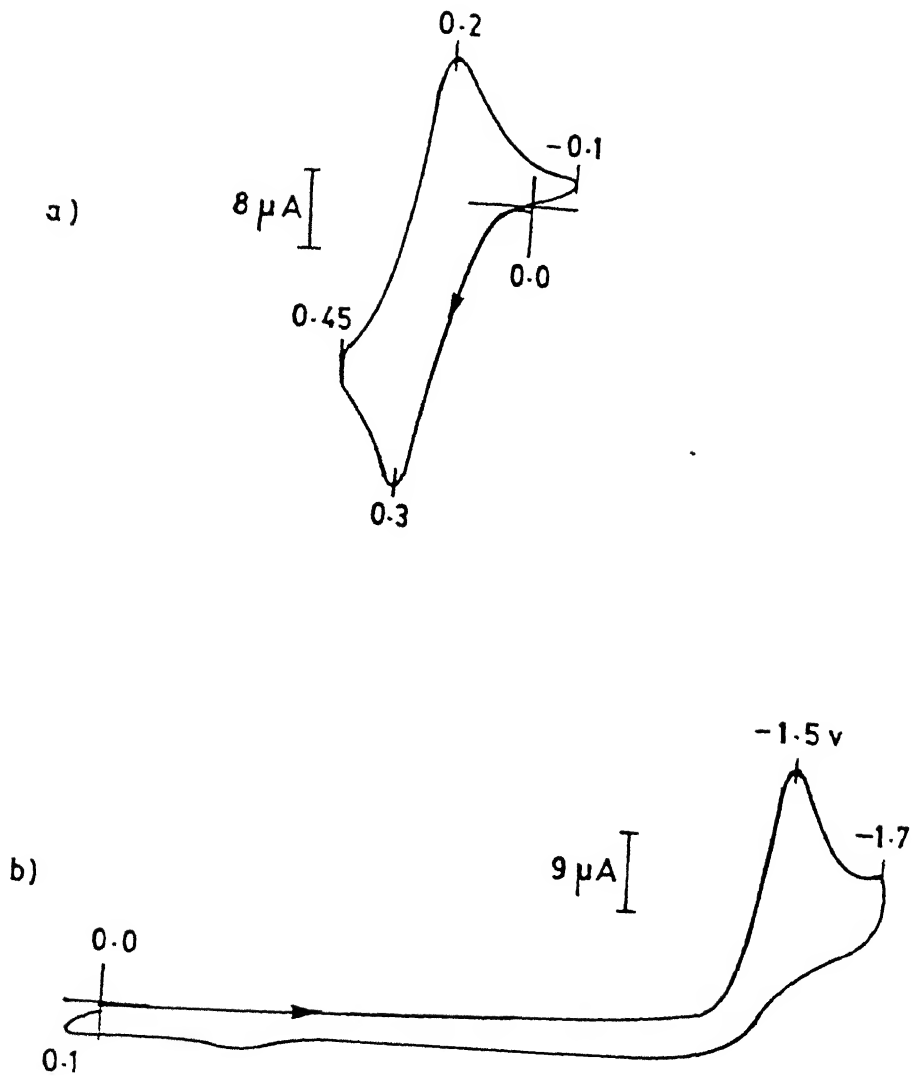


Fig. 3.33 Cyclic voltammograms of $[\text{Et}_4\text{N}]_2[\text{W}^{\text{IV}}\text{O}(\text{mnt})_2]$ (a) and $[\text{Et}_4\text{N}]_2[\text{W}^{\text{VI}}\text{O}_2(\text{mnt})_2]$ (b) in MeCN. Potential vs Ag/AgCl, 0.1M Et_4NClO_4 , 100 mV/s.

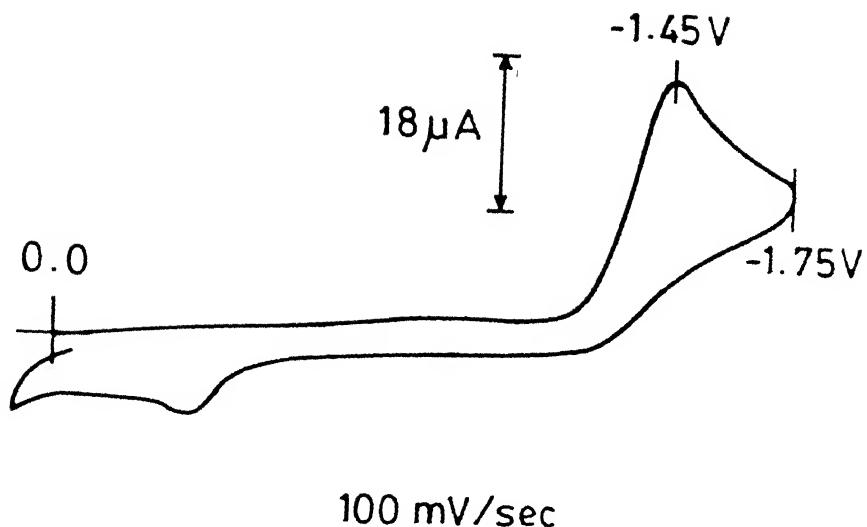


Fig. 3.34 Cyclic voltammogram of $[\text{Et}_4\text{N}]_2[\text{W}^{\text{VI}}\text{O}(\text{S}_2)(\text{mnt})_2]$ in MeCN.
Potential vs Ag/AgCl, 0.1M Et_4NClO_4 , 100 mV/s.

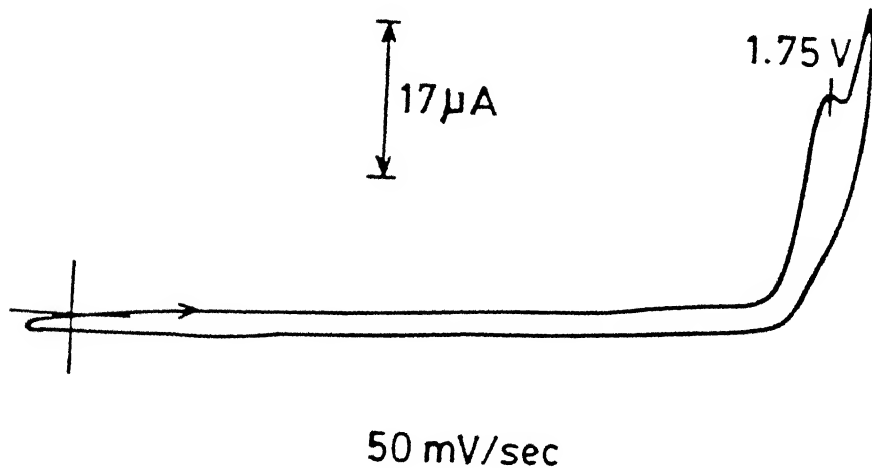


Fig. 3.35 Cyclic voltammogram of $[\text{Et}_4\text{N}]_2[\text{W}^{\text{VI}}\text{O}(\text{mnt})_2(\text{C}_2(\text{CO}_2\text{CH}_3)_2)]$
in MeCN.

Table 3.7 Electrochemical Parameters^a

complex	E_{PC} , v ^b	E_{PA} , v ^c
$[\text{Bu}_4\text{N}]_2[\text{Mo}^{\text{VI}}\text{O}_2(\text{mnt})_2]$	-1.15	-1.05
$[\text{Bu}_4\text{N}]_2[\text{Mo}^{\text{IV}}\text{O}(\text{mnt})_2]$	+0.41	+0.48
$[\text{Bu}_4\text{N}]_2[\text{W}^{\text{VI}}\text{O}_2(\text{mnt})_2]$	-1.50	---
$[\text{Et}_4\text{N}]_2[\text{W}^{\text{IV}}\text{O}(\text{mnt})_2]$	+0.2	+0.3
$[\text{Ph}_3\text{PNPPh}_3][\text{Et}_4\text{N}]^-$ $[\text{Mo}^{\text{V}}\text{OCl}(\text{mnt})_2]^d$	-0.26	-0.14
$[\text{Et}_4\text{N}]_2[\text{W}^{\text{VI}}\text{O}(\text{S})_2(\text{mnt})_2]$	-1.45	---
$[\text{Et}_4\text{N}]_2[\text{W}^{\text{VI}}\text{O}(\text{C}_2(\text{CO}_2\text{CH}_3)_2)]$	-1.75	---

^apotential vs Ag/AgCl, MeCN, 0.1M Et_4NClO_4 , 100 mV/s, room temperature. ^bCV, reduction peak. ^cCV, oxidation peak.

^dpotential vs SCE, CH_2Cl_2 , 0.1M Bu_4NClO_4 .

One electron oxidation of $[\text{Mo}^{\text{IV}}\text{O}(\text{mnt})_2]^{2-}$ at a Pt cathode in CH_2Cl_2 in the presence of Bu_4NClO_4 at room temperature gives ~ 65% monomeric molybdenum(V) product, $[\text{Mo}^{\text{V}}\text{O}(\text{mnt})_2]^{1-}$, which slowly disproportionates to $[\text{Mo}^{\text{IV}}(\text{mnt})_3]^{2-}$ and MoO_3 . The ESR spectrum of $[\text{Mo}^{\text{V}}\text{O}(\text{mnt})_2]^{1-}$ species in CH_2Cl_2 at 77K is indicative of rhombic symmetry with high g values ($\langle g \rangle_{\text{rt}} = 1.991$) (rt = room temperature) and low A values ($\langle A \rangle_{\text{rt}} = 3.025$) as expected for S_4 coordination (Fig. 4.25b, Table 4.5). The same ESR spectrum for $[\text{Mo}^{\text{V}}\text{O}(\text{mnt})_2]^{1-}$ species was obtained when $[\text{Bu}_4\text{N}]_2[\text{Mo}^{\text{IV}}\text{O}(\text{mnt})_2]$ was oxidized chemically by iodine (1:1 stoichiometry) in CH_2Cl_2 . No ESR data for oxo-Mo(V) complexes having dithiolene sulfur donors have been reported so far. The oxo bis(benzene-1,2-dithiolato) Mo(V) complex, $[\text{Ph}_4\text{P}][\text{MoO}(\text{bdt})_2]$ (*vide infra*) has been structurally established but with no ESR data⁹⁰. The ESR spectrum of the molybdenum(V) complex, $[\text{Mo}^{\text{V}}\text{O}(\text{SCH}_2\text{CH}_2\text{S})_2]^{1-}$ at 77K exhibited a rhombic signal with $\langle g \rangle_{\text{rt}} = 1.995$ ¹¹⁶ but the anisotropic ESR spectrum of the thiolate complex, $[\text{Mo}^{\text{V}}\text{O}(\text{SPh}_4)]^{1-}$ is axial with $\langle g \rangle_{\text{rt}} = 1.990$ ¹¹⁷. These observations suggest that the dithiolene sulfur donors are comparable to thiolate sulfur donor or ethane 1,2-sulfur donors in its effect on molybdenum(V) g values. Addition of excess of $[\text{Ph}_3\text{PNPPh}_3]\text{Cl}$ to the species, $[\text{Mo}^{\text{V}}\text{O}(\text{mnt})_2]^{1-}$ in CH_2Cl_2 results in a new molybdenum(V) species with significantly lower g value ($\langle g \rangle_{\text{rt}} = 1.974$) suggesting Cl^- coordination (*vide infra*).

The tungsten(V) species, $[\text{W}^{\text{V}}\text{O}(\text{mnt})_2]^{1-}$ can be identified in CH_2Cl_2 by ESR when $[\text{Et}_4\text{N}]_2[\text{W}^{\text{IV}}\text{O}(\text{mnt})_2]$ was oxidized

chemically by iodine (1:1 stoichiometry) in CH_2Cl_2 . The room temperature ESR spectrum for the $[\text{W}^{\text{V}}\text{O}(\text{mnt})_2]^{1-}$ species is shown in Fig. 3.36 with $\langle g \rangle_{\text{rt}} = 1.956$. Addition of excess of $[\text{Ph}_3\text{PNPPh}_3]\text{Cl}$ to the species, $[\text{W}^{\text{V}}\text{O}(\text{mnt})_2]^{1-}$ in CH_2Cl_2 resulted in one more ESR signal with $\langle g \rangle_{\text{rt}} = 1.895$ (Fig. 3.36) in addition to the ESR signal with $\langle g \rangle_{\text{rt}} = 1.956$. The appearance of ESR signal with lower g value is indicative of Cl^- coordination to tungsten(V). The difference in reactivity of $[\text{M}^{\text{V}}\text{O}(\text{mnt})_2]^{1-}$ ($\text{M} = \text{Mo}$ and W) towards Cl^- is thus apparent wherein the Mo(V)-oxo-chloro complex is completely formed in the presence of Cl^- .

3.2.8 X-RAY STUDY.

X-RAY POWDER DIFFRACTOGRAMS.

X-ray powder diffractograms of $[\text{Et}_4\text{N}]_2[\text{Mo}^{\text{IV}}\text{O}(\text{mnt})_2]$ and $[\text{Et}_4\text{N}]_2[\text{W}^{\text{IV}}\text{O}(\text{mnt})_2]$ were recorded and are reproduced in Fig. 3.37 and Fig. 3.38 respectively. The powder pattern of these two complexes was found to be similar. This suggests that $[\text{Et}_4\text{N}]_2[\text{Mo}^{\text{IV}}\text{O}(\text{mnt})_2]$ and $[\text{Et}_4\text{N}]_2[\text{W}^{\text{IV}}\text{O}(\text{mnt})_2]$ are structurally similar.

X-RAY CRYSTAL STRUCTURE OF $[\text{Bu}_4\text{N}]_2[\text{Mo}^{\text{VI}}\text{O}_2(\text{mnt})_2]$.

The crystal structure was measured at room temperature on CAD4 with FR 590 sealed tube generator with a molybdenum tube at 50 kV, 35 mA. The size of the crystal was $0.5 \times 0.2 \times 0.066$ mm. The diffraction power of the crystal was not great. The structure was solved with MOIEN program package (Delft Instruments X-ray

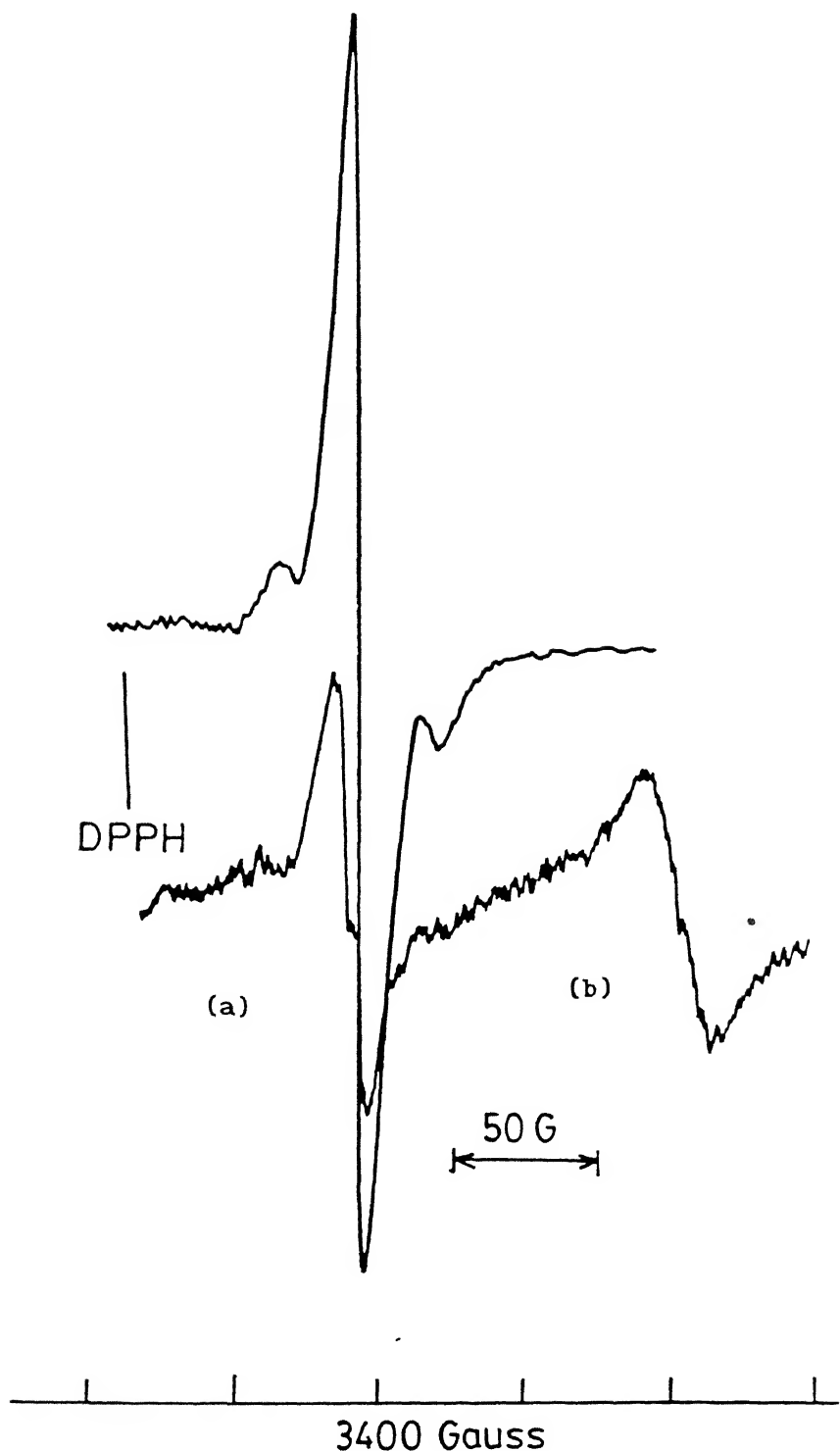


Fig. 3.36. ESR spectrum of $[W^V_0(\text{mnt})_2]^{1-}$ in CH_2Cl_2 formed by the reaction between equivalent amounts of $[\text{Et}_4\text{N}]_2[W^{\text{IV}}_0(\text{mnt})_2]$ and

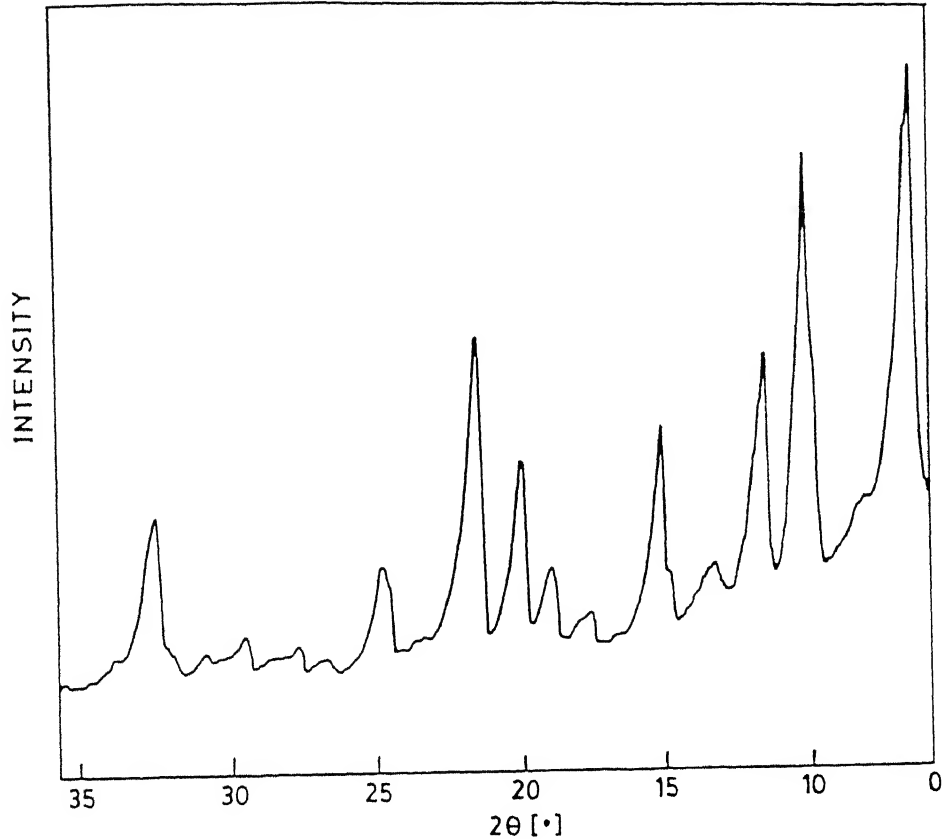


Fig. 3.37 X-ray powder diffractogram of $[\text{Et}_4\text{N}]_2[\text{Mo}^{\text{IV}}\text{O}(\text{mnt})_2]$.

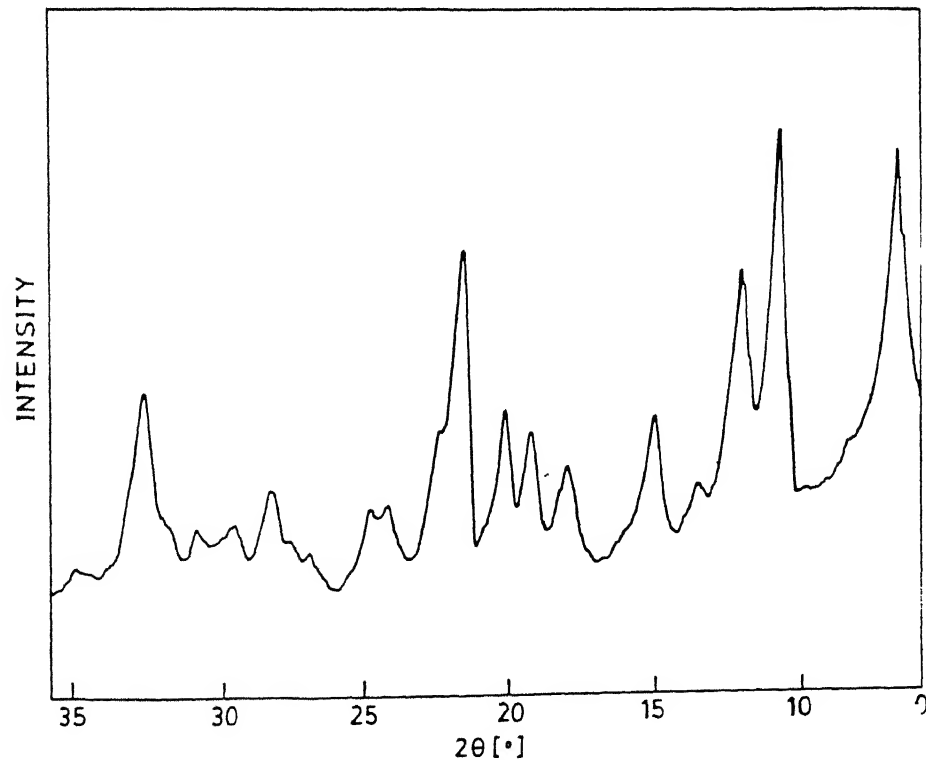


Fig. 3.38 X-ray powder diffractogram of $[\text{Et}_4\text{N}]_2[\text{W}^{\text{IV}}\text{O}(\text{mnt})_2]$.

Diffraction). The thermal parameters are quite large for the outer carbon atoms on the tetrabutylammonium cation and with the present room temperature data it is difficult to refine any atoms with anisotropic thermal parameters, except for the Mo atom and its six donor ligand atoms. To be able to refine this structure with anisotropic B's and all H atoms, it is essential to remeasure this crystal at liquid nitrogen temperature. However, the overall core structure of this complex ion has been identified.

The summary of the crystal data is given in Table 3.8. Positional and isotropic thermal parameters for the non-hydrogen atoms are listed in Table 3.9. The anisotropic thermal parameters for the Mo atom and its six donor ligand atoms are presented in Table 3.10. Selected bond lengths and angles are described in Table 3.11. The structure is shown in Fig. 3.39. The structure of the complex anion is a distorted octahedron with the oxo groups *cis* to each other and *trans* to sulfur atoms. The sulfur atoms *trans* to the oxo groups must compete with the strongly bound oxo groups for the same orbital¹¹⁸. This *trans* effect is reflected in the Mo-S₁ (2.606 Å^o) and Mo-S₃ (2.628 Å^o) distances compared to Mo-S₂ (2.448 Å^o) and Mo-S₄ (2.448 Å^o) distance which are not *trans* to terminal oxo groups. The ligand has the expected geometry. In the reported structure of [Mo^{IV}(mnt)₃]²⁻, in one of the chelate rings the bond angles Mo-S-C_{ethylene} and S-C_{ethylene}-C_{ethylene} are 108.1(4)^o and 120.8(4)^o respectively¹¹⁹. These corresponding angles of the mnt²⁻ ligand in the present complex are nearly similar (Table 3.11). The structure of MoO₂(Et₂dtc)₂ is also a distorted octahedron with the oxo groups *cis* to each other and

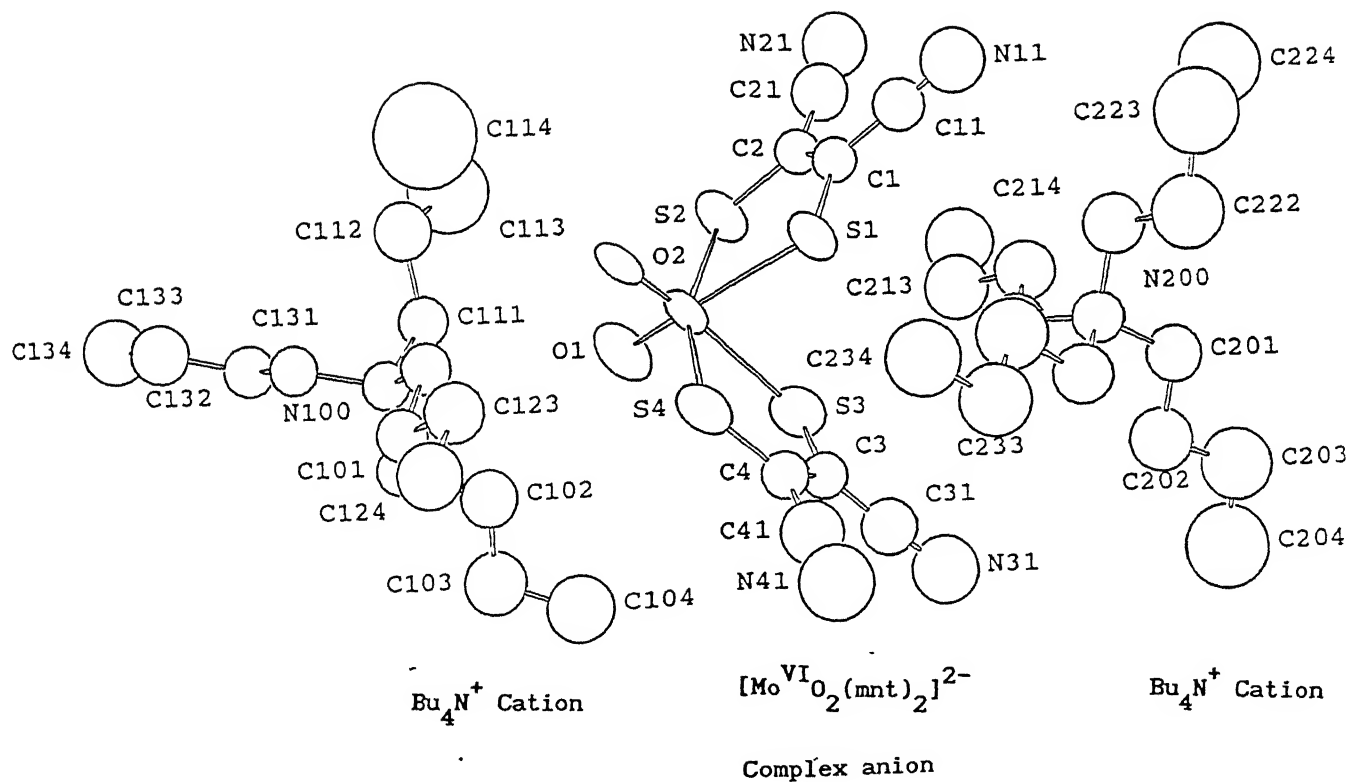


Fig. 3.39 Crystal structure of $[\text{Bu}_4\text{N}]_2[\text{Mo}^{\text{VI}} \text{O}_2(\text{mnt})_2]$.

Table 3.8 Summary of Crystal Data for $[\text{Bu}_4\text{N}]_2[\text{Mo}^{\text{VI}}\text{O}_2(\text{mnt})_2]$

chem. formula	$\text{C}_{40}\text{H}_{72}\text{MoN}_6\text{O}_2\text{S}_4$
fw	893.26
crystal shape	needle
crystal color	red
crystal dimensions, mm	0.5 x 0.2 x 0.066
space group	$\text{P}2_{1}2_{1}2_{1}$ (No. 14) $\text{P}_{\text{Li}/\text{N}}$ ($\text{Iv}, \text{14}$)
a, Å°	11.867 (0.01)
b, Å°	31.618 (0.01)
c, Å°	13. 585 (0.01)
α, deg	89.976 (0.04)
β, deg	102.655 (0.03)
γ, deg	90.032 (0.04)
V, Å°³	4973 (4)
radiation, Å°	λ (Mo-Kα) 0.71073
supplied power	50 kV, 35 mA
unweighted R factor	0.094
weighted R factor	0.109
esd of an observn of unit wt	6.180

**Table 3.9 Positional Parameters and Isotropic Thermal Parameters
(Å²)**

Atom	x	y	z	B (iso)
Mo	0.38255	0.09693	0.54505	
S1	0.50138	0.10058	0.73046	
S2	0.22845	0.08601	0.63634	
S3	0.35765	0.17887	0.56460	
S4	0.56380	0.12297	0.50946	
O1	0.26678	0.10030	0.44347	
O2	0.44031	0.04977	0.53331	
N11	0.48942	0.08457	0.99249	8.501
N21	0.15277	0.06434	0.87830	9.684
N31	0.50938	0.27838	0.59235	9.684
N41	0.76090	0.21058	0.51955	10.819
C1	0.40145	0.08849	0.80211	4.183
C2	0.29107	0.08165	0.76552	4.273
C3	0.48516	0.19924	0.55386	4.378
C4	0.57087	0.17514	0.53043	4.502
C11	0.44766	0.08620	0.90701	5.717
C21	0.21519	0.07273	0.82931	7.193
C31	0.49839	0.24179	0.57358	6.608
C41	0.67366	0.19426	0.52404	7.769
N100	0.31324	0.02354	0.21169	4.807
N200	0.57339	0.22677	0.93063	5.355
C101	0.28912	0.06359	0.15229	5.126

C102	0.30670	0.10539	0.21289	6.979
C103	0.27832	0.14379	0.14474	8.666
C104	0.30122	0.18360	0.20523	9.776
C111	0.22232	0.01936	0.27957	5.506
C112	0.23044	-0.02370	0.33489	7.301
C113	0.11236	-0.01500	0.38967	15.309
C114	0.11660	-0.04560	0.41394	25.036
C121	0.43099	0.02255	0.28253	5.173
C122	0.53091	0.03106	0.23041	5.313
C123	0.64427	0.03123	0.31316	6.725
C124	0.75084	0.03655	0.26742	7.740
C131	0.30614	-0.01402	0.14053	4.943
C132	0.18435	-0.02153	0.07360	5.555
C133	0.19614	-0.05972	0.01007	7.201
C134	0.07381	-0.07001	-0.05701	9.410
C201	0.55398	0.27143	0.97171	6.740
C202	0.52889	0.30425	0.89202	8.373
C203	0.51038	0.34594	0.94414	10.993
C204	0.48977	0.37914	0.86888	15.660
C211	0.46830	0.21183	0.84973	6.289
C212	0.35897	0.20739	0.89079	7.761
C213	0.25925	0.19973	0.80660	9.400
C214	0.14657	0.19463	0.83949	11.095
C221	0.59021	0.19375	1.01628	7.254
C222	0.70242	0.20245	1.09473	10.662
C223	0.71800	0.16545	1.17615	14.401
C224	0.63878	0.16516	1.23329	13.331

C231	0.67965	0.22980	0.87957	6.855
C232	0.71568	0.18538	0.85041	9.589
C233	0.81714	0.19183	0.79534	9.615
C234	0.85484	0.14737	0.76715	10.451

Table 3.10 Anisotropic Thermal Parameters (\AA^2)

Atom	b_{11}	b_{22}	b_{33}	b_{12}	b_{13}	b_{23}
Mo	0.01272	0.00148	0.00301	-0.00027	0.00429	0.00007
S1	0.00943	0.00161	0.00440	0.00024	0.00346	0.00035
S2	0.00979	0.00214	0.00509	-0.00143	0.00242	0.00043
S3	0.01092	0.00161	0.00785	0.00094	0.00542	0.00084
S4	0.01373	0.00173	0.00620	0.00123	0.01025	0.00070
O1	0.01221	0.00272	0.00497	-0.00157	-0.00014	0.00025
O2	0.02050	0.00148	0.00264	-0.00033	0.00476	0.00085

Table 3.11 Selected Bond Angles (deg) and Distances (\AA°)

Bond Distances			
Mo-O1	1.724	C1-C2	1.313
Mo-O2	1.664	C3-C4	1.364
Mo-S1	2.606	C1-S1	1.733
Mo-S2	2.448	C2-S2	1.755
Mo-S3	2.628	C3-S3	1.680
Mo-S4	2.448	C4-S4	1.673

Bond Angles			
O1-Mo-O2	104.57	Mo-S1-C1	103.952
O2-Mo-S2	106.968	C1-C2-S2	122.308
O1-Mo-S4	113.686	C2-C1-S1	124.890
S1-Mo-S2	79.787	C1-C2-C21	121.281
S3-Mo-S4	79.164	C2-C1-C11	120.547
Mo-S2-C2	108.538	Mo-S4-C4	108.115

trans to sulfur atoms¹²⁰. The X-ray structure of MoO₂(dttd) indicates that the molecule adopts distorted octahedral geometry with the thioether atoms trans to the terminal oxo groups which are cis to each other^{80d}. Therefore, the structure of [Mo^{VI}O₂(mnt)₂]²⁻ anion is completely consistent with other dioxomolybdenum complexes with similar donor atoms.

3.3 KINETIC EXPERIMENTS.

NaHSO₃ Saturation Kinetics.

All kinetic measurements were made by spectrophotometric method by use of Shimadzu 160 spectrophotometer provided with piezoelectric type thermostating devise for the regulation of temperature. Since one of the reactant (NaHSO₃) is insoluble in organic medium while the complex [Bu₄N]₂[Mo^{VI}O₂(mnt)₂] is insoluble in aqueous medium, the advantage was taken of a mixed solvent medium. In our preliminary investigation it was found that the oxygen had a profound influence on the kinetics of this redox process therefore all experiments were performed with deaerated solvents. So prior to use of these solvents, these were separately flushed with argon gas for at least half an hour or so depending on the volume required at a time for the experiments. MeCN was flushed for a relatively longer period and was used immediately thereafter. The fixed wave length at which the progress of the

reaction was monitored was chosen from the uv-vis spectrum of the complex and that of the corresponding product such that it gives considerably a large difference in the optical density for the accuracy of the results. As the half life of this reaction was almost of the order of few seconds, a modification¹²¹ of the conventional procedure was adopted for the kinetic measurements due to the unavailability of stopped flow apparatus. The concentration of stock solution of the complex in MeCN and separate stock solutions of NaHSO₃ in MeCN:H₂O (12:13, v/v) of different strength was so prepared such that a desired fixed concentration (4.098×10^{-4} M) of the complex in the reaction mixture was obtained while the NaHSO₃ concentration in the same mixture was of different concentrations. 2.9 ml of NaHSO₃ solution was placed in the spectrophotometer cell with the help of a calibrated pipette and left for a minute or so to acquire the desired temperature. 100 μ L of the complex in MeCN was placed with the help of a micropipette (sigma) on the flat button of glass attached to one end of a glass rod of five inches length. This was lowered into the cell and the solutions were mixed with a few vertical rapid movements of the rod. As soon as the button was dipped into the solution already contained in the cell a stopwatch was started. The progress of the reaction was monitored by the decay of absorbance at 535 nm as a function of time interval. Three to four kinetic runs were made for each NaHSO₃ concentration over the entire range of NaHSO₃ concentration used. The substrate concentration was varied ranging from 50×10^{-4} M to 250×10^{-4} M. The rate law was found to be always first order in Mo(VI) complex.

over this substrate concentration range as found by conventional graphical procedure. The equation for the decay of the Mo(VI) complex in terms of concentration follows the equation

$$C(t) = (A(t) - \epsilon_2 C_0) / \epsilon_1 - \epsilon_2 \quad ----- \quad (27)$$

where $C(t)$ is the concentration of the Mo(VI) complex at time t , $A(t)$ is the absorbance of reaction mixture solution at time t , C_0 is the initial concentration of the complex, $\epsilon_1 = 1580 \text{ M}^{-1} \text{cm}^{-1}$ and $\epsilon_2 = 82 \text{ M}^{-1} \text{cm}^{-1}$ are the molar extinction coefficients of the complex and that of the reduced Mo(IV) coplex respectively at 535 nm. The temperature at which this kinetics was performed was $20 \pm 0.1^\circ\text{C}$. During inhibition studies with Na_2SO_4 and KH_2PO_4 different stock solutions of the mixture of either NaHSO_3 and Na_2SO_4 or NaHSO_3 and KH_2PO_4 in $\text{MeCN:H}_2\text{O}$ (12:13) were so prepared such that in each of these of either type the concentration of inhibitor was fixed while the concentration of NaHSO_3 was varied. This allows the measurement of rate over a desired substrate concentration range when the inhibitor concentration remains fixed. The same substrate range was scanned with atleast two different fixed concentrations of either type of inhibitor. The temperature at which these inhibition studies were performed was 20°C and the monitoring wave length was also the same (535 nm).

Oxygen Atom Transfer Reaction Bestween $[\text{Bu}_4\text{N}]_2^{+} [\text{Mo}^{\text{VI}}\text{O}_2(\text{mnt})_2]^-$ and PPh_3

The experimental procedure in this case was typically that of conventional spectrophotometric type. A stock solution of the Mo(VI) complex of fixed concentration and stock solutions of PPh_3

of different concentrations in MeCN were taken. 1.5 ml of the Mo(VI) complex solution was placed in the spectrophotometer cell and was thermally equilibrated. 1.5 ml of PPh_3 solution was withdrawn from the stock which was thermally preequilibrated at the same temperature and was transferred in the cell. As soon as the solutions were mixed a stopwatch was started. Mixing was achieved gently by inverting the cell quite a few times with its stopper closed. As before the progress of the reaction was monitored at the fixed wave length of 525 nm. The same equation 27 holds for the decay of the Mo(VI) complex with ϵ_1 and ϵ_2 having values 1620 and $110 \text{ M}^{-1} \text{cm}^{-1}$ respectively. The rate law followed A + B type simple second order kinetics which reduces to pseudo first order type with large concentration of PPh_3 . The concentration of Mo(VI) complex in the mixture was $1 \times 10^{-4} \text{ M}$ while the PPh_3 concentration was varied. The experiment was repeated at 15°C , 25°C and 35°C temperatures with fixed different concentration of the PPh_3 . The kinetics of the same reaction was also performed in $\text{MeCN:H}_2\text{O}$ (1:1) medium but owing to solubility restriction, the highest concentration of PPh_3 that could be achieved in the reaction mixture was five times stronger than that of the complex. It was again found that the kinetics follows the same second order rate law but with the increased rate.

Reaction Between $[\text{Et}_4\text{N}]_2[\text{W}^{\text{VI}}\text{O}(\text{S}_2)(\text{mnt})_2]$ and PPh_3

The same procedure as cited just above was followed in this case at the fixed wave length of 478 nm and at four different temperatures with the initial concentration of the complex 1×10^{-4} M and that of the substrate 7.82×10^{-4} M in MeCN. The rate law was found to follow A + 2B type second order kinetics.

Reaction Between $[\text{Bu}_4\text{N}]_2[\text{Mo}^{\text{IV}}\text{O}(\text{mnt})_2]$ and $(\text{CH}_3)_3\text{NO} \cdot 2\text{H}_2\text{O}$

The solution of the complex, $[\text{Bu}_4\text{N}]_2[\text{Mo}^{\text{IV}}\text{O}(\text{mnt})_2]$ and that of $(\text{CH}_3)_3\text{NO} \cdot 2\text{H}_2\text{O}$ were prepared in acetone-acetic acid medium (effective pH 6). The procedure for kinetic measurements was the same as mentioned in the previous case. The reaction was monitored at 525 nm and at 20°C with varied concentrations of trimethylamine N-oxide and fixed concentration of the Mo(IV) complex (1×10^{-4} M). The rate was found to be first order in concentration of the complex when the concentration of the trimethylamine N-oxide was more than five times the concentration of the complex. The growth of optical density corresponding to the decay of Mo(IV) complex follows the equation,

$$C(t) = (\varepsilon_2 C_0 - A(t)) / (\varepsilon_2 - \varepsilon_1),$$

where $C(t)$ is the concentration of Mo(IV) complex at time t , C_0 is its initial concentration, $A(t)$ is the absorbance of reaction solution at 525 nm at time t , ε_1 and ε_2 are the molar extinction coefficients of the Mo(IV) and Mo(VI) complexes respectively having the same values as in MeCN.

Rate constants were determined from either the first order or second order decay curves for the progress of each reaction completing atleast three to four half lives. Since four to five runs carried out at each substrate concentration in most kinetic studies the mean value of the first order or second order rate constants and its standard deviation were computed from the data of the corresponding number of runs and fitting the experimental data by the method of least square. The errors in parameters based on slope measurements of these lines were evaluated according to the formula, $m \pm \frac{(m_1 - m_2)}{2\sqrt{N}}$, where m is the slope of the best fit line, m_1 is the slope of the line joining the top data points lying left of the centroid and the bottom data points lying at its right, while m_2 is the slope of the line joining the bottom data points lying left to the centroid to the top data points lying at its right obtained as the error limit of each data point and N is the number of data points displayed on the plot. The centroid is determined by $x_c = \sum x_i/N$ and $y_c = \sum y_i/N$, x_i and y_i represents the coordinate of the i^{th} data point. The addition, multiplication or division of two parameters having error limits to get the third parameter with error was evaluated by the use of formula for complex errors, such as

$$(A \pm \alpha) + (B \pm \beta) = A + B \pm \sqrt{\alpha^2 + \beta^2}$$

$$(A \pm \alpha) - (B \pm \beta) = A - B \pm \sqrt{\alpha^2 + \beta^2}$$

$$(A \pm \alpha)/(B \pm \beta) = A/B \pm A/B \sqrt{\left(\frac{\alpha}{A}\right)^2 + \left(\frac{\beta}{B}\right)^2}$$

α and β are the error limits of two experimentally determined parameters A and B respectively

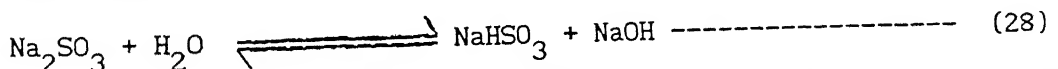
CHAPTER 4

FUNCTIONAL ANALOGUE REACTIONS

As discussed earlier a model complex should respond to react with physiological substrate at least stoichiometrically. If this stoichiometric reaction is feasible then the kinetics of this reaction may be studied to examine if the system follows enzymatic kinetic behavior. Finally this allows examination of substrate binding and product formation which can be substantiated by following inhibition studies.

4.1 FUNCTIONAL ANALOGUE REACTION OF SULFITE OXIDASE.

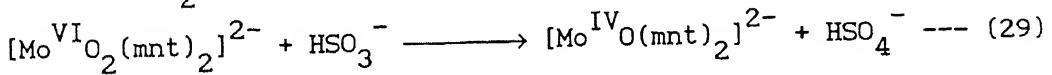
The complex anion, $[\text{Mo}^{\text{VI}}\text{O}_2(\text{mnt})_2]^{2-}$, has been tested first whether it responds with reducing substrate like sulfite (or bisulfite). Na_2SO_3 is not fairly soluble in organic solvents like MeCN. Furthermore, Na_2SO_3 when dissolved in water raises the pH of the solution because of the reaction,



The complex anion, $[\text{Mo}^{\text{VI}}\text{O}_2(\text{mnt})_2]^{2-}$, is not very stable in solution at pH greater than 7. Thus to avoid the hydrolysis of Na_2SO_3 and decomposition of $[\text{Mo}^{\text{VI}}\text{O}_2(\text{mnt})_2]^{2-}$ anion at higher pH than 7 the use of NaHSO_3 has been made. The stability of $[\text{Mo}^{\text{VI}}\text{O}_2(\text{mnt})_2]^{2-}$ anion in solution in presence of acid has been checked by

following electronic spectrum of $[\text{Mo}^{\text{VI}}\text{O}_2(\text{mnt})_2]^{2-}$ in MeCN where on addition of acetic acid the spectrum did not change. This suggests that on acidification protonation of the oxo group in $[\text{Mo}^{\text{VI}}\text{O}_2(\text{mnt})_2]^{2-}$ did not take place and molybdenum-dithiolene ligation remains intact. However, it has been observed that if the pH is lowered than 4 the $[\text{Mo}^{\text{VI}}\text{O}_2(\text{mnt})_2]^{2-}$ species is decomposed.

Thus when a brownish red solution of $[\text{Bu}_4\text{N}]_2[\text{Mo}^{\text{VI}}\text{O}_2(\text{mnt})_2]$ in MeCN-water (1:1) is mixed with NaHSO_3 solution in MeCN-water (1:1), the brown red color is immediately changed to green. The electronic spectrum of the green solution revealed the presence of $[\text{Bu}_4\text{N}]_2[\text{Mo}^{\text{IV}}\text{O}(\text{mnt})_2]$. The progress of the reaction between $[\text{Bu}_4\text{N}]_2[\text{Mo}^{\text{VI}}\text{O}_2(\text{mnt})_2]$ and NaHSO_3 in MeCN-water medium (3.3% water) monitored spectrophotometrically is shown in Fig. 4.1(a). Clean isobestic point is observed at 374 nm. The electronic absorption spectra of $[\text{Bu}_4\text{N}]_2[\text{Mo}^{\text{VI}}\text{O}_2(\text{mnt})_2]$ and $[\text{Bu}_4\text{N}]_2[\text{Mo}^{\text{IV}}\text{O}(\text{mnt})_2]$ are shown in Fig. 4.1(b) for comparison. These figures clearly demonstrate quantitative reduction of $[\text{Mo}^{\text{VI}}\text{O}_2(\text{mnt})_2]^{2-}$ by HSO_3^- to $[\text{Mo}^{\text{IV}}\text{O}(\text{mnt})_2]^{2-}$ according to the reaction (29),



Quantification of the formation of sulfate in the above reaction has been made gravimetrically by BaSO_4 method¹⁰⁵. Blank reactions were performed to take care of the presence of contaminated sulfate in bisulfite used. This analysis confirmed the stoichiometric conversion of bisulfite to sulfate as shown in equation (29).

The kinetics of the oxygen transfer reaction from $[\text{Mo}^{\text{VI}}\text{O}_2(\text{mnt})_2]^{2-}$ by HSO_3^- in MeCN-water (1:1) solution have been

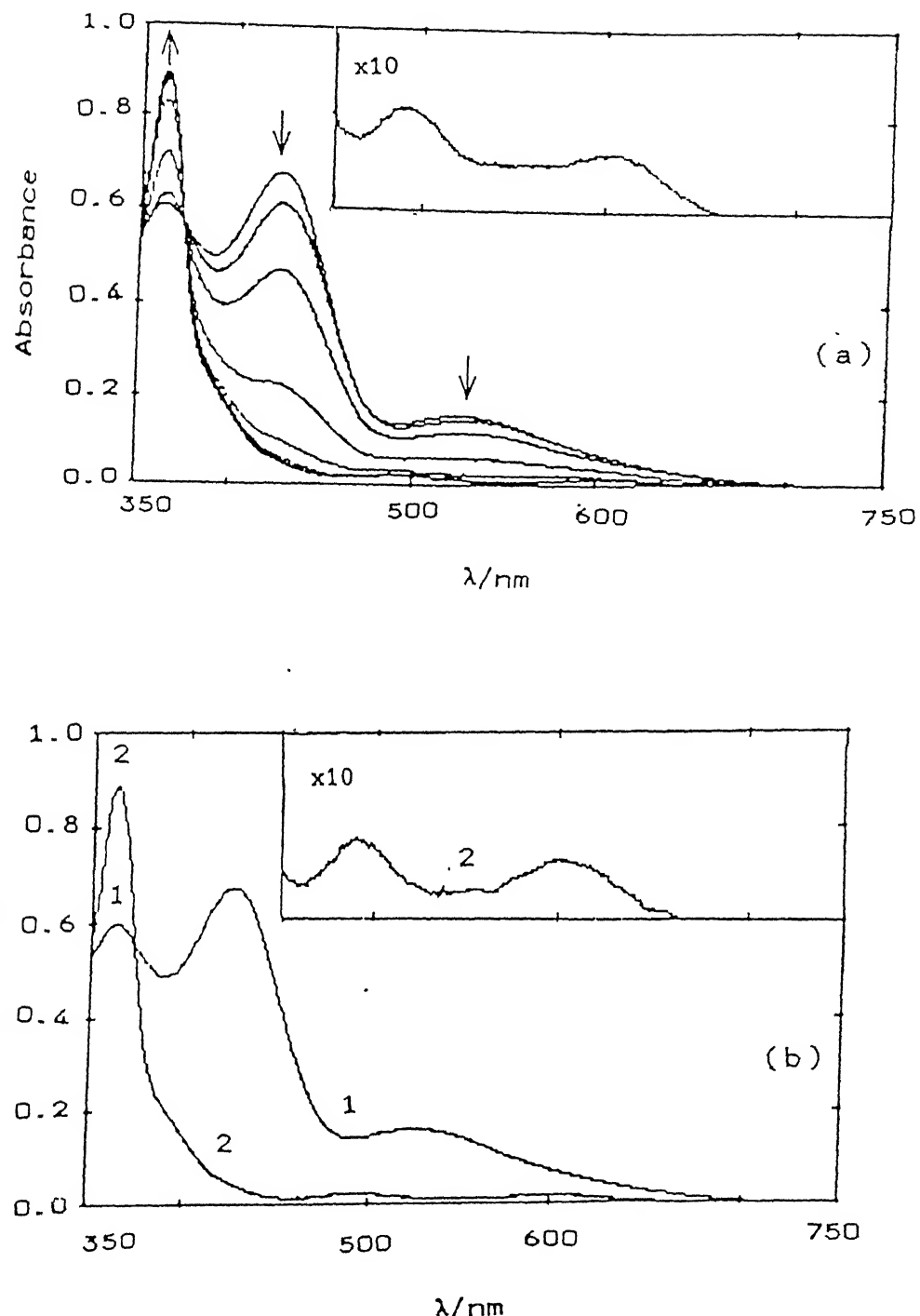
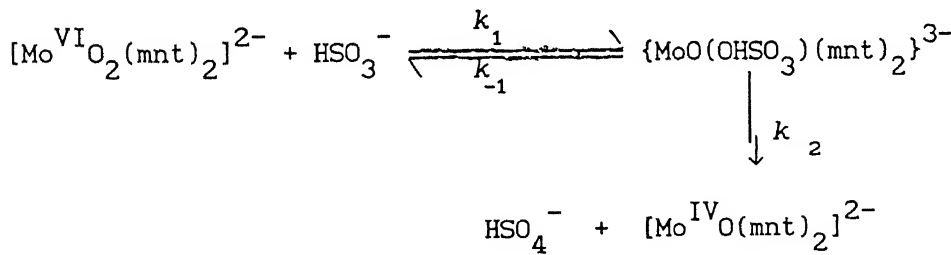


Fig. 4.1 (a) Spectral changes for the reaction between $[\text{Bu}_4\text{N}]_2[\text{Mo}^{\text{VI}}\text{O}_2(\text{mnt})_2]$ (1×10^{-4} M) and NaHSO₃ (2.0×10^{-4} M) in MeCN with 3.3% water at $20 \pm 0.1^\circ\text{C}$. Inset, d-d bands of the end feature in expanded form.

Fig. 4.1 (b) UV-visible absorption spectra of $[\text{Bu}_4\text{N}]_2[\text{Mo}^{\text{VI}}\text{O}_2(\text{mnt})_2]$ 1 and $[\text{Bu}_4\text{N}]_2[\text{Mo}^{\text{IV}}\text{O}(\text{mnt})_2]$ 2. Inset, d-d bands of 2 in expanded

spectrophotometrically monitored. The details of the kinetic experiments have been described in earlier chapter. The reaction is first order in the molybdenum(VI) complex as shown by the linearity of plot of $\log C$ (C = concentrations of Mo^{VI} complex at different intervals obtained from absorptions at different time) vs time in experiments with greater than 12 equivalents of NaHSO_3 . A representative plot of this type is shown in Fig. 4.2. Reaction rates at various NaHSO_3 concentrations were obtained from the slopes of these plots. A plot of observed rate constants vs concentrations of NaHSO_3 is shown in Fig. 4.3. At high concentration of NaHSO_3 the rates virtually become independent of the concentration of NaHSO_3 . This plot of k_{obs} vs $[\text{NaHSO}_3]$ is similar to what one expects for substrate saturation kinetics which can be interpreted as in following Scheme 4.1:



Scheme 4.1

The corresponding double reciprocal plot similar to enzymatic kinetic analysis of Fig. 4.3 is shown in Fig. 4.4. The V_{max} (= k_2 , the k_{obs} value at substrate saturation) and K_m (Michaelis constant) obtained from this double reciprocal plot were calculated to be $0.87 (\pm 0.04) \text{ s}^{-1}$ and $0.01 (\pm 0.001) \text{ M}$ respectively at 20°C (Table A3, Appendix). Thus the most

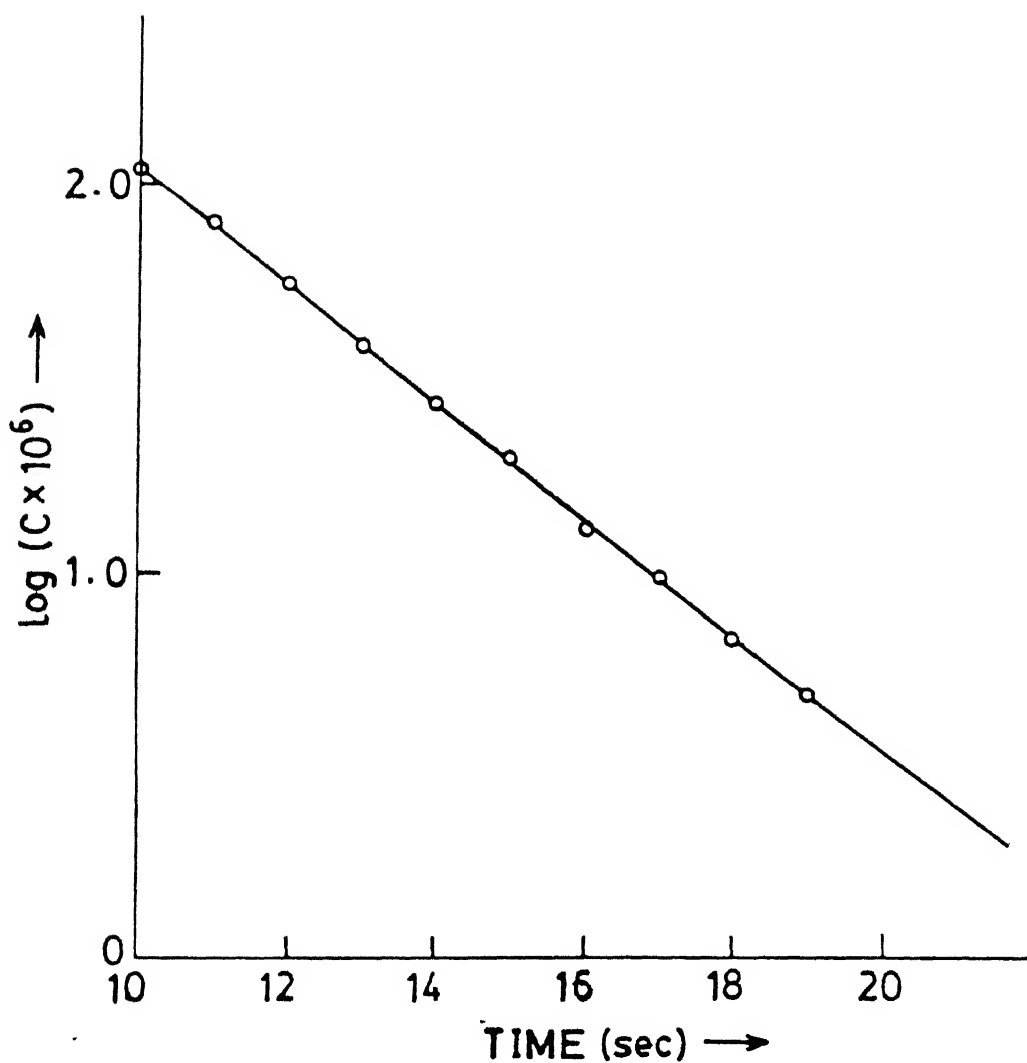


Fig. 4.2 Plot of $\log(C \times 10^6)$ vs Time : Oxidation of HSO_3^- by $[\text{Bu}_4\text{N}]_2^{+} [\text{Mo}^{\text{VI}} \text{O}_2(\text{mnt})_2]$.

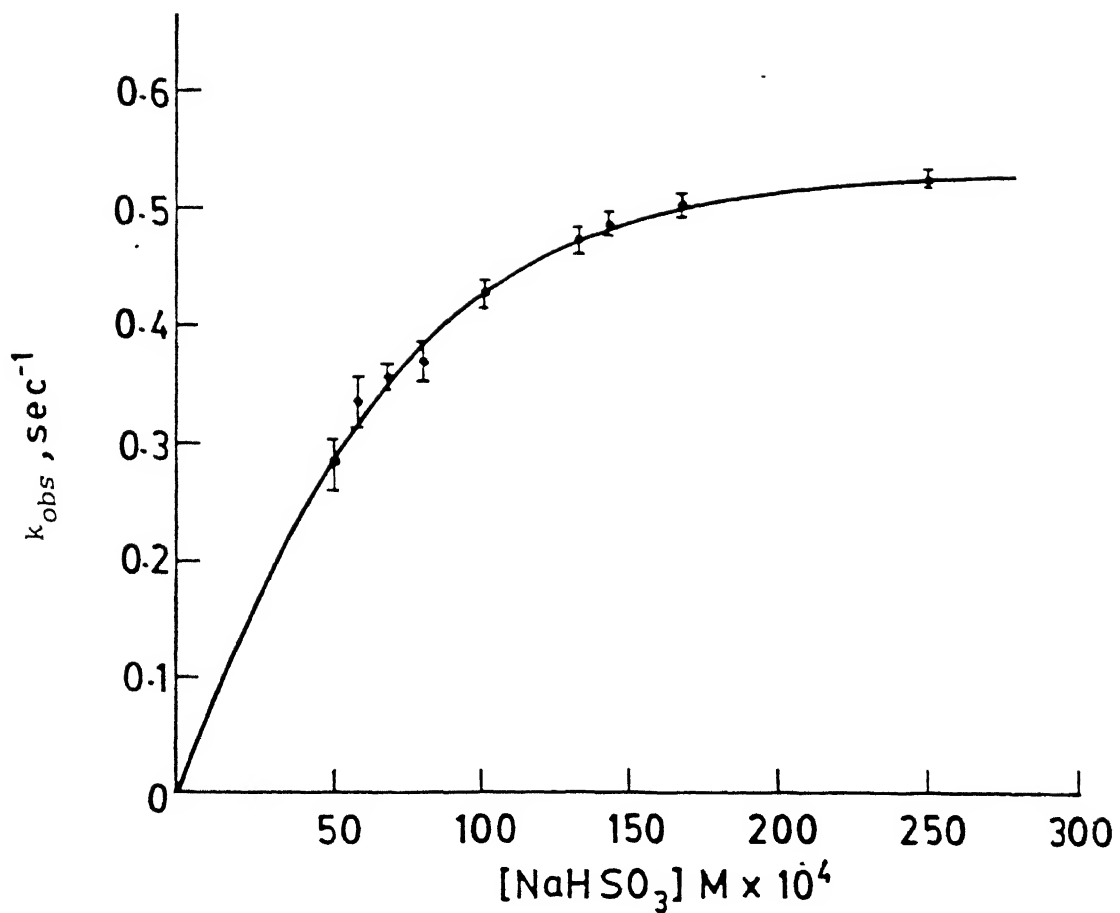


Fig. 4.3 Dependence of the k_{obs} of the reaction of $[\text{Mo}_{2}^{\text{VI}}(\text{mnt})_2]^{2-}$ and 12-62 equivalents of NaHSO_3 in 1:1 MeCN:H₂O at 20°C on $[\text{NaHSO}_3]$ (saturation curve).

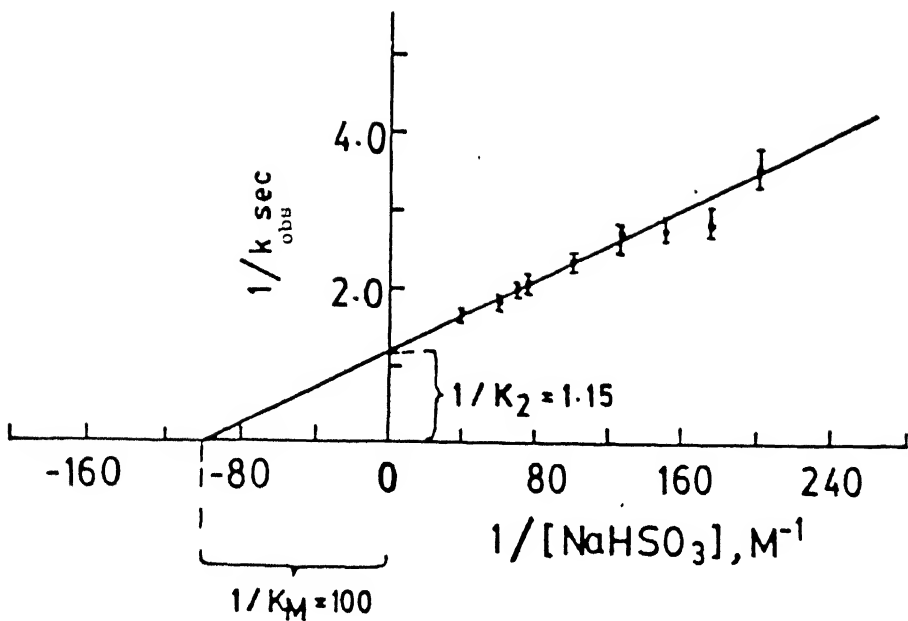


Fig. 4.4 Double reciprocal of Plot of $1/k_{\text{obs}}$ vs $1/[\text{NaHSO}_3]$ for the reaction in Fig. 4.3.

significant observation is made with these studies to demonstrate synthetic analogue reaction of sulfite oxidase.

For this reaction the formation of the intermediate complex, $\{\text{MoO}(\text{OH}\text{SO}_3)(\text{mnt})_2\}^{3-}$ similar to enzyme-substrate (ES) complex is important. In native sulfite oxidase, sulfite (or bisulfite) binds to molybdenum center of the enzyme. Inhibition studies by several anionic inhibitors especially with sulfate and phosphate anions demonstrate that these anions compete with the substrate binding site (*vide supra*). In the present model study, binding of bisulfite to molybdenum center is possible in two ways. Firstly the hexacoordinated complex anion can bind to bisulfite with the dissociation of one of the Mo-S coordination preferentially trans to one of the oxo groups to maintain hexacoordination in the formation of enzyme-substrate (ES) type complex. This would require subsequent steps for rearrangement to yield the final products. Alternatively bisulfite can bind to molybdenum center with coordination expansion to seven. Similar heptacoordinated MoO(VI) complexes are known¹⁰¹⁻¹⁰³. However, heptacoordinated complexes containing $\text{MoO}_2(\text{VI})$ moiety are not known. Thus to invoke heptacoordination for the Mo(VI)-sulfite complex similar to ES complex, the initial $\text{MoO}_2(\text{VI})$ moiety in the complex should transform to Mo(VI) moiety to accomodate bisulfite ligation. Another important aspect here is to consider whether the anionic center of bisulfite is responsible for its binding to molybdenum center or it is some sort of lone pair interaction. To clarify these alternatives saturation kinetics were followed in the presence of different concentrations of SO_4^{2-} and H_2PO_4^- . Double

reciprocal plots of k_{obs} vs varying concentration of bisulfite at two different fixed concentrations of SO_4^{2-} are shown in Fig 4.5 which represent typical competitive inhibition by SO_4^{2-} as observed in enzymatic inhibition reaction¹²². The inhibition constant was found to be $2.256 \times 10^{-2} \text{ M}$ (Table A4, Appendix). This competitive inhibition demonstrates that the substrate or the inhibitor binds to molybdenum center because of their anionic nature similar to native sulfite oxidase. When H_2PO_4^- was used as anionic inhibitor the double reciprocal plots exhibit mixed noncompetitive type inhibition as shown in Fig. 4.6. The inhibition constants K_I and K_I' were found to be $2.785 \times 10^{-3} \text{ M}$ and $3.367 \times 10^{-2} \text{ M}$ respectively (Table A5, Appendix). The mixed noncompetitive behavior of H_2PO_4^- suggests that H_2PO_4^- can combine with $[\text{Mo}^{\text{VI}}\text{O}_2(\text{mnt})_2]^{2-}$ at a second site, not identical, atleast in part, to the HSO_3^- binding site and thereby involving a ternary inhibitor-Mo^{VI} complex- substrate intermediate which is similar to enzymatic IES type of intermediate^{50b,123}. As the respective pK_a values for all the anions like HSO_3^- , SO_4^{2-} and H_2PO_4^- are almost the same and all these reactions were carried out with high bisulfite concentration, any drastic change in pH in these reactions can thus be ruled out. Hexacoordinated dioxocomplex like $\text{MoO}_2(\text{Et}_2\text{dtc})_2$ transforms to heptacoordinated $[\text{MoO}(\text{Et}_2\text{dtc})_2(\text{cat})]$ with catechol (cat)¹⁰¹. A similar reaction between catechol and $[\text{Bu}_4\text{N}]_2[\text{Mo}^{\text{VI}}\text{O}_2(\text{mnt})_2]$ thwarted all attempts to isolate any heptacoordinated species owing to the reduction of $[\text{Mo}^{\text{VI}}\text{O}_2(\text{mnt})_2]^{2-}$ to $[\text{Mo}^{\text{IV}}\text{O}(\text{mnt})_2]^{2-}$ with the oxidation of catechol to benzoquinone. Spectrophotometric time course of this reaction

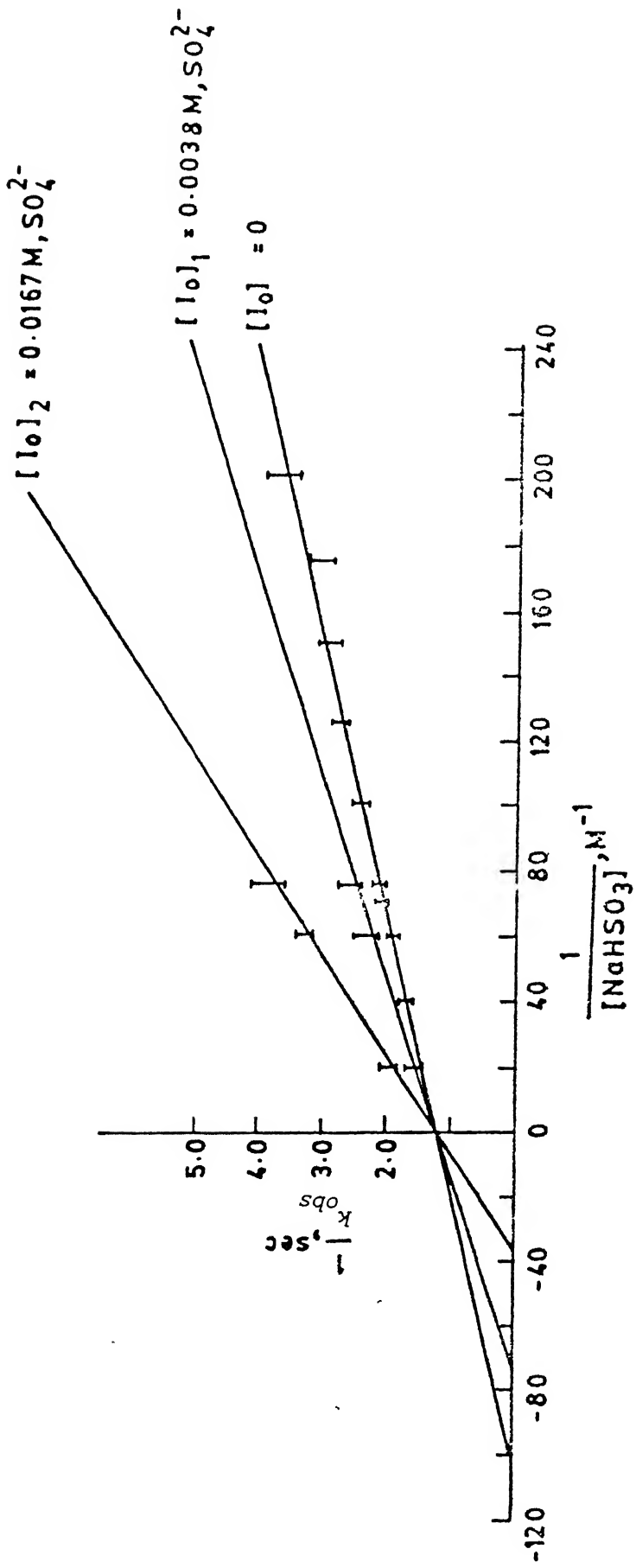


Fig. 4.5 Double reciprocal plots of bisulfite saturation kinetics in the presence of SO_4^{2-} .

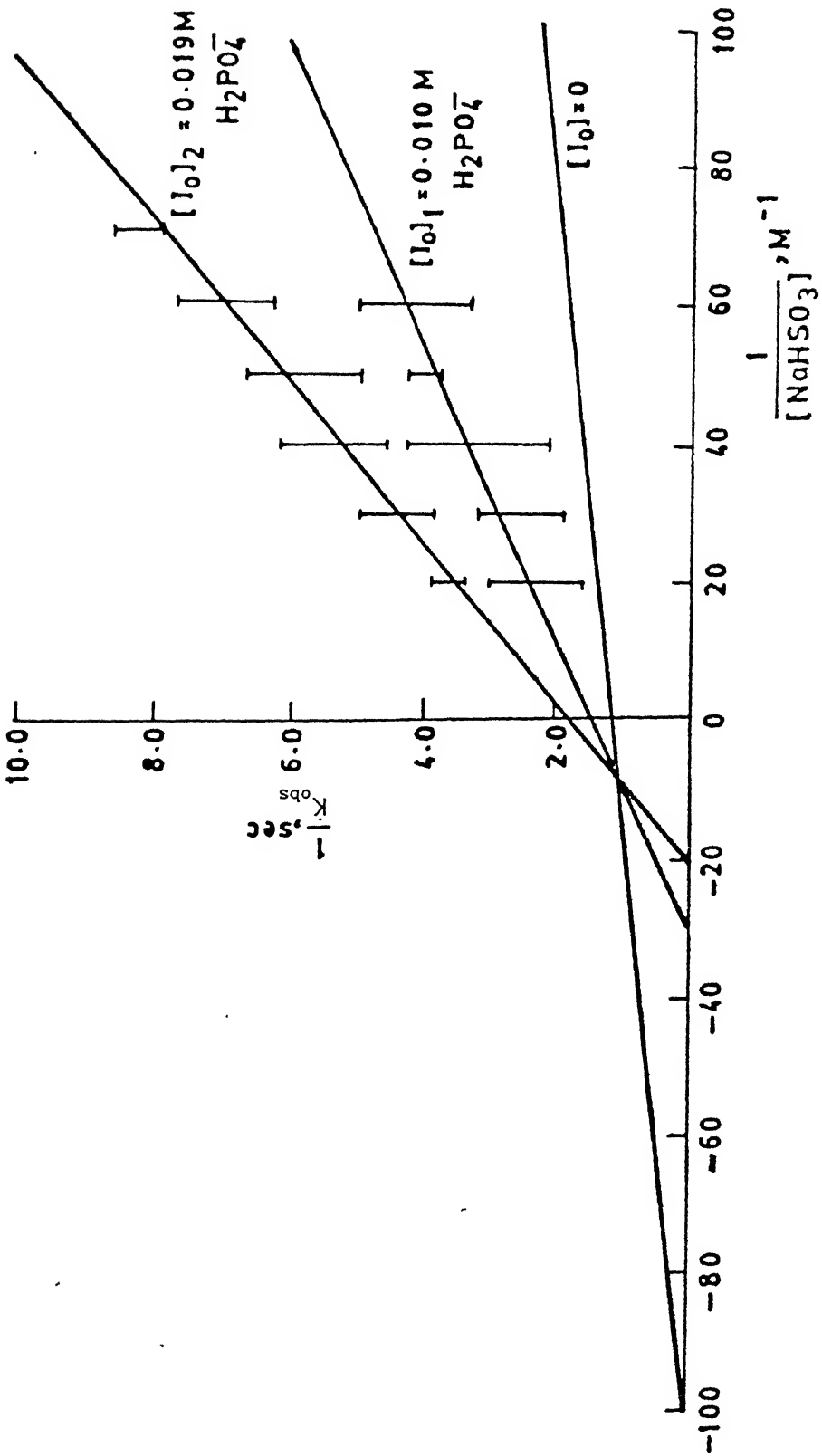


Fig. 4.6 Double reciprocal plots of bisulfite saturation kinetics in the presence of $H_2PO_4^-$.

is shown in Fig. 4.7. From this Figure it is evident that the dioxomolybdenum(VI) complex at the initial stage of the reaction forms an intermediate complex with shift of the lowest energy 525 nm absorption band of $[\text{Mo}^{\text{VI}}\text{O}_2(\text{mnt})_2]^{2-}$ to a more intense absorption band around 640 nm. The isolated heptacoordinated complexes, $[\text{MoO}(\text{R}_2\text{dtc})_2(\text{cat})]$ showed the appearance of an intense charge transfer transition in the energy range 509-572 nm¹⁰¹. Quantitative conversion of $[\text{Mo}^{\text{VI}}\text{O}_2(\text{mnt})_2]^{2-}$ to $[\text{Mo}^{\text{IV}}\text{O}(\text{mnt})_2]^{2-}$ with the formation of oxidized benzoquinone strongly support the formation of intermediate which may possess heptacoordination. During the progress of the reaction, ESR investigation in solution did not show any characteristic signal responsible for the presence of pentavalent molybdenum. From these observations the course of the reaction may be schematically presented as shown in Scheme 4.2. Further support for this type of enhancement of coordination before reduction of MoO_2 (VI) moiety to MoO (IV) moiety may be furnished by the reaction between $[\text{Mo}^{\text{VI}}\text{O}_2(\text{mnt})_2]^{2-}$ and PhSH. Recently Holm and coworkers⁸⁴ have demonstrated that PhSH functions as a potential reducing substrate to react with MoO_2LNS_2 . Similar progress of reaction between $[\text{Mo}^{\text{VI}}\text{O}_2(\text{mnt})_2]^{2-}$ and PhSH when monitored spectrophotometrically (Fig. 4.8a) showed the appearance of a red shifted band around 600 nm for an intermediate complex. This reaction is relatively a slower one and after 8 h the final spectrum was identical to the authentic spectrum of $[\text{Mo}^{\text{IV}}\text{O}(\text{mnt})_2]^{2-}$ (Fig. 4.8b). Contrary to the reaction between $[\text{Mo}^{\text{VI}}\text{O}_2(\text{mnt})_2]^{2-}$ and HSO_3^- these reaction do not show any clean isobestic point during the progress of these reactions. From

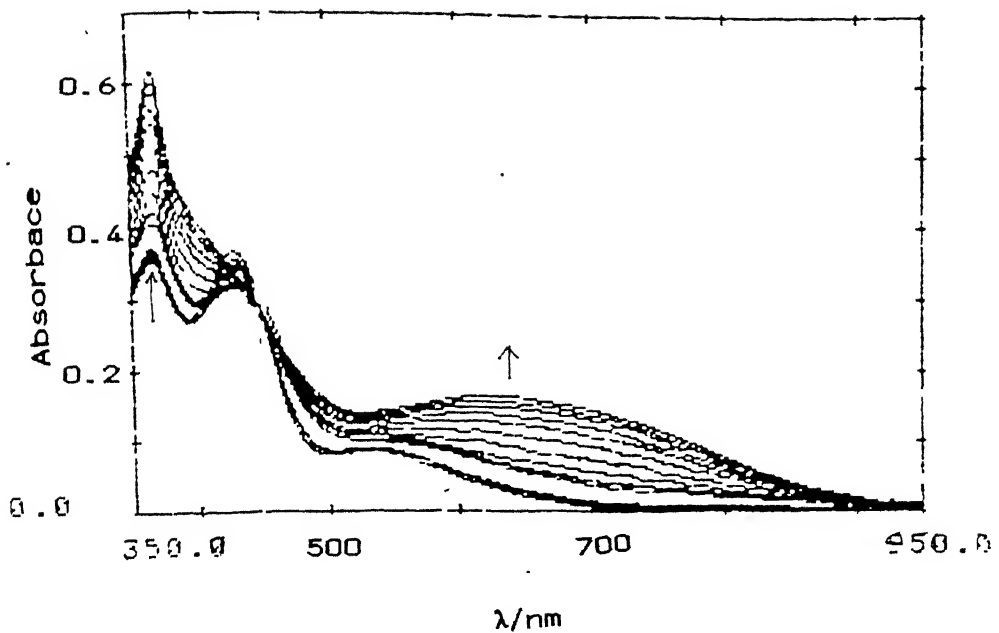
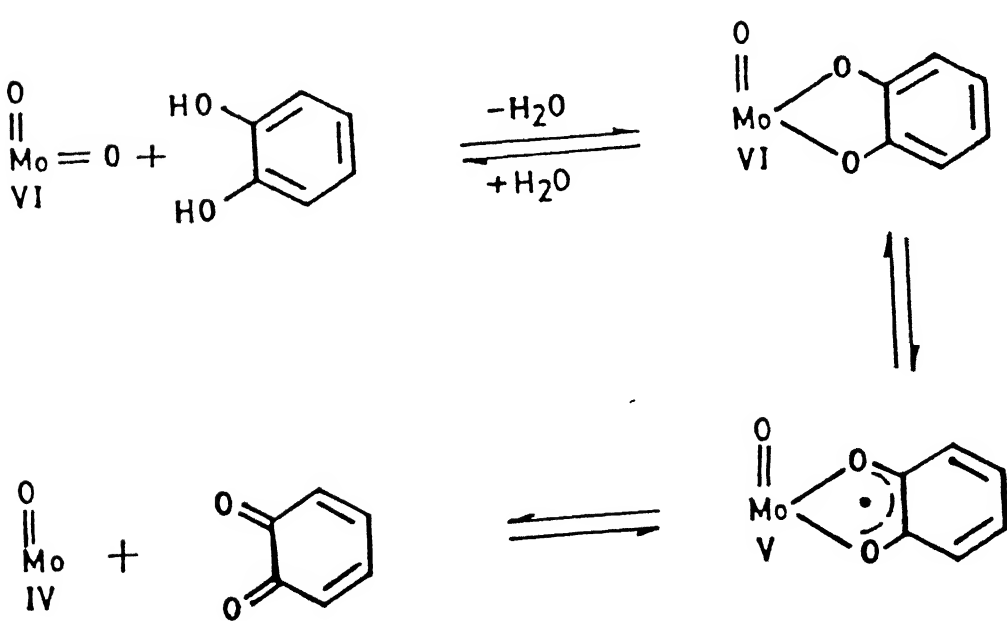


Fig. 4.7 Spectral changes for the reaction between $[\text{Mo}^{\text{VI}}\text{O}_2(\text{mnt})_2]^{2-}$ and catechol in CH_2Cl_2 . Spectra were taken for 50 Minutes.



Scheme 4.2

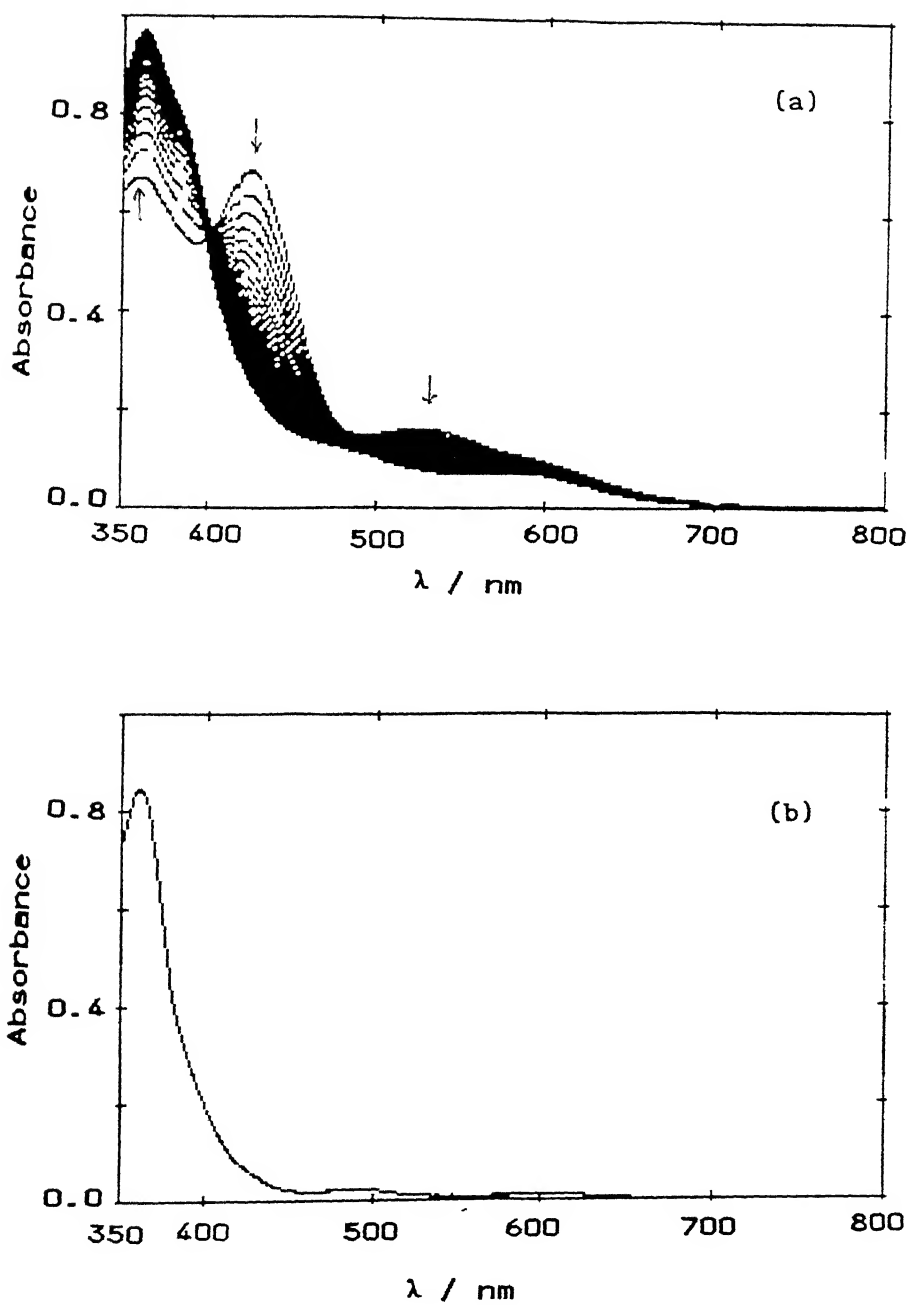


Fig. 4.8 (a) Spectral changes for the reaction between $[\text{Mo}^{\text{VI}}\text{O}_2(\text{mnt})_2]^{2-}$ and PhSH in MeCN, (b) the final spectrum after 8

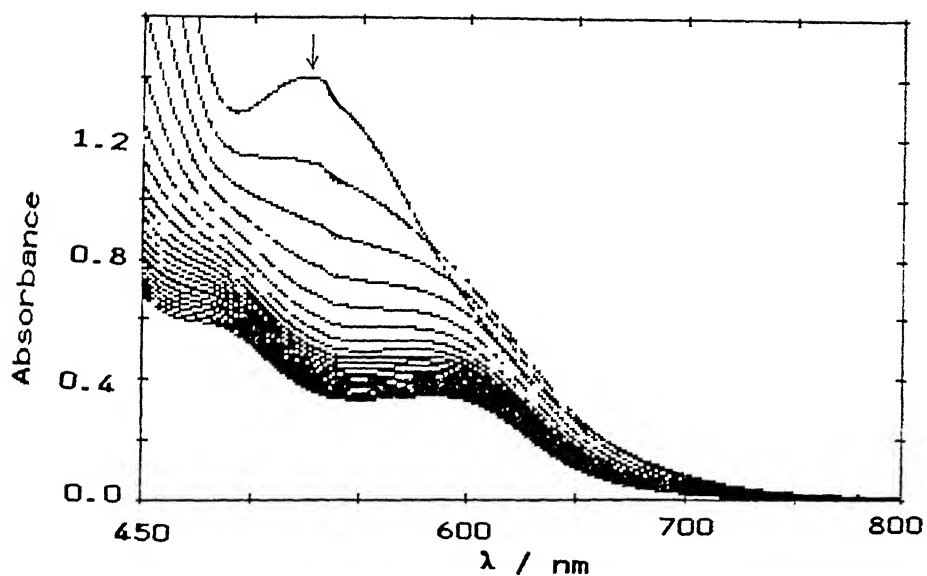


Fig. 4.8 (c) Spectral changes for the reaction between $[\text{Mo}^{\text{VI}}\text{O}_2(\text{mnt})_2]^{2-}$ and PhSH in expanded form.

Fig. 4.8a and its expanded form (Fig. 4.8c) it is evident that there are involvement of more than one reaction. In other words the ultimate quantitative conversion of $[\text{Mo}^{\text{VI}}\text{O}_2(\text{mnt})_2]^{2-}$ to $[\text{Mo}^{\text{IV}}\text{O}(\text{mnt})_2]^{2-}$ by the reducing substrate, PhSH, proceeds via the formation of some intermediate along with the conversion of the intermediate to final products concurrently. The cutting point around 400 nm in Fig. 4.8a at the initial time interval (5 min) may be the isobestic point of the formation of intermediate from $[\text{Mo}^{\text{VI}}\text{O}_2(\text{mnt})_2]^{2-}$ and PhSH. To get some more insight of this reaction, the progress of the reaction was followed cyclicvoltammetrically. Cyclic voltammograms for repetitive scans with time interval of $[\text{Bu}_4\text{N}]_2[\text{Mo}^{\text{VI}}\text{O}_2(\text{mnt})_2]$ in the presence of six times of PhSH were monitored and the voltammograms thus obtained are shown in Fig. 4.9. It is interesting to note the following events: (i) the cathodic reduction peak potential of $[\text{Bu}_4\text{N}]_2[\text{Mo}^{\text{VI}}\text{O}_2(\text{mnt})_2]$ which appeared at -1.15V vs Ag/AgCl (broken line of Fig. 4.9) is shifted to less negative potential -0.97V vs Ag/AgCl on addition of PhSH (PhSH does not have any redox response under the voltage limit of this study); (ii) voltammetric scans with number 1 and 2 were done within five minutes and during this time interval the appearance of the couple $[\text{Mo}^{\text{V}}\text{O}(\text{mnt})_2]/[\text{Mo}^{\text{IV}}\text{O}(\text{mnt})_2]$ did not appear properly; (iii) in subsequent scans the reduction of the current height of the cathodic peak potential at -0.97V vs Ag/AgCl is related to the appearance of the anodic peak potential at + 0.48V and to the corresponding cathodic peak potential at + 0.41V vs Ag/AgCl. This clearly demonstrates that the intermediate compound formed between $[\text{Bu}_4\text{N}]_2[\text{Mo}^{\text{VI}}\text{O}_2(\text{mnt})_2]$ and PhSH is stable

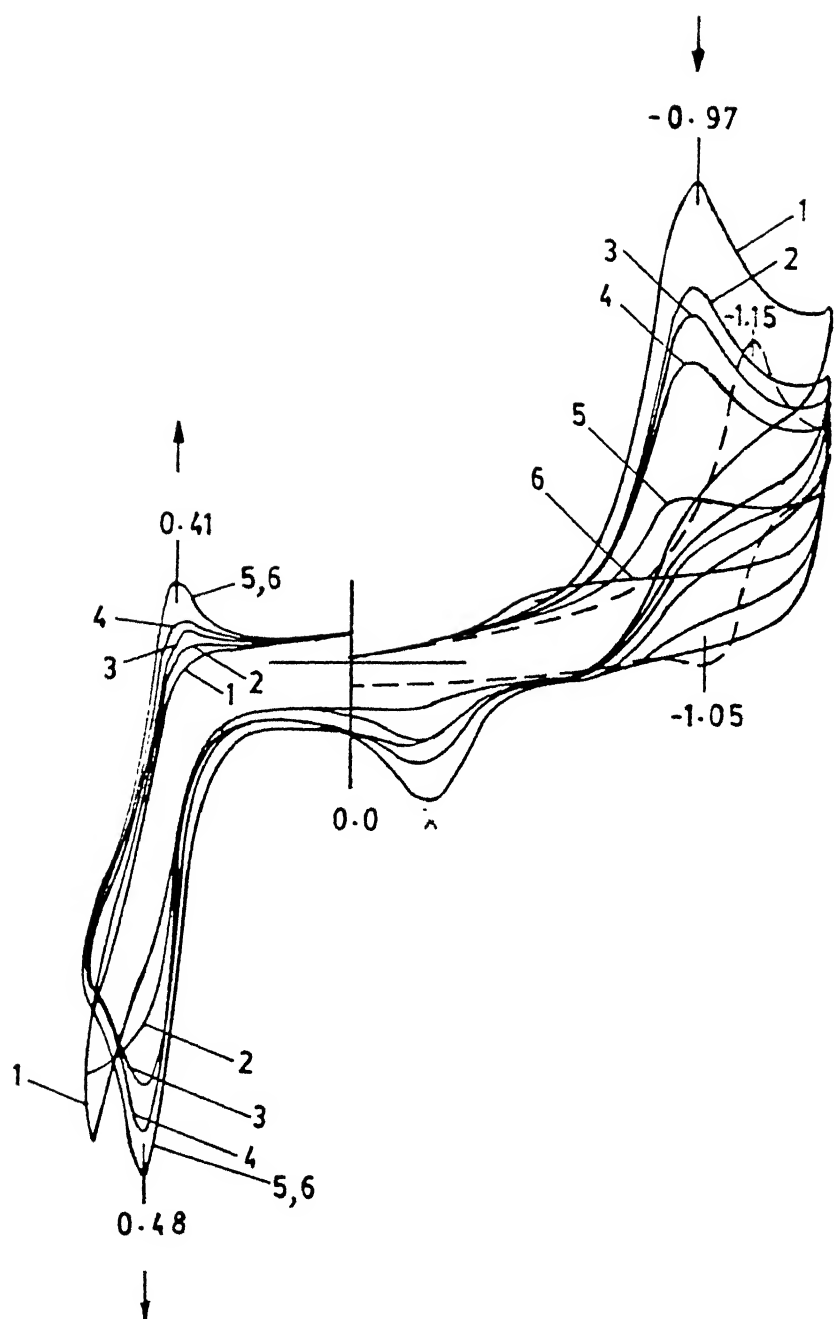
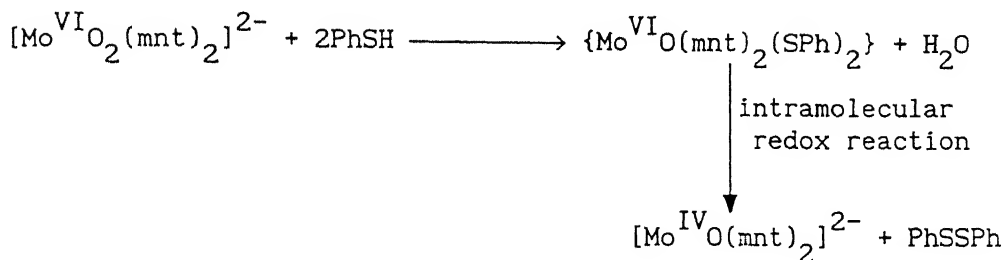


Fig. 4.9 Cyclic voltammetric scans during the progress of reaction between $[Bu_4N]^2[Mo^{VI}O_2(\text{mnt})_2]$ and PhSH in MeCN. The broken line scan is for pure complex. Subsequent scans (1-6) are after addition of PhSH.

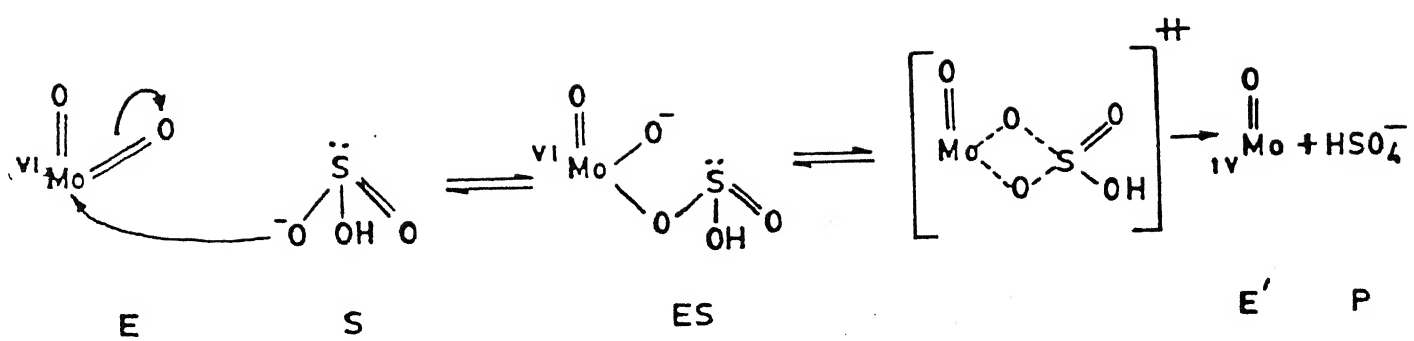
within 5 minutes of the reaction. This complex has its reduction potential peak at -0.97V vs Ag/AgCl. Around few minutes of its formation intramolecular redox reaction sets in with the formation of the reduced $[\text{Mo}^{\text{IV}}\text{O}(\text{mnt})_2]^{2-}$ complex anion as shown in the reaction Scheme 4.3.



Scheme 4.3

All these reactions strongly suggest (but does not prove) the formation of an intermediate heptacoordinated species before intramolecular electron transfer reaction. Thus the reaction between $[\text{Mo}^{\text{VI}}\text{O}_2(\text{mnt})_2]^{2-}$ and HSO_3^- can be proposed to occur in the sequence as shown in the Scheme 4.4. In this scheme it is thus proposed that the anionic binding of HSO_3^- or inhibitor transforms this rigid $[\text{Bu}_4\text{N}]_2[\text{Mo}^{\text{VI}}\text{O}_2(\text{mnt})_2]$ complex to stereochemically nonrigid seven coordinated enzyme-substrate (ES) or enzyme-inhibitor (EI) type intermediate according to "induced fit" theory of Koshland¹²⁴ with the generation of another functional Mo-O⁻ site at the initial event. Subsequent interactions between bonded substrate and functional site's O⁻ may thus lead to the product formation.

The proposition of the expansion of coordination number of hexavalent molybdenum from six to seven in the above discussion is



Scheme 4.4

not ill founded as oxomolybdenum(VI) complexes with seven coordination number are known (*vide supra*).

For native sulfite oxidase the reported inhibition constants of X^- ($X = F^-, Br^-, I^-$) with nucleophilicity⁸ order are $I^- > Br^- > F^-$. It has also been demonstrated that both pH and anions have strong effect on the molybdenum reduction potential of the enzyme¹²⁵ while dioxo group remains intact in the oxidized enzyme at both low pH and high pH¹²⁶. Thus in the course of reductive half reaction of sulfite oxidase it is the initial nucleophilic attack by the anionic substrate, that seems, controls the entire course of reaction. It is worthnoting that $H_2PO_4^-$ binds to present model system in mixed noncompetitive fashion in relation to the reductive half reaction by HSO_3^- . The observations made by Oshino and Chance¹²⁷ with regard to the participation of sulfite oxidase catalyzed reaction in the intermembrane space of mitochondria exclusively through the respiratory chain suggest that Nature has developed this system whereby detoxification of one equivalent of SO_3^{2-} leads to the synthesis of one equivalent of ATP as schematically shown in the Fig. 4.10. The presence of sulfite oxidase in the intermembrane space of mitochondria casts some doubt about the actual form of the substrate, sulfite, in the presence of proton gradient. The cotransport of $H_2PO_4^-$ ion and H^+ ion via the intermembrane space¹²⁸ led to suggest that the actual reducing substrate may be HSO_3^- . The mixed noncompetitive inhibition by $H_2PO_4^-$ may further suggest that the rate of bypass detoxification reaction is probably controlled by the presence of $H_2PO_4^-$ ion flux present therein.

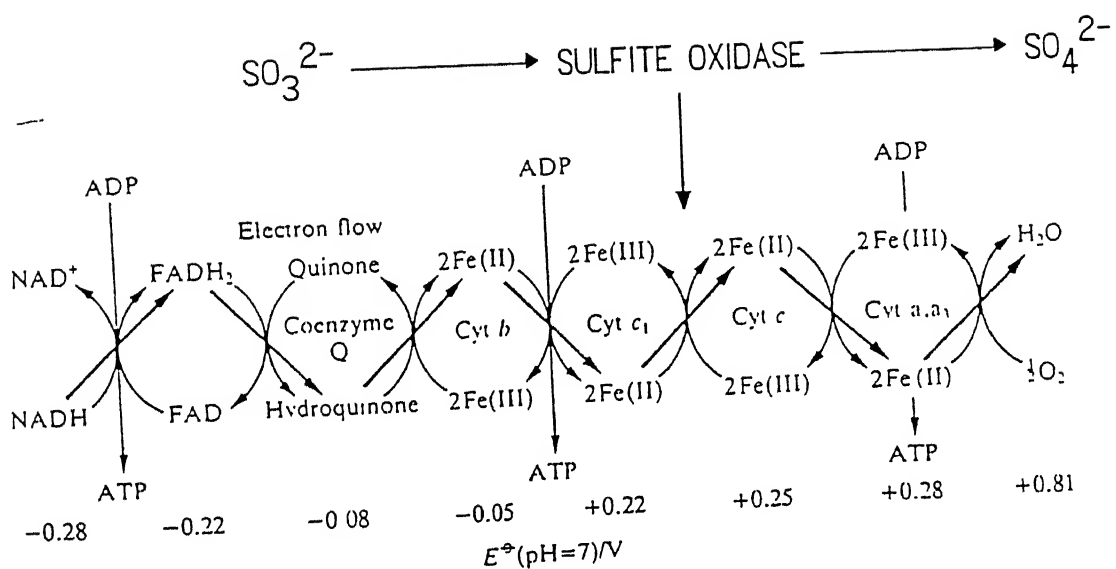


Fig. 4.10 Close association of mitochondrial electron sequence chain with sulfite oxidase catalyzed reaction.

chain with sulfite oxidase catalyzed reaction.

The temperature dependencies of rate constants for the reaction (29) were determined. Activation parameters were obtained by least-squares fit of k_{obs} values measured at different temperatures to the Eyring equation,

$$k_{\text{obs}} = (K_B T/h) e^{[\Delta S^\# / R - \Delta H^\# / RT]} \quad \text{-----(30)}$$

The rate constants for the rection (29) at different temperatures and the activation parameters are summarized in Table 4 1. The Eyring plot of the rate constants is shown in Fig 4.11.

From the Table 4.1 the negative value of entropy requires some explanations. As the reaction is carried out with charge molecules in presence of MeCN-water (1:1) which is strongly polar, the like charges on $[\text{Mo}^{\text{VI}}\text{O}_2(\text{mnt})_2]^{2-}$ and HSO_3^- when form the activated complex lead to increase in charge density; as a result of which the solvent molecules will be more ordered around the complex leading thereby to decrease the entropy. In the present case it is difficult to correct the entropy chnage associated with this electrostiction process.

4.2 OXOTRANSFER REACTION WITH TRIPHENYLPHOSPHINE.

Phosphines, especially, triphenylphosphine, have been used to follow oxotransfer reactions with model dioxomolybdenum(VI) complexes⁵⁵. With the present model dioxomolybdenum(VI) compound, the reaction with PPh_3 has been carried out for two reasons:

Table 4.1 Kinetic Data and Activation Parameters for the Reaction
System 29 (in 1:1 MeCN:H₂O)

T, K	$10^2 k_2$, s ⁻¹	$\Delta H^\#$, Kcal/mol	$\Delta S^\#$, cal/(deg.mol)
288	69.9 (\pm 5.5)		
293	64.5 (\pm 5.1)		
298	61.4 (\pm 5.5)	2.05 (\pm 0.63)	-52.59 (\pm 2.1)
303	51.7 (\pm 3.1)		

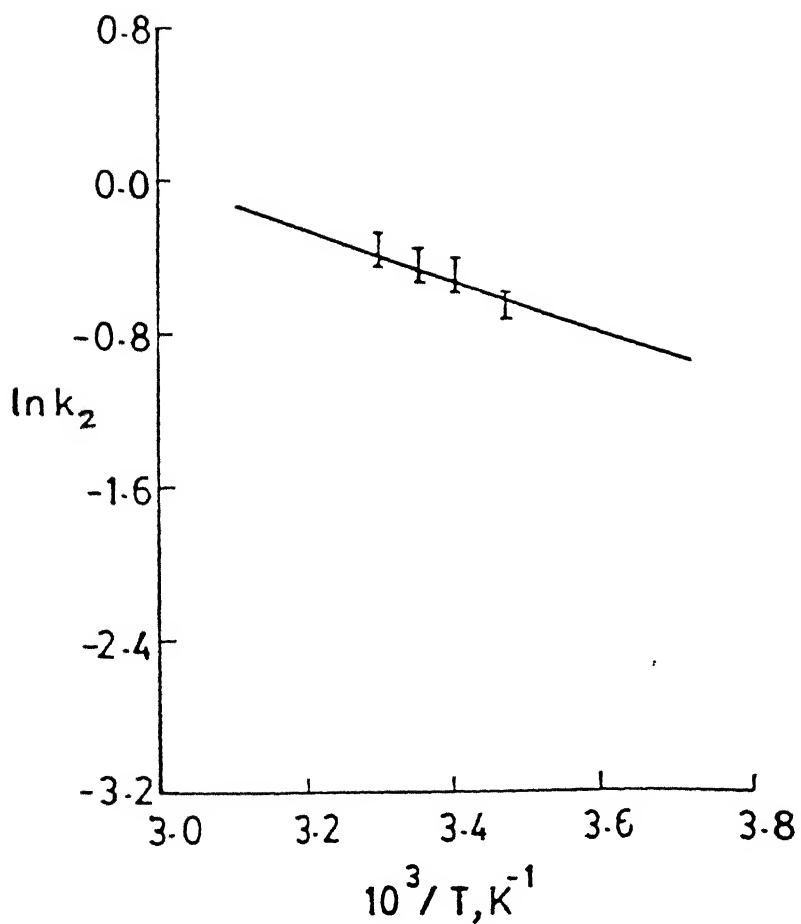
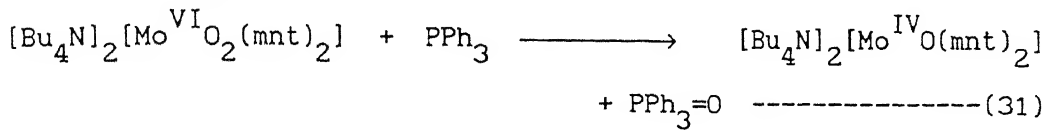


Fig. 4.11 Eyring plot of the rate constants (k_2) for reaction between $[\text{Mo}^{\text{VI}}\text{O}_2(\text{mnt})_2]^{2-}$ and HSO_3^- in 1:1 MeCN: H_2O .

firstly to compare its kinetic data with those of the other model compounds; secondly to understand if there is any medium dependency from pure MeCN to MeCN-water (1:1) of the reaction.

The progress of the oxo transfer reaction in MeCN,



as observed spectrophotometrically is shown in Fig. 4.12. The isobestic point is found at 374 nm. The final spectrum of the reaction was identical with that of the authentic reduced monooxo complex, $[\text{Bu}_4\text{N}]_2[\text{Mo}^{\text{IV}}\text{O}(\text{mnt})_2]$.

Pseudo-first order conditions were used to study the reaction (31) in MeCN the concentration of PPh_3 between ~ 50 fold and ~ 275 fold molar excess over the concentration of complex, $[\text{Bu}_4\text{N}]_2[\text{Mo}^{\text{VI}}\text{O}_2(\text{mnt})_2]$. The reaction was followed by monitoring absorbance changes at 525 nm. The pseudo-first order rate constants k_{obs} ($k_{\text{obs}} = k_1[\text{PPh}_3]$) were determined for each reaction from plots of $\log C$ vs time and values of k_{obs} were obtained at 15°C , 25°C and 35°C . The dependence of k_{obs} on $[\text{PPh}_3]$ is shown in Fig. 4.13. The reaction is first order in both Mo(VI) complex and PPh_3 . Hence the applicable rate equation is

$$\frac{d[\text{Mo(VI)}]}{dt} = k_2[\text{Mo(VI)}][\text{PPh}_3] \quad (32)$$

The specific rate constants, k_2 , were obtained in pure MeCN and in MeCN-water (1:1) medium. Activation parameters were obtained by least squares fit of k_2 values determined at different temperatures to the Eyring equation (30). The Eyring plot for this oxo transfer reaction is shown in Fig. 4.14. The kinetic data and activation parameters are summarized in Table 4.2. In MeCN at

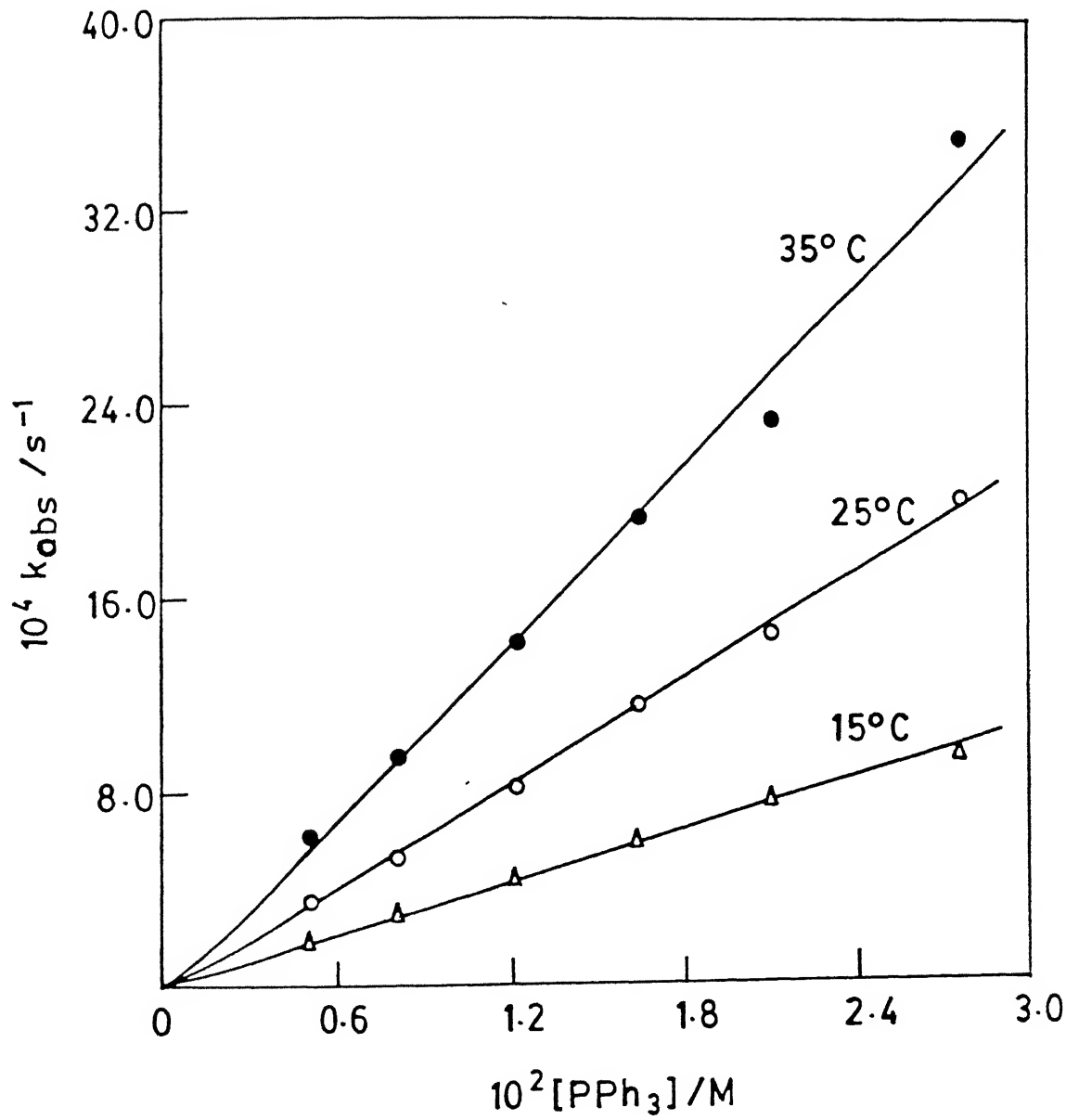


Fig. 4.13 Observed variation of k_{obs} with $[{\text{PPh}}_3]$ at 15°C , 25°C and 35°C .

Table 4.2 Kinetic Data and Activation Parameters for the Reaction
System 31

T, K	$10^3 k_2$, $M^{-1}s^{-1}$	$\Delta H^\#$, Kcal/mol	$\Delta S^\#$ cal/(deg.mol)
<u>in pure MeCN</u>			
288	37.5 (\pm 0.5)		
298	70.4 (\pm 0.4)	9.0 (\pm 0.3)	-33.3 (\pm 1.2)
308	123.3 (\pm 0.8)		
318	205.2 (\pm 4.8)		
<u>in 1:1 MeCN:water</u>			
298	1076 (\pm 20)	5.541 (\pm 0.32)	-39.79 (\pm 0.92)

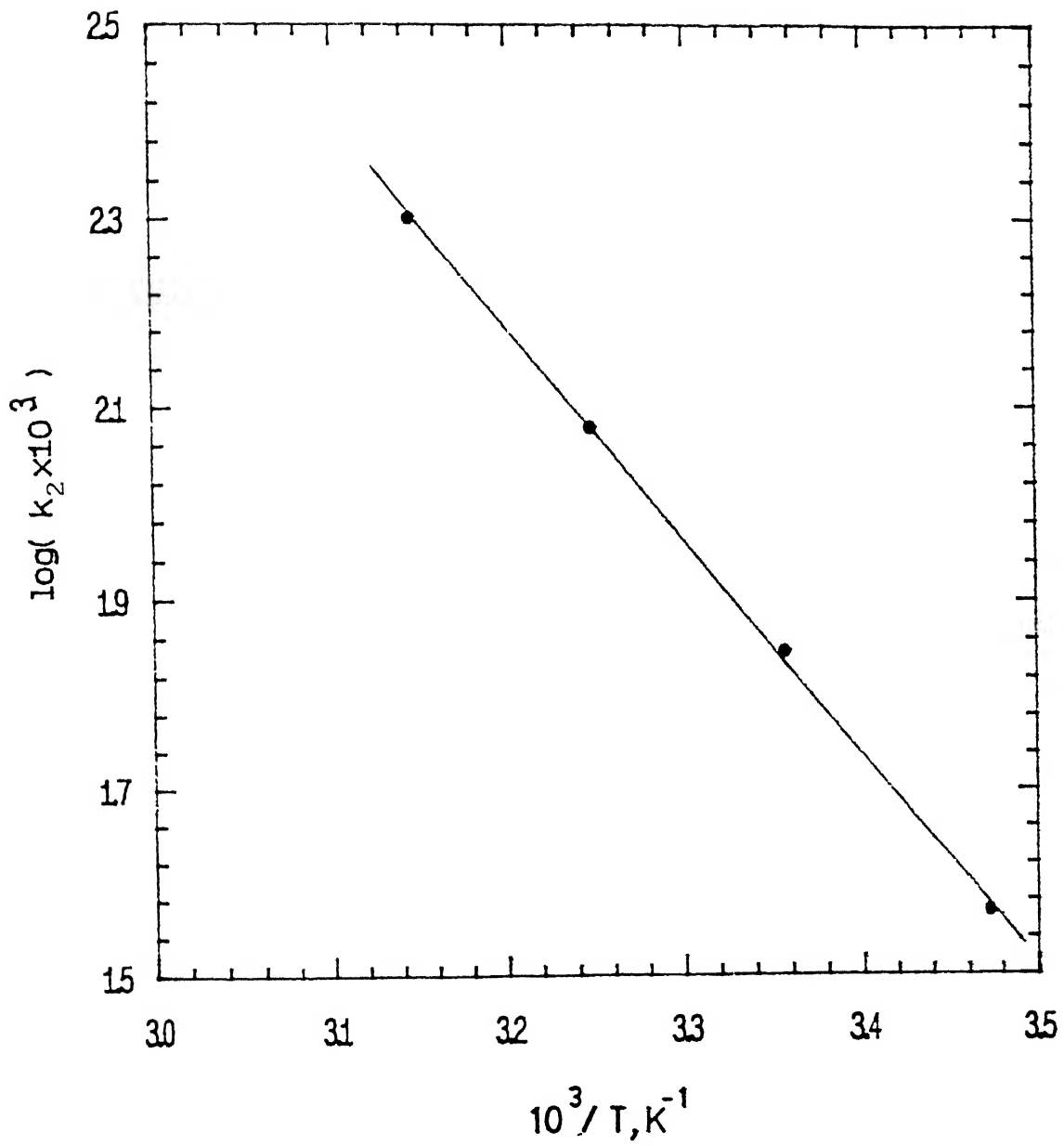


Fig. 4.14 Eyring plot of the rate constants (k_2) for the reaction between $[Mo^{VI}O_2(mnt)_2]^{2-}$ and PPh_3 in MeCN.

100

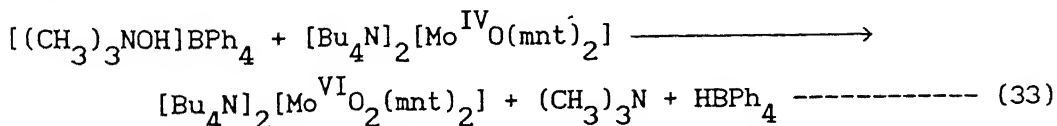
25°C, $\Delta H^\#$ and $\Delta S^\#$ were obtained to be 9 (\pm 0.3) Kcal/mol and -33.3 (\pm 1.2) cal/deg/mol respectively. The $\Delta H^\#$ and $\Delta S^\#$ for the oxo transfer reaction of $\text{MoO}_2(\text{R}_2\text{dtc})_2$ and PPh_3 in MeCN have been reported^{85b} to be 8.4 Kcal/mol and -30 cal/deg/mol respectively at 25°C. These results suggest that the mechanism of the reaction (31) is quite similar to that of the reaction between $\text{MoO}_2(\text{R}_2\text{dtc})_2$ and PPh_3 ^{85a,b}. Thus this is a simple bimolecular reaction involving the interaction between one $[\text{Mo}^{\text{VI}}\text{O}_2(\text{mnt})_2]^{2-}$ and one PPh_3 in the activated complex. The formation of the activated complex then leads to transfer of an oxygen atom via the donation of the lone pair of electrons on phosphorous atom into the antibonding Mo-O π^* orbital. This results in the formation of the P-O bond and oxomolybdenum(IV) complex. This pathway is consistent with the low value of $\Delta H^\#$ obtained here because the formation of activated complex does not require any significant bond breaking or intramolecular reorganization. The similar mechanism^{72c} has been described for the reaction of $\text{MoO}_2(\text{ssp})_2$ and PEtPh_2 . From the Table 4.2 it is evident that the reaction rate is faster in MeCN-water (1:1) medium than in pure MeCN medium. This may be due to the medium effect. But the activation parameters in pure MeCN and in MeCN-water media suggest that the mechanisms occurring in these two solvents are similar.

4.3 FUNCTIONAL ANALOGUE REACTION OF TRIMETHYLAMINE N-OXIDE REDUCTASE.

Trimethylamine N-oxide (TMANO) reductase, an inducible terminal enzyme for anaerobic respiration of bacteria like *Escherichia coli*¹²⁹, *Salmonella typhimurium*¹³⁰ and *Proteus spp*¹³¹, contains molybdenum cofactor common to all oxomolybdoenzymes^{26d, 132}. The molybdenum cofactor is proposed to be a complex of molybdopterin and molybdenum, with the metal linked to dithiolene moiety of molybdopterin^{26d}. This trimethylamine N-oxide reductase generally showed activity with ClO_3^- but no activity with NO_3^- and no or little (pH dependent) activity with dimethylsulfoxide (DMSO)¹³² suggesting that this reductase operates with high potential substrates. The reduced complex, $[\text{Bu}_4\text{N}]_2[\text{Mo}^{\text{IV}}\text{O}(\text{mnt})_2]$ shows redox potential at + 0.445V vs Ag/AgCl for its one electron oxidation in MeCN (*vide supra*). As expected it does not react with NO_3^- but reacts with ClO_3^- . Interestingly when this complex was dissolved even in neat DMSO apparently no oxo transfer reaction takes place for days. Curiously $\text{MoO}(\text{Et}_2\text{dtc})_2$ readily reacts with DMSO^{85a, 133}. As trimethylamine N-oxide is a strong oxo donor it is interesting to see if this can respond oxo transfer reaction to $[\text{Bu}_4\text{N}]_2[\text{Mo}^{\text{IV}}\text{O}(\text{mnt})_2]$. When the reaction between $(\text{CH}_3)_3\text{NO} \cdot 2\text{H}_2\text{O}$ and $[\text{Bu}_4\text{N}]_2[\text{Mo}^{\text{IV}}\text{O}(\text{mnt})_2]$ was carried out in MeCN or in dimethylformamide (DMF) the green color of the complex rapidly changed to reddish brown. Spectrophotometric investigation of this reaction in these solvents showed the formation of

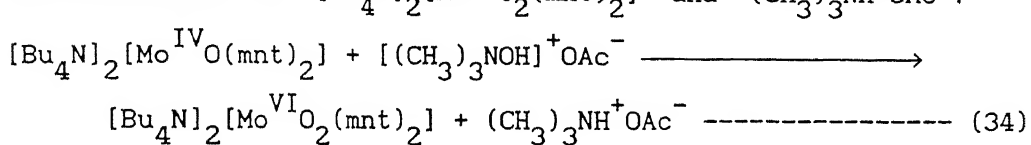
$[\text{Mo}^{\text{VI}}\text{O}_2(\text{mnt})_2]^{2-}$ ion; however, reaction in these solvents never attend quantitatively. In MeCN solubility of $(\text{CH}_3)_3\text{NO}\cdot 2\text{H}_2\text{O}$ is restricted. However, in DMF when $(\text{CH}_3)_3\text{NO}\cdot 2\text{H}_2\text{O}$ was dissolved in excess the progress of the reaction demonstrated the rapid formation of $[\text{Mo}^{\text{VI}}\text{O}_2(\text{mnt})_2]^{2-}$ to nearly 60% followed by decomposition of the oxidized complex. When anhydrous $(\text{CH}_3)_3\text{NO}$ was used in DMF the oxo trasfer reaction was improved but never attend to completion.

When $[\text{Bu}_4\text{N}]_2[\text{Mo}^{\text{IV}}\text{O}(\text{mnt})_2]$ was dissolved in CH_2Cl_2 and mixed with an aqueous solution of $(\text{CH}_3)_3\text{NO}\cdot 2\text{H}_2\text{O}$, no reaction takes place. Interestingly when aqueous $(\text{CH}_3)_3\text{NO}\cdot 2\text{H}_2\text{O}$ solution was acidified with dil. H_2SO_4 , CH_3COOH or with benzoic acid, then immediately the green layer of CH_2Cl_2 changed to reddish brown. Spectrophotometry revealed the formation of $[\text{Mo}^{\text{VI}}\text{C}_2(\text{mnt})_2]^{2-}$ complex ion. This suggests that the oxo transfer capability of trimethylamine N-oxide facilitates with formation of proper ion pair like $[(\text{CH}_3)_3\text{NOH}]^+ \parallel \text{x}^-$ ($\text{x}^- = \text{CH}_3\text{COO}^-$, $\text{C}_6\text{H}_5\text{COO}^-$ etc.). As a test when $[(\text{CH}_3)_3\text{NOH}] \text{BPh}_4$ was used in solvent like acetone or CH_2Cl_2 the oxo transfer reaction has been found to be smooth and quantitative. Interestingly $[(\text{CH}_3)_3\text{NOH}] \text{BPh}_4$ when allowed to react with $[\text{Bu}_4\text{N}]_2[\text{Mo}^{\text{IV}}\text{O}(\text{mnt})_2]$ in DMF, the rection was once more not quantitative. This can be explained by the strong cation solvating property of DMF^{134} . The reaction like,



liberates equivalent amounts of an acid and base as byproducts.

To maintain the pH of the reactive solution we found that if $(\text{CH}_3)_3\text{NO} \cdot 2\text{H}_2\text{O}$ was treated with glacial acetic acid and then dissolved in acetone then an effective pH around 6 could be maintained. The effective pH 6 was chosen because the kinetics of the native trimethylamine N-oxide reductase¹²⁹⁻¹³¹ has been performed mainly in the pH range 5.5 to 6.5. The reaction between $(\text{CH}_3)_3\text{NO} \cdot 2\text{H}_2\text{O}$ dissolved in acetic acid in acetone with an effective pH 6 and $[\text{Bu}_4\text{N}]_2[\text{Mo}^{\text{VI}}\text{O}(\text{mnt})_2]$ followed quantitatively with formation of $[\text{Bu}_4\text{N}]_2[\text{Mo}^{\text{VI}}\text{O}_2(\text{mnt})_2]$ and $(\text{CH}_3)_3\text{NH}^+\text{OAc}^-$.



The byproduct, $(\text{CH}_3)_3\text{NH}^+\text{OAc}^-$ has been tested by standard chemical method¹³⁵. The progress of this reaction as monitored spectrophotometrically is shown in Fig. 4.15. The appearance of clean isobestic points at 356 nm and 374 nm confirmed the formation of $[\text{Mo}^{\text{VI}}\text{O}_2(\text{mnt})_2]^{2-}$ from $[\text{Mo}^{\text{IV}}\text{O}(\text{mnt})_2]^{2-}$ without the formation of any other molybdenum species. For comparison purpose electronic spectra of $[\text{Bu}_4\text{N}]_2[\text{Mo}^{\text{IV}}\text{O}(\text{mnt})_2]$ and its oxidized form, $[\text{Bu}_4\text{N}]_2[\text{Mo}^{\text{VI}}\text{O}_2(\text{mnt})_2]$ taken in the same solvent (acetone-acetic acid) have been shown in Fig. 4.16. Saturation kinetics of $[\text{Bu}_4\text{N}]_2[\text{Mo}^{\text{IV}}\text{O}(\text{mnt})_2]$ with $(\text{CH}_3)_3\text{NO} \cdot 2\text{H}_2\text{O}$ in acetone-acetic acid medium (effective pH 6) was observed and the plot of observed first order rate constants, k_{obs} , vs concentration of trimethylamine N-oxide has been shown in Fig. 4.17. The first order rate constants were determined from the slope of the linear plot of $\log C$ (C = concentrations at different time intervals, obtained from absorptions at different time intervals) vs time. A

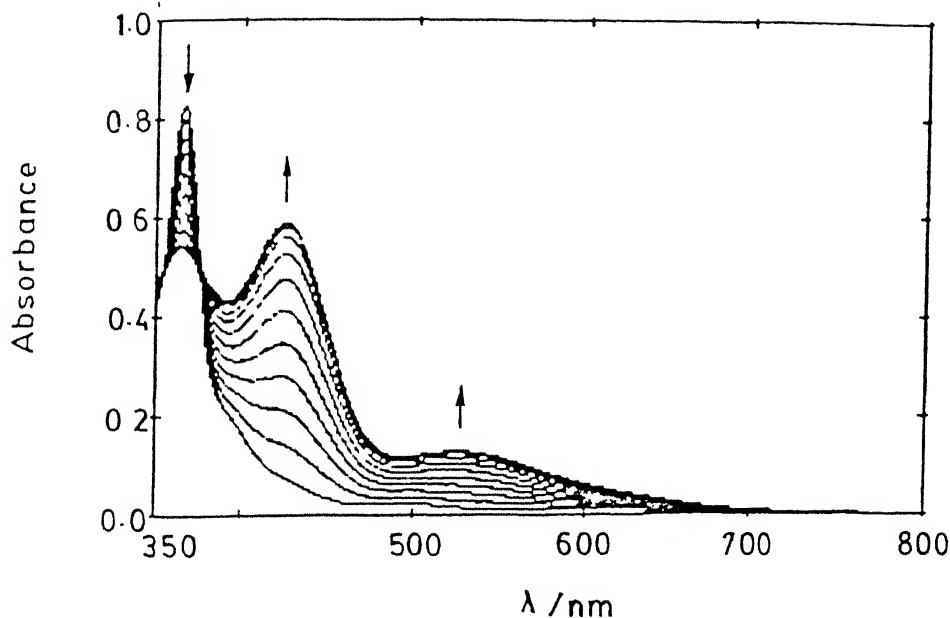


Fig. 4.15 Spectral changes for the reaction between $[\text{Bu}_4\text{N}]_2^{+}$
 $[\text{Mo}^{\text{IV}}\text{O}(\text{mnt})_2]$ (0.9×10^{-4} M) and $(\text{CH}_3)_3\text{NO} \cdot 2\text{H}_2\text{O}$ (1.8×10^{-3} M) in
acetone-acetic Acid (effective pH = 6) at $20 \pm 0.1^\circ\text{C}$.

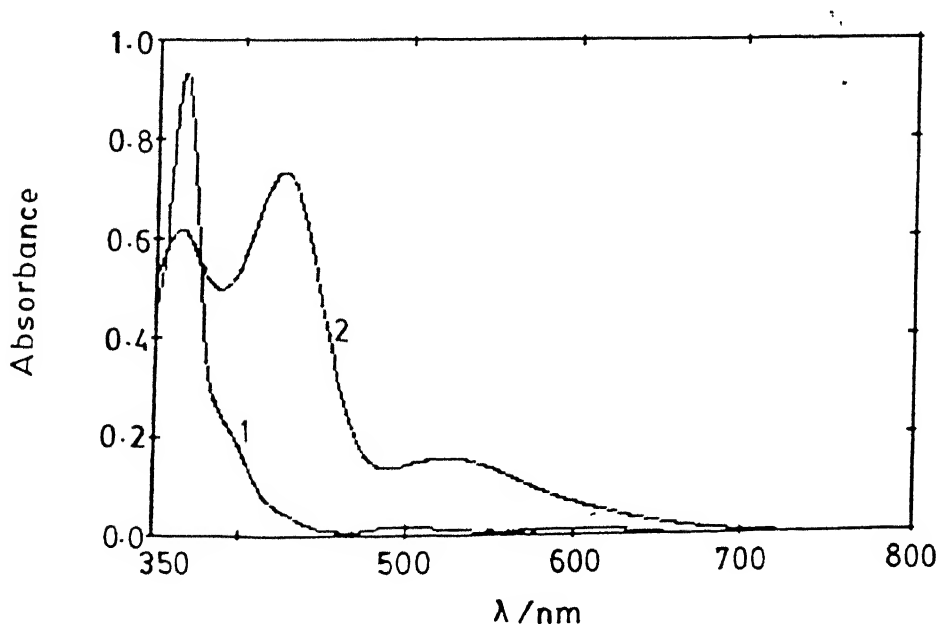


Fig. 4.16 UV-visible absorption spectra of $[\text{Bu}_4\text{N}]_2^{+}[\text{Mo}^{\text{IV}}\text{O}(\text{mnt})_2]$ 1
and $[\text{Bu}_4\text{N}]_2^{+}[\text{Mo}^{\text{VI}}\text{O}_2(\text{mnt})_2]$ 2 in acetone-acetic Acid (effective pH
6).

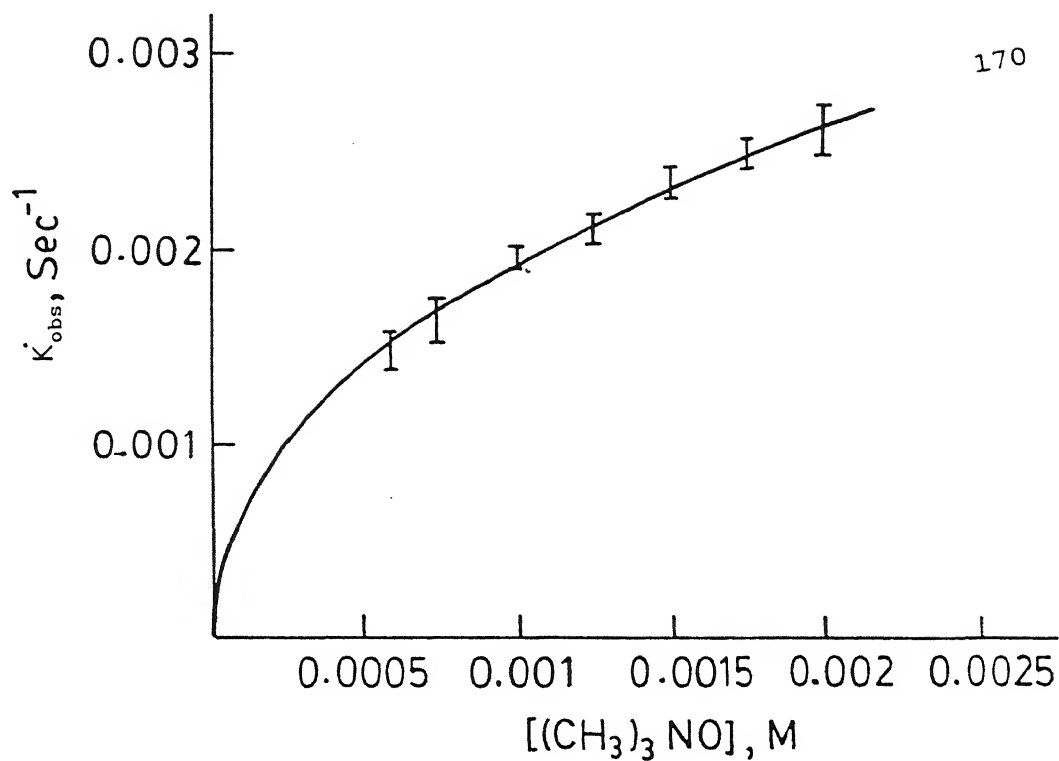


Fig. 4.17 Substrate saturation plot of k_{obs} vs $[(\text{CH}_3)_3\text{NO}.2\text{H}_2\text{O}]$ for the reaction between $[\text{Mo}^{\text{IV}}_0(\text{mnt})_2]^{2-}$ and $(\text{CH}_3)_3\text{NO}.2\text{H}_2\text{O}$ in acetone-acetic acid (effective pH 6)

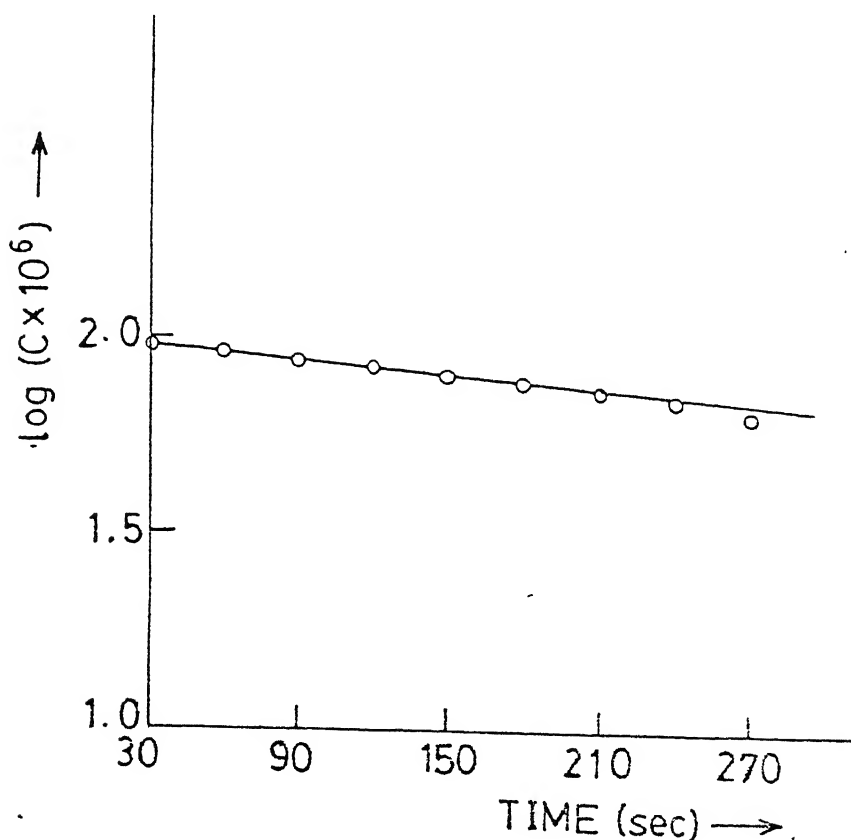


Fig. 4.18 Plot $\log(C \times 10^6)$ vs Time: reduction of $(\text{CH}_3)_3\text{NO}.2\text{H}_2\text{O}$ by $[\text{Mo}^{\text{IV}}_0(\text{mnt})_2]^{2-}$

representative plot is shown in Fig. 4.18. The first order rate was observed when trimethylamine N-oxide was taken five equivalents and more, and when taken less than five equivalents, second order reaction was followed.

From the recent EXAFS studies for sulfite oxidase it has been conclusively demonstrated that in the oxidized state the molybdenum center remains in MoO_2^{VI} form in both high pH and low pH. Thus protonation of dioxo species around pH 6 should not be anticipated for a good model compound in the oxidized state. However, EXAFS studies also demonstrated that in the fully reduced or in the half reduced form of sulfite oxidase, Cl^- binds to molybdenum center¹²⁶. This observation has also been substantiated by microcoulometric experiments¹²⁵ in presence of Cl^- . To test similar interaction between $[\text{Bu}_4\text{N}]_2^{+} [\text{Mo}^{\text{IV}}\text{O}(\text{mnt})_2]$ and Cl^- during oxo transfer reaction (34) saturation kinetics was followed in presence of Bu_4NCl with two fixed concentrations of 8×10^{-4} M and 15×10^{-4} M respectively. Double reciprocal plots each containing 1×10^{-4} M of $[\text{Bu}_4\text{N}]_2^{+} [\text{Mo}^{\text{IV}}\text{O}(\text{mnt})_2]$ with varying concentrations of $(\text{CH}_3)_3\text{NO}.2\text{H}_2\text{O}$ (in acetone-acetic acid): I_0 , in the absence of inhibitor, Bu_4NCl ; I_1 , in the presence of 8×10^{-4} M inhibitor, Bu_4NCl ; I_2 , in the presence of 15×10^{-4} M Bu_4NCl are shown in Fig. 4.19. These plots clearly showed competitive inhibition by Cl^- anion in this oxo transfer reaction. The V_{max} (= k_2 , the k_{obs} at substrate saturation) and K_m values are $3.81 \times 10^{-3} \text{ s}^{-1}$ and $9.1 (\pm 0.9) \times 10^{-4}$ M respectively (Table A8, Appendix) and inhibition constant K_I is 2.4×10^{-3} M (Table A9, Appendix).

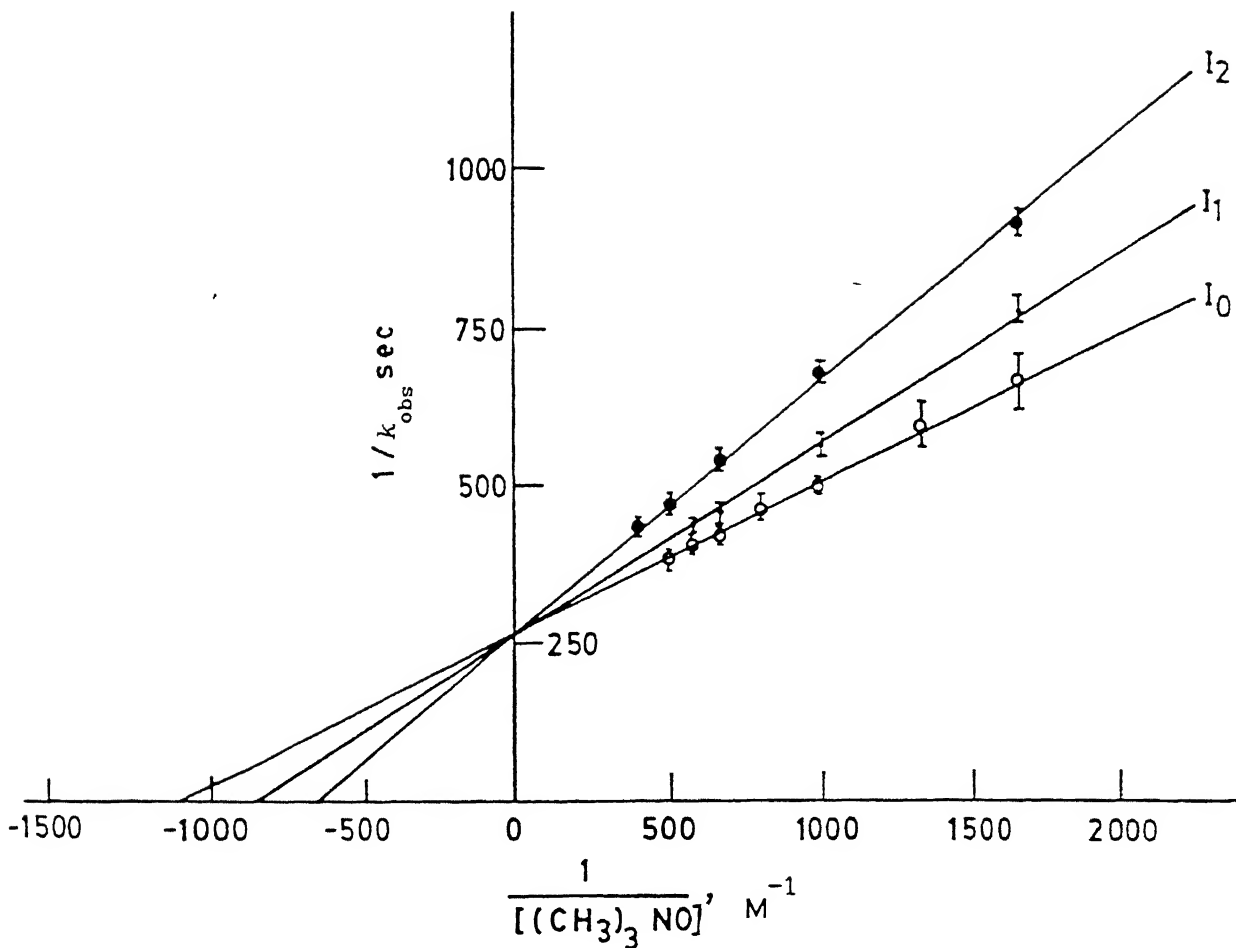


Fig. 4.19 Double reciprocal plots, each containing $1 \times 10^{-4} \text{ M}$ of $[\text{Bu}_4\text{N}]_2[\text{Mo}^{\text{IV}}_0(\text{mnt})_2]$ with varying concentrations of $(\text{CH}_3)_3\text{NO} \cdot 2\text{H}_2\text{O}$; I_0 represents reaction without Cl^- as inhibitor. I_1 and I_2 represent reactions carried out in the presence of Bu_4NCl as inhibitor with fixed concentrations of $8 \times 10^{-4} \text{ M}$ and $15 \times 10^{-4} \text{ M}$ respectively (reaction medium: acetone-acetic acid with effective

Activation parameters were obtained by least squares fit of k_{obs} values determined at different temperatures to the Eyring equation (30). The Eyring plot for this reaction has been shown in Fig. 4.20. All the kinetic data and activation parameters are summarized in Table 4.3. The negative entropy value is indicative of associative type of mechanism.

4.4 CONFIRMATIONS OF BINDING OF CHLORIDE ANION TO MOLYBDENUM.

In the previous section the competitive inhibition of Cl^- anion in trimethylamine N-oxide saturation kinetics has been demonstrated. These kinetic results imply that Cl^- binds at the same site where the oxo group of trimethylamine N-oxide binds. Hence Mo-Cl bond must be *cis* to Mo=O bond in $[\text{Mo}^{\text{IV}}\text{O}(\text{mnt})_2]^{2-}$ during oxidation process. However, there is also the possibility that Cl^- can bind *trans* to Mo=O bond in this monooxo complex. All isolation procedures in the presence of excess Cl^- ion containing cation with $[\text{Mo}^{\text{IV}}\text{O}(\text{mnt})_2]^{2-}$ failed to isolate Mo-Cl bond containing complex ion, $[\text{Mo}^{\text{IV}}\text{OCl}(\text{mnt})_2]^{3-}$, even with bulky cation. Similarly electronic spectrum of $[\text{Mo}^{\text{IV}}\text{O}(\text{mnt})_2]^{2-}$ in relatively weak coordinating solvent like CH_2Cl_2 did not change on addition of strongly donor solvents like DMF, DMSO, hexamethyl phosphoramide (HMPA) etc. However, the electronic spectrum of $[\text{Mo}^{\text{IV}}\text{O}(\text{mnt})_2]^{2-}$ in CH_2Cl_2 was identical to that taken in MeCN. But when spectra were taken in neat oxo donor solvents like DMF, DMSO and HMPA, the spectral band positions slightly change. Table 4.4

Table 4.3 Kinetic Data and Activation Parameters for the Reaction System 34 in acetone-acetic acid (effective pH 6)

T, K	$10^3 k_{\text{obs}}$, s^{-1}	ΔH^\ddagger , Kcal/mol	ΔS^\ddagger , cal/(deg.mol)
283	1.01 (\pm 0.06)		
288	1.62 (\pm 0.01)		
293	2.6 (\pm 0.03)	15.52 (\pm 0.95)	-17.29 (\pm 3.2)
298	4.47 (\pm 0.31)		

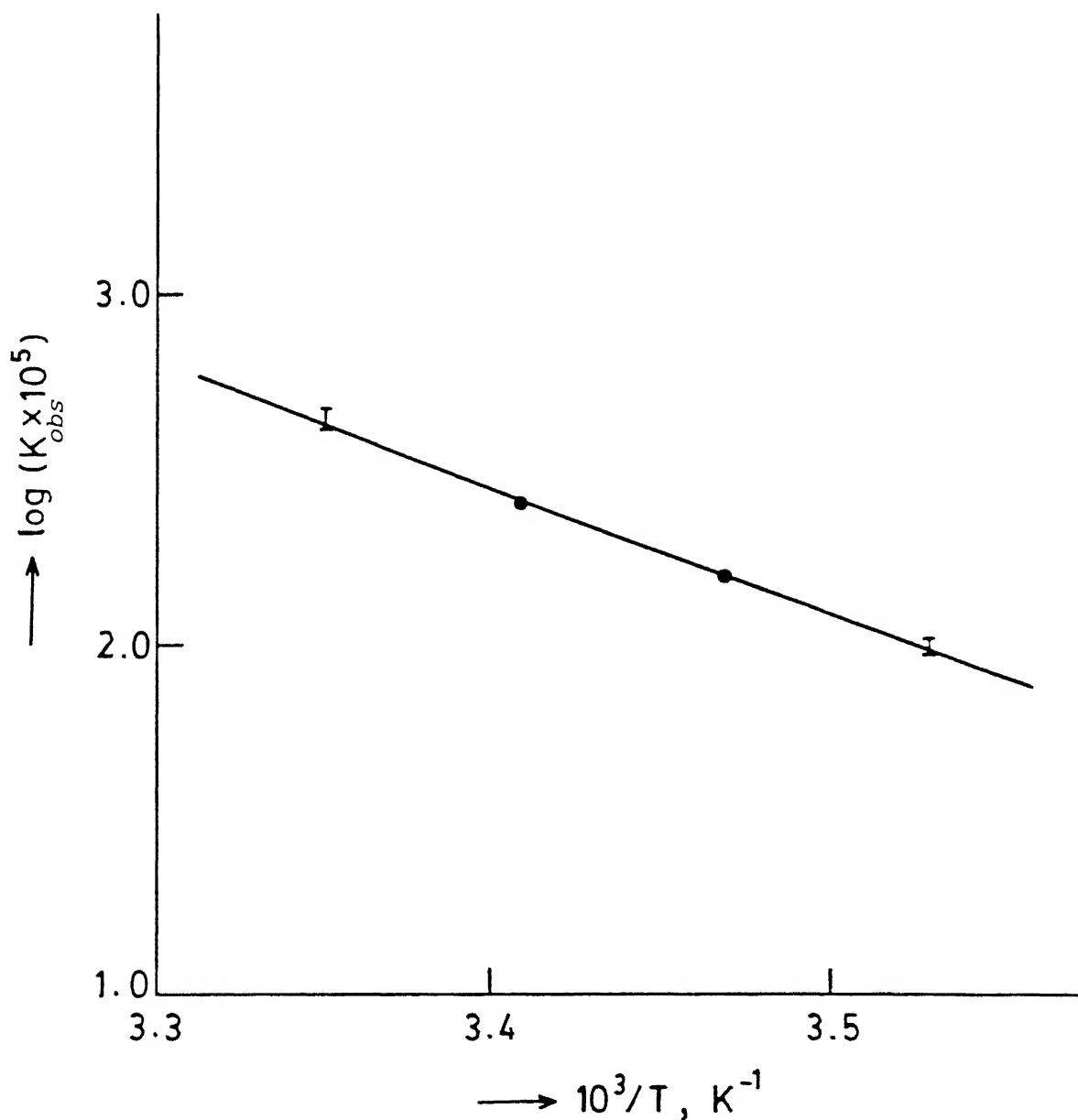


Fig. 4.20 Eyring plot of the rate constants (k_{obs}) for the reaction between $[Mo^{IV}O(mnt)_2]^{2-}$ and $(CH_3)_3NO \cdot 2H_2O$ in acetone-acetic acid (effective pH 6).

represents this change when spectra were taken in neat solvents. Red shift of the weak d-d bands was observed in the order HMPA > DMSO > DMF > acetone which correlates the donor property of the solvents. It is curious to note that MeCN has good donor property albeit being weakest among all oxo donor solvents mentioned above, yet no spectral change in CH_2Cl_2 and in MeCN suggest something which can not be explained readily. This difference in behavior was also reflected in cyclic voltammetric response of $[\text{Bu}_4\text{N}]_2^{+} [\text{Mo}^{\text{IV}}\text{O}(\text{mnt})_2]$ in these solvents. The one electron oxidation couple Mo(V)/Mo(IV) was found to be reversible in CH_2Cl_2 or in MeCN and also in acetone whereas in the rest of the solvents this oxidation process became irreversible. Cyclic voltammograms of $[\text{Bu}_4\text{N}]_2^{+} [\text{Mo}^{\text{IV}}\text{O}(\text{mnt})_2]$ in different solvents are shown in Fig. 4.21. Similar cyclic voltammetric response was observed in the oxidation of $\text{MoO}(\text{R}_2\text{dtc})_2$, especially, in solvents like MeCN, DMSO¹³³. For $\text{MoO}(\text{R}_2\text{dtc})_2$, DMSO clearly responds to oxo transfer reaction^{85a} with the formation of *cis*- $\text{MoO}_2(\text{R}_2\text{dtc})_2$. The present complex did not undergo any oxo transfer reaction with DMSO. However, the difference in CV response for both the complexes in N-donor solvent like MeCN and oxo donor solvent like DMSO suggests but definitely did not prove that in the present case these strong oxo donor solvents bind to *cis* position of Mo=O group in the complex. When cyclic voltammetry was done in the presence of Cl^- anion even in CH_2Cl_2 , the reversible oxidation process (Fig. 4.22a) became irreversible (Fig. 4.22b). When the scan speed was increased to 500 mV/s, another quasireversible couple centered at -0.20V vs SCE appeared alongwith the irreversible one. It is

Table 4.4 Visible / UV Spectral Data for $[\text{Mo}^{\text{IV}}\text{O}(\text{mnt})_2]^{2-}$ in Various Solvents^a

solvent	$\text{d} \longrightarrow \text{d}$	charge transfer
acetonitrile	602(110), 491(187)	365(10055), 395(sh)
acetone	608(130), 495(212)	365(9390), 397(sh)
dimethyl formamide	612(165), 499(246)	368(10934), 399(sh)
dimethyl sulfoxide	613(150), 500(225)	369(11317), 400(sh)
hexamethyl-phosphoramide	619(167), 505(238)	371(12049), 401(sh)
methylene chloride	603(132), 491(219)	366(9796), 395(sh)

^a λ_{max} in nm, ϵ in parentheses, conc. taken 1×10^{-4} M.

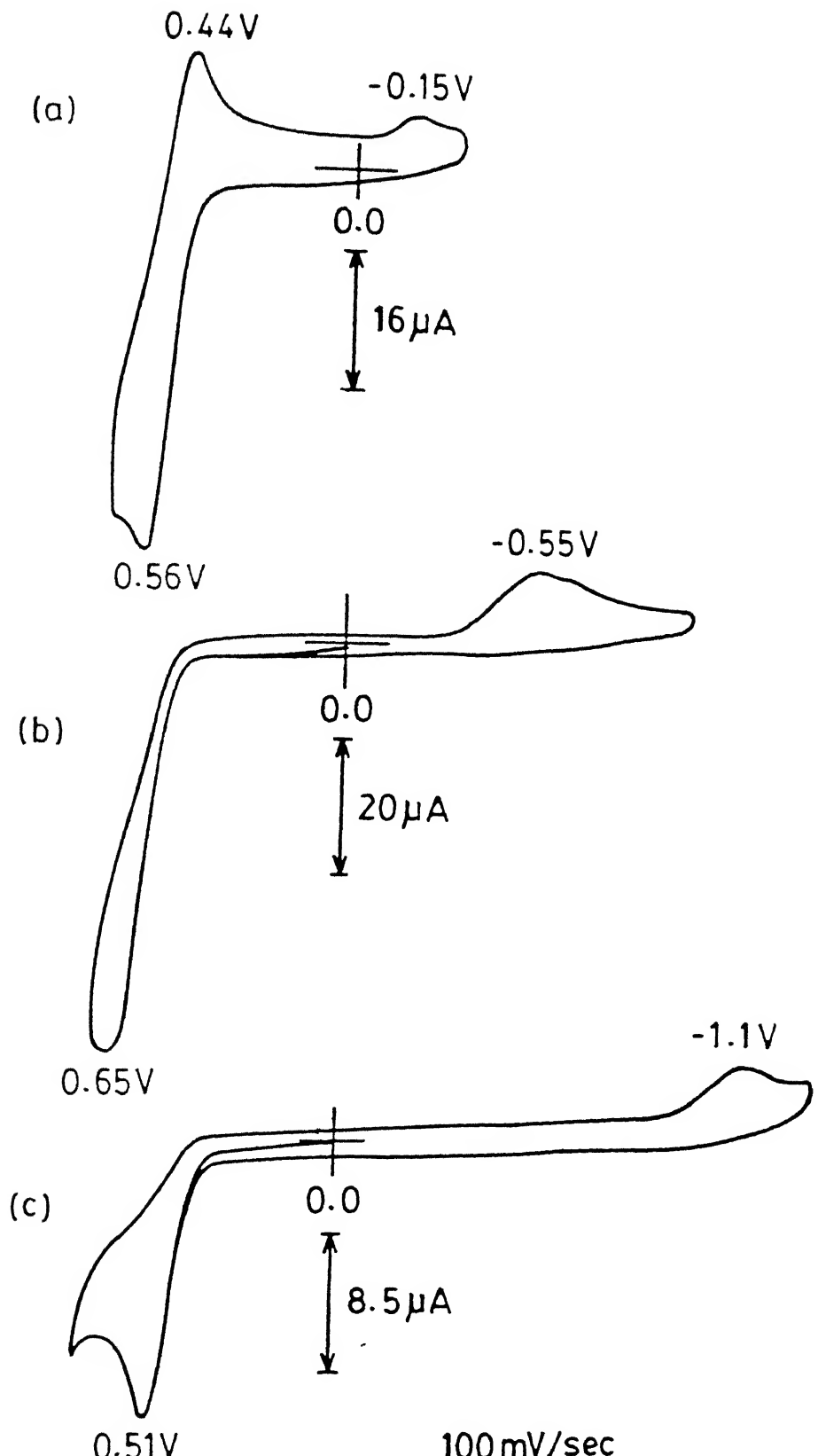


Fig. 4.21 Cyclic voltammograms of $[Bu_4N]_2[Mo^{IV}O(mnt)_2]$ in different solvents: (a) DMF, (b) DMSO and (c) HMPA . Potential vs Ag/AgCl, 0.1M Et_4NClO_4 , 100mV/s.

generally known that Cl^- binds to Mo(V) center in this type of complexes which can readily be seen when cyclic voltammograms were recorded in the presence of supporting electrolyte in chloride form^{78,80d}.

In the chapter 3 the isolation of $[\text{Ph}_3\text{PNPPh}_3][\text{Et}_4\text{N}]^-[Mo^{\text{V}}\text{OCl}(\text{mnt})_2]$ has already been described. The CV of this complex in the presence of $[\text{Ph}_3\text{PNPPh}_3]\text{Cl}$ as supporting electrolyte showed the quasireversible redox couple at -0.20V vs SCE which was identical to that recorded in cyclic voltammogram of $[\text{Mo}^{\text{IV}}\text{O}(\text{mnt})_2]^{2-}$ in presence of excess $[\text{Ph}_3\text{PNPPh}_3]\text{Cl}$ which has been shown in the inset of Fig. 4.22b. This electrochemical analysis implicate the binding of Cl^- to molybdenum in the redox process:



Further confirmation on the binding of Cl^- was made by ESR measurement of isolated $[\text{Ph}_3\text{PNPPh}_3][\text{Et}_4\text{N}]^-[Mo^{\text{V}}\text{OCl}(\text{mnt})_2]$. When this was dissolved in CH_2Cl_2 and subjected to room temperature ESR measurement, two molybdenum(V) signals having g values at 1.991 and 1.974 respectively appeared as shown in Fig. 4.23. With time the intensity of the signal with $g = 1.974$ decreased with the increase of the intensity of the signal of $g = 1.991$. When $[\text{Ph}_3\text{PNPPh}_3]\text{Cl}$ was added in excess into the test solution the ESR signal of $g = 1.991$ completely vanished with the appearance of signal with $g = 1.974$. When $[\text{Et}_4\text{N}]^2[\text{Mo}^{\text{IV}}\text{O}(\text{mnt})_2]$ was oxidized by one equivalent of iodine in CH_2Cl_2 and subjected to room temperature ESR measurement only molybdenum(V) species with $g = 1.991$ was observed. Into this when excess of $[\text{Ph}_3\text{PNPPh}_3]\text{Cl}$ was added the signal with $g = 1.991$ changed to the form with $g =$

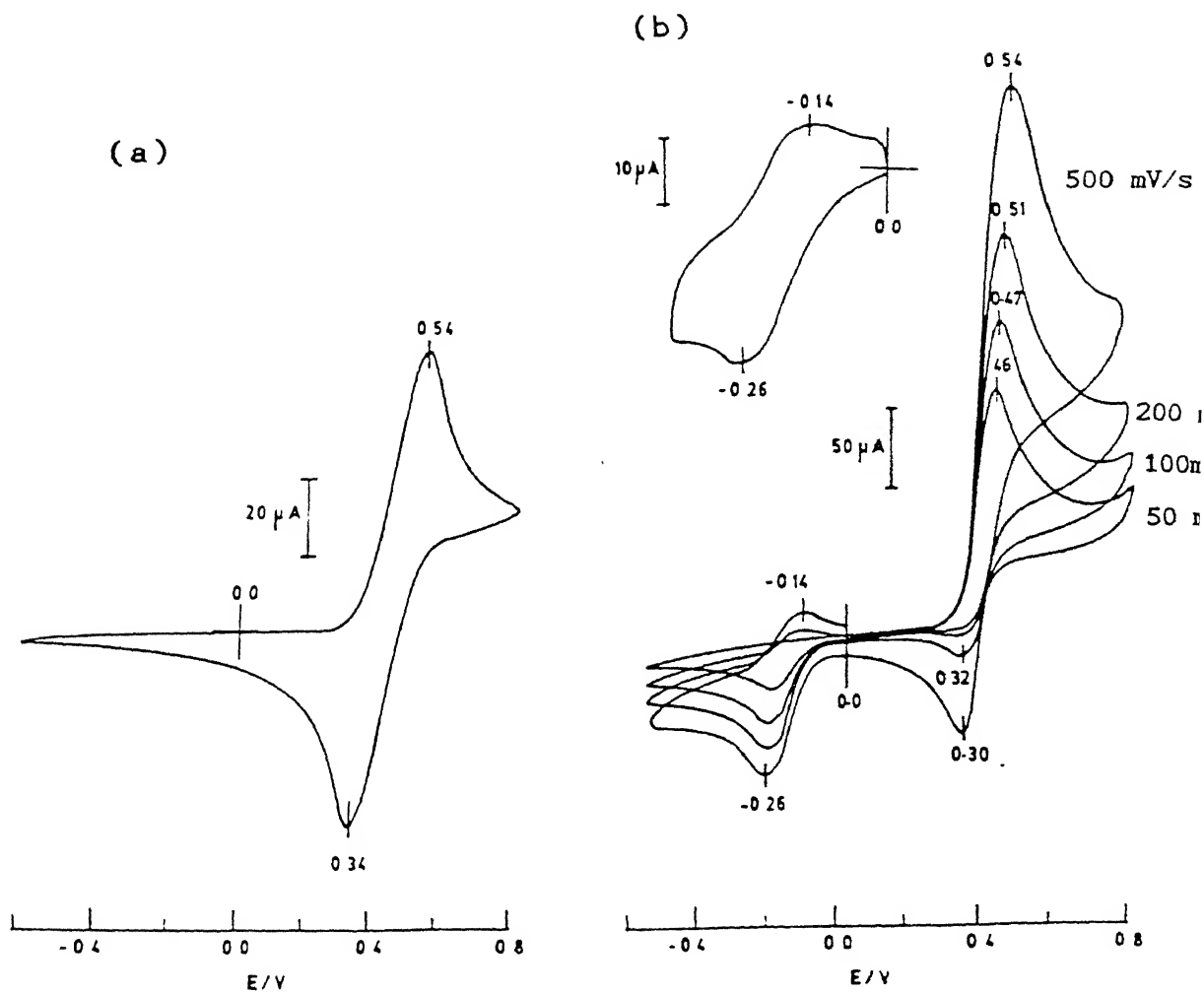


Fig. 4.22 (a) Cyclic voltammogram of $[\text{Bu}_4\text{N}]_2[\text{Mo}^{\text{IV}}\text{O}(\text{mnt})_2]$ in CH_2Cl_2 ; **4.22 (b)** Cyclic voltammograms at different scan rates (50, 100, 200 and 500 mV/s) of the compound in CH_2Cl_2 in the presence of excess of $[\text{Ph}_3\text{PNPPh}_3]\text{Cl}$. Inset, cyclic voltammogram of $[\text{Ph}_3\text{PNPPh}_3][\text{Et}_4\text{N}]^-\text{[Mo}^{\text{V}}\text{OCl}(\text{mnt})_2]$, scan rate 500 mV/s. Potential vs SCE, supporting

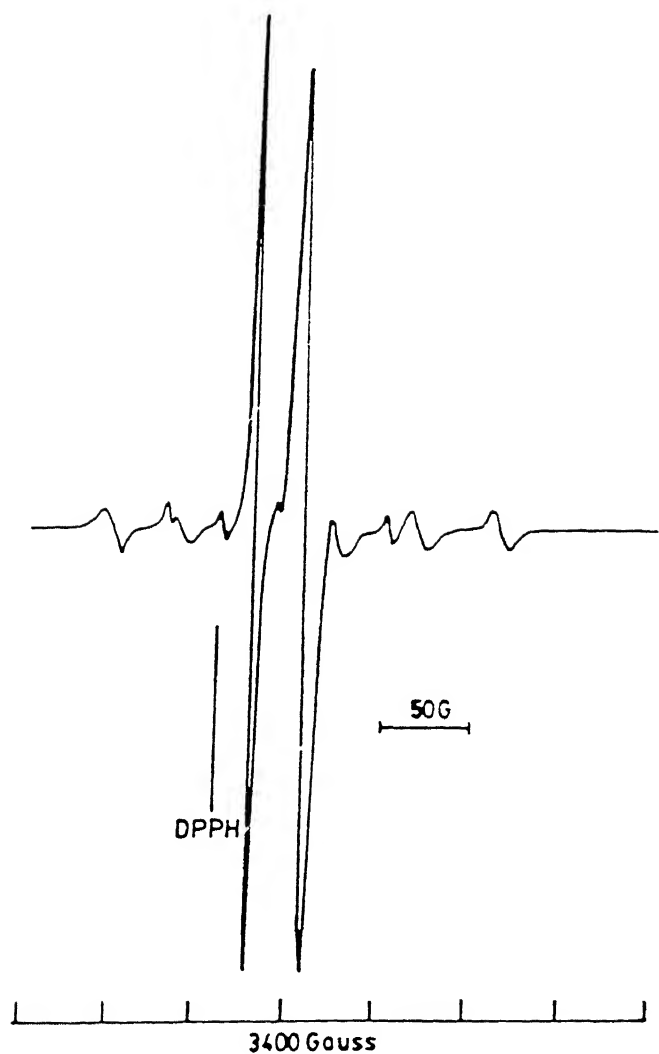
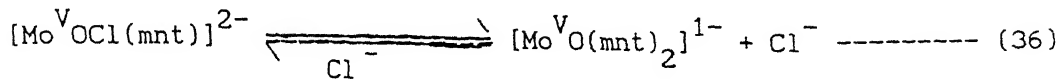


Fig. 4.23 ESR spectrum of $[\text{Ph}_3\text{PNPPh}_3][\text{Et}_4\text{N}]_2[\text{Mo}^{\text{V}}\text{OCl}(\text{mnt})_2]$ in CH_2Cl_2 at room temperature.

1.974 [Fig. 4.24]. These experiments clearly demonstrate the presence of two different molybdenum(V) species: one is in pentacoordinated form and another is in hexacoordinated form with Cl^- binding which are in equilibrium as shown below.



Chloride has two isotopes of ^{35}Cl and ^{37}Cl and both have $I = 3/2$ with combined natural abundance 100%. $^{35,37}\text{Cl}$ superhyperfine splitting (four components) could be observed if the attachment of Cl^- is *cis* to Mo=O group because the unpaired electron in the pentavalent complex is located in d_{xy} orbital. If the attachment of the Cl^- is *trans* to Mo=O group then no superhyperfine splitting out of Cl^- interaction could be observed. A careful search of the main signal (with $g = 1.974$) clearly showed superhyperfine splitting due to Cl^- interaction as shown in the inset of Fig. 4.24. Similar interaction of Cl^- has been reported for the complex¹³⁶, $[\text{MoOCl}(\text{S}_2\text{CNET}_2)_2]$. The magnitude of the chlorine superhyperfine splitting is small because of its low nuclear magnetic moment value. It has been thought that the corresponding bromo system having higher nuclear magnetic moment value will respond to this type of superhyperfine splitting with larger separation. However, addition of PPh_4Br in excess into $[\text{Mo}^{\text{V}}\text{O}(\text{mnt})_2]^{1-}$ generated by iodine oxidation of $[\text{Mo}^{\text{IV}}\text{O}(\text{mnt})_2]^{2-}$ did not affect the g of 1.991 suggesting that Br^- does not bind to molybdenum center. Verification of this was made with the kinetic experiment as described in the previous section. Thus when trimethylamine N-oxide saturation kinetics was followed in the

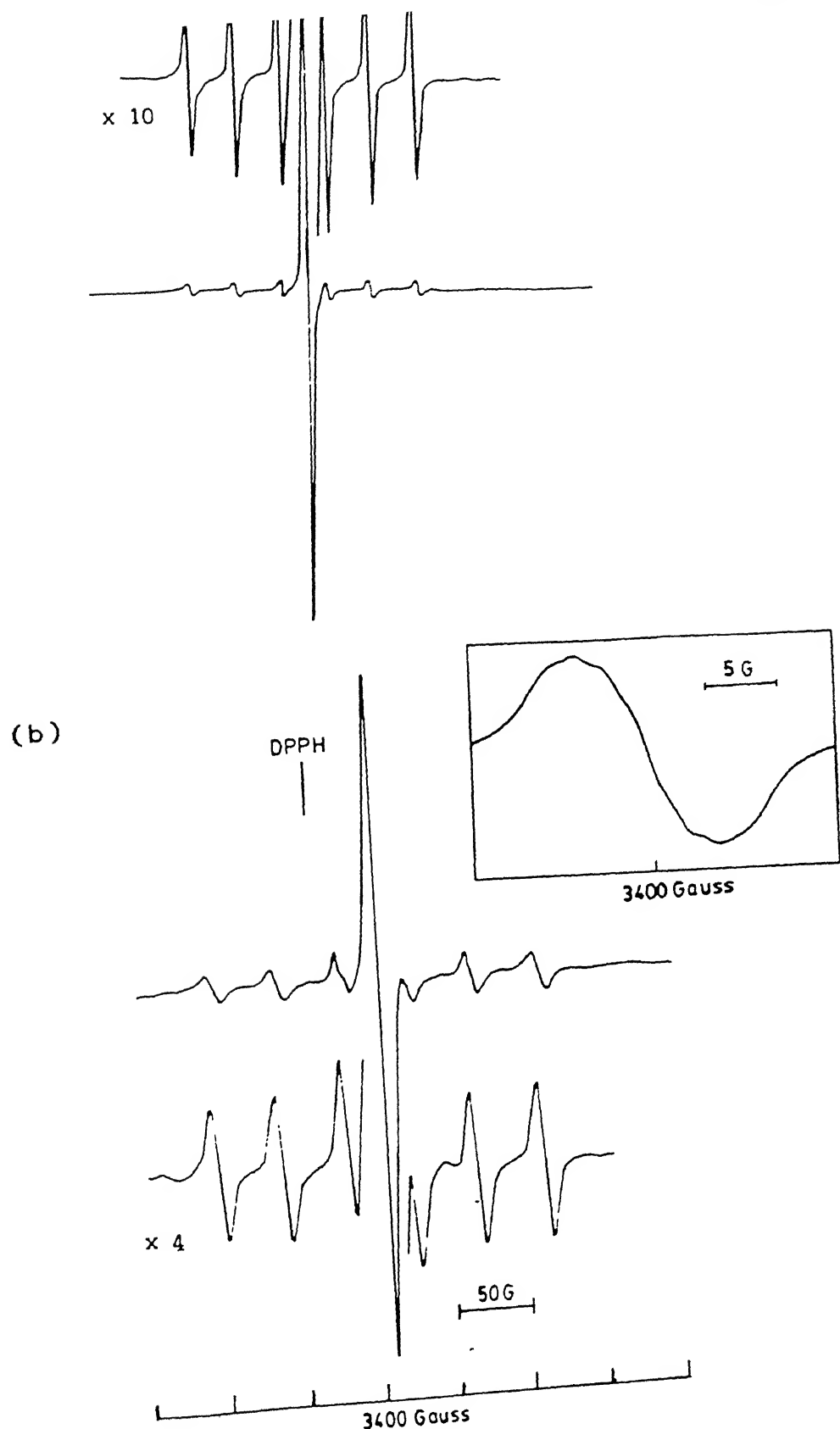


Fig. 4.24 (a) Room temperature ESR spectrum $[\text{Mo}^{\text{V}}\text{O}(\text{mnt})_2]^{1-}$ in CH_2Cl_2 formed by the reaction between $[\text{Bu}_4\text{N}]_2[\text{Mo}^{\text{IV}}\text{O}(\text{mnt})_2]$ and equivalent amount of iodine; (b) room temperature ESR spectrum

presence of PPh_4Br there was no apparent change in the k_{obs} values compared to those found without the presence of Br^- .

Thus from kinetics, cyclic voltammetry and by ESR spectroscopy it has been confirmed that in $[\text{Mo}^{\text{IV}}\text{O}(\text{mnt})_2]^{2-}$, Cl^- binds at *cis* position to Mo=O group. The ^{19}F hyperfine coupling in the ESR spectrum of molybdenum(V) species of sulfite oxidase at low pH form indicates the presence of Mo-F ligation¹²⁶ presumed to be analogous to the Mo-Cl interaction found by the effect of Cl^- on the molybdenum(V) ESR signal of chicken liver sulfite oxidase¹³⁷. ESR spectra of Cl^- bound and unbound forms of the species when carried out at liquid nitrogen (frozen) distinctly showed different patterns which are shown in Fig. 4.25. The axial pattern of the chloride bound complex in frozen solution (chloride unbound complex shows rhombic ESR signal in frozen solution) further support the *cis* chloride addition to Mo=O group¹³⁸. All the ESR parameters are tabulated in Table 4.5.

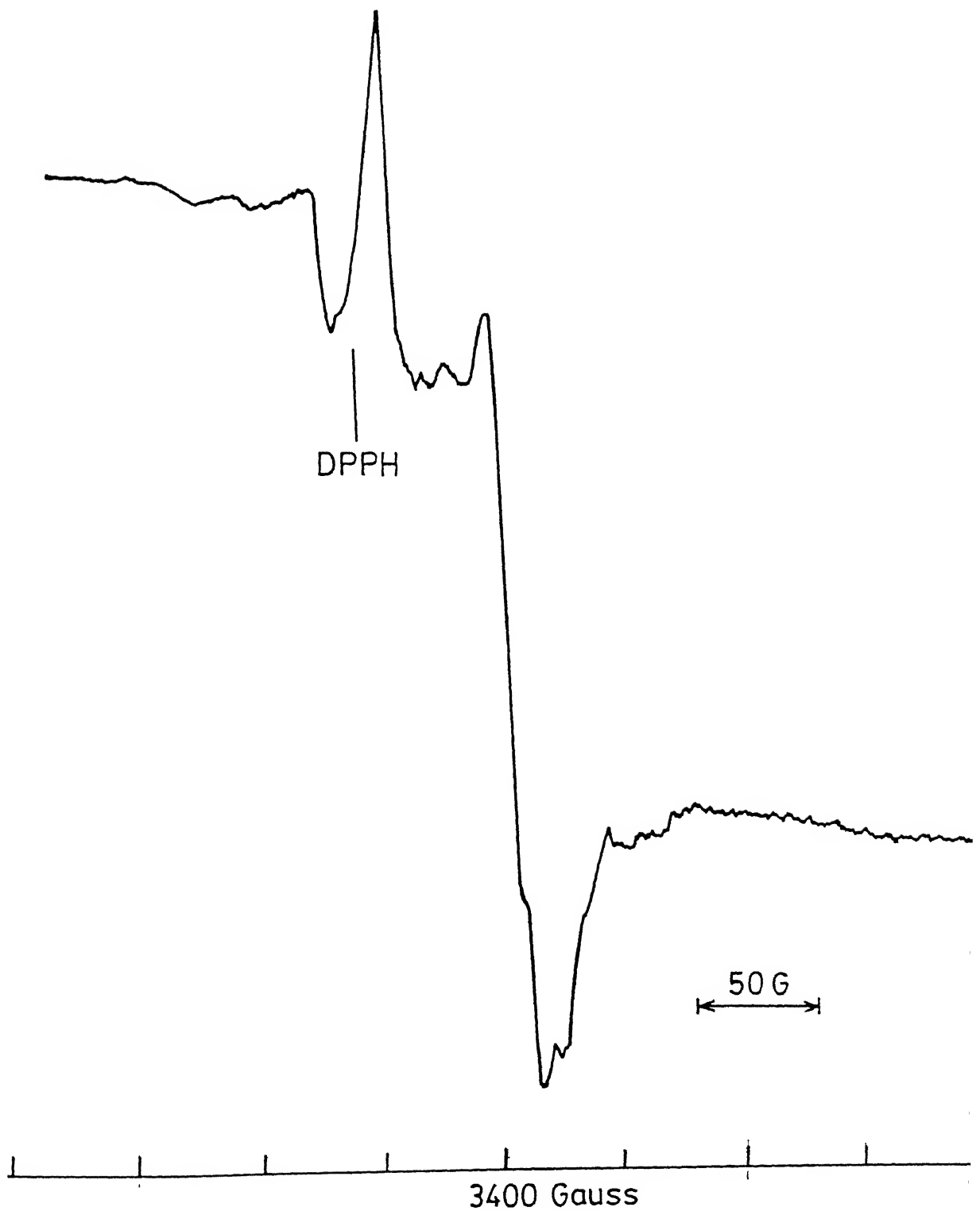


Fig. 4.25 (a) ESR spectrum of $[\text{Ph}_3\text{PNPPh}_3][\text{Et}_4\text{N}]_2[\text{Mo}^{\text{V}}\text{OC}_1(\text{mnt})_2]$, 1×10^{-3} M in CH_2Cl_2 . 0.10M $[\text{Ph}_3\text{PNPPh}_3]\text{Cl}$, 77K.

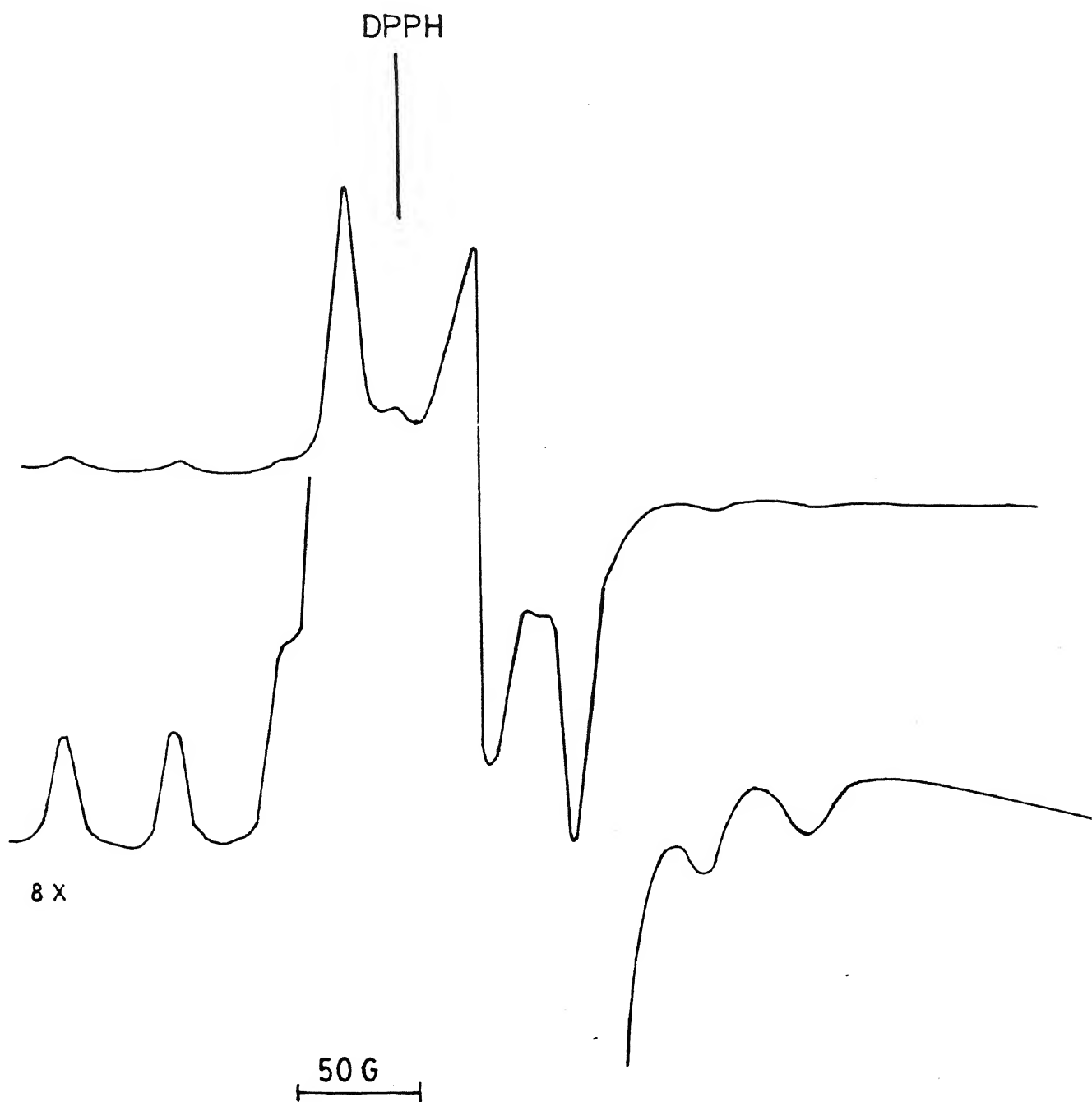


Fig. 4.25 (b) ESR spectrum of $[\text{Mo}^{\text{V}}_0(\text{mnt})_2]^{1-}$ formed by the reaction between $[\text{Bu}_4\text{N}]_2[\text{Mo}^{\text{IV}}_0(\text{mnt})_2]$ and equivalent amount of iodine in CH_2Cl_2 , 77K.

Table 4.5 ESR Parameters^a for $[\text{Mo}^{\text{V}}\text{O}(\text{mnt})_2]^{1-}$ (X) and $[\text{Mo}^{\text{V}}\text{OCl}(\text{mnt})_2]^{2-}$ (Y)^b

center	g_1	g_2	g_3	$\langle g \rangle_{\text{rt}}$	$^{95, 97}\text{Mo}$ (mT)			$\langle A \rangle_{\text{rt}}$
					A_1	A_2	A_3	
X	2.015	1.982	1.960	1.991	4.5	0.59	4.0	3.025
Y	1.998	1.963	1.950	1.974				4.35

^a CH_2Cl_2 . g values and $\langle A \rangle$, A_1 , A_3 values obtained from spectra, A_2 calculated from $\langle g \rangle \langle A \rangle = 1/3 (g_1 A_1 + g_2 A_2 + g_3 A_3)$. rt = room temperature, all other values at 77 K.

^bin the presence of excess $[\text{Ph}_3\text{PNPPh}_3]\text{Cl}$.

4.5 PROTON COUPLED ELECTRON TRANSFER REACTION.

As discussed in earlier chapters, a good model system should perform three important reactions involved in a catalytic cycle of oxomolybdoenzyme. Thus dioxomolybdenum(VI) species should respond to proton coupled electron transfer reaction. It is equally important that the monooxo species should be reverted back to dioxo species on treating with electron acceptor in aqueous medium whereby incorporation of the oxo group should proceed from water to molybdenum center.

Cyclic voltammograms of $[Bu_4N]_2[Mo^{VI}O_2(mnt)_2]$ in MeCN showed a quasireversible reduction at -1.1V vs Ag/AgCl. Interestingly the electronic spectrum of this complex in MeCN was identical to that when MeCN contained 0.13M CH_3COOH and 3.5M H_2O . This observation is in accord to the EXAFS results of oxidized form of sulfite oxidase¹²⁶ wherein it was shown that the dioxo form in the oxidized state does not protonate in low pH. When cyclic voltammogram was recorded in this mixed solvent the quasireversible reduction couple became irreversible and the reduction peak potential shifted to less negative potential at -0.77V vs Ag/AgCl. The change from quasireversible to irreversible reduction can be understood easily because the reduced species containing $MoO_2(V)$ being more basic in nature gets protonated⁷⁸. The drop in reduction potential may be due to proton coupled electron transfer reaction. Confirmation of this has been made when the same experiment was carried out in the presence of 0.13M CH_3COOD and 3.5M D_2O in MeCN. All the three voltammograms are shown in Fig. 4.26. The isotopic kinetic effect with the change of proton to deuterium can be

clearly understood by observing the profile of reduction peak in these two cases as shown in 4.26b and 4.26c. The broad nature of cathodic peak potential in deuterated system compared to that in protonated system confirmed the participation of proton coupled electron transfer in this electrochemical reduction¹³⁹. To understand the fate of this species upon reduction, controlled potential coulometry in identical mixed solvent at -1.0V has been performed. The value of n (number of electrons) has been found to be 2.5 (when still coulomb count was increasing). After electrolysis the solution was ESR silent and its electronic spectrum showed the presence of $[\text{Mo}^{\text{IV}}\text{O}(\text{mnt})_2]^{2-}$ along with some free dithiolene ligand. The coulometric time scale as well as the applied potential at -1.0V in acidic medium may be responsible for the decomposition of the complex and for solvent reduction resulting in the formation of free ligand with the increase of number of coulomb count beyond 2.

Stepwise oxidation of the reduced species, $[\text{Mo}^{\text{IV}}\text{O}(\text{mnt})_2]^{2-}$ has been tried in different solvent media. It has already been discussed earlier that in solvent like CH_2Cl_2 iodine oxidation led to the formation of $[\text{Mo}^{\text{V}}\text{O}(\text{mnt})_2]^{1-}$. It has also been shown (*vide supra*) that constant potential coulometric oxidation would lead to same pentavalent species which on prolonged keeping responded disproportionation reaction (*vide supra*). Oxidation of $[\text{Mo}^{\text{IV}}\text{O}(\text{mnt})_2]^{2-}$ has also been tried in aqueous solvent by making use of the $(\text{PyH})_2[\text{Mo}^{\text{IV}}\text{O}(\text{mnt})_2]$ salt which is soluble in water. Addition of an aqueous solution of $\text{K}_3[\text{Fe}(\text{CN})_6]$ into an aqueous solution of $(\text{PyH})_2[\text{Mo}^{\text{IV}}\text{O}(\text{mnt})_2]$ immediately changed the green

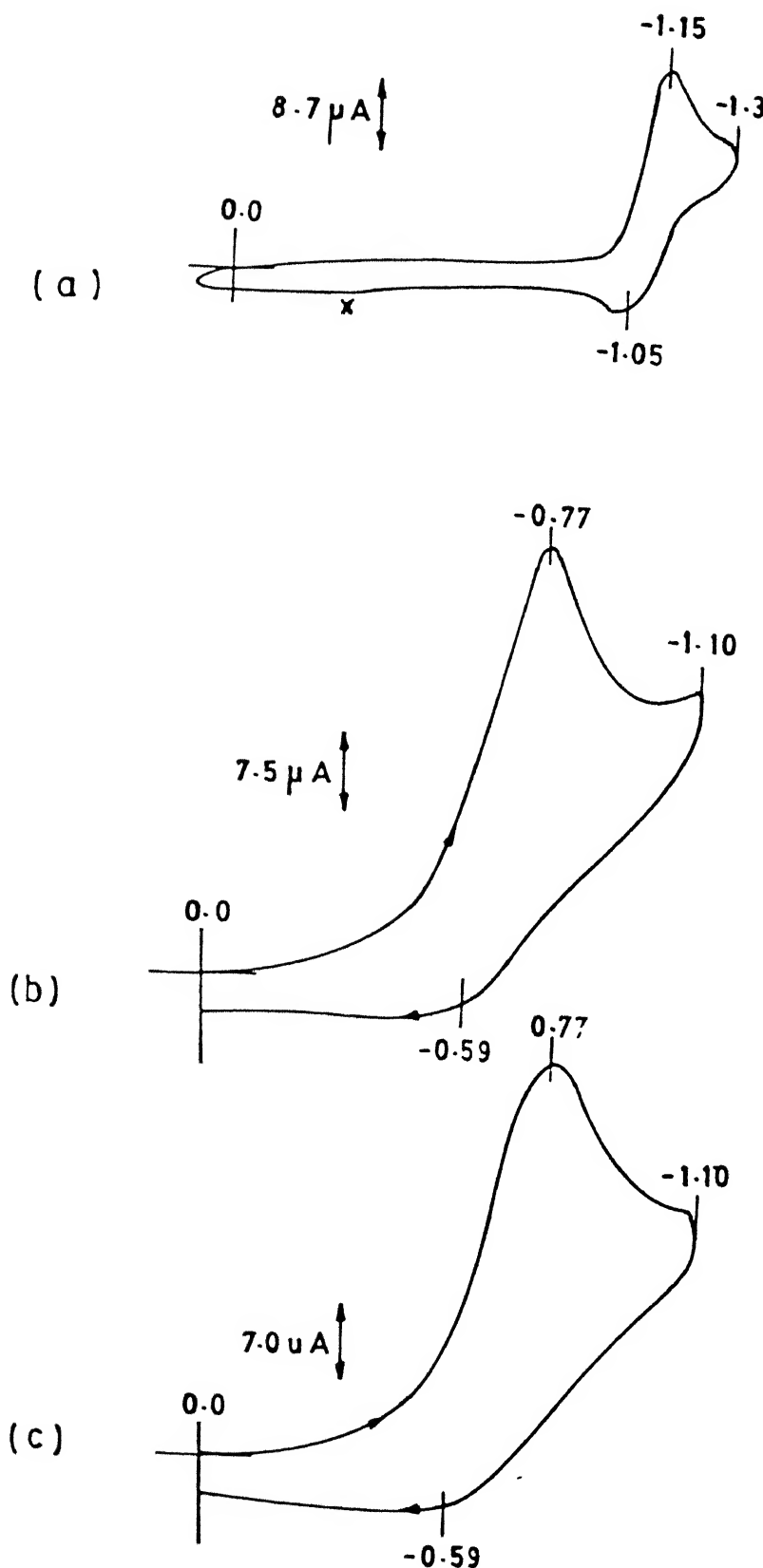


Fig. 4.26 Cyclic voltammograms of $[Bu_4N]_2[Mo^{VI}O_2(\text{mnt})_2]$: (a) in MeCN, (b) in MeCN containing 0.13M CH_3COOH and 3.5M H_2O , (c) in MeCN containing 0.13M CH_3COOD and 3.5M D_2O .

color to red brown. Immediate addition of excess of Bu_4^-NBr caused precipitation of brown gummy compound which after washing with water, isopropanol and ether and extracted by minimum MeCN on treating with isopropanol and ether gave $[\text{Bu}_4^-\text{N}]_2[\text{Mo}^{\text{VI}}\text{O}_2(\text{mnt})_2]$ in 10% yield. Simple redox potential of $[\text{Fe}(\text{CN})_6]^{4-}/[\text{Fe}(\text{CN})_6]^{3-}$ does not justify the oxidation of $(\text{PyH})_2[\text{Mo}^{\text{IV}}\text{O}(\text{mnt})_2]$ because its irreversible oxidation occurred in MeCN-water medium with an anodic peak potential +0.56V vs Ag/AgCl. This can be explained in the following way. $[\text{Fe}(\text{CN})_6]^{3-}$ may bind to $[\text{Mo}^{\text{IV}}\text{O}(\text{mnt})_2]^{2-}$ species and once these two are together electron transfer can take place. The oxidation potential of $[\text{Fe}(\text{CN})_6]^{3-}$ bound $[\text{Mo}^{\text{IV}}\text{O}(\text{mnt})_2]^{2-}$ may be suitable for intra or inter molecular electron transfer for which there is no simple way to confirm it. However, when $[\text{Fe}(\text{CN})_6]^{3-}$ was added into $[\text{Et}_4^-\text{N}]_2[\text{Mo}^{\text{IV}}\text{O}(\text{mnt})_2]$ in MeCN-water medium containing traces of acetic acid, the red brown color thus developed on spectrophotometric investigation showed the presence of an absorption band centered around 535 nm alongwith a strong and broad charge transfer band centered around 380 nm. When $[\text{Bu}_4^-\text{N}]_2[\text{Mo}^{\text{VI}}\text{O}_2(\text{mnt})_2]$ was dissolved in MeCN-water containing traces of acetic acid and one equivalent of $\text{K}_4[\text{Fe}(\text{CN})_6]$ was added to it, the electronic spectra of the resulting solution was identical to that observed with $[\text{Mo}^{\text{IV}}\text{O}(\text{mnt})_2]^{2-}$ and $\text{K}_3[\text{Fe}(\text{CN})_6]$ in MeCN-water medium containing acetic acid. It was difficult to analyze this intermediate further because of its instability. These observations suggest the formation of similar complex between $[\text{Mo}^{\text{VI}}\text{O}_2(\text{mnt})_2]^{2-}$ and $\text{K}_4[\text{Fe}(\text{CN})_6]$ as has been observed with reduced monooxo species and $\text{K}_3[\text{Fe}(\text{CN})_6]$.

color to red brown. Immediate addition of excess of Bu_4NBr caused precipitation of brown gummy compound which after washing with water, isopropanol and ether and extracted by minimum MeCN on treating with isopropanol and ether gave $[\text{Bu}_4\text{N}]_2[\text{Mo}^{\text{VI}}\text{O}_2(\text{mnt})_2]$ in 10% yield. Simple redox potential of $[\text{Fe}(\text{CN})_6]^{4-}/[\text{Fe}(\text{CN})_6]^{3-}$ does not justify the oxidation of $(\text{PyH})_2[\text{Mo}^{\text{IV}}\text{O}(\text{mnt})_2]$ because its irreversible oxidation occurred in MeCN-water medium with an anodic peak potential +0.56V vs Ag/AgCl. This can be explained in the following way. $[\text{Fe}(\text{CN})_6]^{3-}$ may bind to $[\text{Mo}^{\text{IV}}\text{O}(\text{mnt})_2]^{2-}$ species and once these two are together electron transfer can take place. The oxidation potential of $[\text{Fe}(\text{CN})_6]^{3-}$ bound $[\text{Mo}^{\text{IV}}\text{O}(\text{mnt})_2]^{2-}$ may be suitable for intra or inter molecular electron transfer for which there is no simple way to confirm it. However, when $[\text{Fe}(\text{CN})_6]^{3-}$ was added into $[\text{Et}_4\text{N}]_2[\text{Mo}^{\text{IV}}\text{O}(\text{mnt})_2]$ in MeCN-water medium containing traces of acetic acid, the red brown color thus developed on spectrophotometric investigation showed the presence of an absorption band centered around 535 nm alongwith a strong and broad charge transfer band centered around 380 nm. When $[\text{Bu}_4\text{N}]_2[\text{Mo}^{\text{VI}}\text{O}_2(\text{mnt})_2]$ was dissolved in MeCN-water containing traces of acetic acid and one equivalent of $\text{K}_4[\text{Fe}(\text{CN})_6]$ was added to it, the electronic spectra of the resulting solution was identical to that observed with $[\text{Mo}^{\text{IV}}\text{O}(\text{mnt})_2]^{2-}$ and $\text{K}_3[\text{Fe}(\text{CN})_6]$ in MeCN-water medium containing acetic acid. It was difficult to analyze this intermediate further because of its instability. These observations suggest the formation of similar complex between $[\text{Mo}^{\text{VI}}\text{O}_2(\text{mnt})_2]^{2-}$ and $\text{K}_4[\text{Fe}(\text{CN})_6]$ as has been observed with reduced monooxo species and $\text{K}_3[\text{Fe}(\text{CN})_6]$.

In this context it is important to take note that sodium dithionite has been taken as the universal *invitro* reductant for any oxomolybdoenzyme. The standard reduction potential¹⁴⁰ measured for dithionite is -0.666V vs NHE at pH 7. The basic question one can raise here whether dithionite transfers electron to all the oxomolybdoenzymes in the bound form or not. From chemistry point of view if dithionite is treated as a substrate and if it is bound to, say, molybdenum center in sulfite oxidase in the position of anion binding site, then the reduction potential of dithionite may not be identical in bound and in unbound forms. This argument is valid whenever electron transfer proceeds by inner sphere mechanism. This point could be once more addressed later (*vide infra*).

Thus the present model system accounts for sulfite oxidase analogue reaction wherein regeneration of the dioxo species can be achieved by $K_3[Fe(CN)_6]$ oxidation in aqueous medium. One electron oxidation of the tetravalent species does produce a pentavalent monooxo species which under high Cl^- concentration binds to Cl^- in *cis* position to Mo=O demonstrating the viability of this position over nonenzymatic *trans* position. The facile proton coupled electron transfer has also been demonstrated wherein the unstable pentavalent species, $MoO_2(V)$, changes to fully reduced tetravalent $MoO(IV)$ species. That salient changes in the apoprotein or molybdopterin substituent in the molybdenum cofactor can tune redox potential of the molybdenum center for selective substrate also been demonstrated with the present system in the light of trimethylamine N-oxide reduction. Better reactivity of

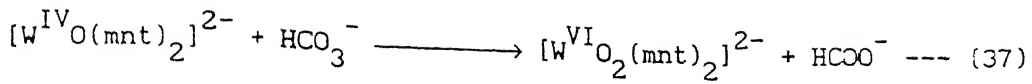
trimethylamine N-oxide in the form of ion pair, $[(\text{CH}_3)_3\text{NOH}]^+ \parallel \text{x}^-$ may relates with its role in lipid cell membrane of *E.coli* which possibly provides hydrophobic site for such reaction. In both the oxidase and reductase type of model reactions, the demonstration of anionic inhibitions has been made. In the sulfite oxidase analogue reaction, the demonstration of mixed noncompetitive inhibition by H_2PO_4^- is unique in a model reaction. This is because of the fact that in native sulfite oxidase, the detoxification of sulfite proceeds with a hidden bypass oxidative phosphorylation reaction in the presence of H^+ and H_2PO_4^- in mitochondria.

4.6 FUNCTIONAL ANALOGUE REACTION OF TUNGSTEN CONTAINING FORMATE DEHYDROGENASE.

The tungste formate dehydrogenase endogeneous to *Clostridium thermoaceticum* catalyses NADPH-dependent reduction of CO_2 to HCOO^- as the first step in acetogenic glucose fermentation^{53a,b}. This functional tungsten enzyme has been shown to contain the cofactor common to molybdenum hydroxylases^{26d} by *Neurospora crassa nit-1* reconstitution assay^{53c} and thus may contain a $\{\text{W}^{\text{IV}}=\text{O}\}$ moiety with a dithiolene chelated ligand in its reduced form. Preliminary EXAFS data from reduced sample of the formate dehydrogenase from *Clostridium thermoaceticum* have been reported¹⁴¹. A detailed analysis of this data was not possible because of the presence of mixture of $\text{W}(\text{IV})$, $\text{W}(\text{V})$ and $\text{W}(\text{VI})$ in the reduced samples¹⁴².

However, it was suggested that the formate dehydrogenase of *Clostridium thermoaceticum* may have tungsten site similar to that of the assimilatory molybdenum containing nitrate reductase of *E. coli*¹⁴³. Pentavalent state of tungsten in *Clostridium thermoaceticum* formate dehydrogenase has been reported by observing ESR signal¹⁴². In other related tungstoenzymes, specially for aldehyde ferredoxin oxidoreductase, the proposed EXAFS structure is almost identical to what is observed for sulfite oxidase^{54e, 126}. Based on the reconstitution assay of Deaton and coworkers^{53c}, a tungsten pterin cofactor also seems to be present in the *Clostridium thermoaceticum* formate dehydrogenase.

It was decided to check the reactivity of the reduced W(IV) complex, $[\text{Et}_4\text{N}]_2[\text{W}^{\text{IV}}\text{O}(\text{mnt})_2]$, in the light of actual biological substrate like CO_2 . $\text{CO}_2/\text{HCOO}^-$ couple has $E^\circ = -0.42\text{V}$ vs NHE. The E_{pa} of $[\text{W}^{\text{IV}}\text{O}(\text{mnt})_2]^{2-}$ at $+0.48\text{V}$ vs NHE in MeCN-water suggests that the oxidation of this W(IV) complex is thermodynamically possible by CO_2 . Under strict anaerobic conditions, $[\text{Et}_4\text{N}]_2[\text{W}^{\text{IV}}\text{O}(\text{mnt})_2]$ in MeCN-water (1:1) in the presence of excess of $\text{CO}_2/\text{HCO}_3^-$ (pH 7.5 adjusted by HCl), slowly changed to $[\text{Et}_4\text{N}]_2[\text{W}^{\text{VI}}\text{O}_2(\text{mnt})_2]$ within a day and on keeping the reaction mixture at a temperature of 50°C this change was completed after 6 h. From the reaction mixture, $[\text{Et}_4\text{N}]_2[\text{W}^{\text{VI}}\text{O}_2(\text{mnt})_2]$ was removed by repeated acetone treatment with the precipitation of a white solid largely containing $\text{NaHCO}_3/\text{Na}_2\text{CO}_3$. This was subjected to chromotropic acid test for formate assay¹⁴⁴ which proves the presence of 55% formate based on $[\text{Et}_4\text{N}]_2[\text{W}^{\text{IV}}\text{O}(\text{mnt})_2]$ thus demonstrating the reaction (37).



The reduction of HCO_3^- to HCOO^- with the formation of $[W^{VI}O_2(\text{mnt})_2]^{2-}$ clearly suggests that this synthetic system operates to fix CO_2 . Whether tungsten containing formate dehydrogenase of *Clostridium thermoaceticum* thus contains $W^{VI}O_2$ and $W^{IV}O$ moieties in the fully oxidized and in fully reduced states respectively or not can only be decided by refined EXAFS study or proper X-ray investigation of the native tungsten containing formate dehydrogenase.

Another important point in relevance to the predicting power of redox potential for two redox couples could be misleading when reaction follows inner sphere mechanism. It has been observed that $[\text{Et}_4\text{N}]_2[W^{VI}O_2(\text{mnt})_2]$ has the irreversible reduction peak potential at -1.50V vs Ag/AgCl. Sodium dithionite has the mid point potential -0.666V vs NHE at pH 7¹⁴⁰. This clearly suggests that sodium dithionate can not reduce $[W^{VI}O_2(\text{mnt})_2]^{2-}$ at pH 7. However, when $[\text{Et}_4\text{N}]_2[W^{VI}O_2(\text{mnt})_2]$ was dissolved in MeCN-water containing acetic acid with pH 5.5 and excess of sodium dithionite was added into it under anaerobic condition, $[W^{IV}O(\text{mnt})_2]^{2-}$ was indeed formed. The mid point potential of dithionite varies with pH as $\Delta E/\Delta \text{pH} = -59$ mV below pH 6.9¹⁴⁰. Even correcting the potential for this pH change reduction of $[W^{VI}O_2(\text{mnt})_2]^{2-}$ is not anticipated by sodium dithionite. The synthesis of $[\text{Et}_4\text{N}]_2[W^{IV}O(\text{mnt})_2]$ was achieved by dithionite reduction of tungstate (*vide supra*) clearly pointed out that for reaction following inner sphere mechanism as in the case of oxo transfer reaction in this class of model reaction it is important to take

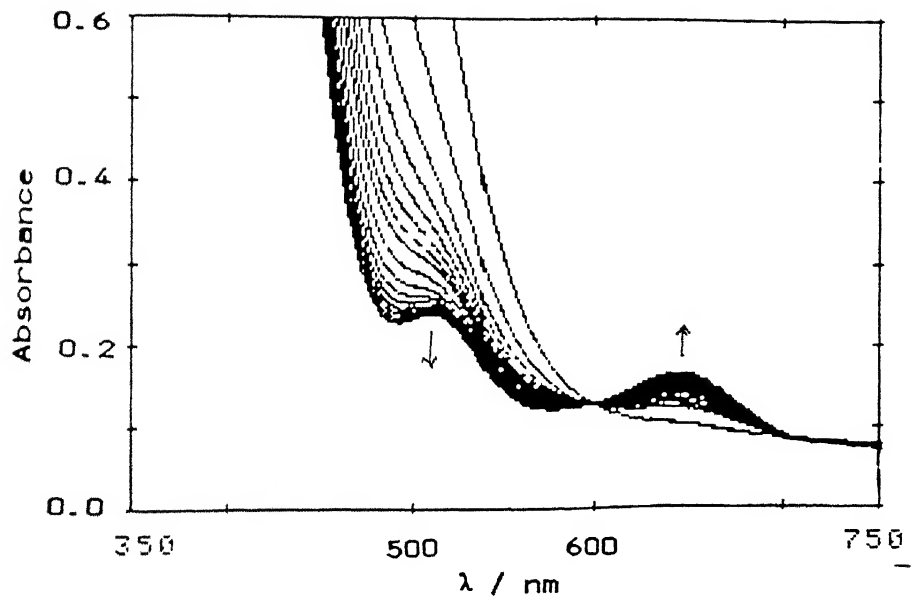
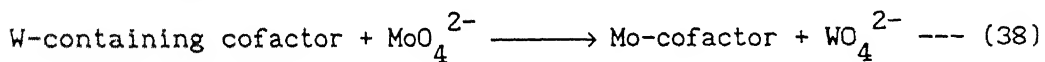


FIG. 4.27 Spectral changes for the reaction between $[\text{Et}_4\text{N}]_2[\text{W}^{\text{VI}}\text{O}_2(\text{mnt})_2]$ and sodium dithionite in 1:1 MeCN:H₂O (pH 5.5 adjusted by adding acetic acid).

note that on coordination of reducting substrate to the oxidized metal center should generate chemically entirely a new species. This might respond to intramolecular electron transfer reaction. The formation of $[W^{IV}O(mnt)_2]^{2-}$ from the reaction of $[W^{VI}O_2(mnt)_2]^{2-}$ and sodium dithionite in MeCN-water (pH 5.5 in the presence of acetic acid) is shown in Fig. 4.27.

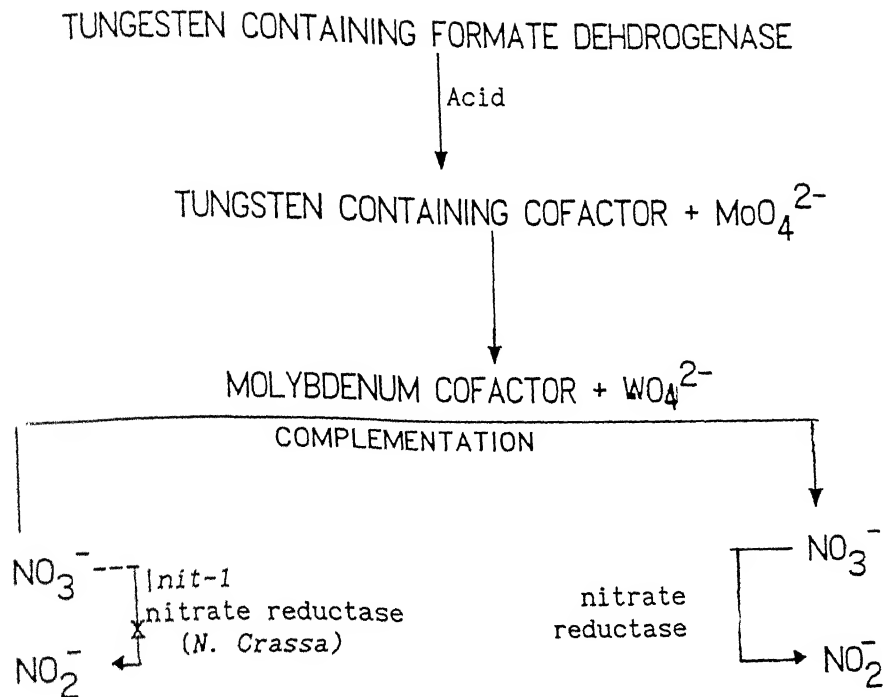
4.7 INTERMETALLIC ELECTRON TRANSFER REACTION.

The reconstitution assay of *N.crassa nit-1* by tungsten containing formate dehydrogenase of *Clostridium thermoacetecum* in the presence of molybdate can be viewed as shown in the Scheme 4.5. From this scheme it is evident that intermetallic electron transfer reaction takes place as



alongwith exchange of cofactor ligation from tungsten to molybdenum.

To decide whether our reduced WO(IV) compound, $[\text{Et}_4\text{N}]_2[W^{IV}O(mnt)_2]$, respond to similar reaction with MoO_4^{2-} , the following experiment was performed. When $[\text{Et}_4\text{N}]_2[W^{IV}O(mnt)_2]$ was taken in MeCN-acetate buffer in water (pH 5) was treated with equivalent amount of sodium molybdate, the purple color of the species slowly started to change under anaerobic condition which finally acquired green color. The progress of this reaction as observed spectrophotometrically is shown in Fig. 4.28a. For comparison the electronic spectra of $[\text{Et}_4\text{N}]_2[W^{IV}O(mnt)_2]$ and



Scheme 4.5

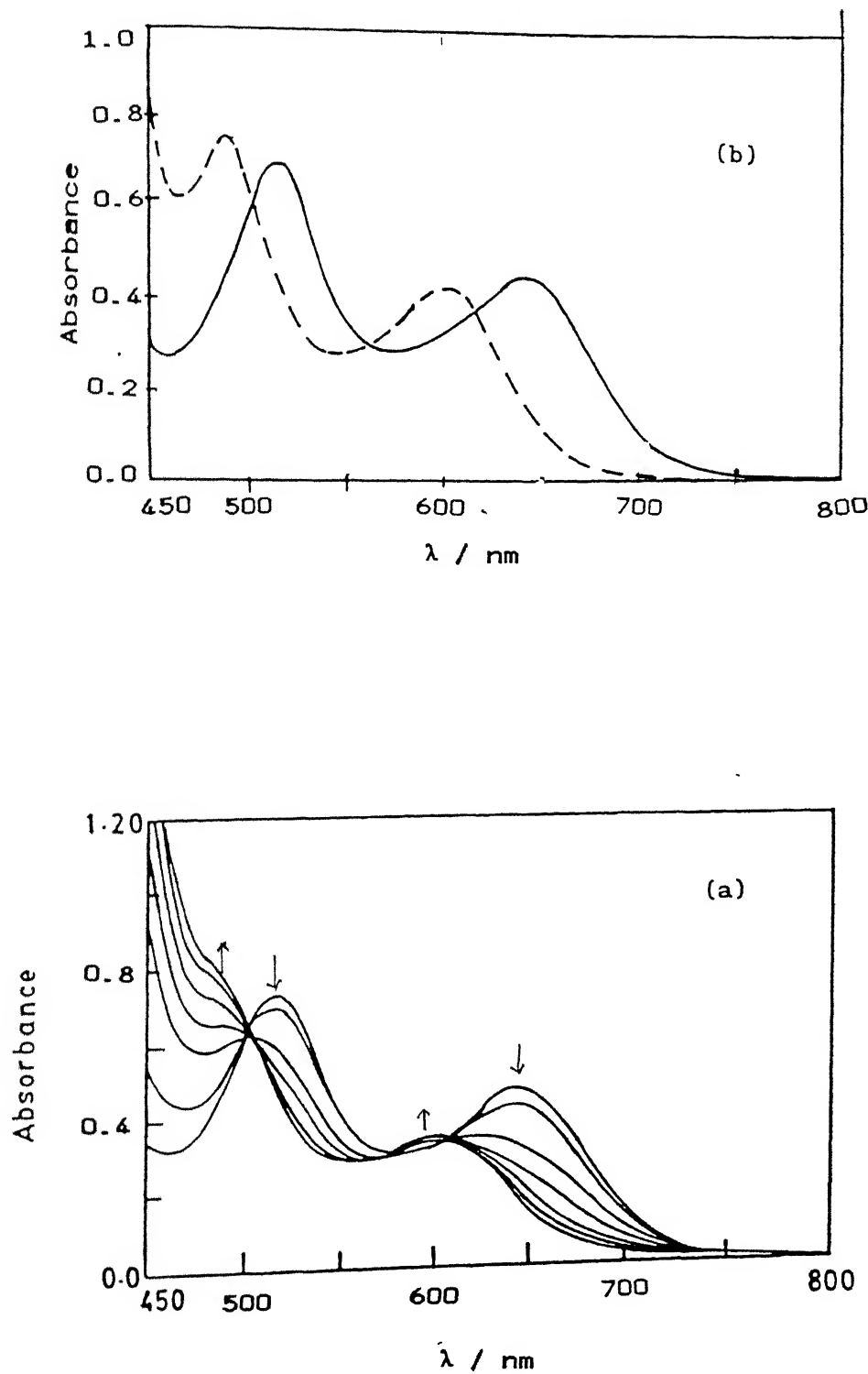


Fig. 4.28 (a) Spectral changes for the reaction between $[\text{Et}_4\text{N}]_2[\text{W}^{\text{IV}}\text{O}(\text{mnt})_2]$ and Na_2MoO_4 in MeCN-acetate buffer in water (pH 5.0); (b) UV-visible absorption spectra of $[\text{Et}_4\text{N}]_2[\text{Mo}^{\text{IV}}\text{O}(\text{mnt})_2]$ (----) and $[\text{Et}_4\text{N}]_2[\text{W}^{\text{IV}}\text{O}(\text{mnt})_2]$ (—) in the same medium.

$[\text{Et}_4\text{N}]_2[\text{Mo}^{\text{IV}}\text{O}(\text{mnt})_2]$ are shown in Fig. 4.28b. Fig 4.28a distinctly shows the conversion of $[\text{W}^{\text{IV}}\text{O}(\text{mnt})_2]^{2-}$ to $[\text{Mo}^{\text{IV}}\text{O}(\text{mnt})_2]^{2-}$ with isobestic points at 620 nm, 565 nm and 501 nm. However the reaction did not go for completion leading to some dissociation of free ligand which appeared with strong absorption near the highest energy isobestic point. Using this method 70% of $[\text{Et}_4\text{N}]_2[\text{Mo}^{\text{IV}}\text{O}(\text{mnt})_2]$ was isolated and from spectroscopic observation 80% conversion is observed. Thus with this model system it was shown that similar exchange reaction as observed in the native enzyme (equation 38) can be demonstrated with synthetic compound. It is important to comment on the two events operating in this reaction. The spectrophotometry clearly showed the exchange of dithiolene ligation from tungsten center to molybdenum center. However, to account for the electron transfer, time dependent ESR study was performed. When stoichiometric amount of $[\text{Et}_4\text{N}]_2[\text{W}^{\text{IV}}\text{O}(\text{mnt})_2]$ and sodium molybdate were taken in same media as used in spectrophotometric study and subjected to room temperature ESR measurement, at the initial stage no ESR signal was appeared. A scan after 15 min did show the appearance of ESR signals with $\langle g \rangle = 1.956$ and $\langle g \rangle = 1.92$ respectively. With the progress of time intensity of both the signals increase and after 2 h the signal at $\langle g \rangle = 1.956$ started to disappear whereas the intensity of signal with $\langle g \rangle = 1.92$ started to increase. After 6 h, the ESR signal with $\langle g \rangle = 1.956$ was not found but the signal at $\langle g \rangle = 1.92$ gained maximum intensity. On prolonged keeping (36 h) this signal also started decreasing in its intensity and finally vanished. The color of the reaction

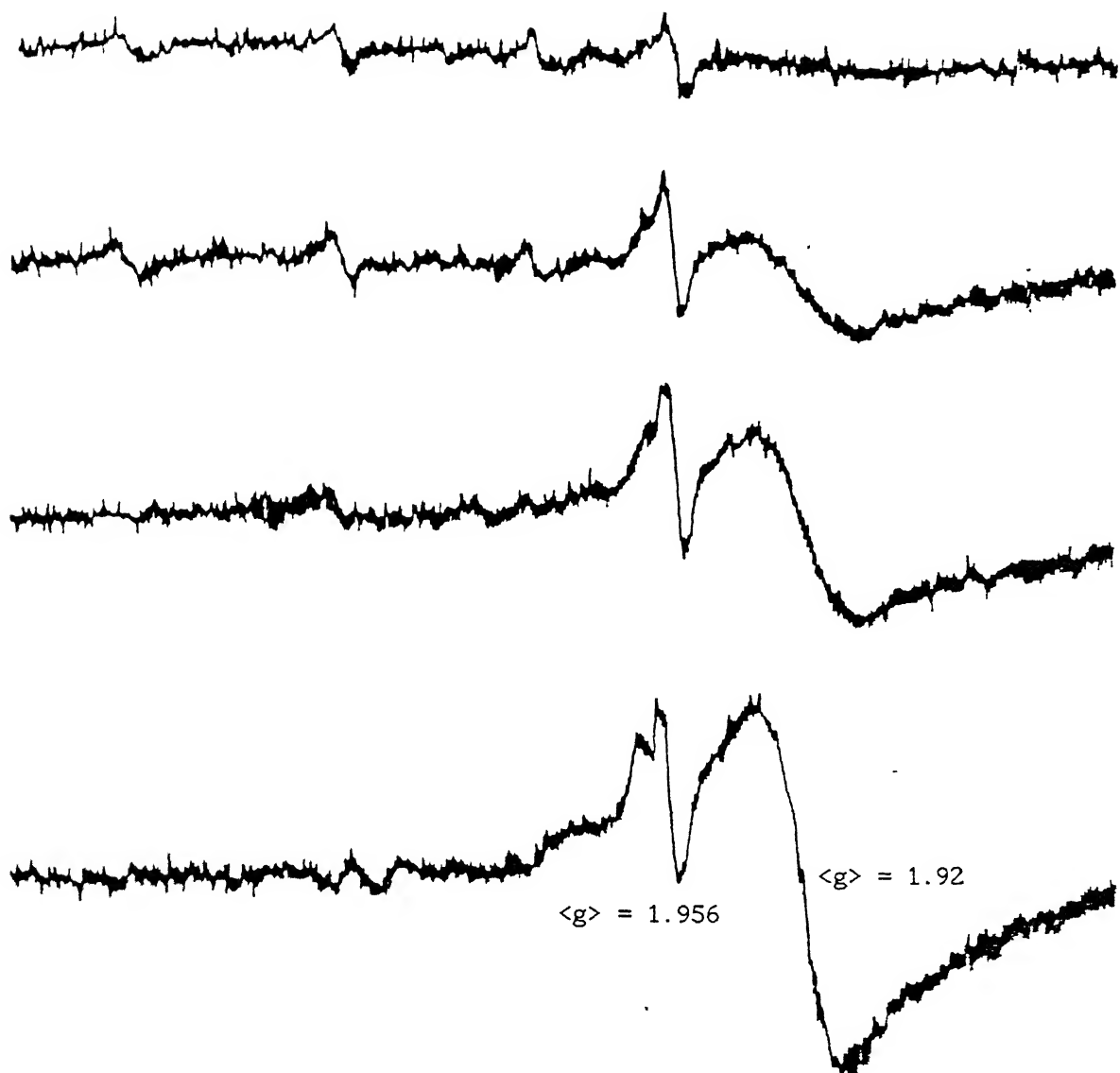


Fig. 4.29 (a) Time dependent ESR spectra for the reaction between $[W^{IV}O(\text{mnt})_2]^{2-}$ and Na_2MoO_4 in MeCN-acetate buffer in water (pH

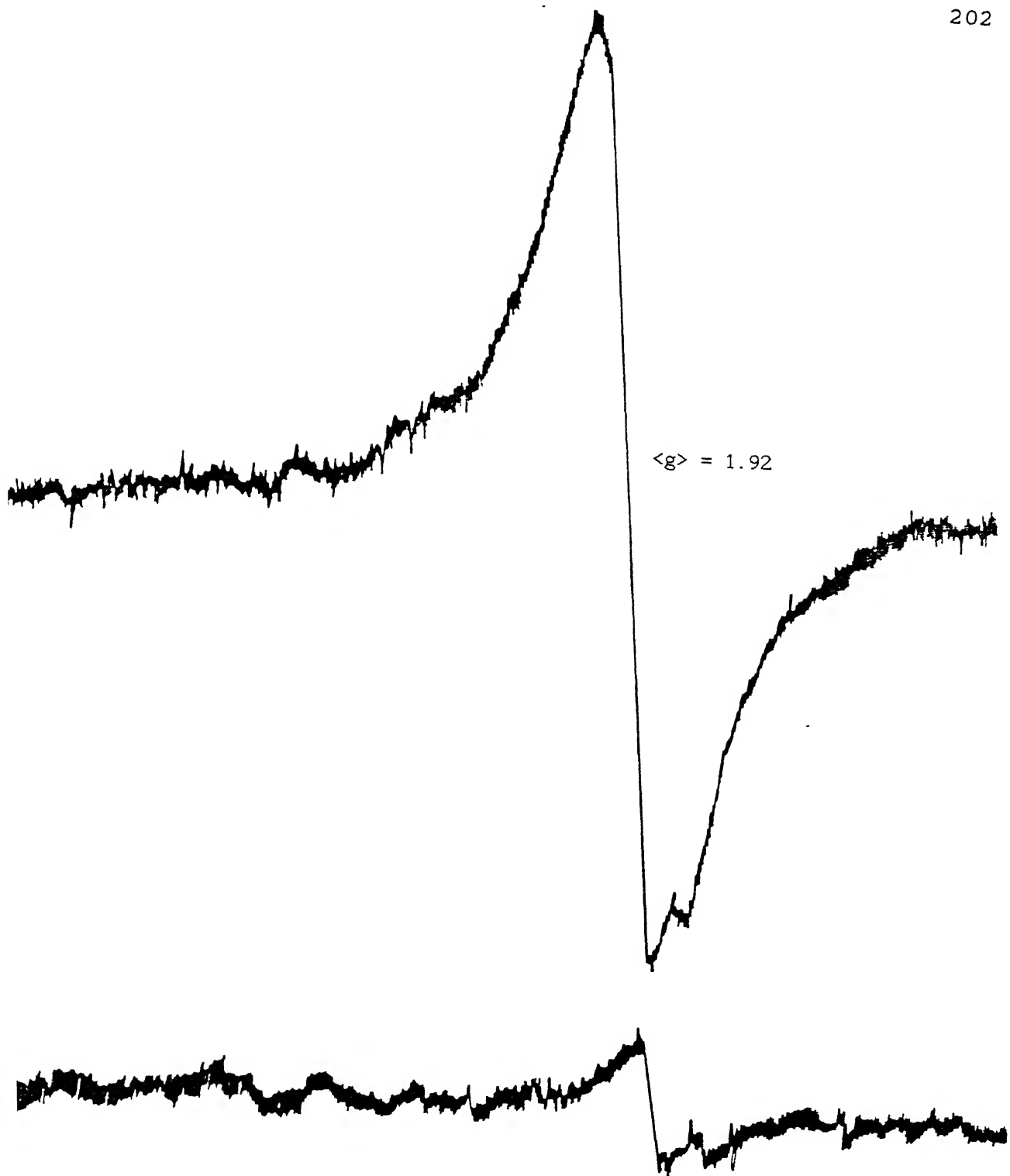
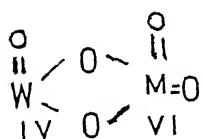


Fig. 4.29 (b) The ESR spectra for the reaction in Fig. 4.29(a)
after 36 h

mixture was green at the end point and spectrophotometric analysis suggests that it contain only $[\text{Mo}^{\text{IV}}\text{O}(\text{mnt})_2]^{2-}$ with some free ligand but without $[\text{W}^{\text{IV}}\text{O}(\text{mnt})_2]^{2-}$. $[\text{Et}_4\text{N}]_2[\text{W}^{\text{IV}}\text{O}(\text{mnt})_2]$ on iodine oxidation in CH_2Cl_2 did produce pentavalent $[\text{W}^{\text{V}}\text{O}(\text{mnt})_2]^{1-}$ with $\langle g \rangle = 1.956$ as shown earlier (*vide supra*). This clearly suggests that the second signal with $\langle g \rangle$ at 1.92 is due to molybdenum(V) predominantly in oxo environment³³.

In the entire course of this electron transfer reaction, atleast, in the ESR active pentavalent states of tungsten and molybdenum moieties, the apparent no change in g values strongly suggest that dithiolene ligands were not dissociated from tungsten so long tungsten is in W(V) oxidation state. Similarly $\langle g \rangle = 1.92$ for Mo(V) suggests that dithiolene is not coordinated to Mo(V) center which should have affect the g value during the course of the reaction. The best possible way to represent this redox reaction is to consider that pentacoordinated $[\text{W}^{\text{IV}}\text{O}(\text{mnt})_2]^{2-}$ reacts with Mo(VI) to make a heptacoordinated tungsten species containing bimetallic moiety as



in the initial stage. Intramolecular electron transfer takes place between these two centers and when both the centers acquired pentavalent state the moiety remains stable. Spectrophotometric investigation (Fig. 4.28a) proved that at the initial event the isobestic points were tight. However, at the later stage appearance of the free ligand could be seen. Thus when W(V) was

oxidized to W(VI) state the release of dithiolene ligand took place. Dithiolene preferentially binds to Mo(IV) state thus demonstrating the appearance of only one ESR active Mo(V) species for the entire course of reaction. The progress of this reaction as followed by ESR spectroscopy is shown in Fig. 4 29a,b.

CHAPTER 5

OXIDATIVE ADDITION REACTION

In the last part of the preceding chapter the reducing property of $[W^{IV}O(mnt)_2]^{2-}$ has been recognized. In this regard it has also been noticed that this pentacoordinated species can bind donors even in the form of MoO_4^{2-} presumably with the intermediate formation of heptacoordinated tungsten species. If after the intermetallic electron transfer reaction the bimetallic intermediate with tungsten(VI) and molybdenum(IV) would have been isolated the system could have been regarded as an example of oxidative addition reaction.

Five coordinated dithiocarbamato complexes of molybdenum(IV), $MoO(R_2dtc)_2$, demonstrate oxidative addition reaction with elemental sulfur¹⁰² as well as with activated acetylenes¹⁰³. Similar tungsten-acetylene species are reported, but the syntheses of these have been achieved by a different synthetic route¹⁴⁵. Furthermore the difficulty of formation of $WO(IV)$ core from $WO_2(VI)$ core by oxygen atom transfer reaction is mainly considered due to thermodynamic reasons as reflected in the reduction potential of $WO_2(VI)$ core. Recently Nakamura *et al* have demonstrated oxygen atom transfer of $[M^{VI}O_2(bdt)_2]^{2-}$ ($M = Mo$ and W) with benzoin (*vide supra*)⁹³. They have shown that the observed rates of these reactions are very similar, albeit the reduction potential peak of tungsten system is -1.34V vs SCE compared to molybdenum system (-0.97V vs SCE) implicating that the

irreversible reduction potential peak is not a good thermodynamic measure alone to predict the viability of a reaction. Based on these, the reactivity study between $[\text{Et}_4\text{N}]_2[\text{W}^{\text{IV}}\text{O}(\text{mnt})_2]$ and elemental sulfur or activated acetylene like demethyl acetylenedicarboxylate (DMAC) has been undertaken.

The syntheses of $[\text{Et}_4\text{N}]_2[\text{W}^{\text{VI}}\text{O}(\text{mnt})_2(\text{C}_2(\text{CO}_2\text{CH}_3)_2)]$ and $[\text{Et}_4\text{N}]_2[\text{W}^{\text{VI}}\text{O}(\text{S}_2)(\text{mnt})_2]$ have already been described earlier. In this chapter some kinetic aspects related to these complexes have been presented.

5.1 OXIDATIVE ADDITION REACTION WITH DMAC.

The oxidative addition reaction in MeCN,

$$[\text{Et}_4\text{N}]_2[\text{W}^{\text{IV}}\text{O}(\text{mnt})_2] + \text{DMAC} \xrightleftharpoons[k_{-1}]{k_{+1}} [\text{Et}_4\text{N}]_2[\text{W}^{\text{VI}}\text{O}(\text{mnt})_2(\text{C}_2(\text{CO}_2\text{CH}_3)_2)] \quad (39)$$

when followed spectrophotometrically under sufficient excess of DMAC concentration showed the desired conversion upto 80% with isobestic points at 364 nm and 581 nm as shown in Fig. 5.1. The K_{eqm} (k_{+1}/k_{-1}) was calculated by observing the formation of product by monitoring its absorption at 435 nm when the reaction attended equilibrium using excess DMAC at different concentrations. The K_{eqm} has been found to be $14 (\pm 1) \text{ M}^{-1}$ at 25°C in MeCN. At sufficiently high concentration of DMAC i.e. under pseudo first order condition the first order rate constant k_{+1} has been found to be $11.2 (\pm 1.0) \times 10^{-4} \text{ s}^{-1}$. From K_{eqm} and k_{+1} values, the k_{-1} has been calculated to be $0.8 (\pm 0.1) \times 10^{-4} \text{ s}^{-1}$.

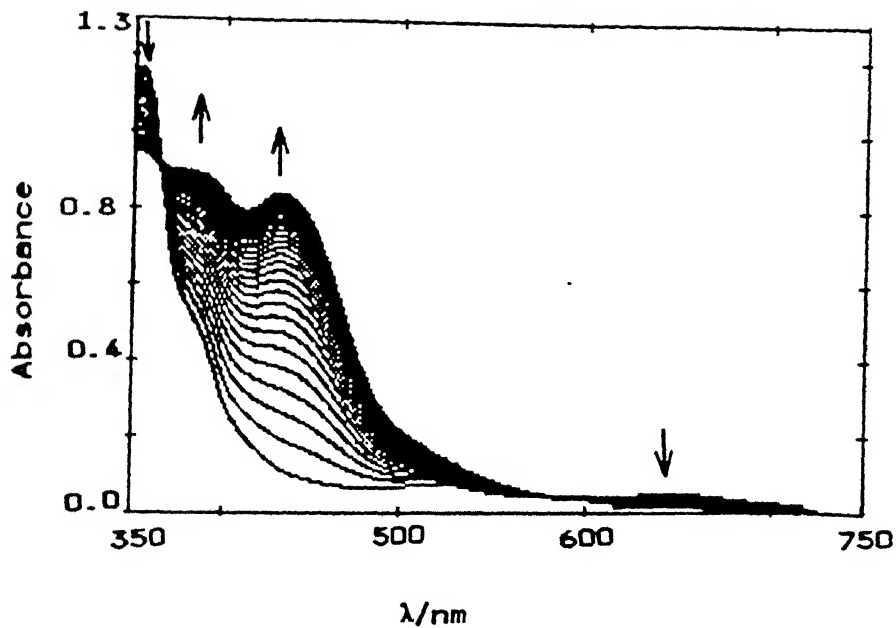


Fig. 5.1 Spectral changes for the reaction between $[\text{Et}_4\text{N}]_2^-$ $[\text{W}^{\text{IV}}\text{O}(\text{mnt})_2]$ (2×10^{-4} M) and DMAC (0.26 M) in MeCN at $25 + 0.1^\circ\text{C}$.

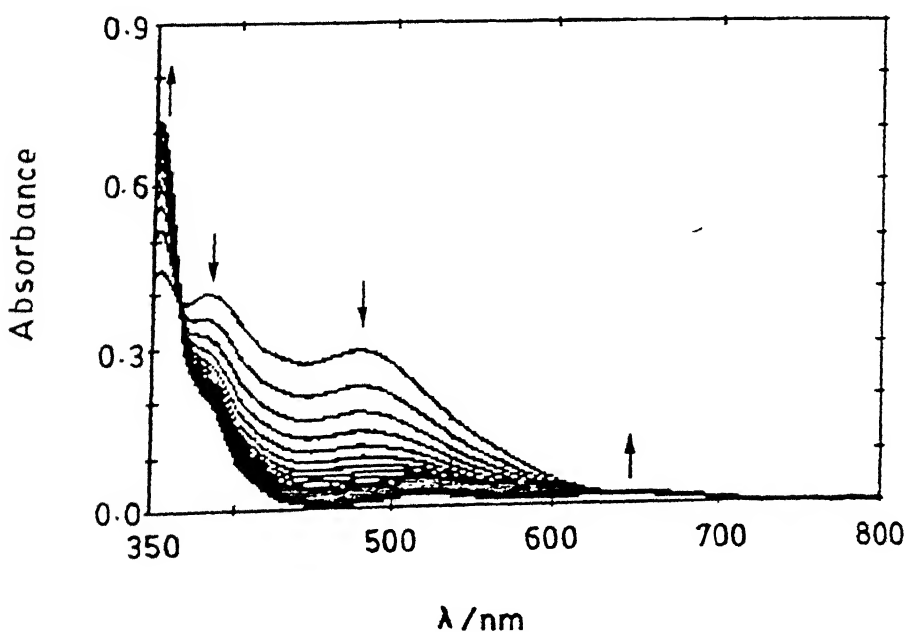
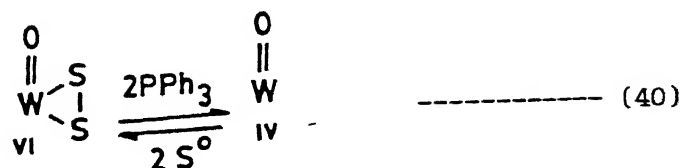


Fig. 5.2 Spectral changes for the reaction between $[\text{Et}_4\text{N}]_2^-$ $[\text{W}^{\text{VI}}\text{O}(\text{S}_2)(\text{mnt})_2]$ (0.8×10^{-4} M) and PPh_3 (5.83×10^{-4} M) in MeCN

5.2 REACTIVITY OF $[\text{Et}_4\text{N}]_2[\text{W}^{\text{VI}}\text{O}(\text{S}_2)(\text{mnt})_2]$.

The complex, $[\text{Et}_4\text{N}]_2[\text{W}^{\text{VI}}\text{O}(\text{S}_2)(\text{mnt})_2]$ has been synthesized by oxidative addition reaction of $[\text{Et}_4\text{N}]_2[\text{W}^{\text{IV}}\text{O}(\text{mnt})_2]$ with elemental sulfur (*vide supra*) in a similar fashion as is known¹⁰² for the synthesis of $[\text{Mo}^{\text{VI}}\text{O}(\text{S}_2)(\text{Et}_2\text{dtc})_2]$. This tungsten(VI) disulfur complex, $[\text{Et}_4\text{N}]_2[\text{W}^{\text{VI}}\text{O}(\text{S}_2)(\text{mnt})_2]$ readily reacts with two equivalents of PPh_3 to produce $[\text{Et}_4\text{N}]_2[\text{W}^{\text{IV}}\text{O}(\text{mnt})_2]$ and Ph_3PS quantitatively and the progress of the reaction as observed spectrophotometrically is shown in Fig. 5.2. Clean isobestic point is found at 365 nm. For comparison purpose the electronic spectra of $[\text{Et}_4\text{N}]_2[\text{W}^{\text{VI}}\text{O}(\text{S}_2)(\text{mnt})_2]$ and $[\text{Et}_4\text{N}]_2[\text{W}^{\text{IV}}\text{O}(\text{mnt})_2]$ are shown together in Fig. 5.3. Addition of one equivalent of PPh_3 led to 0.5 equivalent conversion of $[\text{Et}_4\text{N}]_2[\text{W}^{\text{VI}}\text{O}(\text{S}_2)(\text{mnt})_2]$ to $[\text{Et}_4\text{N}]_2[\text{W}^{\text{IV}}\text{O}(\text{mnt})_2]$ and the resultant electronic spectrum was superposition of equivalent amounts of $[\text{Et}_4\text{N}]_2[\text{W}^{\text{VI}}\text{O}(\text{S}_2)(\text{mnt})_2]$ and $[\text{Et}_4\text{N}]_2[\text{W}^{\text{IV}}\text{O}(\text{mnt})_2]$ (Fig. 5.4). Similar conversion using $[\text{Mo}^{\text{VI}}\text{O}(\text{S}_2)(\text{Et}_2\text{dtc})_2]$ has been reported¹⁴⁶. Thus the synthesis of $[\text{Et}_4\text{N}]_2[\text{W}^{\text{VI}}\text{O}(\text{S}_2)(\text{mnt})_2]$ from $[\text{Et}_4\text{N}]_2[\text{W}^{\text{IV}}\text{O}(\text{mnt})_2]$ and the above sulfur abstraction reaction demonstrate the following interconversion (40).



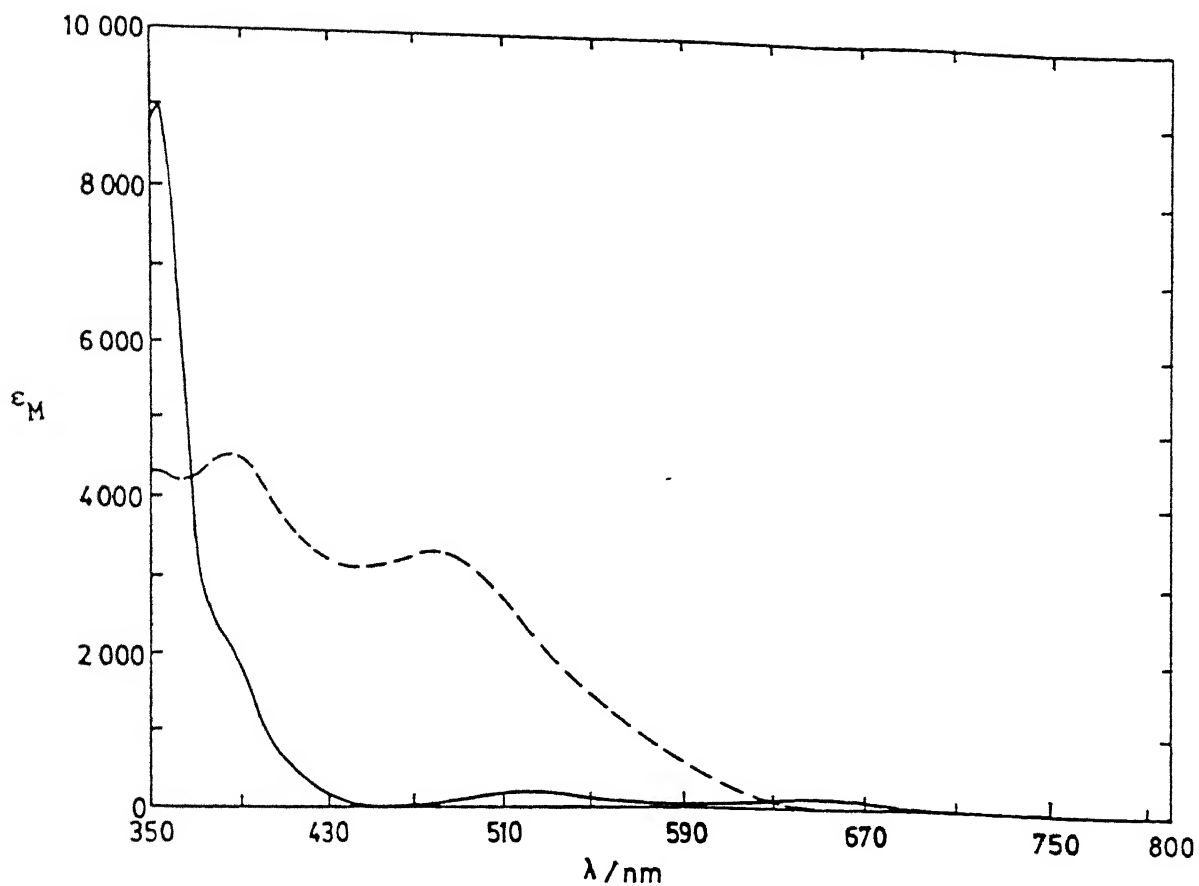


Fig. 5.3 UV-visible absorption spectra of $[\text{Et}_4\text{N}]_2[\text{W}^{\text{IV}}\text{O}(\text{mnt})_2]$ (—) and $[\text{Et}_4\text{N}]_2[\text{W}^{\text{VI}}\text{O}(\text{S}_2)(\text{mnt})_2]$ (----) in MeCN solutions.

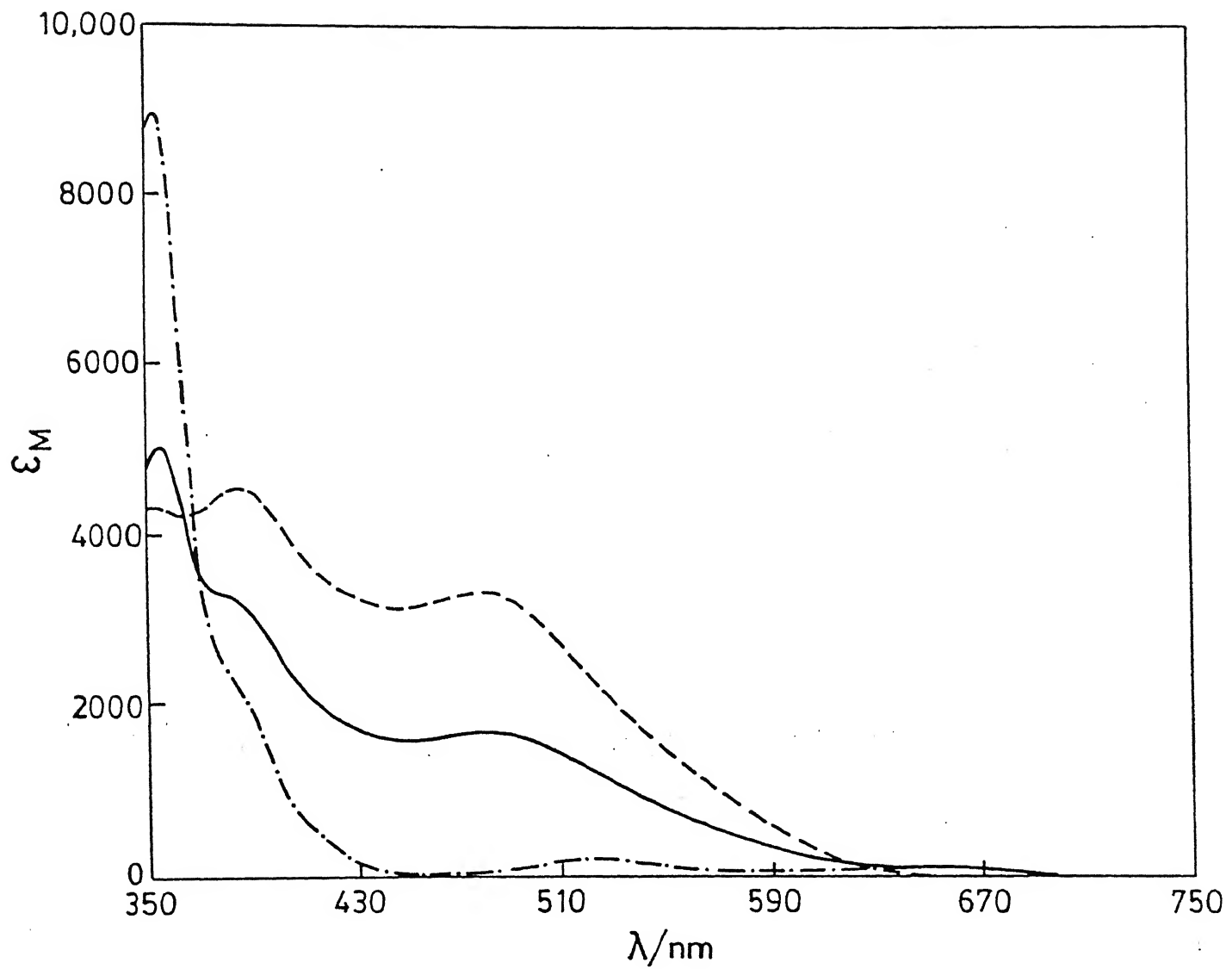


Fig. 5.4 UV-visible absorption spectra in MeCN: -.-.-. for $[\text{Et}_4\text{N}]_2[\text{W}^{\text{IV}}\text{O}(\text{mnt})_2]$; ----- for $[\text{Et}_4\text{N}]_2[\text{W}^{\text{VI}}\text{O}(\text{S}_2)(\text{mnt})_2]$; — for equivalent amounts $[\text{Et}_4\text{N}]_2[\text{W}^{\text{VI}}\text{O}(\text{S}_2)(\text{mnt})_2]$ and $[\text{Et}_4\text{N}]_2[\text{W}^{\text{IV}}\text{O}(\text{mnt})_2]$

The kinetics of the forward reaction was followed by monitoring the decay of 478 nm absorption band of $[\text{Et}_4\text{N}]_2[\text{W}^{\text{VI}}\text{O}(\text{S}_2)(\text{mnt})_2]$ in MeCN. This reaction followed a second order (A + 2B type) kinetics with $k_{\text{obs}} = 4.3 (\pm 0.06) \text{ M}^{-1} \text{ s}^{-1}$ in MeCN at 25°C. Activation parameters were obtained by least-squares fit of k_{obs} values measured at different temperatures to the Eyring equation (30). The rate constants for this reaction at different different temperatures and the activation parameters are described in Table 5.1. For a side on bound S_2^{2-} ligand it is known that a cycloaddition of an acetylene or alkene to metal side on bound S_2^{2-} could be a symmetry forbidden process. Thus the reaction between $[\text{Mo}_2\text{S}_6\text{O}_2]^{2-}$ with activated acetylene, DMAC resulted in insertion of the alkyne across Mo-S bond instead of S-S bond^{89,147}. In the present case the simultaneous attack by two phosphines to WS_2 moiety can be viewed similarly.

Attempts have been made to understand the possible attack by phosphine across the W-S bond by monitoring the progress of this reaction using time dependent cyclic voltammetric study. This is shown in Fig. 5.5. When phosphine was not added the reduction peak potential was at -1.45V vs Ag/AgCl. Within two minutes of the addition of PPh_3 the E_{pc} of $[\text{Et}_4\text{N}]_2[\text{W}^{\text{VI}}\text{O}(\text{S}_2)(\text{mnt})_2]$ distinctly shifted to less negative potential by 40 mV. Similar progress of reaction between $[\text{Bu}_4\text{N}]_2[\text{Mo}^{\text{VI}}\text{O}_2(\text{mnt})_2]$ and PPh_3 has been monitored cyclic voltammetrically for comparison and is shown in Fig 5.6. This reaction followed a simple second order kinetics (vide supra). In this case during the progress of the reaction there was no apparent change in position of the E_{pc} of the complex anion

Table 5.1 Kinetic Data and Activation Parameters for the Forward Reaction of 40

T, K	$k_{obs}, M^{-1}s^{-1}$	$\Delta H^\ddagger, Kcal/mol$	$\Delta S^\ddagger, cal/(deg.mol)$
298	4.30 (± 0.06)		
303	4.99 (± 0.03)		
308	5.785 (± 0.025)	5.14 (± 0.46)	-38.35 (± 1.5)
313	6.75 (± 0.09)		

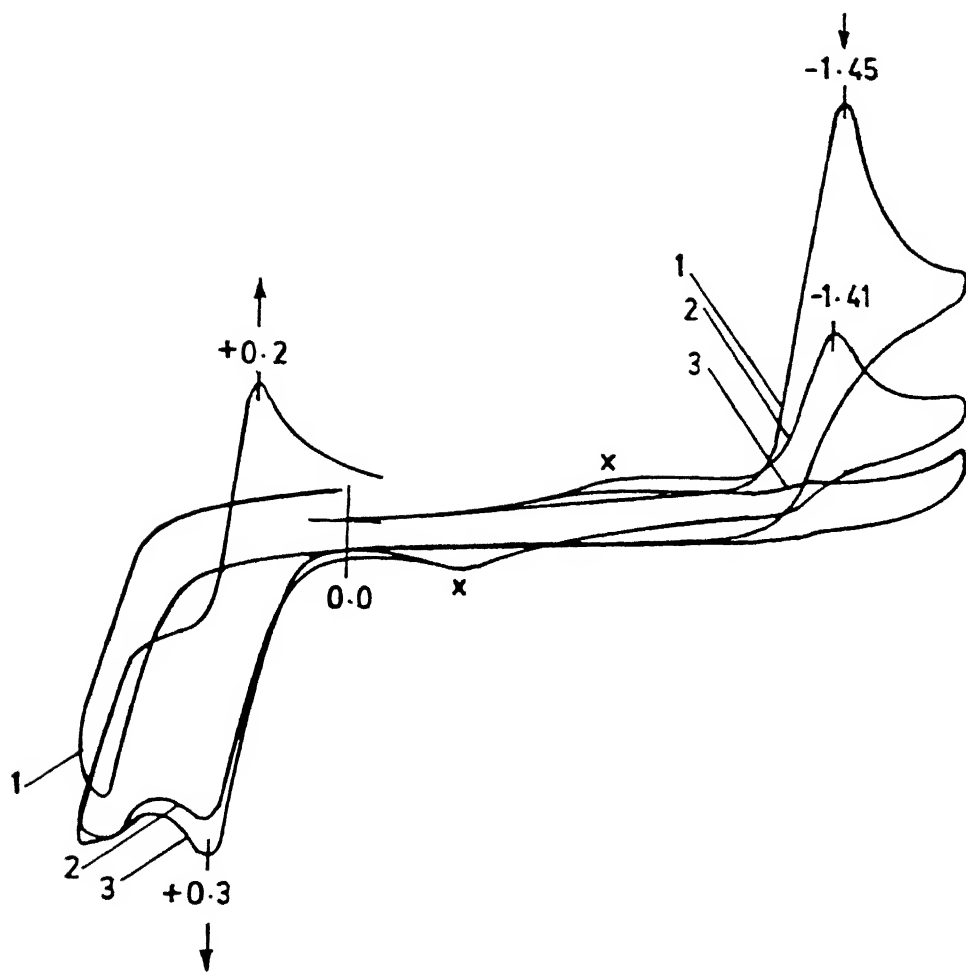


Fig. 5.5 Cyclic voltammetric scans during the progress of reaction between $[\text{Et}_4\text{N}]_2[\text{W}^{\text{VI}}\text{O}(\text{S}_2)(\text{mnt})_2]$ and two equivalents of PPh_3 . The first scan is pure complex. Second scan after addition of two equivalents of PPh_3 with lapse of ca Two min, 3rd scan after 10 min from the 2nd scan. $\Delta E_{\text{PC}} = 40 \text{ mV}$ towards less negative potential between first and second scans. On the positive side the appearance of $\text{WO}(\text{IV})/\text{WO}(\text{V})$ couple is observed. x marked peaks are

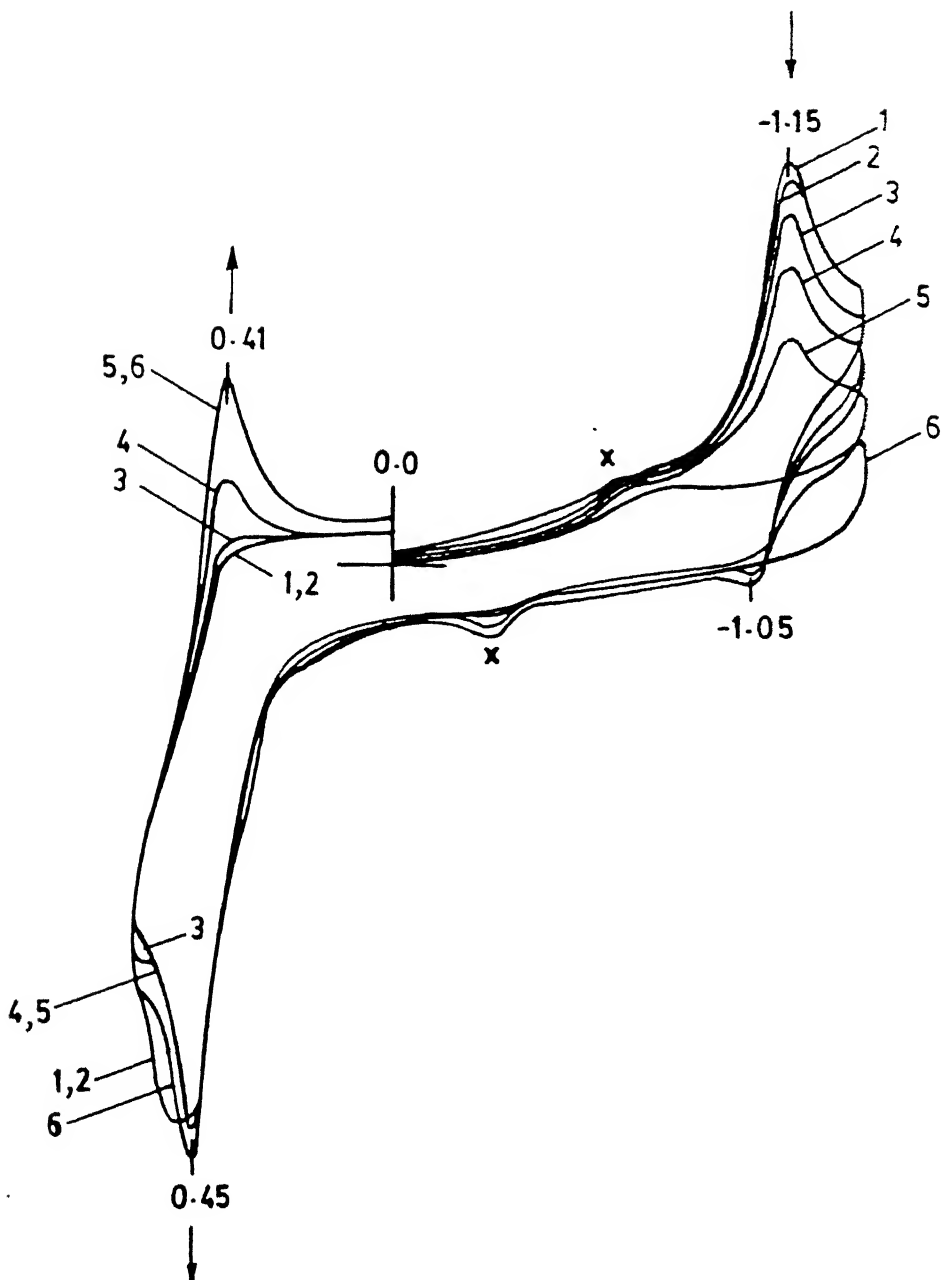


Fig. 5.6 Cyclic voltammetric scans during the progress of reaction between $[Bu_4N]^2[Mo^{VI}O_2(mnt)_2]$ and one equivalent of PPh_3 . First scan is for pure complex, second scan after addition of PPh_3 with lapse of ca two min, 3rd scan (after 5 min), 4th scan (after 30 min), 5th scan (after 60 min) and 6th scan (after 240 min). On the positive side the appearance of $MoO(IV)/MoO(V)$ couple after the

during the course of the reaction (Fig. 5.6). For this type of reaction the attack by phosphine on a terminal oxo group has been proposed^{55,85a,72c}. The shift in cathodic peak potential as observed in Fig. 5.5 thus could be the manifestation of direct PPh_3 attack on tungsten center which made its reduction easier.

The facile reductive "S" abstraction with PPh_3 demonstrated the importance of kinetic aspect in atom transfer reactions. In the present case the irreversible reduction peak potential as high as -1.45V vs Ag/AgCl of $[\text{Et}_4\text{N}]_2^{+} [\text{W}^{\text{VI}}\text{O}(\text{S}_2^-)(\text{mnt})_2^-]$ thus attests that such type of irreversible reduction potential does not really say much for a reaction to occur smoothly at ambient conditions.

CHAPTER 6

FUTURE SCOPE

In the earlier chapters, attempts have been made to model some oxomolybdenum and oxotungsten complexes in relevance to the bioinorganic aspects of these metals. The field is still in its stage of infancy and many more questions are yet to be answered. The involvement of pterin component in the molybdenum cofactor has not been addressed in any synthetic model compound so far. Furthermore the most appropriate model compound should have one dithiolene ligation instead of two. Hence the future strategy should involve to synthesize complexes incorporating these essential and important aspects in mind. For sulfite oxidase, the regeneration stage of the catalytic cycle involves electron transfer via cytochrome b_5 . Demonstration of such reaction in synthetic system would be of great value. To synthesize similar complexes with $\{Mo^{VI}OS\}$ moiety would be of great challenge to model the related xanthine oxidase and other similar enzymes. Once structural aspects and functional analogue reactions become similar to those of molybdenum cofactor, reconstitution assay with the synthetic analogue would testify the perfectness of the said model compound. A similar treatment should be followed with the newly developed tungsten systems.

REFERENCES

1. F. A. Cotton and R. A. Walton, *Multiple Bonds Between Metal Atoms*, Wiley-Interscience, New York, 1982.
2. M. H. Chisholm, *Angew. Chem. Int. Ed. Engl.*, 1980, **25**, 21.
3. F. E. Massoth, *Adv. Catal.*, 1978, **27**, 164.
4. R. R. Chianelli, *Catal. Rev.-Sci. Eng.*, 1984, **26**, 361.
5. R. J. Angelici, *Acc. Chem. Res.*, 1988, **21**, 387.
6. W. H. Orme-Johnson, *Ann. Rev. Biophys. Biochem.*, 1985, **14**, 419.
7. T. G. Spiro (ed.), *Molybdenum Enzymes*, Wiley-Interscience, New York, 1985.
8. M. Coughlan (ed.), *Molybdenum and Molybdenum Containing Enzymes*, Pergamon, Oxford, 1980.
9. R. C. Bray, *Adv. Enzymol.*, 1980, **51**, 107.
10. K. V. Rajagopalan, *Biochem. Elem.*, 1984, **3**, 149.
11. R. C. Bray, *Q. Rev. Biophys.*, 1988, **21**, 299.
12. P. W. Wilson, in *The Chemistry and Biochemistry of Nitrogen Fixation*, ed. J. R. Postage, Plenum Press, New York, 1971, p. 1.
13. V. K. Shah and W. J. Brill, *Proc. Natl. Acad. Sci. U.S.A.*, 1977, **74**, 3249.
14. W. G. Zumft, *Eur. J. Biochem.*, 1978, **91**, 354.
15. (a) S. P. Cramer, K. O. Hodgson, W. O. Gillum and L. E. Mortenson, *J. Am. Chem. Soc.*, 1978, **100**, 3398; (b) S. P. Cramer, *Adv. Inorg. Bioinorg. Mech.*, 1983, **2**, 259.
16. (a) T. E. Wolff, J. M. Berg and R. H. Holm, *Inorg. Chem.*, 1981, **20**, 174; (b) R. H. Holm, *Chem. Soc. Rev.*, 1981, **10**, 455; (c) R. E. Palermo, P. P. Power and R. H. Holm, *Inorg. Chem.*, 1982, **21**,

173; (d) W. H. Armstrong, P. K. Mascharak and R. H. Holm, *Inorg. Chem.*, 1982, 21, 1699; (e) J. A. Kovacs, J. K. Bakshin and R. H. Holm, *J. Am. Chem. Soc.*, 1985, 107, 1784; (f) C. D. Garner, in *Transition Metal Clusters*, ed. B. F. G. Johnson, John Wiley and Sons, 1980, p 265.

17. (a) M. M. Georgiadis, H. Komiya, P. Chakrabarti, D. Woo, J. J. Kornuc and D. C. Rees, *Science*, 1992, 257, 1653; (b) J. Kim and D. C. Rees, *Science*, 1992, 257, 1677.

18. R. H. Holm and E. D. Simhon, in *Molybdenum Enzymes*, ed. T. G. Spiro, Wiley-Interscience, New York, 1985, Ch. 1.

19. (a) T. A. Krenitsky, M. N. Shannon, G. B. Elion and G. H. Hitchings, *Arch. Biochem. Biophys.*, 1972, 150, 585; (b) F. Bergmann, L. Levene, I. Tamir and M. Rahat, *Biochim. Biophys. Acta*, 1977, 480, 21; (c) F. Bergmann, L. Levene, H. Govrin and A. Frank, *Biochim. Biophys. Acta*, 1977, 480, 39.

20. (a) E. C. DeRenzo, *Advanc. Enzymol.*, 1956, 17, 293; (b) R. C. Bray, *Enzymes*, 1963, 7, 533; (c) V. Massey, in *Iron-sulfur Proteins*, ed. W. Lovenberg, V 1, Academic Press, New York, 1973, p 301; (d) K. Tatsumi, S. Kitamura, H. Yoshimura and Y. Kawazoe, *Chem. Pharm. Bull.*, 1978, 26, 1713.

21. P. Subramanian, B. B. Kaul and J. T. Spence, *J Mol. Catalysis*, 1984, 23, 163.

22. J. Horbaczewski, *Monatsch. Chem.*, 1891, 12, 221.

23. J. A. Pateman, D. J. Cove, B. M. Rever and D. B. Roberts, *Nature*, 1964, 201, 58.

24. (a) P. A. Ketchum, H. Y. Cambier, W. A. Frazier III, C. H. Madansky and A. Nason, *Proc. Natl. Acad. Sci. U.S.A.*, 1970, 66,

1016, (b) A. Nason, A. D. Antoine, P. A. Ketchum, W. A. Frazier III and K. D. Lee, *Proc. Natl. Acad. Sci. U.S.A.*, 1970, **65**, 137; (c) A. Nason, K-Y Lee, S-S Pan, P. A. Ketchum, A. Lamberti and J. DeVries, *Proc. Natl. Acad. Sci. U.S.A.*, 1971, **68**, 3242; (d) A. Nason, K-Y Lee, S-S Pan and R. H. Erickson, *J. Less. Common Metals*, 1974, **36**, 449.

25. J. L. Johnson, in *Molybdenum and Molybdenum Containing Enzymes*, ed. M. P. Coughlan, Pergamon Press, Oxford, 1980, p 345.

26. (a) R. C. Wahl, R. V. Hageman and K. V. Rajagopalan, *Arch. Biochem. Biophys.*, 1984, **230**, 264; (b) S. Kramer, R. V. Hageman and K. V. Rajagopalan, *Arch. Biochem. Biophys.*, 1984, **233**, 821; (c) J. L. Johnson, B. E. Hainline, K. V. Rajagopalan and B. H. Arison, *J. Biol. Chem.*, 1984, **259**, 5414; (d) S. P. Kramer, J. L. Johnson, A. A. Ribeiro, D. S. Millington and K. V. Rajagopalan, *J. Biol. Chem.*, 1987, **262**, 16357.

27. (a) B. Kruger and O. Meyer, *Eur. J. Biochem.*, 1986, **157**, 121; (b) B. Kruger and O. Meyer, *Biochim. Biophys. Acta*, 1987, **912**, 357.

28. J. L. Johnson, N. R. Bastian and K. V. Rajagopalan, *Proc. Natl. Acad. Sci. U.S.A.*, 1990, **87**, 3190.

29. J. L. Johnson, K. V. Rajagopalan and O. Meyer, *Arch. Biochem. Biophys.*, 1990, **283**, 542.

30. G. Borner, M. Karrasch and R. K. Thauer, *FEBS. Lett.*, 1991, **290**, 31.

31. G. N. George, R. C. Prince, C. A. Kipke, R. A. Sunde and J. H. Enemark, *Biochem. J.*, 1988, **256**, 307.

32. S. P. Cramer, L. P. Solomonson, M. W. W. Adams and L. E. Mortenson, *J. Am. Chem. Soc.*, 1984, 106, 1467.

33. B. A. Goodman and J. B. Raynor, *Adv. Inorg. Chem. Radiochem.*, 1970, 13, 136.

34. H. J. Cohen, I. Fridovich and K. V. Rajagopalan, *J. Biol. Chem.*, 1971, 246, 367.

35. R C. Bray, in *Molybdenum Chemistry of Biological Significance*, eds. W. E. Newton and S. Otsuka, Plenum Press, New York, 1980, p 117.

36. (a) R. Cammack, M. J. Barber and R. C. Bray, *Biochem. J.*, 1976, 157, 469; (b) M. J. Barber, R. C. Bray, R. Cammack and M. J. Coughlan, *Biochem. J.*, 1977, 163, 279; (c) S. P. Vincent, *Biochem. J.*, 1979, 177, 757.

37. E. I. Stiefel, *Proc. Natl. Acad. Sci. U.S.A.*, 1973, 70, 988.

38. S. Gutteridge, S. J. Tanner and R. C. Bray, *Biochem. J.*, 1978, 175, 869.

39. R. C. Bray in *2nd International Conference on the Chemistry and Uses of Molybdenum*, eds. P. C. H. Mitchell and A. Seaman, Climax Molybdenum Company, London, 1976, p 271.

40. J. S. Olson, D. P. Ballon, G. Palmer and V. Massey, *J. Biol. Chem.*, 1974, 249, 4343.

41. (a) R. C. Bray, *Biochem. J.*, 1961, 81, 189; (b) R. C. Bray and R. Petterson, *Biochem. J.*, 1961, 81, 194; (c) R. C. Bray, G. Palmer and H. Beinert, *J. Biol. Chem.*, 1964, 239, 2667; (d) R. C. Bray, D. T. Lowe, C. Capeillere-Blandin and E. M. Fielder, *Biochem. Soc. Trans.*, 1973, 1, 1067.

42. J. S. Olson, D. P. Ballou, G. Palmer and V. Massey, *J. Biol. Chem.*, 1974, 249, 4350.

43. (a) W. W. Cleland, *Biochim. Biophys. Acta*, 1963, 67, 104; (b) W. W. Cleland, *Nature*, 1963, 198, 463.

44. (a) K. V. Rajagopalan and P. Handler, *J. Biol. Chem.*, 1967, 242, 4097; (b) I. H. Segel, *Enzyme Kinetics*, Wiley, New York, 1975.

45. D. B. Northrop, *J. Biol. Chem.*, 1969, 244, 5808.

46. K. V. Rajagopalan in *Molybdenum and Molybdenum Containing Enzymes*, ed. M. P. Coughlan, Pergamon Press, Oxford, 1980, p 241.

47. K. N. Murray, J. G. Watson and S. Chaykin, *J. Biol. Chem.*, 1966, 241, 4798.

48. G. Stohrer and G. B. Brown, *J. Biol. Chem.*, 1969, 244, 2498.

49. R. Hille and H. Sprecher, *J. Biol. Chem.*, 1987, 262, 10914.

50 (a) H. R. Mahler and E. H. Cordes, *Biological Chemistry*, 2nd edn., Harper & Row, New York, 1986; (b) M. Dixon and E. C. Webb, *Enzymes*, 3rd edn., Longman, London, 1979.

51. L. G. Howell and I. Fridovich, *J. Biol. Chem.*, 1968, 243, 8941.

52. G. A. Heath, K. A. Moock, D. W. A. Sharpe and L. J. Yellowless, *J. Chem. Soc. Chem. Commun.*, 1985, 1503.

53. (a) I. Yamamoto, T. Saiki, S-M Liu and L. G. Ljungdahl, *J. Biol. Chem.*, 1983, 258, 1826; (b) J. R. Andersen and L. G. Ljungdahl, *J. Bacteriol.*, 1974, 120, 6; (c) J. C. Deaton, E. I. Solomon, C. N. Durfor, P. J. Wetherbee, B. K. Burges and D. B. Jacobs, *Biochem. Biophys. Res. Commun.*, 1984, 121, 1042.

54. (a) H. White, G. Strobl, R. Feicht, H. Simon, *Eur. J.*

Biochem., 1989, 184, 89; (b) S. Mukund and M. W. W. Adams, *J. Biol. Chem.*, 1990, 265, 11508; (c) S. Mukund and M. W. W. Adams, *J. Biol. Chem.*, 1991, 266, 14208, (d) G. N. George, Y. Gea, R. C. Prince, S. Mukund and M. W. W. Adams, *J. Inorg. Biochem.*, 1991, 43, 241; (e) G. N. George, R. C. Prince, S. Mukund and M. W. W. Adams, *J. Am. Chem. Soc.*, 1992, 114, 3521.

55. R. H. Holm, *Coord. Chem. Rev.*, 1990, 100, 183.

56. (a) M. L. Larson and F. W. Moore, *Inorg. Chem.*, 1966, 5, 801; (b) H. L. Krauss and W. Huber, *Chem. Ber.*, 1961, 94, 2864; (c) S. M. Horner and S. Y. Tyree, Jr., *Inorg. Chem.*, 1962, 1, 122.

57. (a) E. Wendling, *Bull. Soc. Chim. France*, 1965, 427; (b) W. P. Griffith and T. D. Wickins, *J. Chem. Soc. (A)*, 1967, 675.

58. (a) B. Kojic-Prodic, Z. Ruzic-Toros, D. Grdenic, and L. Golic, *Acta Cryst.*, 1974, B30, 300; (b) B. Kamenar and M. Penavic, *Cryst. Struct. Commun.*, 1973, 2, 41; (c) F. W. Moore and R. E. Rice, *Inorg. Chem.*, 1968, 7, 2511; (d) M. M. Jones, *J. Am. Chem. Soc.*, 1959, 81, 3188; (e) H. Gehrke, Jr. and J. Veal, *Inorg. Chim. Acta*, 1969, 4, 623.

59 (a) L. Malatesta, *Gazz. Chim. Ital.*, 1939, 69, 752; (b) L. Malatesta, *Gazzetta*, 1939, 69, 408. (c) D. Coucounanis, *Prog. Inorg. Chem.*, 1969, 11, 233.

60. (a) F. W. Moore and M. L. Larson, *Inorg. Chem.*, 1967, 6, 998; (b) R. N. Jowitt and P. C. H. Mitchell, *J. Chem. Soc. (A)*, 1970, 1702; (c) W. E. Newton, J. L. Corbin, D. C. Bravard, J. E. Searles and J. W. McDonald, *Inorg. Chem.*, 1974, 13, 1100; (d) R. Colton and G. G. Rose, *Austral. J. Chem.*, 1970, 23, 1111.

61. R. Barral, C. Bocard, I. Seree de Roch and L. Sajus, *Kinet. and Catal.*, 1973, **14**, 130.

62 (a) L. R. Melby, *Inorg. Chem.*, 1969, **8**, 349; (b) A. Kay and P. C. H. Mitchell, *J. Chem. Soc. (A)*, 1970, 2421.

63. (a) J. T. Spence and P. Kroneck, *J. Less Common Metals*, 1974, **36**, 465; (b) C. D. Garner, R. Durant and F. E. Mabbs, *Inorg. Chim. Acta*, 1977, **24**, L29; (c) R. A. D. Wentworth, *Inorg. Chem.*, 1977, **16**, 3385.

64. R. D. Taylor, J. P. Street, M. Minelli and J. T. Spence, *Inorg. Chem.*, 1978, **17**, 3207.

65. A. Nakamura, M. Nakayama, K. Sugihashi and S. Otsaka, *Inorg. Chem.*, 1979, **18**, 394.

66. E. I. Stiefel, K. F. Miller, A. E. Bruce, J. L. Corbin, J. M. Berg and K. O. Hodgson, *J. Am. Chem. Soc.*, 1980, **102**, 3624.

67. N. Yoshinaga, N. Ueyama, T. Okamura and A. Nakamura, *Chem. Lett.*, 1990, 1655.

68. P. Palanca, T. Picher, V. Sanz, P. Gomez-Romero, E. Llopis, A. Domenech and A. Cervilla, *J. Chem. Soc., Chem. Commun.*, 1990, 531.

69. B. E. Schultz, S. F. Gheller, M. C. Muettterties, M. J. Scott and R. H. Holm, *J. Am. Chem. Soc.*, 1993, **115**, 2714.

70. (a) O. A. Rajan and A. Chakravorty, *Inorg. Chim. Acta*, 1979, **37**, L503; (b) O. A. Rajan and A. Chakravorty, *Inorg. Chem.*, 1981, **20**, 660.

71. J. A. Craig, E. W. Harlan, B. S. Synder, M. A. Whitener and R. H. Holm, *Inorg. Chem.*, 1989, **28**, 2082.

72. (a) I. W. Boyd and J. T. Spence, *Inorg. Chem.*, 1982, **21**, 1602; (b) J. Topich and J. T. Lyon, III., *Polyhedron*, 1984, **3**, 55, 61;

(c) J. Topich and J. T. Lyon, III., *Inorg. Chem.*, 1984, 23, 3252.

73. J. M. Berg and R. H. Holm, *Inorg. Chem.*, 1983, 22, 1768.

74. (a) S. Bhattacharjee and R. G. Bhattacharyya, *J. Chem. Soc., Dalton Trans.*, 1992, 1357; (b) S. Bhattacharjee and R. G. Bhattacharyya, *J. Chem. Soc., Dalton Trans.*, 1993, 1151.

75. C. D. Garner and S. Bristow, in *Molybdenum Enzymes*, ed. T. G. Spiro, Wiley-Interscience, New York, 1985, p 360.

76. S. A. Roberts, C. G. Young, C. A. Kipke, W. E. Cleland, Jr., K. Yamanouchi, M. D. Carducci and J. H. Enemark, *Inorg. Chem.*, 1990, 29, 3650.

77. S. A. Roberts, C. G. Young, W. E. Cleland, Jr., R. B. Ortega and J. H. Enemark, *Inorg. Chem.*, 1988, 27, 3044.

78. J. M. Berg and R. H. Holm, *J. Am. Chem. Soc.*, 1985, 107, 917.

79. J. M. Hawkins, J. C. Dewan and K. B. Sharpless, *Inorg. Chem.*, 1986, 25, 1501.

80 (a) A. Bruce, J. L. Corbin, P. L. Dahlstrom, J. R. Hyde, M. Minelli, E. I. Stiefel, J. T. Spence and J. Zubieta, *Inorg. Chem.*, 1982, 21, 917; (b) P. L. Dahlstrom, J. H. Hyde, P. A. Vella and J. Zubieta, *Inorg. Chem.*, 1982, 21, 927; (c) P. Subramanian, J. T. Spence, R. Ortega and J. H. Enemark, *Inorg. Chem.*, 1984, 23, 2564; (d) B. B. Kaul, J. H. Enemark, S. L. Merbs and J. T. Spence, *J. Am. Chem. Soc.*, 1985, 107, 2885.

81. (a) R. A. Walton, P. C. Crouch and B. J. Brisdon, *Spectrochim. Acta Part A*, 1968, 24, 601; (b) E. B. Fleischer and T. S. Srivastava, *Inorg. Chim. Acta*, 1971, 5, 151; (c) T. Imamura, T. Numatatsu, M. Terni and M. Fujimoto, *Bull. Chem. Soc., Jpn.*, 1981, 54, 170.

82. (a) F. Farchione, G. R. Hanson, C. G. Rodrigues, T. D. Bailey, R. N. Bagchi, A. M. Bond, J. R. Pilbrow and A. G. Wedd, *J. Am. Chem. Soc.*, 1986, 108, 831; (b) G. L. Wilson, R. J. Greenwood, J. R. Pilbrow, J. T. Spence and A. G. Wedd, *J. Am. Chem. Soc.*, 1991, 113, 6803.

83. R. N. Jowitt and P. C. H. Mitchell, *J. Chem. Soc. (A)*, 1969, 1476.

84. E. W. Harlan, J. M. Berg and R. H. Holm, *J. Am. Chem. Soc.*, 1986, 108, 6992.

85. (a) M. S. Reynolds, J. M. Berg and R. H. Holm, *Inorg. Chem.*, 1984, 23, 3057; (b) R. Durant, C. D. Garner, M. R. Hyde and F. E. Mabbs, *J. Chem. Soc., Dalton Trans.*, 1977, 955; (c) R. Barral, C. Bocard, I. Seree de Roch and L. Sajus, *Tetrahedron Lett.*, 1972, 1693; (d) D. B. McDonald and J. I. Shulman, *Anal. Chem.*, 1975, 47, 2023.

86. J. A. McCleverty, J. Locke, B. Ratcliff and E. J. Wharton, *Inorg. Chim. Acta*, 1969, 3, 283.

87. E. I. Stiefel, L. E. Bennett, Z. Dori, T. H. Crawford, C. Simo and H. B. Gray, *Inorg. Chem.*, 1970, 9, 281.

88. M. A. Ansari, J. Chandrasekaran and S. Sarkar, *Inorg. Chim. Acta*, 1987, 133, 133.

89. D. Coucouvanis, A. Hajikyriacou, M. Draganjac, M. G. Kanatzidis and O. Illeperuma, *Polyhedron*, 1986, 5, 349.

90. S. Boyde, S. R. Ellis, C. D. Garner and W. Clegg, *J. Chem. Soc., Chem. Commun.*, 1986, 1541.

91. G. J-J. Chen, J. W. McDonald, W. E. Newton, *Inorg. Chim. Acta*, 1976, 19, L67.

92. S. Yu and R. H. Holm, *Inorg. Chem.*, 1989, 28, 4385.
93. N. Ueyama, H. Oku and A. Nakamura, *J. Am. Chem. Soc.*, 1992, 114, 7310.
94. M. A. Ansari, J. Chandrasekaran and S. Sarkar, *Inorg. Chem.*, 1988, 27, 763.
95. E. I. Stiefel, in *Molybdenum and Molybdenum Containing Enzymes*, ed. M. Coughlan, Pergamon, Oxford, 1980, p. 41.
96. L. Ricard, J. Estienne, P. Karagiannidis, P. Toledano, A. Mitschler and R. Weiss, *J. Coord. Chem.*, 1974, 3, 277.
97. S. Gruber, L. Kilpatrick, N. R. Bastian, K. V. Rajagopalan and T. G. Spiro, *J. Am. Chem. Soc.*, 1990, 112, 8179.
98. P. Subramanian, S. Burgmayer, S. Richards, V. Szalai and T. G. Spiro, *Inorg. Chem.*, 1990, 29, 3849.
99. Cited as unpublished results in ref. 75.
100. A. Muller, E. Diemann, R. Jostes, H. Bogge, *Angew. Chem. Int. Ed. Engl.*, 1981, 20, 934.
101. J. R. Bradbury and F. A. Schultz, *Inorg. Chem.*, 1986, 25, 4416.
102. J. W. McDonald and W. E. Newton, *Inorg. Chim. Acta*, 1980, 44, L81.
103. W. E. Newton, J. W. McDonald, J. L. Corbin, L. Ricard and R. Weiss, *Inorg. Chem.*, 1980, 19, 1997 and references cited therein.
104. J. Deistung and R. C. Bray, *Biochem. J.*, 1989, 263, 477.
105. A. I. Vogel, in *A Text Book of Quantitative Inorganic Analysis*, 4th edn., Longman, London, 1978.
106. J. A. McCleverty, J. Locke, E. J. Wharton and M. Gerloch, *J. Chem. Soc. (A)*, 1968, 816.

107. R. J. P. Williams, *The Biological Role of Molybdenum*, Climax Molybdenum Company Ltd., Oxford, 1978.

108. H. E. Simmons, D. C. Blomstrom and R. D. Vest, *J. Am. Chem. Soc.*, 1962, **84**, 4756.

109. R. Lozano, E. Alarcon, A. L. Doadrio and A. Doadrio, *Polyhedron*, 1983, **2**, 435.

110. E. I. Stiefel, *Prog. Inorg. Chem.*, 1977, **22**, 1.

111. C. W. Schlapfer and K. Nakamoto, *Inorg. Chem.*, 1975, **14**, 1338.

112. K. V. Rajagopalan and J. L. Johnson, *J. Biol. Chem.*, 1992, **267**, 10199.

113. P. Subramanian, S. Burgmayer, S. Richards, V. Szalai and T. G. Spiro, *Inorg. Chem.*, 1990, **29**, 3849.

114. (a) A. B. P. Lever and H. B. Gray, *Acc. Chem. Res.*, 1978, **11**, 348; (b) M. A. Ansari, Ph.D. Thesis, I. I. T., Kanpur, 1986.

115. (a) H. B. Gray and C. R. Hare, *Inorg. Chem.*, 1962, **1**, 363; (b) C. R. Hare, I. Bernal and H. B. Gray, *Inorg. Chem.*, 1962, **1**, 831.

116. S. R. Ellis, D. Collison, C. D. Garner, W. Clegg, *J. Chem. Soc. Chem. Commun.*, 1986, 1483.

117. R. G. Hanson, A. A. Brunette, A. E. McDonnell, K. S. Murray, A. G. Wedd, *J. Am. Chem. Soc.*, 1981, **103**, 1953.

118. F. A. Cotton, *Proceedings of the First International Conference of the Chemistry and Uses of Molybdenum*, Climax Molybdenum Company, London, 1973, p. 6.

119. G. F. Brown and E. I. Stiefel, *Inorg. Chem.*, 1973, **12**, 2140.

120. J. M. Berg and K. O. Hodgson, *Inorg. Chem.*, 1980, **19**, 2180.

121. J. F. Below, R. E. Connick, C. P. Coppel, *J. Am. Chem. Soc.*,

1958, 80, 2961.

122. D. L. Kessler and K. V. Rajagopalan, *Biochim. Biophys. Acta*, 1974, 370, 389.

123. R. M. Krupka and K. L. Laidler, *J. Am. Chem. Soc.*, 1961, 83, 1445.

124. D. E. Koshland, Jr., *Proc. Nat. Acad. Sci. (U. S. A.)*, 1958, 44, 98.

125. J. T. Spence, C. A. Kipke, J. H. Enemark and R. A. Sunde, *Inorg. Chem.*, 1991, 30, 3011.

126. G. N. George, C. A. Kipke, R. C. Prince, R. A. Sunde, J. H. Enemark and S. P. Cramer, *Biochemistry*, 1989, 28, 5075.

127. N. Oshino and B. Chance, *Arch. Biochem. Biophys.*, 1975, 170, 514.

128. A. L. Lehninger, *Principles of Biochemistry*, Worth Publishers, Inc, U. S. A., 1982.

129. (a) M. Ishimoto and O. Shimokawa, *Z. Allg. Mikrobiol.*, 1978, 18, 173; (b) M. Takagi, T. Tschiya and M. Ishimoto, *J. Bacteriol.*, 1981, 148, 762.

130. (a) K. E. Kim and G. W. Chang, *Can. J. Microbiol.*, 1974, 20, 1745; (b) H. S. Kwan and E. L. Barrett, *J. Bacteriol.*, 1983, 155, 1455.

131. (a) E. Stenberg, O. B. Styrvold and A. R. Strom, *J. Bacteriol.*, 1982, 149, 22; (b) A. R. Strom, J. A. Olafsen and H. Larsen, *J. Gen. Microbiol.*, 1979, 112, 315.

132. I. Yamamoto, N. Okubo and M. Ishimoto, *J. Biochem.*, 1986, 99, 1773.

133. L. J. De-Hayes, H. C. Faulkner, W. H. Doub Jr. and D. T.

Sawyer, *Inorg. Chem.*, 1975, **14**, 2110.

134. A. J. Parker, *Quart. Rev. (London)*, 1962, **16**, 163.

135. F. Feigl, *Spot Tests in Organic Analysis*, Elsevier Publishing Company, Amsterdam, 1960.

136 G. J-J. Chen, J. W. McDonald and W. E. Newton, *Inorg. Chim. Acta*, 1980, **41**, 49.

137. R. C. Bray, S. Gutteridge, M. T. Lamy and T. Wilkinson, *Biochem. J.*, 1983, **211**, 227.

138. M. I. Scullane, R. D. Taylor, M. Minelli, J. T. Spence, K. Yamanouchi, J. H. Enemark and N. D. Chasteen, *Inorg. Chem.*, 1979, **18**, 3213.

139. R. Manchanda, H. H. Thorp, G. W. Brudvig and Crabtree, *Inorg. Chem.*, 1991, **30**, 494.

140. S. G. Mayhew, *Eur. J. Biochem.*, 1978, **85**, 535.

141. S. P. Cramer, C.-L. Lui, L.E. Mortenson, S. M. Lui, I. Yamamoto and L. Lundahl, *J. Inorg. Biochem.*, 1985, **23**, 119.

142. J. C. Deaton, E. I. Solomon, G. D. Watt, P. J. Wetherbee and C. N. Dunfor, *Biochem. Biophys. Res. Commun.*, 1987, **149**, 424.

143. G. N. George, N. A. Turner, R. C. Bray, F. F. Morpeth, D. H. Boxer and S. P. Cramer, *Biochem. J.*, 1989, **259**, 693.

144. W. M. Grant, *Anal. Chem.*, 1948, **2**, 267.

145. J. L. Templeton, B. C. Ward, G. J-J. Chen, J. W. McDonald and W. E. Newton, *Inorg. Chem.*, 1981, **20**, 1248.

146. K. Leonard, K. Plute, R. C. Haltiwanger and M. R. DuBois, *Inorg. Chem.*, 1979, **18**, 3246.

147. T. R. Halbert, W-H. Pan and E. I. Stiefel, *J. Am. Chem. Soc.*, 1983, **105**, 5476.

APPENDIX.

KINETIC DATA

TABLE A1

Oxidation of HSO_3^{1-} by $[\text{Bu}_4\text{N}]_2[\text{Mo}^{\text{VI}}\text{O}_2(\text{mnt})_2]$ (Fig. 4.2)

[Complex] = $4.098 \times 10^{-4} \text{ M}$

$[\text{HSO}_3^{1-}] = 57.5 \times 10^{-4} \text{ M}$

Temp. $20.0 \pm 0.1^\circ\text{C}$

Solvent = 1:1 MeCN:H₂O

Time (sec)	Conc. (C)	$\log(C \times 10^6)$
10	$1.0 \times 10^{-4} \text{ M}$	2.029
11	$0.803 \times 10^{-4} \text{ M}$	1.904
12	$0.563 \times 10^{-4} \text{ M}$	1.750
13	$0.396 \times 10^{-4} \text{ M}$	1.577
14	$0.283 \times 10^{-4} \text{ M}$	1.451
15	$0.202 \times 10^{-4} \text{ M}$	1.305
16	$0.136 \times 10^{-4} \text{ M}$	1.133
17	$0.102 \times 10^{-4} \text{ M}$	1.008
18	$0.0694 \times 10^{-4} \text{ M}$	0.841
19	$0.0493 \times 10^{-4} \text{ M}$	0.692

Plot: $\log(C \times 10^6)$ vs time $k_{\text{obs}} = 0.353 \text{ s}^{-1}$

The formula used to calculate concentration (C) is:

$C(t) = (A(t) - \epsilon_2 C_0) / (\epsilon_1 - \epsilon_2)$, where C(t) is the concentration of $[\text{Bu}_4\text{N}]_2[\text{Mo}^{\text{VI}}\text{O}_2(\text{mnt})_2]$ at time t, A(t) is the absorbance of the reaction mixture at 535 nm at time t, C_0 is the initial concentration of the complex, ϵ_1 is molar extinction coeff. of above complex and ϵ_2 is that of reduced complex, $[\text{Bu}_4\text{N}]_2[\text{Mo}^{\text{IV}}\text{O}(\text{mnt})_2]$ at the monitoring wave length 535 nm.

TABLE A2

Kinetic Data for Substrate Saturation Curve (Fig. 4.3)

Complex = $[\text{Bu}_4\text{N}]_2[\text{Mo}^{\text{VI}}\text{O}_2(\text{mnt})_2]$ $[\text{Complex}] = 4.098 \times 10^{-4} \text{ M}$ Temp. = $20.0 \pm 0.1^\circ\text{C}$ Solvent = 1:1 MeCN:H₂OSubstrate = NaHSO₃ $10^4 [\text{NaHSO}_3], \text{ M}$ $10^2 k_{\text{obs}}, \text{ s}^{-1}$ 50.0 27.885 (± 2.145)57.5 33.16 (± 2.14)67.5 35.3 (± 1.0)80.0 36.63 (± 1.65)100.0 42.405 (± 1.155)132.5 47.025 (± 1.155)142.5 48.51 (± 0.99)167.5 49.83 (± 0.99)250.0 52.8 (± 0.66)

TABLE A3

Kinetic Data for the Double Reciprocal Plot of $1/k_{\text{obs}}$ vs $1/[S]$
 (Fig. 4.4)

Complex = $[\text{Bu}_4\text{N}]_2[\text{Mo}^{\text{VI}}\text{O}_2(\text{mnt})_2]$ $[\text{Complex}] = 4.098 \times 10^{-4} \text{ M}$

Solvent = 1:1 MeCN:H₂O Temp. = $20 \pm 0.1^\circ\text{C}$

S = Substrate = NaHSO₃

$1/[S], \text{ M}^{-1}$	$1/k_{\text{obs}}, \text{ s}^{-1}$
200.0	3.6075 (± 0.2775)
174.0	3.0282 (± 0.1954)
148.12	2.8351 (± 0.0803)
125.0	2.7355 (± 0.1232)
100.0	2.3599 (± 0.0643)
75.5	2.1277 (± 0.0522)
70.12	2.06225 (± 0.04205)
59.7	2.0076 (± 0.0399)
40.0	1.8942 (± 0.0237)

From the double reciprocal plot (Fig. 4.4) ,

V_{max} (= k_2 , the k_{obs} at substrate saturation) = $0.87 (\pm 0.04) \text{ s}^{-1}$;

and K_m (Michaelis constant) = $0.01 (\pm 0.001) \text{ M}$.

TABLE A4

Kinetic Data for the Double Reciprocal Plots of $1/k_{\text{obs}}$ vs $1/[S]$ in the Presence of Inhibitor SO_4^{2-} (Fig. 4.5)

$$[\text{Complex}] = 4.098 \times 10^{-4} \text{ M} \quad \text{Complex} = [\text{Bu}_4\text{N}]_2[\text{Mo}^{\text{VI}}\text{O}_2(\text{mnt})_2]$$

$$\text{S} = \text{Substrate} = \text{NaHSO}_3 \quad \text{Temp.} = 20^\circ\text{C}$$

$$\text{Solvent} = 1:1 \text{ MeCN:H}_2\text{O} \quad \text{I} = \text{Inhibitor} = \text{Na}_2\text{SO}_4$$

$[I] = 0.0038\text{M}$	$[I] = 0.0167\text{M}$		
$1/[S], \text{ M}^{-1}$	$1/k_{\text{obs}}, \text{ s}^{-1}$	$1/[S], \text{ M}^{-1}$	$1/k_{\text{obs}}, \text{ s}^{-1}$
75.5	2.55 (± 0.2)	75.5	3.85 (± 0.25)
60.0	2.3 (± 0.2)	60.0	3.275 (± 0.125)
20.0	1.55 (± 0.15)	20.0	1.95 (± 0.15)

$K_I = 2.256 \times 10^{-2} \text{ M}$, K_I is inhibition constant which was calculated from the formula,

$$\text{slope} = \frac{K_m}{k_2 = V_{\text{max}}} \left(1 + \frac{[I]}{K_I} \right) \quad (\text{for competitive inhibition})$$

K_m (Michaelis constant), k_2 ($= V_{\text{max}}$) and slope were calculated from the double reciprocal plots.

TABLE A5

Kinetic Data for the Double Reciprocal Plots of $1/[S]$ vs $1/k_{obs}$
in the Presence of $H_2PO_4^-$ (Fig. 4.6)

[Complex] = $4.098 \times 10^{-4} M$

Complex = $[Bu_4N]_2[Mo^{VI}O_2(mnt)]_2$

S = Substrate = $NaHSO_3$

Temp. = $20^\circ C$

Solvent = 1:1 MeCN:H₂O

I = Inhibitor = KH_2PO_4

$[I] = 0.010M$		$[I] = 0.019M$	
$1/[S], M^{-1}$	$1/k_{obs}, s$	$1/[S], M^{-1}$	$1/k_{obs}, s$
60.0	4.175 (± 0.825)	70.0	8.25 (± 0.35)
50.0	4.05 (± 0.25)	60.0	7.0 (± 0.7)
40.0	3.225 (± 1.075)	50.0	5.85 (± 0.85)
30.0	2.55 (± 0.65)	40.0	5.40 (± 0.8)
20.0	2.3 (± 0.7)	30.0	4.45 (± 0.55)
		20.0	3.65 (± 0.25)

$H_2PO_4^-$ behaves as mixed noncompetitive inhibitor. Hence in this case there are two inhibition constants, K_I and K_I' . K_I is the inhibition constant for the reaction between model complex (E) and inhibitor and K_I' is the inhibition constant for the reaction between inhibitor and E-S complex. K_I and K_I' were calculated from the double reciprocal plots (Fig. 4.6) using the formulae (for mixed noncompetitive inhibition) described in Table 1.5. The K_I and K_I' were found to be $2.785 \times 10^{-3} M$ and $3.367 \times 10^{-2} M$ respectively.

TABLE A6

Kinetic Data for the Oxygen Atom Transfer Reaction (30) Between
 $[\text{Bu}_4\text{N}]_2[\text{Mo}^{\text{VI}}\text{O}_2(\text{mnt})_2]$ and PPh_3 (Fig. 4.13)

T K	10^4 [Complex] M	10^2 [PPh_3] M	$10^4 k_{\text{abs}}^*$ s^{-1}
	M	M	s^{-1}
288	1.0	0.50	1.9
	1.0	0.80	3.05
	1.0	1.21	4.365
	1.0	1.63	6.035
	1.0	2.10	7.63
	1.0	2.75	9.745
298	1.0	0.50	3.555
	1.0	0.80	5.29
	1.0	1.21	8.20
	1.0	1.63	11.6
	1.0	2.10	14.48
	1.0	2.75	20.01
308	1.0	0.50	6.22
	1.0	0.80	9.48
	1.0	1.21	14.15
	1.0	1.63	19.25
	1.0	2.10	23.20
	1.0	2.75	33.00

* Typically an average of two measurements.

TABLE A7

Reduction of $(\text{CH}_3)_3\text{NO} \cdot 2\text{H}_2\text{O}$ (TMANO) by $[\text{Bu}_4\text{N}]_2[\text{Mo}^{\text{IV}}\text{O}(\text{mnt})_2]$
 $[\text{Complex}] = 1 \times 10^{-4}\text{M}$ Temp. = $20 \pm 0.1^\circ\text{C}$
 $[\text{TMAO}] = 12.5 \times 10^{-4}\text{M}$ Solvent = Acetone-acetic acid (effective pH 6)
Fig. 4.18

Time (sec)	Conc. (C)	$\log(C \times 10^6)$
30	$0.961 \times 10^{-4}\text{M}$	1.982
60	$0.934 \times 10^{-4}\text{M}$	1.970
90	$0.894 \times 10^{-4}\text{M}$	1.951
120	$0.867 \times 10^{-4}\text{M}$	1.938
150	$0.821 \times 10^{-4}\text{M}$	1.914
180	$0.787 \times 10^{-4}\text{M}$	1.895
210	$0.740 \times 10^{-4}\text{M}$	1.869
240	$0.694 \times 10^{-4}\text{M}$	1.841

Plot: $\log(C \times 10^6)$ vs time $k_{\text{obs}} = 1.192 \times 10^{-3} \text{ s}^{-1}$

The formula used to calculate concentration (C), is:

$$C(t) = (C_0 \varepsilon_2 - A(t)) / (\varepsilon_2 - \varepsilon_1)$$

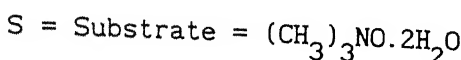
$C(t)$ is concentration of the Mo(IV) complex at time t , C_0 is the initial concentration of this complex (at $t = 0$), $A(t)$ is absorbance of reaction mixture at time t at the monitoring wave length, 525 nm, ε_1 is the molar extinction coeff. of Mo(IV) complex and ε_2 is that of Mo(VI) complex, $[\text{Bu}_4\text{N}]_2[\text{Mo}^{\text{VI}}\text{O}_2(\text{mnt})_2]$ at the wave length 525 nm.

TABLE A8

Kinetic Data for the Substrate Saturation Curve (Fig. 4.17) and Corresponding Double Reciprocal Plot (I_o) for Fig. 4.19



Solvent = acetone-acetic acid (effective pH 6) Temp. = 20°C



$10^4 [S]$, M	$10^3 k_{obs}$, s ⁻¹	$1/[S]$, M ⁻¹	$1/k_{obs}$, s
6.0	1.49 (\pm 0.09)	1666.6	673.595 (\pm 40.685)
7.5	1.65 (\pm 0.11)	1333.3	608.765 (\pm 40.585)
10.0	1.97 (\pm 0.05)	1000.0	509.435 (\pm 14.395)
12.5	2.12 (\pm 0.08)	800.0	472.365 (\pm 17.825)
15.0	2.36 (\pm 0.08)	666.6	424.21 (\pm 14.38)
17.5	2.5 (\pm 0.08)	571.4	400.395 (\pm 12.805)
20.0	2.63 (\pm 0.13)	500.0	381.15 (\pm 18.85)

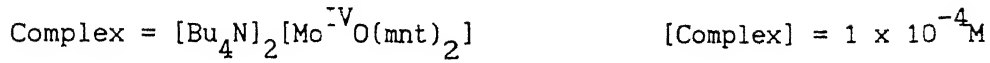
From the double reciprocal plot (I_o) (Fig. 4.19),

$$V_{max} (= k_2, k_{obs} \text{ at substrate saturation}) = 3.81 \times 10^{-3} \text{ s}^{-1}$$

$$K_m \text{ (Michaelis constant)} = 9.1 (\pm 0.9) \times 10^{-4} \text{ M}$$

TABLE A9

Kinetic Data for Double Reciprocal Plots (I_1 and I_2) for Competitive Inhibition by Cl^- (Fig. 4.19)



Solvent = acetone-acetic acid (effective pH 6) Temp. = 20°C

S = Substrate = $(\text{CH}_3)_3\text{NO}.2\text{H}_2\text{O}$ I = Inhibitor = Bu_4NCl

$[I] = 8 \times 10^{-4} \text{ M}$		$[I] = 15 \times 10^{-4} \text{ M}$	
$1/[S], \text{ M}^{-1}$	$1/k_{\text{obs}}, \text{ s}^{-1}$	$1/[S], \text{ M}^{-1}$	$1/k_{\text{obs}}, \text{ s}^{-1}$
1662.5	784.375 (± 21.875)	1662.5	925.0 (± 25.0)
1000.0	568.75 (± 18.75)	1000.0	681.25 (± 18.75)
662.5	456.25 (± 18.75)	662.5	543.75 (± 18.75)
575.0	437.5 (± 12.5)	500.0	468.75 (± 18.75)
		400.0	437.5 (± 12.5)

Cl^- behaves as competitive inhibitor (Fig. 4.19).

The inhibition constant, K_I for the reaction of inhibitor (Cl^-) with Mo(IV) complex was calculated (from double reciprocal plots, Fig. 4.19) to be

$$K_I = 2.4 \times 10^{-3} \text{ M.}$$

TABLE A10

Oxygen Atom Transfer Reaction Between $[Bu_4N]_2[Mo^{VI}O_2(mnt)_2]$ and PPh_3 : A Representative Table of Time vs Concentration for the Calculation of k_{obs}

$$[Complex] = 1 \times 10^{-4} M$$

Solvent = MeCN

$$[PPh_3] = 8 \times 10^{-2} M$$

Temp. = 25°C

Time (sec)	Concentration (C)	$\log(C \times 10^6)$
15	$0.9048 \times 10^{-4} M$	1.956
135	$0.8435 \times 10^{-4} M$	1.923
255	$0.7891 \times 10^{-4} M$	1.897
375	$0.7415 \times 10^{-4} M$	1.870
495	$0.6939 \times 10^{-4} M$	1.841
615	$0.6462 \times 10^{-4} M$	1.810
735	$0.6122 \times 10^{-4} M$	1.787
855	$0.5714 \times 10^{-4} M$	1.757
975	$0.5374 \times 10^{-4} M$	1.730
1095	$0.5034 \times 10^{-4} M$	1.702
1215	$0.4694 \times 10^{-4} M$	1.671

The formula used to calculate C (from absorbance) has been described in Table A1. In this case the monitoring wave length is 525 nm.

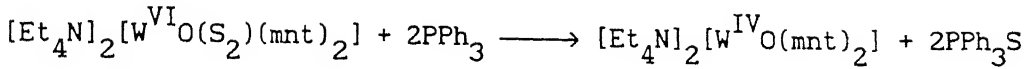
Plot: $\log(C \times 10^6)$ vs time

$$k_{obs} = 5.3 \times 10^{-4} s^{-1}$$

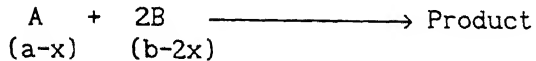
TABLE A11

The KInetics of the Reaction of $[\text{Et}_4\text{N}]_2[\text{W}^{\text{VI}}\text{O}(\text{S}_2)(\text{mnt})_2]$ with PPh_3

The reaction,



follows A + 2B type second order kinetics.



x denotes the concentrations of the reactants which disappear in time t,

then, the rate,

$\frac{dx}{dt} = k(\text{a}-\text{x})(\text{b}-\text{x})$, integrating followed by taking logarithm,

$$\log \frac{a(b-2x)}{b(a-x)} = -\frac{(b-2a)kT}{2.303}$$

Hence $\log \frac{a(b-2x)}{b(a-x)}$ vs T should give straight line, the slope of which will be $\frac{(b-2a)k}{2.303}$, from which k can be calculated.

TABLE A12

Reaction Between $[\text{Et}_4\text{N}]_2[\text{W}^{\text{VI}}\text{O}(\text{S}_2)(\text{mnt})_2]$ and PPh_3 : A

Representative Table for Calculation of k_{obs}

$$a = [\text{Complex}] = 1 \times 10^{-4} \text{ M} \quad b = [\text{PPh}_3] = 7.28 \times 10^{-4} \text{ M}$$

Solvent = MeCN

Temp. = 25°C

$$a/b = 0.137$$

$$(b-2a) = 5.282 \times 10^{-4} \text{ M}$$

Time (sec)	$10^4 (a-x)$	$10^4 (b-2x)$	$\log \frac{a(b-2x)}{b(a-x)}$
------------	--------------	---------------	-------------------------------

30	0.9211	7.1214	0.0521
90	0.7671	6.8162	0.0854
150	0.6500	6.5820	0.1422
210	0.5514	6.3848	0.2004
270	0.4713	6.2246	0.2575
330	0.4066	6.0952	0.3125
390	0.3512	5.9844	0.3682
450	0.3019	5.8858	0.4266
510	0.2619	5.8058	0.4824

$(a-x)$ = concentration of the complex at time $t = C(t) =$
 $(A(t) - \epsilon_2 C_0) / (\epsilon_1 - \epsilon_2)$, where $A(t)$ = absorbance of the reaction
mixture at time t at the monitoring wave length 478 nm, C_0 =
concentration of the complex at time $t = 0$, ϵ_1 molar extinction
coeff. of the complex at the monitoring wave length, and the ϵ_2 =
molar extinction coeff. of the reduced complex,
 $[\text{Et}_4\text{N}]_2[\text{W}^{\text{IV}}\text{O}(\text{mnt})_2]$ at the same wave length.
Plot: $\log \frac{a(b-2x)}{b(a-x)}$ vs time $k_{\text{obs}} = 4.24 \text{ M}^{-1} \text{s}^{-1}$.

LIST OF PUBLICATIONS

1. S. Sarkar and S. K. Das, Synthesis of the active sites of molybdoenzymes: MoO_2 (VI) and $\text{MoO}(\text{IV})$ -dithiolene complexes mimicking enzymatic reactions of sulphite oxidase with saturation kinetics, *Proc. Indian Acad. Sci. (Chem. Sci.)*, 1992, 104, 437.
2. S. Sarkar and S. K. Das, CO_2 fixation by $[\text{W}^{\text{IV}}\text{O}(\text{S}_2\text{C}_2(\text{CN})_2)_2]^{2-}$: functional model for the tungsten-formate dehydrogenase of *Clostridium thermoaceticum*, *Proc. Indian Acad. Sci. (Chem. Sci.)*, 1992, 104, 533.

Three manuscripts are under preparation.